Fate of nutrients in a subtropical reservoir according to hydrodynamic processes and its effects on phytoplankton dynamics

by

Mayra Matsume Ishikawa

from Curitiba, Brazil

Accepted Dissertation thesis for the partial fulfillment of the requirements for a

Doctor of Natural Sciences

Fachbereich 7: Natur- und Umweltwissenschaften

Universität Koblenz-Landau

Thesis examiners:

Prof. Dr. Andreas Lorke, Landau

Prof. Dr. Tobias Bleninger, Curitiba

06 September 2022

This dissertation is based on the following articles, published in peer-reviewed journals (ordered by date):

Ishikawa, M., Haag, I., Krumm, J., Teltscher, K., & Lorke, A. (2021). The effect of stream shading on the inflow characteristics in a downstream reservoir. River Research and Applications, 37(7), 943-954. doi: 10.1002/rra.3821

Ishikawa, M., Bleninger, T., & Lorke, A. (2021). Hydrodynamics and mixing mechanisms in a subtropical reservoir. Inland Waters, 11(3), 286-301. doi: 10.1080/20442041.2021.1932391

Ishikawa, M., Gonzalez, W., Golyjeswski, O., Sales, G., Rigotti, J. A., Bleninger, T., Mannich, M., and Lorke, A. (2022). Effects of dimensionality on the performance of hydrodynamic models for stratified lakes and reservoirs. Geosci. Model Dev., 15(5), 2197-2220. doi: 10.5194/gmd-15-2197-2022

Ishikawa, M., Gurski, L., Bleninger, T., Rohr, H., Wolf, N., Lorke, A. (2022). Hydrodynamic drivers of nutrient and phytoplankton dynamics in a subtropical reservoir. Water, 14(10), 1544, doi: 10.3390/w14101544.

Table of Contents

Abstract

Manmade dams have been constructed from centuries for multiple purposes, and in the past decades they have been constructed in a fast pace, with the hotspot in tropical and subtropical regions. However, studies that explore hydrodynamics in these areas are scarce and biased to the rich literature available for temperate regions. Lakes and reservoirs have the same controlling mechanisms for physical processes and primary production, hence, analyses that were initially conceptualized for lakes are frequently applied for reservoirs. Nevertheless, longitudinal gradients in reservoirs challenges the application of these approaches.

Degradation of water quality in reservoirs is a major concern, and it is expected to be aggravated with climate change. Therefore, studies that explore mechanisms controlling water quality are essential for the maintenance of these systems, especially in tropical and subtropical regions. The aim of this thesis is to comprehend the role of hydrodynamic processes in the fate of nutrients in reservoirs and its implications on water quality, in a subtropical region. With focus on the relevance of different density current patterns. For that, analyses combining field measurements and numerical simulations were performed in a medium to small size subtropical drinking water reservoir for a complete seasonal cycle. Measurements were conducted combining several approaches: traditional sampling, sensors in high temporal and spatial resolution, and remote sensing. Besides, hydrodynamic models were set up and calibrated to reproduce observations, and to simulate scenarios that assisted on the analysis.

Results showed that different flow paths of density currents did not influence on phytoplankton dynamics. At the regions where the main nutrient supply was the river inflow (upstream), the density currents did not vary, the euphotic zone usually covered the entire depth, and vertical mixing was observed on a daily basis, turning the flow path of the density currents irrelevant. At downstream regions, the remobilization of nutrients in the sediment was the main source for primary production. Even though density currents had a seasonal pattern in the downstream region, thermal stratification conditions were the driver for variations in chlorophyll-a concentrations, with peaks after vertical mixing. This mechanism had in its favor the frequent anoxic conditions in the hypolimnion that enhanced the dissolution of reactive phosphorus from the sediment. Anoxic conditions were easily reached because the sediment in the downstream area was rich in organic matter. Phytoplankton produced in the upstream area was transported by the density currents, and for this reason, large concentrations of chl-a was observed below the euphotic zone. Further, the extensive measurements of temperature, and flow velocities,

together with the hydrodynamic models, provided insights about the hydrodynamics of reservoirs. For instance, that the relevant processes occurred along the longitudinal, and mixing conditions varied along it. The relevance of inflow conditions regarding the presence of structures such as forebays and pre-dams, and the degree of stream shading in the catchment was assessed. And turbulence and internal waves had different features than the documented for high latitudes. Those findings can assist on the management of reservoirs, based on the comprehension of the physical processes.

1 Introduction

1.1 Bias of limnology studies to temperate regions and the boom of tropic reservoirs

Since the first studies about limnology, started by François-Alphonse Forel at the end of the XIX century in Switzerland (Forel, 1892), most of the progress in the subject have been developed in Europe and North America. And until this date a bias towards temperate inland waters exist (Winton et al., 2019). Although limnology comprise all inland waters including rivers and estuaries, natural lakes are concentrated at high latitudes (see Figure 1), which among others reasons can explain the bias.

On the other hand, manmade dams have been constructed from centuries for multiple purposes, such as water supply, irrigation, flood control, and energy generation (Lehner et al., 2011). As a consequence, reservoirs disrupt the natural course of running waters, changing the water body completely altering nutrient balances, flow of particulate matter, oxygen concentration, and temperature (Friedl and Wüest, 2002). On top of that, in the past decades dams have been constructed in a fast pace, the International Commission of Large Dams (i.e. dams with a height > 15 m) has the register of 58713 dams worldwide. Tropical regions are the hotspot for the construction of new dams (Zarfl et al., 2014), from 2001 to 2011 there was one project per year of dams larger than 10^3 km^3 in tropical regions (Winton et al., 2019). However, small to medium-sized reservoirs are the most abundant. Based on data from Messager et al. (2016), reservoirs with a surface area between 1 and a 10 km^2 and volume ranging from 10^6 to 10^8 m^3 were 37% of their estimates.

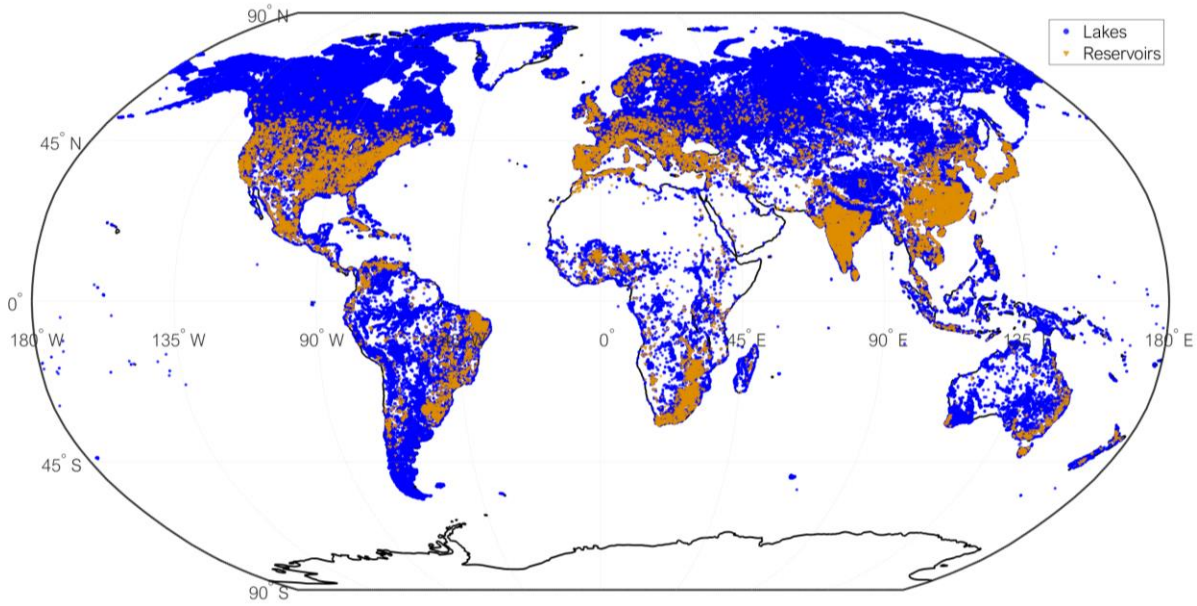

Figure 1: worldwide distribution of natural lakes and dams, data from Mulligan et al. (2020) and Messager et al. (2016), respectively.

Major differences between inland waters in low and high latitudes rely on the discrepant distribution of seasonal solar radiation, from that different dynamics develop regarding mixing and stratification patterns, nutrient cycle, and dissolved oxygen concentrations (Lewis Jr, 1996; MacIntyre and Melack, 2010). These are basic processes that regulate mechanisms of great importance for the management of lakes and reservoirs and their impacts, such as the maintenance of the quality of the impounded area and downstream rivers (Winton et al., 2019), and the emission of greenhouse gases (Rosentreter et al., 2021). Winton et al. (2019) showed that data from reservoirs in tropical and subtropical regions are scarce, and even the classification of the mixing regime is difficult to define in those regions.

1.2 Lakes vs. Reservoirs

Natural lakes differ from reservoirs in several aspects. Starting from the morphometry, lakes have predominantly oval or elliptical shapes with maximum depths usually located at a central region, while reservoirs can be quite variable in shape (ovoid, triangular, dendritic, valley, etc.) and present continuous gradient of increasing depths from inflows to dam (Wetzel, 2001). In addition, there are also differences in water level fluctuations, inflow and outflow dynamics, residence time, deposition of sediments, and substance concentration gradients (Wetzel, 2001). These differences impact on physical and biogeochemical processes.

Reservoirs are usually built from the damming of rivers, therefore they transit from riverine to lacustrine environments. Kimmel and Groeger (1984) observed strong longitudinal gradients formed in reservoirs due to this transition, therefore they suggested the zonation of reservoirs in three parts: riverine, transitional and lacustrine zones. In this conceptual model the three regions differ in morphometry from narrow to broader areas, and the high flow velocities from the running waters gradually decrease. As a consequence, from the inflow to the dam direction, the turbidity decreases due to the settling of particles, and nutrient concentrations are still sufficient, making the transitional zone the ideal location for the growth of phytoplankton. However, the identification of zones is not always trivial because variable shapes of reservoirs, possible multiple inflows, and large variability in volumetric discharges of inflows and outflows can expand and compress the zones (Kimmel et al., 1990).

Despite the differences between lakes and reservoirs, both aquatic environments share the same controlling mechanisms of both physical processes (Imberger and Hamblin, 1982), and primary production (Kimmel and Groeger, 1984). Hence, analyses that were initially conceptualized for lakes are frequently applied for reservoirs, such as the thermal classification of mixing regimes proposed by Lewis Jr (1983) (e.g. Winton et al., 2019), the application of 1D vertical models (Weber et al., 2017), dimensionless numbers as Lake and Wedderburn Number (Rueda et al., 2007), and linear relationships to predict chlorophyll-a (chl-a) concentration through total phosphorus (TP) inputs (Dillon and Rigler, 1974). However, horizontal heterogeneity in reservoirs challenges the application of these approaches.

1.3 Water quality

The maintenance of the water quality of inland waters is of great importance for several reasons, the basic is to assure the access of potable water and keep sustainable ecosystems in those environments. This is such an important topic that sustainable water security is one of the development goals proposed by the United Nations (Griggs et al., 2013), which the aim is provide universal access to clean water and basic sanitation.

Water quality usually is assessed by their trophic state, which quantifies the biological productivity. The classification varies from oligo-, meso-, eutro- and hypereutrophic, corresponding for good, fair and poor estates (the last two), they usually are estimated through indices that account for concentrations of chl-a, TP, total nitrogen (TN), and turbidity (Cunha et al., 2021). Chl-a is used as a proxy for phytoplankton biomass, which is relevant since primary

production is associated to it. In turn, primary production depends on nutrient availability (TP and TN), and ambient conditions such as temperature, residence time and light availability (turbidity) (Le Moal et al., 2019). And algal blooms are episodic events where excessive phytoplankton biomass is developed, usually associated to nutrient over-enrichment (Paerl and Otten, 2013).

Both, eutrophication and algal blooms, can deplete dissolved oxygen concentrations to hypoxic or anoxic levels due to the decomposition of organic matter that consume oxygen. The low levels of dissolved oxygen are problematic for biodiversity, nutrient biogeochemistry, emission of greenhouse gases, among others (Jane et al., 2021). Thus, the degradation of water quality due to eutrophication and algal blooms can result in alteration of odor and color, and the mortality of fish due to the depletion of oxygen concentrations to anoxic conditions and liberation of toxins. These problems can rise the costs for water treatment (Pretty et al., 2003), develop diseases during the events with acute intoxication (Roberts et al., 2020), and can potentially be a problem to humans through the bioaccumulation of toxins (Weirich and Miller, 2014; Alves and Mafra, 2018), in addition entire communities are impacted on social, economic, and cultural aspects (Ellis et al., 2022).

Therefore, algal blooms became a major concern regarding the water quality of inland waters (Brooks et al., 2016), and their incidence in lakes increased considerably since the decade of 1980 (Ho et al., 2019). There are indications that with climate changes blooms will be even more frequent due to warmer water temperatures, prolonged stratification with low levels of oxygen concentrations in the hypolimnion, and inflow regimes alterations (Nazari-Sharabian et al., 2018; Ho et al., 2019; Jane et al., 2021; Akomeah et al., 2021).

Reservoirs are more susceptible to eutrophication, the accumulation of suspended solids traps organic matter and nutrients, turning the sediment into an internal supply of nutrients for algal growth (Maavara et al., 2020). And reservoirs usually are located in areas of high anthropogenic activities that can potentially increase nutrient loads (Kimmel and Groeger, 1984). On top of that, climate changes are expected to enhance those features by the increase input of sediment and nutrients from the catchment (Yasarer and Sturm, 2016).

1.4 The role of hydrodynamics on water quality

Relationships between nutrients and phytoplankton were first identified in the decade of 1970 and 80, when the eutrophication of lakes and reservoirs was a massive problem (Dillon and Rigler, 1974; Walker Jr, 1983). Thereafter, some regions made efforts on the reduction of point source

nutrients inputs, especially phosphorous, were successfully made to control and/or restore the trophic state of such systems (Gibson, 1986; Cullen and Forsberg, 1988). However, as previously mentioned, eutrophication still is a major concern for managers of reservoirs.

Highly eutrophic water bodies can take a long time to respond to point source reductions of nutrients, remobilization of phosphorus from the sediment, i.e. internal loading, can supply phytoplankton for a long period (Marsden, 1989). It was the case of Lake Constance in Germany, that took approximately 20 years for re-oligotrophication (Gaedke et al., 1991; Gaedke, 1998). The remobilization of phosphorus from a particulate form in the sediment to a dissolved reactive form depends on the biological structure in the pelagic zone, temperature, pH, and especially dissolved oxygen concentrations, since phosphorus release is redox dependent (Søndergaard et al., 2003). Hence, in such environments physical processes regulate the availability of the reactive phosphorus produced in the deepest layers to the euphotic zone.

For shallow water bodies strong winds that mix the entire water depth can be sufficient to resuspend solids from the bed and bring nutrients to the surface (Søndergaard et al., 2003). For stratified systems, mechanisms that can trigger the development of phytoplankton are the variations on the thickness of the upper mixed layer (UML) (e.g. Liu et al., 2012; Xu et al., 2021), and the upwelling of the hypolimnion forced by standing waves (e.g. Rao et al., 2012). More complex set ups involving hydrodynamics also interfere on water quality, for instance, results of a numerical simulation showed that Dianshan Lake would have less frequent algal blooms with the reduction of residence time (through flow discharges regulations), than the reduction of nutrient inputs (Chen et al., 2016). And algal blooms at Xiangxi Bay, a tributary of the Three Gorges Reservoir, are driven by nutrients inputs of the main reservoir, depending on an interplay of stratification conditions of the bay and main reservoir, and inflow conditions of the tributary, when certain density currents are formed the blooms occur (Long et al., 2019; Xu et al., 2021).

Catchment characteristics also affects the water quality of the water body, depending on the activities in the area, such as agriculture that use fertilizes, nutrients loads from diffuse sources can be significant (Schindler, 2006). Therefore, for reservoirs that usually have one main inflow (Wetzel, 2001), the flow path of the inflowing river into the reservoir can rule the phytoplankton dynamics (Vincent et al., 1991). The water masses entering water bodies can be classified in three flow paths: under-, inter-, and overflows, see Figure 2. The currents enter the water bodies pushing the water with its initial momentum, then pass through an initial dilution when entering the reservoir, and afterwards follow a path of neutral buoyance, for this reason

they are called density or gravity currents. Their fate will depend on the density stratification of the reservoir and the inflow conditions; mainly temperature and substances concentrations that can potentially alter its density (Alavian et al., 1992). Hence, when the inflow density is larger than the observed in the reservoir an underflow is formed and the current moves along the bed; overflows occur when the inflow density is smaller and/or equal to the UML and the current goes over the surface; and interflows are resulted from currents of densities equal to the ones found in middle depths.

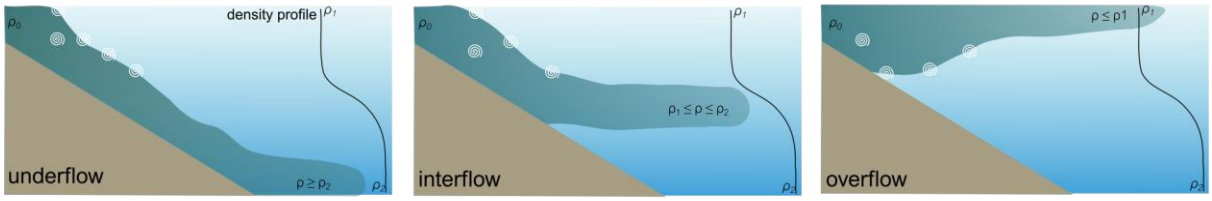

Figure 2: Scheme of the different density currents flow paths, each panel demonstrates the different flow paths according to the interaction between inflow conditions and density stratification of the reservoir.

1.5 Research needs

Advances on the comprehension of the physical mechanism of density currents have been developed for years. For instance, Alavian et al. (1992) presented a good overview of the involved mechanisms and described the stages of the development of a density current. Rueda et al. (2007) pointed the uncertainties regarding the initial mixing of density currents and how they could influence on the prediction of density currents formation, and as consequence uncertainties on nutrients pathways. Progress on the physical process itself was made through modeling, laboratorial experiments and field data (Cortés et al., 2014a; Cortés et al., 2014b; Cortés et al., 2015; Rueda and MacIntyre, 2009, 2010). And the use of tracers in hydrodynamic models to predict the flow path of density current was proven to be a good approach (Owens et al., 2014).

The influence of the different flow paths of density currents on water quality was investigated by a few studies. Vincent et al. (1991) and Gibbs (1992) linked the density currents dynamics to water quality of Lake Rotoiti, a deep lake in New Zealand with two main basins. Depending on the flow path of the inflowing current, it passed through the lake directly to the outflow, or it entered into the main basin bringing nutrients and algae, and altering the residence time and its oxygenation. Lake Toolik, located in Alaska, was monitored over its summer stratification and the increase of primary production driven by overflows was captured (MacIntyre et al., 2006).

Although the existing interest in improve the knowledge of processes that degrade water quality and trigger algal blooms, not many studies linked the response of primary production in accordance to density currents patterns. Such relationships have not been assessed for reservoirs, which can potentially have its effects augmented by some of their peculiarities. For instance, their location on catchments with larger loads of nutrients, the predominance of a single major inflow, and the continuous bottom slope. Therefore this thesis explore the relationship between density currents and water quality in a subtropical reservoir. It presents an extensive description of hydrodynamics processes, providing a contribution to reduce the gaps related to the knowledge about low latitude environments, with focus on features that are specific for reservoirs.

In the next chapter the objectives and tested hypotheses of the thesis will be presented, followed by the outline containing an overview of the methods, publications that support the findings, and the study site. Then results are discussed, and lastly the conclusions are stated.

2 Objectives

The principal objective of this thesis is advance in the comprehension of the role of hydrodynamic processes in the fate of nutrients in reservoirs and its effect on water quality, in a subtropical region, especially the impact of different density current patterns. For that, the following research questions with their respective hypotheses are going to be addressed:

Q1. Which are the main hydrodynamic processes in a subtropical reservoir?

Hypothesis 1.1. Physical processes in a subtropical region are significantly different than in a temperate region, regarding their relevance, and temporal dynamics. Distinct dynamics in mixing and stratification, turbulence, and internal waves, are expected due to distinguish meteorological conditions of each climate zone.

Hypothesis 1.2. Forebays and pre-dams play an important role in the hydrodynamic processes of reservoirs. In such systems the rates of heat exchange with the atmosphere are faster than in the deeper regions inside the reservoir. As consequence, they alter the water inflow temperature dynamics and associated processes.

Hypothesis 1.3. Changes in river inflow temperature, due to stream shading conditions in the catchment area, can alter the flow path dynamics within the reservoir. Alterations are caused by changes in inflow water density driven by temperature.

Q2. In which dimensionality do the relevant processes occur?

Hypothesis 2.1. The usual continuous bed slopes observed in reservoirs create a depth gradient along the longitudinal. Thus, processes over the vertical dimension have their relevance and characteristics altered towards the downstream direction.

Hypothesis 2.2. Owning to the strong longitudinal gradients observed in reservoirs, the hypothesis that physical processes along the longitudinal regulate thermal stratification is tested through the application of hydrodynamic models of distinct dimensionalities. While, the relevance of the transversal dimension is negligible.

Q3. Which are the main relationships between hydrodynamics and water quality?

Hypothesis 3.1. Seasonal variations of chlorophyll-a depend on internal loading, therefore they are ruled by thermal stratification.

Hypothesis 3.2. Seasonal variations of chlorophyll-a are driven by different density currents entering the reservoir. Overflows result in larger concentrations of chlorophyll-a, because nutrients are being delivered at the euphotic zone. Likewise, underflows result in lower concentrations of chlorophyll-a.

Hypothesis 3.3. Density currents can also influence on chlorophyll-a distribution patterns through the advection/redistribution of phytoplankton biomass.

3 Outline

To address the objectives and to test the hypotheses, analyses combining field measurements and numerical simulations were performed in a medium to small size subtropical drinking water reservoir. The reservoir was monitored for a complete seasonal cycle. In situ measurements were conducted through different approaches: traditional sampling (for water quality parameters), and sensors in high temporal and spatial resolution (for water quality parameters, flow velocities, and temperature). In addition, remote sensing images were used to estimate chl-a concentrations at the surface. Hydrodynamic models were set up and calibrated to reproduce observations, and later to simulate scenarios that assisted on the test of the hypotheses. Results from a hydrological model were used to feed the boundary conditions of inflow discharges and water temperature of the hydrodynamic model. Besides, the hydrological model considered different degrees of stream shading conditions in the catchment to simulate changes in water temperature. Figure 3 presents an overview of the studied system indicating the associated processes, monitoring approaches, and related parameters.

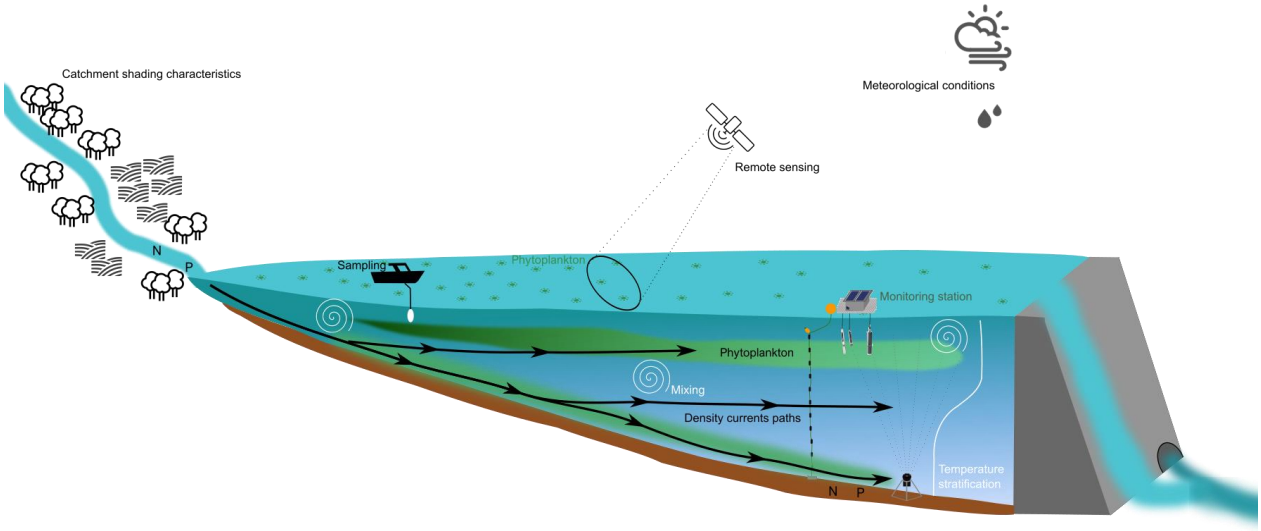

Figure 3: Graphical abstract of the study showing the assessed processes, indicating the relevant parameters and applied methods.

Four peer-reviewed publications contain the main findings supporting this thesis (Appendices). Following, there is a brief description of each publication highlighting their contributions to the research questions and hypotheses, at the end of the section the study site is presented.

Hydrodynamics and mixing mechanisms in a subtropical reservoir

Ishikawa, M., Bleninger, T., & Lorke, A. (2021). Hydrodynamics and mixing mechanisms in a subtropical reservoir. Inland Waters, 11(3), 286-301. doi: 10.1080/20442041.2021.1932391 (***Appendix I***)

The characterization of the main physical processes occurring in a subtropical reservoir was performed through high resolution observations of temperature, flow velocities and meteorological conditions (**Q1**). Over the study it was explored the main drivers of mixing and stratification, water movement, wave motion, and turbulence, in diel and seasonal scales (*H1.1*). An investigation of the flow path of density currents was performed. It considered temperature as a proxy for density, and with observations of temperatures at the inflow, after the forebay, and the profile in a deeper region of the reservoir the flow paths were estimated (*H1.2* and *H1.3*).

The effect of stream shading on the inflow characteristics in a downstream reservoir

Ishikawa, M., Haag, I., Krumm, J., Teltscher, K., & Lorke, A. (2021). The effect of stream shading on the inflow characteristics in a downstream reservoir. River Research and Applications, 37(7), 943-954. doi: 10.1002/rra.3821 (***Appendix II***)

Based on the potential effect of inflow temperature on flow paths within the reservoir, this study evaluated different scenarios of stream shading in the catchment to assess its influence on density currents within the reservoir. For that, inflow temperatures were simulated with the distributed water-balance model LARSIM-WT with 0 and 100% stream shading in the catchment. The results were assessed together with the measured temperature profile (*H1.3*).

Effects of dimensionality on the performance of hydrodynamic models for stratified lakes and reservoirs

Ishikawa, M., Gonzalez, W., Golyjeswski, O., Sales, G., Rigotti, J. A., Bleninger, T., Mannich, M., and Lorke, A. (2022). Effects of dimensionality on the performance of hydrodynamic models for stratified lakes and reservoirs. Geosci. Model Dev., 15, 2197-2220. doi: 10.5194/gmd-15-2197-2022 (***Appendix III***)

Three hydrodynamic models of distinct dimensionalities were applied for the same subtropical reservoir, all of them are widely used to simulate stratified lakes and reservoirs. The models are General Lake Model (GLM), a 1D vertical model which is horizontally averaged, CE-QUAL-W2 a 2D model laterally averaged, and the 3D model was Delft3D-FLOW. Their performance regarding water level, temperature stratification, substance transport as a proxy for density currents, and flow velocities (only for the 2 and 3 D) were compared with the aim to understand how the physical processes were affected according to their simplifications. Thus, it was possible to identify which dimensions were paramount for the processes and the mechanisms behind them (**Q2**, *H2.1, H2.2*).

Hydrodynamic drivers of nutrient and phytoplankton dynamics in a subtropical reservoir

Ishikawa, M., Gurski, L., Bleninger, T., Rohr, H., Wolf, N., Lorke, A. (2022). Hydrodynamic drivers of nutrient and phytoplankton dynamics in a subtropical reservoir. Water, 14(10), 1544, doi: 10.3390/w14101544. (*Appendix IV*)

This work explored the water quality dynamics based on the fate of nutrients within the reservoir according to physical processes, and its response on primary production (**Q3**). For that, extensive measurements were performed combining different approaches: traditional sampling and in-situ sensors for nutrients and chlorophyll-a (chla), remote sensing images for chla, and the 3D hydrodynamic model for the physical processes. Measurements provided temporal and spatial dynamics, thus observations of chla were explained accordingly (*H3.1, H3.2* and *H3.2*). And the simulation of two scenarios with the hydrodynamic model assisted on the evaluation of the influence of inflow temperatures and the role of the forebay on reservoir hydrodynamics (**Q1**, *H1.2* and *H1.3*).

Passaúna Reservoir

Passaúna reservoir is located between the latitudes 25.44° S and 25.54° S, it has an area of ~ 9 km^2, volume of 60×10^6 m^3 and maximum depth of 17.5 m close to its dam, thus it is in the size range of small to medium (Figure 4). Thirty-four percent of the reservoirs in the tropical and subtropical region are in the same size range of Passaúna, and they represent 14% of all reservoirs worldwide (estimation based on data from Messager et al., 2016).

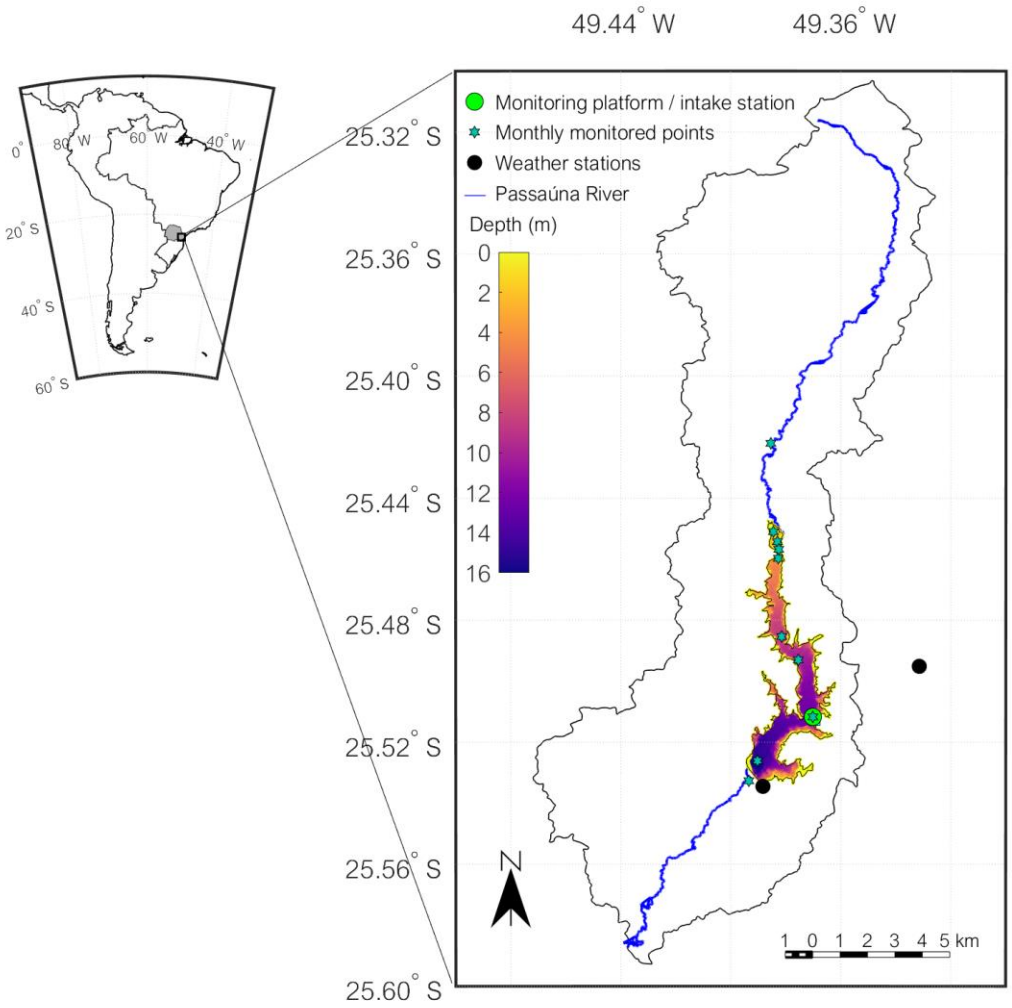

Figure 4: Map of the study site within the South American continent in the left panel, where the gray background indicates the location of Paraná state in Brazil. Right panel shows in blue line the Passaúna River with its respective catchment area in black line. Passaúna Reservoir area is presented with colors indicating the depths (data from Sotiri et al., 2019). Within the right panel there is the indication of the weather stations, the monthly monitored points, and the monitoring platform (in front of the intake station). The legend of each symbol is present inside the right panel at the top left.

A bridge crosses the reservoir at latitude 25.45° S, which constrain the reservoir and forms a forebay of 0.28 km^2 and mean depth of ~1 m^2, other than that it has an elongated valley shape with a continuous slope. In operation since 1990, it was constructed for water supply of part of Curitiba and other three neighbor cities attending ~ 600 million people with an average production rate of 1.8 $m^3 s^{-1}$. The main inflow is Passaúna River (75% of the total annual inflow), followed by Ferraria River at latitude 25.47° S (average flow discharge of 0.15 $m^3 s^{-1}$), the remaining inflows are intermittent. The outflows are the intake for water production, and at the dam through a bottom outlet (continuous discharge of approximately 0.5 $m^3 s^{-1}$) and a spillway.

4 Discussion

This chapter presents discussions merging the results from the four published articles presented in Chapter 3. The articles are referenced according to their respective location in the appendices section, and presenting their contributions to reject or retain the raised hypotheses. Each subchapter correspond to a research question following the same order as they were presented in the outline.

4.1 Hydrodynamics in a subtropical reservoir

The main characteristics of the physical processes in a subtropical reservoir were identified based on high resolution measurements of meteorological conditions, flow velocities, and temperature, performed over a year. The dynamics of mixing and stratification, longitudinal transport, flow velocities, turbulence and wave motion were explored in diel and seasonal scales (***Appendix I***).

According to observations of the temperature profile at the intake region, the mixing regime of Passaúna Reservoir was classified as warm discontinuous polymictic, which is expected for lakes of medium depths in tropical and subtropical regions (Lewis Jr, 1983). Intermittent mixing occurred over the autumn and winter season, while persistent stratification was observed over spring and summer. Mixing events were driven by prolonged periods of heat loss by the water surface when air temperatures dropped, wind was not relevant due to its low intensities (***Appendix I***). On the other hand, stratification was promoted by the warming of the surface, and also by the addition of cold inflow waters at the bottom layers of the water column (***Appendix I***). This mechanism was caused by density currents in the underflow form, which can be significant for the formation of temperature stratification in low latitudes (Lewis Jr, 2000; Xing et al., 2014)

For this reason, the temperature of inflowing waters into the reservoir were assessed, considering the river inflow temperature and the temperature measured right after the forebay (***Appendix I***). The shallow depths at the forebay promoted fast heat exchanges, as consequence water temperature entering the reservoir after the forebay was warmer and varied more than the river temperature, respective mean ± standard variation of 19.6 ± 3.6 and 16.8 ± 2.6 °C. This mechanism is similar to differential cooling, where the littoral regions of lakes cool faster than the pelagic zone, creating a horizontal temperature gradient that enables water circulations (Doda et al., 2022).

Hence, to test the influence of the forebay and the inflow temperature on thermal stratification of the reservoir, a 3 dimensional hydrodynamic model was used to reproduce the monitored year (Appendix III). Results had a good agreement with observations, and errors were comparable to values found in the literature. Thermal stratification and mixing events were well reproduced, while flow velocities had the main pattern well reproduced, but rather underestimated magnitudes. Then, other two scenarios were set up (*Appendix IV*), to test to which extent the forebay was influencing on inflow temperatures and on downstream temperature profiles. Scenario (i) had the forebay completely removed. While scenario (ii) had warmer inflow temperatures (according to changes on catchment stream shading, *Appendix II*), to understand the role of the river inflow temperature on density currents. At the end, the simulated temperatures from the scenarios had minor differences with the original simulation at the intake region (where the temperature profile was measured continuously), temperatures differed in the second decimal. This result indicates that the temperature stratification at lacustrine regions of the reservoir had minor influence from changes in inflow temperatures and the forebay. Although a few underflows events were relevant for the re-stratification of the intake region, they occurred when the inflow temperature had the largest difference with reservoir bottom temperatures (inflow colder). Which provided the conditions for consistent underflows, also for the simulated scenarios, that are independent from the forebay (scenario i) and the overall warmer water inflow temperature (scenario ii). Hence, *H1.2* and *H1.3* are rejected when considering the thermal stratification of the lacustrine zone, since the alterations to test the relevance of the forebay and the water inflow temperature were not significant.

Density currents patterns were evaluated through the model using a tracer as a proxy (*Appendix III*), similar to the application done by Owens et al. (2014). At the intake region it was observed that density currents had a seasonal variability, with predominantly underflows over autumn and winter, coinciding with the period where re-stratification was promoted by them, while spring and summer varied between inter- and overflows (*Appendix III*). The simulated scenarios had not great differences in density current results, similar to what was observed with temperatures. Thus, *H1.2* and *H1.3* were also rejected for alterations in density current patters at the lacustrine region. Both hypotheses were expected to be retained, however it is likely that the long residence time of the study site reduce the influence of inflow/upstream characteristics and meteorological conditions were more relevant for thermal stratification at the downstream region for most of the time. And it is possible that in systems with shorter residence time density

currents along the entire reservoir have a greater influence from inflow temperatures and the presence of the forebay, which as consequence have relevance on thermal stratification.

Monthly averaged temperature profiles were smooth over depth, and marked layers of epi-, meta- and hypolimnion were not observed (***Appendix I***), which is a feature commonly found in higher latitudes (e.g. Pernica and Wells, 2012), confirming that dynamics of a same process differ from temperate to subtropical, as stated in *H1.1*. Owning to the medium depths of the reservoir and air temperatures varying in a range of 10 °C every day, the temperature profiles had large variability within 24 hours, and for this reason the averaged profiles were close to a continuous gradient (***Appendix I***). Even though, flow velocities had as main characteristic opposing flow directions in upper and lower layers, which are only possible when the water column is divided in layers of different densities (***Appendix I***). Passaúna Reservoir had stable density layers due to the larger dependency of density at warmer temperatures, the minimum observed temperature at the reservoir was of 16 °C at the bed.

In turn, flow velocities were driven by wind following a dynamic similar to the observed in standing waves (Mortimer and Horn, 1982), however they did not developed to oscillating internal seiches. Motivated by this finding, de Carvalho Bueno et al. (2022) investigated the reasons for the absence of seiches in Passaúna Reservoir. The study concluded that the continuous bottom slope and the curvature of the reservoir damped the development of the wave. Besides that, high frequency internal waves (HFIW) were observed all year round, while most studies on the subject were performed only over seasons of stable stratification (e.g. Saggio and Imberger, 1998; Antenucci and Imberger, 2001). The premise for the formation of such HFIW is the presence of layers of distinct densities (Thorpe et al., 1977), for this reason most of studies aiming in explore the phenomena focused on periods of stable stratification. Due to the warm temperatures (≥ 16 °C) of Passaúna Reservoir, stable stratification was easily formed during autumn and winter through intermittent mixings and stratifications, which was unexpected since previous studies were performed in temperate regions. The presence of HFIW in all seasons is a marked difference of the subtropical reservoir when compared to the temperate region, which is another feature confirming *H1.1*. Although observed in all seasons, the HFIW had different frequencies and amplitudes, but comparable kinetic energy (***Appendix I***).

Dissipation rates of turbulent kinetic energy (ε) were estimated from continuous measurements of vertical flow velocity in high resolution, hence, seasonal and diel patterns of ε were assessed, from 0.5 m above the bed until middle depths (***Appendix I***). Dissipation rates

were similar over seasons, and the main distinctions were observed close to the bed at the largest flow velocities intensities where ε also increased indicating the laminarization of the bottom boundary layer. And at night-time, when ε was on average one order of magnitude larger than day-time. It coincided with stronger acoustic backscatter signal from measurements of the acoustic Doppler current profiler, which is an evidence of biomixing due to the diel migration of zooplankton (Lorke et al., 2004).

The role of the turbulent mixing produced by aquatic biota is not well solved, and only a few studies were able to captured data to assess it. Simoncelli et al. (2018) did not find a significant contribution of vertically migrating zooplankton (*Daphnia magna*) to observations of turbulence in small manmade lakes, similar to results from Noss and Lorke (2014) based on laboratory observations. On the other hand, Simpson et al. (2021) estimated that ~36 % of the ε in the bottom boundary layer was driven by biogenic mixing (most likely zooplankton, although fish in the study site had the same migrating pattern). More recently Fernández Castro et al. (2022) demonstrated with observations in the ocean, that turbulence generated by a large aggregation of anchovies was comparable to geophysical mixing. Therefore, observations in Passaúna Reservoir indicated that biomixing was significant, in compliance with the recent literature. However subtropical environments potentially have other species to the ones found on temperate regions. Different organisms have distinct migrating patterns and moving mechanisms that possibly reflect on dissipation rates intensities and diel distribution. For example, the diel variations of ε presented by Simpson et al. (2021) depended on depth, while in Passaúna Reservoir ε variations within one day were consistent in all depths where measurements were performed, which also supports *H1.1*.

4.2 Longitudinal processes

According to the simulated scenarios the temperature profiles at the lacustrine region had rather minor influence from the forebay and inflow temperatures, rejecting *H1.2* and *H1.3*. However, water temperatures at the upstream region of the reservoir had significant changes in the simulated scenarios, until approximately 1.7 km from the bridge after the forebay, therefore for this region *H1.2* and *H1.3* are retained for thermal stratification. The temperature difference between surface and bottom (ΔT) increased on average 0.5 °C for scenario (i), due to the cold inflows along the bed, and scenario (ii) decrease ΔT in 0.2 °C (average calculated for ΔT in all grid cells that had a significant difference from the original simulation). Until the farthest location

from inflow where differences were significant the mean depth is 5.8 m, and for this area persistent stratification was not observed through the hydrodynamic model. Instead, thermal stratification was formed during the day and mixing occurred over nights, which fits on the classification of warm continuous polymictic. The wide diel variation of air temperature that resulted in smooth averaged temperature profiles and diel stratification of the UML in regions of larger depths, whereas in shallower locations it promoted the entire mixing of the water column over every night. Thus, the distinct mixing regimes from upstream to downstream regions supports *H2.1*.

In the same way, density currents simulated by scenarios were also significant different in upstream parts. The absence of the forebay increased underflows (scenario i), and warmer inflow temperatures brought inflows closer to the surface (overflows, in scenario ii). Both differences were observed in the same region where temperature was altered (***Appendix IV***), which complies with *H1.2* and *H1.3* also for density currents. Nevertheless, in the most upstream parts, region that could be considered the riverine zone, most of the flow path was in the form of underflows (>90% of the simulation period) for the three simulations. The river inflow temperature was consistently colder than temperatures observed inside the reservoir (***Appendix I***), hence it had larger density and formed underflows. It agrees with the theoretical description of density currents, inside the reservoir the current will pass through a dilution due to the entrainment of the surrounding water and may change the flow path (Alavian et al., 1992).

After the initial underflow, the density current in inner parts of the reservoir could follow three paths. The first was to keep moving through the bed as underflow, which mainly occurred in cold seasons when inflow had the lowest temperatures. In the second, the density current eventually detached from the bed and entered in a layer of neutral buoyance, as the reservoir increases the depth due to its constant bottom slope, thus forming an interflow. And lastly, an overflow usually was only formed after a mixing of the water column where the tracer was then carried over the surface. Vertical mixings were common at upstream regions where significant differences were observed in the simulated scenarios.

Although the influence in temperature stratification and the flow path of the density currents were minor in the lacustrine region according to the simulated scenarios, the processes occurring along the longitudinal dimension of the reservoir were essential for the dynamics of downstream regions. This was clear when simulating the reservoir with models of distinct dimensionalities (***Appendix III***). When using a 1D vertical model, considering that the reservoir

was homogeneous along horizontal layers, thermal stratification was more stable than observations due to colder temperatures at the deepest layers. The longitudinal dynamic of density currents described in the previous paragraph was disregarded by the 1 D model, and inflowing waters were placed close to the bed for most of the time (***Appendix III***). Similar to the dynamics observed with the substance transport of the 3D model at the most upstream part of the reservoir where >90 % of flow paths were underflows (***Appendix IV***). The 2D model, that disregard the transversal dimension, had results closer to the observations with comparable thermal stratification to the observations (***Appendix III)***.

Therefore, vertical mixing processes had relevant differences along the longitudinal dimension (supporting *H2.1*). And although thermal stratification in the lacustrine region did not depend on physical conditions upstream (i.e. inflow temperature and the presence forebay), the process of the longitudinal transport was relevant for it. Hence, *H2.2* is confirmed.

4.3 Relationships among hydrodynamics, nutrient delivery, and phytoplankton dynamics

Continuous measurements of chlorophyll-a (chl-a) at the monitoring platform located at the intake region did not presented marked seasonal variations (***Appendix IV***), however, peaks were observed after mixing events. Dividing the data in mixed and stratified season, with mixed season during from the first to the last mixing event of the monitored year, the mixed period had significant larger concentrations than the remaining time (***Appendix IV***). This result highlights that the phytoplankton dynamics in this region depended mainly on thermal stratification with nutrient supply from internal loadings from the sediment, supporting *H3.1*. At lacustrine zones, internal loads usually are the main source of nutrients, since nutrients from inflowing waters are consumed and/or sediment before reaching lower reaches of the reservoir (Kimmel et al., 1990).

On the other hand, upstream regions had greater influence from nutrients of inflowing waters. This was clear from the longitudinal concentrations measurements of total phosphorus and total nitrogen that had strong decays from the river to regions not much farther to the forebay (***Appendix IV***). Chl-a did not presented a continuous decay gradient from headwaters to dam, but larger concentrations were always located closer to the forebay (***Appendix IV***). The pronounced longitudinal gradients were in accordance with the descriptions of Kimmel and Groeger (1984), but the riverine, transitional, and lacustrine zones were not identified. Although other studies usually do this classification (e.g. de Oliveira et al., 2020; de Moura-Júnior et al., 2021), for

Passaúna Reservoir the comprehension of the drivers for the longitudinal gradient was more important than have clear delimitations of the zones.

It was expected that each pattern of density currents could influence on phytoplankton dynamics according to the depth where nutrients were inserted. As stated in *H3.2*, overflows were expected to enhance primary production with the delivery of nutrients at the euphotic zone, while inter- and underflows would be unfavorable for algal growth when located below the euphotic zone (Vincent et al., 1991; Cortés et al., 2014a). However, density currents did not have great impact on phytoplankton, rejecting *H3.2*. At the lacustrine region density currents had a seasonal pattern, however nutrient concentrations were low and phytoplankton depended on the remobilization of nutrients from the sediment through the mixing of the water column. And at upstream regions, where nutrients from river inflow was the main supply for primary production, density currents did not varied seasonally being mainly underflows. There were a few moments when overflows occurred through the entire reservoir, but these were isolate events. The shallow depths at the entrance of the reservoir provided an environment where the active euphotic zone was covering the entire water column (***Appendix IV***). In addition, the frequent mixing at the upstream region redistributed nutrient concentrations over depth, turning the density current type irrelevant, and seasonal variations in phytoplankton in accordance with the density currents were not observed.

With the identification of the euphotic zone reaching the bed of the reservoir in upstream regions, it was possible to identify that in that area the large concentrations of chl-a at the deepest layers were in a productive zone. Then, with the measurements over the longitudinal it was clear that the phytoplankton produced close to the inflow was being carried to downstream parts of the reservoir according to the density currents, supporting *H3.3*. Thus, it was common to observe large concentrations of chl-a at depths below the euphotic zone in areas closer to the dam (***Appendix IV***). Furthermore, the transport of phytoplankton to deep layers close to the dam resulted in the deposition of fresh organic matter in the sediment of the lacustrine region. This was confirmed by Marcon et al. (2022), where the organic matter content in the sediment was assessed for different regions of Passaúna Reservoir. According to the study, at downstream regions the organic matter content was in the range of 20-50%, while upstream it was 23%, and both locations had comparable sediment thickness.

The transport of fresh organic matter to the sediment at the lacustrine zone of the reservoir, resulted in areal hypolimnetic oxygen deficit (AHOD) rates in the same order of

magnitude of eutrophic lakes (Müller et al., 2012), although the reservoir ranges from oligo- to mesotrophic (Fonseca Xavier et al., 2017). Passaúna Reservoir had warmer water temperatures when compared to temperate lakes, which contributes to the high AHOD rates, caused by the decrease of solubility of dissolved oxygen in larger temperatures. Anoxic conditions are favorable for the remobilization of phosphate from the sediment to the water column (Søndergaard et al., 2003; Jane et al., 2021), the most available form of phosphorus for phytoplankton consumption. Passaúna Reservoir had the AHOD of 1.0 g of O_2 m^{-2} day^{-1}, therefore anoxic conditions at the hypolimnion were easily reached over thermal stratification even during the cold seasons. Hence, it is reasonable that peaks of chl-a were observed after mixing events. Moreover, the emission of greenhouse gases depend on sediment properties, therefore the patches of sediment composition induced by the transport of phytoplankton through density currents can be a relevant aspect to be considered in order to map emissions in reservoirs.

5 Conclusions

Over this thesis the assessment of the water quality of a subtropical drinking water reservoir was done through the interpretation of its hydrodynamics. High resolution measurements during a complete seasonal cycle, combined with hydrodynamic models assisted on the identification of the main processes involved, and provided insights about the interpretation of reservoirs physical processes.

The assessment of mixing and stratification processes, one of the few in such resolution, confirmed the expected mixing regime by former studies (Lewis Jr, 1983). In addition, it was observed that physical processes had contrasts in temporal dynamics between subtropical and temperate regions, confirming *H1.1*. For instance, the smooth temperature profiles due to the larger diel variation of air temperature; internal waves, where oscillating internal seiches were absent (feature that was already explored by other study), and high frequency internal waves were observed during all seasons. Further, biomixing caused diel variability on turbulence, a topic yet not much explored in general and with potential to have a relevant difference from high latitudes.

The influence of the forebay and inflow water temperature were tested (*H1.2* and *H1.3*), and based on results from the 3D hydrodynamic model both were relevant, for water temperature and density currents dynamics, until a certain extent of the reservoir. For locations far from the inflow (lacustrine zone) alterations on inflow water temperature and the removal of the forebay were not relevant. In the downstream region water temperature profile was mostly driven by meteorological conditions, and density currents in the form of underflows. The difference between the two regions indicates the presence of a longitudinal gradient on physical processes, an insight that confirms *H2.1*. Besides, the mixing regime in the shallower region of the reservoir was warm continuous polymictic, since it mixed and stratified on a daily basis. While the lacustrine zone was warm discontinuous polymictic with a marked seasonal variability. On top of that, the downstream region was not affected by alterations at the inflow but it depended on processes occurring along the longitudinal. Through the 1D hydrodynamic model it was possible to see that if the longitudinal dimension was disregarded the thermal stratification was not well reproduced, nevertheless, the same was not observed when disregarding only the transversal dimension. Thus, confirming *H2.2*, the longitudinal dimension contain relevant processes for downstream regions.

With the comprehensive understanding of the hydrodynamic processes it was possible to make links with water quality. Seasonal variations were small and only observed at downstream

regions, where larger concentrations of chl-a were driven by the supply of nutrients from sediment remobilization caused by vertical mixing, retaining *H3.1* for the lacustrine zone. Density currents had a marked seasonal variability in the region, however they were not a source of nutrients for phytoplankton. On the contrary, at upstream regions density currents were mostly underflows, the euphotic zone usually covered the entire depth which turns the flow path irrelevant, and daily vertical mixings diminished possible seasonal properties, rejecting *H3.2*. And lastly, it was confirmed that density currents transported phytoplankton to deeper layers of the reservoir (*H3.3*).

Insights regarding the management of reservoir can be derived from this thesis. For example, at the lacustrine zone algal blooms have higher chances to occur during the mixing seasons. In addition, the phytoplankton formed upstream is carried downstream by density currents and deposits in the lacustrine region, forming is a stock of nutrients for internal loading, and consuming dissolved oxygen in fast rates. The different flow paths of density currents did not affected water quality dynamics, therefore the presence of forebays or pre-dams, and alterations of stream shading in the catchment were not a harm for the water quality of the reservoir. Nevertheless, further studies in environments with shorter residence time and steeper slopes should be conducted, since these are features that could change the observed results. And it should be highlighted that the application of methods initially developed for lakes should be applied with caution to reservoirs, since the second have strong gradients not only on substance concentrations, but also on physical processes.

Lastly, the findings regarding hydrodynamics not only contributed to the comprehension of the water quality, but also to the literature of tropical and subtropical inland waters. The novel aspects presented, for instance the observed diel variability of dissipation rates, indicating a relevance of biomixing; and the high frequency internal waves, leave open questions for further research about their relevance in such systems.

References

Akomeah, E., Morales-Marın, L. A., Carr, M., Sadeghian, A., and Lindenschmidt, K. E.: The impacts of changing climate and streamflow on nutrient speciation in a large Prairie reservoir, Journal of environmental management, 288, 112262, https://doi.org/10.1016/j.jenvman.2021.112262, 2021.

Alavian, V., Jirka, G. H., Denton, R. A., Johnson, M. C., and Stefan, H. G.: Density Currents Entering Lakes and Reservoirs, Journal of Hydraulic Engineering, 118, 1464-1489, https://doi.org/10.1061/(ASCE)0733-9429(1992)118:11(1464), 1992.

Alves, T. P., and Mafra, L. L.: Diel Variations in Cell Abundance and Trophic Transfer of Diarrheic Toxins during a Massive Dinophysis Bloom in Southern Brazil, Toxins, 10, 232, 2018.

Antenucci, J. P., and Imberger, J.: On internal waves near the high-frequency limit in an enclosed basin, Journal of Geophysical Research: Oceans, 106, 22465-22474, 2001.

Brooks, B. W., Lazorchak, J. M., Howard, M. D., Johnson, M. V., Morton, S. L., Perkins, D. A., Reavie, E. D., Scott, G. I., Smith, S. A., and Steevens, J. A.: Are harmful algal blooms becoming the greatest inland water quality threat to public health and aquatic ecosystems?, Environmental toxicology and chemistry, 35, 6-13, 10.1002/etc.3220, 2016.

Chen, Y., Lin, W., Zhu, J., and Lu, S.: Numerical simulation of an algal bloom in Dianshan Lake, Chinese journal of oceanology and limnology, 34, 231-244, 2016.

Cortés, A., Fleenor, W., Wells, M., de Vicente, I., and Rueda, F.: Pathways of river water to the surface layers of stratified reservoirs, Limnology and Oceanography, 59, 233-250, https://doi.org/10.4319/lo.2014.59.1.0233, 2014a.

Cortés, A., Rueda, F., and Wells, M.: Experimental observations of the splitting of a gravity current at a density step in a stratified water body, Journal of Geophysical Research: Oceans, 119, 1038-1053, 2014b.

Cortés, A., Wells, M. G., Fringer, O. B., Arthur, R. S., and Rueda, F. J.: Numerical investigation of split flows by gravity currents into two-layered stratified water bodies, Journal of Geophysical Research: Oceans, 120, 5254-5271, https://doi.org/10.1002/2015JC010722, 2015.

Cullen, P., and Forsberg, C.: Experiences with reducing point sources of phosphorus to lakes, Hydrobiologia, 170, 321-336, 10.1007/BF00024912, 1988.

Cunha, D. G. F., Finkler, N. R., Lamparelli, M. C., Calijuri, M. d. C., Dodds, W. K., and Carlson, R. E.: Characterizing Trophic State in Tropical/Subtropical Reservoirs: Deviations among Indexes in the Lower Latitudes, Environmental Management, 68, 491-504, 10.1007/s00267-021-01521-7, 2021.

de Carvalho Bueno, R., Bleninger, T., Boehrer, B., and Lorke, A.: Physical mechanisms of internal seiche attenuation for non-ideal stratification and basin topography, Limnology and Oceanography, Submitted to:, 2022.

de Moura-Júnior, E. G., Severi, W., Kamino, L. H. Y., and de Lemos-Filho, J. P.: To what degree do spatial and limnological predictors explain the occurrence of a submerged macrophyte species in lotic and semi-lotic/lentic environments of a dammed river?, Limnology, 22, 101-110, 10.1007/s10201-020-00638-8, 2021.

de Oliveira, T. F., de Sousa Brandão, I. L., Mannaerts, C. M., Hauser-Davis, R. A., Ferreira de Oliveira, A. A., Fonseca Saraiva, A. C., de Oliveira, M. A., and Ishihara, J. H.: Using hydrodynamic and water quality variables to assess eutrophication in a tropical hydroelectric reservoir, Journal of environmental management, 256, 109932, https://doi.org/10.1016/j.jenvman.2019.109932, 2020.

Dillon, P. J., and Rigler, F. H.: The phosphorus-chlorophyll relationship in lakes1,2, Limnology and Oceanography, 19, 767-773, https://doi.org/10.4319/lo.1974.19.5.0767, 1974.

Doda, T., Ramón, C. L., Ulloa, H. N., Wüest, A., and Bouffard, D.: Seasonality of density currents induced by differential cooling, Hydrol. Earth Syst. Sci., 26, 331-353, 10.5194/hess-26-331-2022, 2022.

Ellis, I., Bates, W., Martin, S., McCrabb, G., Koehn, J., Heath, P., and Hardman, D.: How fish kills affected traditional (Baakandji) and non-traditional communities on the Lower Darling–Baaka River, Marine and Freshwater Research, 73, 259-268, https://doi.org/10.1071/MF20376, 2022.

Fernández Castro, B., Peña, M., Nogueira, E., Gilcoto, M., Broullón, E., Comesaña, A., Bouffard, D., Naveira Garabato, A. C., and Mouriño-Carballido, B.: Intense upper ocean mixing due to large aggregations of spawning fish, Nature Geoscience, 15, 287-292, 10.1038/s41561-022-00916-3, 2022.

Fonseca Xavier, C., Neiva Dias, L., and Brunkow, R. F.: Qualidade das águas dos reservatórios do estado do Paraná, IAP - Instituto Ambiental do Paraná, 219, 2017.

Forel, F. A.: Le Léman: monographie limnologique, F. Rouge, 1892.

Friedl, G., and Wüest, A.: Disrupting biogeochemical cycles-Consequences of damming, Aquatic Sciences, 64, 55-65, https://doi.org/10.1007/s00027-002-8054-0, 2002.

Gaedke, U., Schweizer, A., Beese, B., and Wieser, T.: Interannual variability of phytoplankton productivity and related parameters in Lake Constance: no response to decreased phosphorus loading?, Journal of Plankton Research - J PLANKTON RES, 13, 755-777, 10.1093/plankt/13.4.755, 1991.

Gaedke, U.: The response of the pelagic food web to re-oligotrophication of a large and deep lake (L. Constance): Evidence for scale-dependent hierarchical patterns?(with 2 figures and 2 tables), Ergebnisse der Limnologie, 53, 317-333, 1998.

Gibbs, M. M.: Influence of hypolimnetic stirring and underflow on the limnology of Lake Rotoiti, New Zealand, New Zealand Journal of Marine and Freshwater Research, 26, 453-463, 10.1080/00288330.1992.9516538, 1992.

Gibson, C. E.: Preliminary results on phosphorus reduction in Lough Neagh - Assessing the effect against a background of change, Hydrobiological Bulletin, 20, 173-182, 10.1007/BF02291161, 1986.

Griggs, D., Stafford-Smith, M., Gaffney, O., Rockström, J., Öhman, M. C., Shyamsundar, P., Steffen, W., Glaser, G., Kanie, N., and Noble, I.: Policy: Sustainable development goals for people and planet, Nature, 495, 305, 2013.

Ho, J. C., Michalak, A. M., and Pahlevan, N.: Widespread global increase in intense lake phytoplankton blooms since the 1980s, Nature, 574, 667-670, 10.1038/s41586-019-1648-7, 2019.

Imberger, J., and Hamblin, P. F.: Dynamics of Lakes, Reservoirs, and Cooling Ponds, Annual Review of Fluid Mechanics, 14, 153-187, 10.1146/annurev.fl.14.010182.001101, 1982.

Jane, S. F., Hansen, G. J. A., Kraemer, B. M., Leavitt, P. R., Mincer, J. L., North, R. L., Pilla, R. M., Stetler, J. T., Williamson, C. E., Woolway, R. I., Arvola, L., Chandra, S., DeGasperi, C. L., Diemer, L., Dunalska, J., Erina, O., Flaim, G., Grossart, H.-P., Hambright, K. D., Hein, C., Hejzlar, J., Janus, L. L., Jenny, J.-P., Jones, J. R., Knoll, L. B., Leoni, B., Mackay, E., Matsuzaki, S.-I. S., McBride, C., Müller-Navarra, D. C., Paterson, A. M., Pierson, D., Rogora, M., Rusak, J. A., Sadro, S., Saulnier-Talbot, E., Schmid, M., Sommaruga, R., Thiery, W., Verburg, P., Weathers, K. C., Weyhenmeyer, G. A., Yokota, K., and Rose, K. C.: Widespread deoxygenation of temperate lakes, Nature, 594, 66-70, 10.1038/s41586-021-03550-y, 2021.

Kimmel, B. L., and Groeger, A. W.: FACTORS CONTROLLING PRIMARY PRODUCTION IN LAKES AND RESERVOIRS: A PERSPECTIVE, Lake and Reservoir Management, 1, 277-281, 10.1080/07438148409354524, 1984.

Kimmel, B. L., Lind, O. T., and Paulson, L. J.: Reservoir primary productivity, in: Reservoir Limnology: Ecological Perspectives, John Wiley & Sons, Inc., Canada, 133-199, 1990.

Le Moal, M., Gascuel-Odoux, C., Ménesguen, A., Souchon, Y., Étrillard, C., Levain, A., Moatar, F., Pannard, A., Souchu, P., Lefebvre, A., and Pinay, G.: Eutrophication: A new wine in an old bottle?, Science of The Total Environment, 651, 1-11, https://doi.org/10.1016/j.scitotenv.2018.09.139, 2019.

Lehner, B., Liermann, C. R., Revenga, C., Vörösmarty, C., Fekete, B., Crouzet, P., Döll, P., Endejan, M., Frenken, K., and Magome, J.: High-resolution mapping of the world's reservoirs and dams for sustainable river-flow management, Frontiers in Ecology and the Environment, 9, 494-502, https://doi.org/10.1890/100125, 2011.

Lewis Jr, W. M.: A revised classification of lakes based on mixing, Canadian Journal of Fisheries and Aquatic Sciences, 40, 1779-1787, https://doi.org/10.1139/f83-207, 1983.

Lewis Jr, W. M.: Tropical lakes: how latitude makes a difference, Perspectives in tropical limnology, 4364, 1996.

Lewis Jr, W. M.: Basis for the protection and management of tropical lakes, Lakes & Reservoirs: Research & Management, 5, 35-48, 2000.

Liu, L., Liu, D., Johnson, D. M., Yi, Z., and Huang, Y.: Effects of vertical mixing on phytoplankton blooms in Xiangxi Bay of Three Gorges Reservoir: Implications for management, Water research, 46, 2121-2130, 2012.

Long, L., Ji, D., Yang, Z., Ma, J., Wells, S. A., Liu, D., and Lorke, A.: Density-driven water circulation in a typical tributary of the Three Gorges Reservoir, China, River Research and Applications, 35, 833-843, https://doi.org/10.1002/rra.3459, 2019.

Lorke, A., McGinnis, D. F., Spaak, P., and Wuest, A.: Acoustic observations of zooplankton in lakes using a Doppler current profiler, Freshwater Biology, 49, 1280-1292, 10.1111/j.1365-2427.2004.01267.x, 2004.

Maavara, T., Chen, Q., Van Meter, K., Brown, L. E., Zhang, J., Ni, J., and Zarfl, C.: River dam impacts on biogeochemical cycling, Nature Reviews Earth & Environment, 1, 103-116, 10.1038/s43017-019-0019-0, 2020.

MacIntyre, S., Sickman, J. O., Goldthwait, S. A., and Kling, G. W.: Physical pathways of nutrient supply in a small, ultraoligotrophic arctic lake during summer stratification, Limnology and Oceanography, 51, 1107-1124, 2006.

MacIntyre, S., and Melack, J.: Mixing dynamics in lakes across climatic zones, Lake ecosystem ecology: a global perspective, 86-95, 2010.

Marcon, L., Sotiri, K., Bleninger, T., Lorke, A., Männich, M., and Hilgert, S.: Acoustic Mapping of Gas Stored in Sediments of Shallow Aquatic Systems Linked to Methane Production and Ebullition Patterns, Frontiers in Environmental Science, 10, 10.3389/fenvs.2022.876540, 2022.

Marsden, M. W.: Lake restoration by reducing external phosphorus loading: the influence of sediment phosphorus release, Freshwater Biology, 21, 139-162, https://doi.org/10.1111/j.1365-2427.1989.tb01355.x, 1989.

Messager, M. L., Lehner, B., Grill, G., Nedeva, I., and Schmitt, O.: Estimating the volume and age of water stored in global lakes using a geo-statistical approach, Nature Communications, 7, 13603, 10.1038/ncomms13603, 2016.

Mortimer, C. H., and Horn, W.: Internal wave dynamics and their implications for plankton biology in the Lake of Zurich, Vier. Natur. Gesell. Zurich, 127, 299-318, 1982.

Müller, B., Bryant, L. D., Matzinger, A., and Wüest, A.: Hypolimnetic Oxygen Depletion in Eutrophic Lakes, Environmental science & technology, 46, 9964-9971, 10.1021/es301422r, 2012.

Mulligan, M., van Soesbergen, A., and Sáenz, L.: GOODD, a global dataset of more than 38,000 georeferenced dams, Scientific data, 7, 31, 10.1038/s41597-020-0362-5, 2020.

Nazari-Sharabian, M., Ahmad, S., and Karakouzian, M.: Climate change and eutrophication: a short review, Engineering, Technology and Applied Science Research, 8, 3668, 2018.

Noss, C., and Lorke, A.: Direct observation of biomixing by vertically migrating zooplankton, Limnology and Oceanography, 59, 724-732, 2014.

Owens, E. M., Effler, S. W., O'Donnell, D. M., and Matthews, D. A.: Modeling the Fate and Transport of Plunging Inflows to Onondaga Lake, JAWRA Journal of the American Water Resources Association, 50, 205-218, https://doi.org/10.1111/jawr.12130, 2014.

Paerl, H. W., and Otten, T. G.: Harmful cyanobacterial blooms: causes, consequences, and controls, Microbial ecology, 65, 995-1010, 10.1007/s00248-012-0159-y, 2013.

Pernica, P., and Wells, M.: Frequency of episodic stratification in the near surface of Lake Opeongo and other small lakes, Water Quality Research Journal of Canada, 47, 227, 10.2166/wqrjc.2012.001, 2012.

Pretty, J. N., Mason, C. F., Nedwell, D. B., Hine, R. E., Leaf, S., and Dils, R.: Environmental costs of freshwater eutrophication in England and Wales, Environmental science & technology, 37, 201 - 208, https://doi.org/10.1021/es020793k, 2003.

Rao, Y. R., Milne, J. E., and Marvin, C. H.: Hydrodynamics and water quality in western Lake Ontario, Journal of Great Lakes Research, 38, 91-98, 10.1016/j.jglr.2012.04.001, 2012.

Roberts, V. A., Vigar, M., Backer, L., Veytsel, G. E., Hilborn, E. D., Hamelin, E. I., Vanden Esschert, K. L., Lively, J. Y., Cope, J. R., Hlavsa, M. C., and Yoder, J. S.: Surveillance for Harmful Algal Bloom Events and Associated Human and Animal Illnesses - One Health Harmful Algal Bloom System, United States, 2016-2018, MMWR Morb Mortal Wkly Rep, 69, 1889-1894, 10.15585/mmwr.mm6950a2, 2020.

Rosentreter, J. A., Borges, A. V., Deemer, B. R., Holgerson, M. A., Liu, S., Song, C., Melack, J., Raymond, P. A., Duarte, C. M., Allen, G. H., Olefeldt, D., Poulter, B., Battin, T. I., and Eyre, B. D.: Half of global methane emissions come from highly variable aquatic ecosystem sources, Nature Geoscience, 14, 225-230, 10.1038/s41561-021-00715-2, 2021.

Rueda, F. J., Fleenor, W. E., and de Vicente, I.: Pathways of river nutrients towards the euphotic zone in a deep-reservoir of small size: uncertainty analysis, Ecological modelling, 202, 345-361, https://doi.org/10.1016/j.ecolmodel.2006.11.006, 2007.

Rueda, F. J., and MacIntyre, S.: Flow paths and spatial heterogeneity of stream inflows in a small multibasin lake, Limnology and Oceanography, 54, 2041-2057, https://doi.org/10.4319/lo.2009.54.6.2041, 2009.

Rueda, F. J., and MacIntyre, S.: Modelling the fate and transport of negatively buoyant storm–river water in small multi-basin lakes, Environmental Modelling & Software, 25, 146-157, https://doi.org/10.1016/j.envsoft.2009.07.002, 2010.

Saggio, A., and Imberger, J.: Internal wave weather in a stratified lake, Limnology and oceanography, 43, 1780-1795, 1998.

Schindler, D. W.: Recent advances in the understanding and management of eutrophication, Limnology and oceanography, 51, 356-363, 2006.

Simoncelli, S., Thackeray, S. J., and Wain, D. J.: On biogenic turbulence production and mixing from vertically migrating zooplankton in lakes, Aquatic Sciences, 80, 10.1007/s00027-018-0586-z, 2018.

Simpson, J. H., Woolway, R. I., Scannell, B., Austin, M. J., Powell, B., and Maberly, S. C.: The Annual Cycle of Energy Input, Modal Excitation and Physical Plus Biogenic Turbulent Dissipation in a Temperate Lake, Water Resources Research, 57, e2020WR029441, https://doi.org/10.1029/2020WR029441, 2021.

Søndergaard, M., Jensen, J., and Jeppesen, E.: Role of sediment and internal loading of phosphorus in shallow lakes, Hydrobiologia, 506-509, 135-145, https://doi.org/10.1023/B:HYDR.0000008611.12704.dd, 2003.

Sotiri, K., Hilgert, S., and Fuchs, S.: Sediment classification in a Brazilian reservoir: Pros and cons of parametric low frequencies, Advances in Oceanography and Limnology, 10, https://doi.org/10.4081/aiol.2019.7953, 2019.

Thorpe, S., Hall, A., Taylor, C., and Allen, J.: Billows in Loch Ness, Deep Sea Research, 24, 371-IN373, 1977.

Vincent, W. F., Gibbs, M. M., and Spigel, R. H.: Eutrophication processes regulated by a plunging river inflow, Hydrobiologia, 226, 51-63, 10.1007/BF00007779, 1991.

Walker Jr, W. W.: Significance of eutrophication in water supply reservoirs, Journal-American Water Works Association, 75, 38-42, https://doi.org/10.1002/j.1551-8833.1983.tb05056.x, 1983.

Weber, M., Rinke, K., Hipsey, M. R., and Boehrer, B.: Optimizing withdrawal from drinking water reservoirs to reduce downstream temperature pollution and reservoir hypoxia, Journal of environmental management, 197, 96-105, https://doi.org/10.1016/j.jenvman.2017.03.020, 2017.

Weirich, C. A., and Miller, T. R.: Freshwater harmful algal blooms: toxins and children's health, Current problems in pediatric and adolescent health care, 44, 2-24, 10.1016/j.cppeds.2013.10.007, 2014.

Wetzel, R. G.: Limnology: Lake and River Ecosystems, Academic Press, Gulf Professional Publishing, 2001.

Winton, R. S., Calamita, E., and Wehrli, B.: Reviews and syntheses: Dams, water quality and tropical reservoir stratification, Biogeosciences, 16, 1657-1671, https://doi.org/10.5194/bg-16-1657-2019, 2019.

Xing, Z., Fong, D. A., Yat-Man Lo, E., and Monismith, S. G.: Thermal structure and variability of a shallow tropical reservoir, Limnology and Oceanography, 59, 115-128, 2014.

Xu, H., Yan, M., Long, L., Ma, J., Ji, D., Liu, D., and Yang, Z.: Modeling the Effects of Hydrodynamics on Thermal Stratification and Algal Blooms in the Xiangxi Bay of Three Gorges

Reservoir, Frontiers in Ecology and Evolution, 8, https://doi.org/10.3389/fevo.2020.610622, 2021.

Yasarer, L. M. W., and Sturm, B. S. M.: Potential impacts of climate change on reservoir services and management approaches, Lake and Reservoir Management, 32, 13-26, 10.1080/10402381.2015.1107665, 2016.

Zarfl, C., Lumsdon, A. E., Berlekamp, J., Tydecks, L., and Tockner, K.: A global boom in hydropower dam construction, Aquatic Sciences, 77, 161-170, https://doi.org/10.1007/s00027-014-0377-0, 2014.

Author contributions

This thesis is based on four original research articles provided in Appendix I - IV which were conceived by all of the authors. I am the lead author of all articles. The contributions of all authors are explained in the following:

Hydrodynamics and mixing mechanisms in a subtropical reservoir

Mayra Ishikawa, Tobias Bleninger, and Andreas Lorke

Designing of the research: AL, TB, MI
Performing the research (field work): MI, TB
Data analysis: MI, AL
Writing the manuscript: MI, AL, TB

The effect of stream shading on the inflow characteristics in a downstream reservoir

Mayra Ishikawa, Ingo Haag, Julia Krumm, Katharina Teltscher, and Andreas Lorke

Designing of the research: AL, IH, JK
Performing the research (field work): MI
Data analysis / LARSIM-WT modeling: KT, JK, IH
Data analysis of density currents: MI
Writing the manuscript: MI, AL, IH, JK, KT

Effects of dimensionality on the performance of hydrodynamic models for stratified lakes and reservoirs

Mayra Ishikawa, Wendy Gonzalez, Orides Golyjeswski, Gabriela Sales, J. Andreza Rigotti, Tobias Bleninger, Michael Mannich, and Andreas Lorke

Conceptualization, application of Delft3D, formal analysis, and investigation: MI
Set up of Delft3D, adjustment of grids, bathymetry, and analysis of water balance: WG
First set up of Delft3D and application of CE-QUAL-W2: OG
Application of GLM: GS and J.AR
Supervision of GS and OG master thesis, advisor in all models and concepts: TB
Co-supervision of GS, and advisor for the ms concept: MM
Supervision of MI PhD thesis, advisor for the ms concept: AL
Writing – original draft preparation: MI, WG, J.AR, GS, and OG.
Writing – review & editing: AL, TB, and MM.

Hydrodynamic drivers of nutrient and phytoplankton dynamics in a subtropical reservoir

Mayra Ishikawa, Luziadne Gurski, Tobias Bleninger, Harald Rohr, Nils Wolf, and Andreas Lorke

Conceptualization: MI, AL, LG and TB
Field campaigns: MI, LG, HR, and TB

Laboratorial analysis: LG
Validation of sensor's data: HR, LG and MI
Formal analysis: MI and LG
Remote sensing images acquisition, processing and validation: NW
Writing – original draft preparation: MI and LG
Writing – review and editing: AL, TB, NW and HR
Supervision: AL and TB

Declaration

I hereby declare that the thesis entitled "*Fate of nutrients in a subtropical reservoir according to hydrodynamic processes and its effects on phytoplankton dynamics*" is the result of my own work except where otherwise indicated. It has not been submitted for any other degree at another university or scientific institution.

Landau, 30 May 2022

Mayra Ishikawa

Curriculum Vitae

Mayra Matsume Ishikawa

Date of birth	26 Aug 1990
Place of birth	Curitiba
Nationality	Brazilian
E-mail	mayraishikawa@gmail.com

Background

Aug 2017 – May 2018	PhD student, Institute for Environmental Sciences, University of Koblenz-Landau, Germany *"Fate of nutrients in a subtropical reservoir according to hydrodynamic processes and its effects on phytoplankton dynamics"*
Mar 2014 – Mar 2016	Master in Water Resources and Environmental Engineering, Graduate Program of Water Resources and Environmental Engineering (PPGERHA), Federal University of Paraná (UFPR) *"Methodology to classify and visualize time-series simulations using dilution contour maps"*
Aug 2009 – Dec 2013	Bachelor in Environmental *Engineering*, Federal University of Paraná (UFPR) *"Application of Cormix model in time series to analyze the performance of submarine outfalls"*

Acknowledgments

I would like to start thanking my supervisor Andreas Lorke, for the time invested on me so this thesis could be completed. Over this path I was able to learn from him not only about turbulence, internal waves, and how an ADCP works, but also on how to conduct research with excellence. I am sure that these are skills that will help me for a lifetime. And Tobias Bleninger with whom I gave my first steps into the research field, and kept being around to assist me whenever I needed. Thank you for always show me the bright side of my results, and realize that outliers are beautiful.

Secondly, I am thankful for all other people that were somehow involved in my thesis. The co-authors of the four published articles. For me it was a challenge to work with so many people at the same time, but the effort paid off. Receiving the feedback of professionals in different fields was an excellent exercise to keep an open mind to listen to other points of view, and be aware of particularities that would never cross my mind. Clara Mendonza-Lera, Cristovão Fernandes, Michael Mannich and Stephan Hilgert, thank you for proofreading my thesis and giving me valuable comments to improve it. And all the team from MuDak-WRM project, the Graduate Program in Water Resources and Environmental Engineering of the Federal University of Paraná, and the Environmental Physics Group of the University of Koblenz-Landau. A special thanks to Christoph Bohrs who helped me to carry so many equipments to cross the Atlantic.

Then, I am glad that my PhD journey was surrounded by such amazing persons trilling the same path so we could share experiences, frustrations, and motivate each other. Eliana Bohórquez Bedoya, Gerrit Rau, Lediane Marcon, Lianghong Long, Liege Wosiacki, Luziadne Gurski, and Sofya Guseva, thank you for being good friends, listening to my nonending list of complains, and always being ready to discuss any silly or big questions. And Echo (Ka yee) Kowalski and Fernanda Rocha, thank you for remind me from time to time that life exists besides the PhD. I also own a thanks to my family for comprehending my path, and althoug the distance being present over the whole process. And lastly, I thank Danny Thiessen for joining me in this journey and for supporting me in all possible aspects.

Appendices

Appendix I

This is an 'Accepted/Original Manuscript' of an article published by Taylor & Francis Group in Inland Waters on 16 Aug 2021, available online: https://wwww.tandfonline.com/10.1080/20442041.2021.1932391

Hydrodynamics and mixing mechanisms in a subtropical reservoir

Mayra Ishikawa[1], Tobias Bleninger[2], and Andreas Lorke[1]

[1] *Institute for Environmental Sciences, University of Koblenz-Landau, Landau, Germany*

[2] *Graduate Program in Water Resources and Environmental Engineering, Federal University of Paraná, Curitiba, Brazil*

Abstract

With the aim to improve current knowledge on physical processes in tropical and subtropical reservoirs, we explore the dynamics of prevailing hydrodynamic processes in a small to medium-size reservoir based on one-year continuous measurements of temperature, flow velocity and turbulence. The mixing regime of the reservoir is characterized as warm polymictic and extended periods of comparably strong density stratification were observed during all seasons, interrupted by several mixing periods between autumn and winter. The stratification was affected by lateral, density-driven flows from the main river inflow. A forebay through which the river enters the reservoir influenced the density currents and reduced the occurrence of underflows. Flow velocities in the middle of the reservoir were generally small and higher velocities (currents >3.5 cm s^{-1}) were driven by wind. These currents were more frequent during stratified than during mixed periods. No basin-scale internal waves (seiches) were observed, but propagating, high-frequency internal waves with periods between 2 and 17 min were present at all seasons. Dissipation rates of turbulent kinetic energy were generally small (10^{-10} – 10^{-9} W kg^{-1}). Wind-driven currents were associated with enhanced dissipation rates at the bottom-boundary layer, but represented only 10% of the total monitored period. We identified several aspects, in which the observed hydrodynamics of the reservoir differed from that of more commonly studied temperate aquatic systems. We expect that our findings are representative for a large number of small to medium sized lakes and for a growing number of reservoirs located in the tropical and subtropical zone.

Keywords: forebay, density currents, subtropical reservoir, physical limnology

Introduction

Reservoirs have been constructed for diverse purposes including hydropower production, flood control and water storage for drinking water production and irrigation (Lehner et al. 2011). During the last two decades, their number as well as plans for, and construction of, new reservoirs has been strongly increasing, with tropical regions, including Southeast Asia, South America and Africa being hotspots of dam construction (Zarfl et al. 2014; Best 2019). Despite the socioeconomic benefits that reservoirs provide, they disrupt the natural course of substances by trapping large amounts of sediments, organic matter, nutrients and pollutants (Friedl and Wüest 2002; Vörösmarty et al. 2003; Mendonça et al. 2017). Consequently, existing reservoirs suffer from continuous reduction in storage volume (Wisser et al. 2013), poor water quality and harmful

algae blooms (Winton et al. 2019), and are a globally significant source of the greenhouse gas methane (Deemer et al. 2016). A profound understanding of the processes that control these adverse effects of reservoir construction is urgently required to identify and to implement potential mitigation measures during design and operation of existing and future reservoirs.

The fate of particulate and dissolved substances entering reservoirs with river inflow depends on flow velocity, density stratification, turbulent mixing and other hydrodynamic processes in the reservoirs. Two physical quantities are of paramount importance, the distribution of the rate of dissipation of turbulent kinetic energy and the path along which water and particles travel (Imberger 1998). River inflows, rich in nutrients and organic matter, can enter the reservoir as underflows, favoring the deposition of particles on the bed, or as overflows, delivering nutrients to the photic zone and thus promote phytoplankton growth (Rueda et al. 2007; Cortés et al. 2014). The lack of deep-water renewal by underflows and weak vertical mixing promote the formation of hypoxic or anoxic conditions in deeper layers of stratified reservoirs (Fer et al. 2002; Yoshimizu et al. 2010; Lemmin 2020). Oxygen depletion triggers the formation of toxic substances, such as hydrogen sulfide, causes enhanced release of phosphorus and promotes the production and potential emission of the greenhouse gases methane and nitrous oxide (Friedl and Wüest 2002; Bastviken et al. 2004; Baulch et al. 2011).

Besides density currents formed by inflowing water, the main energy sources inducing currents and vertical mixing in reservoirs are wind and convection (Imberger and Hamblin 1982; Wüest and Lorke 2003). Convective mixing mainly occurs when air temperature falls below water surface temperature and plays a major role in the seasonal mixing dynamics. Wind energizes mixing in the surface layer and induces flows that can cause tilting of density gradients and internal waves. Processes driven by wind and convection contain most of the kinetic energy in small and medium-sized stratified lakes and reservoirs (Woolway and Simpson 2017), for larger water bodies, circulation patterns are more relevant (Imberger 1998).

Although physical processes in reservoirs have been studied and conceptualized comprehensively (Imberger and Hamblin 1982; Stevens 1999; Cortés et al. 2014), most existing studies were based in temperate regions. Similar to a general bias in limnological studies towards mid/high latitudes (Lewis Jr 1987; Winton et al. 2019), field observations of reservoir hydrodynamics in tropical and subtropical regions, where dam building is now concentrated, are sparse. Comprehension of reservoir hydrodynamics is essential for successful mitigation of

adverse effects of reservoir construction, for achieving good water quality and drinking water safety, as well as for predicting future changes.

The objective of this study is to contribute to the understanding of prevalent hydrodynamic processes and main drivers of density stratification in small to medium-size subtropical reservoirs. We analyze continuous measurements of temperature, flow velocity and turbulence over a complete seasonal cycle in a drinking water reservoir located in South Brazil. The analysis includes diel to seasonal dynamics of stratification and flow paths of inflowing water, typical patterns of wind-generated currents and internal wave motion, as well as the vertical distribution of dissipation rates of turbulent kinetic energy. We relate these patterns to existing concepts for describing hydrodynamic process and emphasize differences to more widely studied temperate lakes and reservoirs.

Study Site

Passaúna Reservoir is a valley-shaped drinking water reservoir. It has a surface area of 9 km^2, a volume of approximately 60×10^6 m^3, it is 11 km long and has a maximum depth of 15 m (Carneiro et al. 2016). With a production rate of approximately 1.8 m^3 s^{-1}, it provides the water supply for 650,000 inhabitants of the western region of Curitiba and three neighbouring cities (SANEPAR 2013). The Passaúna River enters the reservoir at the northern end through a forebay, which has a geometrical constriction due to the embankment of a bridge (Ferraria Bridge). This region of approximately 0.28 km^2 area and an average depth of 1 m is called the Buffer, as it attenuates variations of the river inflow. The intake tower of the treatment facility is located close to the reservoir bank and water is abstracted near the surface. The reservoir outflows are a spillway and a bottom outlet at the dam (Figure).

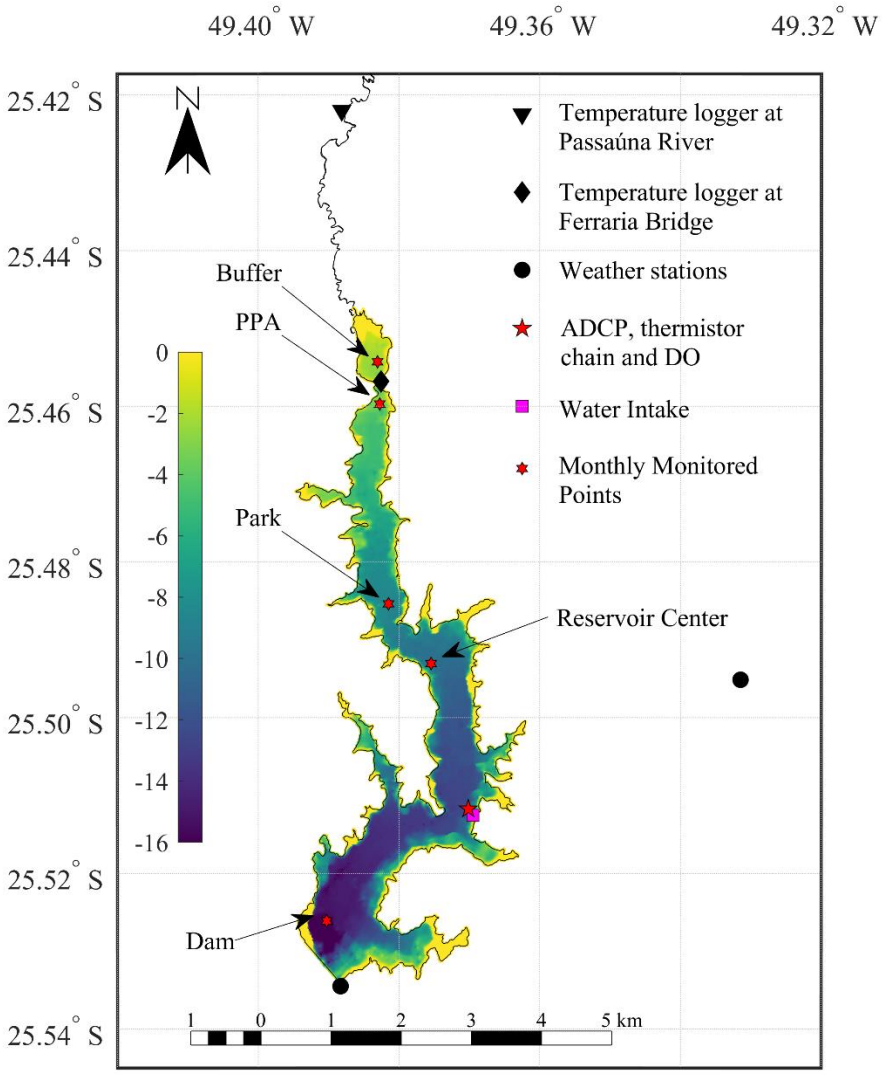

Figure 1: Bathymetric map of Passaúna Reservoir with colors representing water depth in meter (Sotiri et al. 2019). Passaúna River enters the reservoir in the North through a shallow forebay (Buffer). The intake location of the water treatment plant and the locations of monitoring and weather stations are marked by symbols.

According to the Environmental Protection Agency of Paraná (Fonseca Xavier et al. 2017), the reservoir is classified as oligotrophic to moderately degraded, based on monitoring data from 1999 to 2013.

Methods

Data collection and processing

The measurements for this study were made between February 2018 and February 2019. The locations of the sampling sites are marked on the map shown in Figure .

Temperature – Inflow temperature in Passaúna River was recorded by a combined temperature oxygen sensor (miniDOT, Precision Measurement Engineering, Inc) at a sampling interval of 15 min, accuracy of ± 0.1 °C and resolution of 0.01 °C. At the boundary between the Buffer region and the main reservoir (Ferraria Bridge) water temperature was measured by a thermistor logger (Minilog-II-T, Vemco) with a sampling interval of 1 min, precision of ± 0.1ºC and 0.01ºC resolution. This logger was lost and its last record was on 12 Aug 2018. Eleven temperature loggers of the same type were deployed as a vertical chain nearby the intake station, at a mean water depth of 12 m. The vertical spacing of the loggers was 1 m starting with the first logger at 1 m above the bed. The chain was deployed with a subsurface up-drift buoy located 11 m above the bed. Therefore, the thermistors measured at fixed distances above the bottom when the water level was larger than 11 m, and at fixed distances below the surface at lower water levels. Additional temperature profiles were measured at monthly intervals at five locations along the main axis of the reservoir (Figure) with a CTD (Conductivity-Temperature-Depth profiler, Sontek Cast-Away). Sampling took place in February, April, May, June, August, November and December 2018, and in February 2019.

Dissolved oxygen concentration – In addition to the oxygen sensor in the Passaúna River, two optical oxygen sensors (miniDOT, Precision Measurement Engineering, Inc) were deployed together with the second-lowest thermistor (2 m above the bed) and with the uppermost thermistor (between the water surface and around 1 m depth, depending on water level). They measured at a sampling interval of 5 min, with a resolution of 0.01 mg L^{-1} and an accuracy of ± 0.3 mg L^{-1}. The sensors were cleaned during the monthly sampling campaigns.

Flow velocity - Nearby the thermistor chain (< 50 m distance), an upward-looking acoustic Doppler current profiler (ADCP Signature 1000, Nortek AS) was deployed at the bottom of the reservoir (approximately 12 m water depth). The instrument configuration was modified during the sampling period to improve the data quality and to have better usage of batteries according to the maintenance schedule (deployment configurations are summarized in Table SI 1). All types of measurement started around 0.60 m above the bed, including frame height and the blanking distance above the instrument. Vertical profiles of the mean three-dimensional flow velocity were measured along four inclined beams up to a depth of 1.5 m below the water surface and with spatial and temporal resolution of 0.5 m and 5 or 10 min, respectively. High-resolution profiles of the vertical flow velocity, including turbulent velocity fluctuations, were measured along a vertically oriented beam. The maximum range of these measurements varied between 5.62 and

8.20 m above the bed, with a vertical resolution of 2 to 4 cm and a sampling frequency of 1 or 4 Hz (Table SI 1).

In addition to flow velocity, the ADCP recorded profiles of acoustic echo intensity along its vertical beam. The measurements were made using the instrument's echo sounder mode and resolved the entire water column with a vertical resolution of 1.2 cm and a sampling frequency of 1or 4 Hz.

Initial ADCP data processing was conducted using a commercial software provided by the manufacturer (Ocean Contour, Nortek AS). The velocity processing included bin mapping, removal of unreliable data near the water surface (side lobe interference), thresholds for minimum signal correlation as well as for minimum and maximum signal amplitudes. Echo amplitude was converted into volume backscatter strength using corrections for speed of sound and the two-way transmission loss along the beam. In addition to quality screening, spike removal was applied to the high resolution data of vertical velocities using the method of Goring and Nikora (2002) with adaptions following the suggestions of Wahl (2003).

Reservoir operation and water level - From the built-in pressure sensor of the ADCP, the water level was derived by assuming a constant density of water, and by taking ADCP frame height into account. Water abstraction rates at the intake station, as well as water level and volumetric outflows at the dam (spillway and bottom outlet) were provided by the reservoir operator (SANEPAR, Sanitation Company of Paraná).

Meteorological conditions – We used measurements of air temperature, wind speed, shortwave radiation, humidity and air pressure from two different weather stations. For the period February to May 2018 we used data from the Solarimetric station operated within the Smart Energy project at the Technology Institute of Paraná (TECPAR), which is located 4 km east of the reservoir. Measurements were recorded with a temporal resolution of 1 min, which we subsequently averaged over 10 min. In May 2018, SANEPAR installed a weather station directly at the dam and its data was used instead of the TECPAR station, as it is closer to the reservoir. The dam station provided data in 10 min intervals.

Surface heat balance – Estimations were made following Imboden and Wüest (1995):

$$S = SW_{net} + LW_{in} - LW_{out} - E + H \quad (1)$$

where S is the surface heat flux, SW_{net} is the net shortwave radiation, LW_{in} is the incoming longwave radiation from the atmosphere, LW_{out} is the outgoing longwave radiation from the water surface, E is the latent heat flux and H is the sensible heat flux, all fluxes in W m^{-2}.

Mixing and stratification indices – Buoyancy frequency (N), Schmidt Stability (S_T), Lake number (L_N), thermocline depth and Upper Mixed Layer (UML) thickness were calculated, using Lake Analyzer (Read et al. 2011).

The mixed layer Richardson number (Ri_{UML}) was computed using equation 2:

$$Ri_{UML} = \frac{g' z_e}{u_*^2} \quad (2)$$

g' (m s^{-2}) is the reduced gravity due to density differences, $g' = -g(\rho_h - \rho_e/\rho_h)$ where ρ_h and ρ_e are the water densities (kg m^{-3}) in the hypolimnion and in the epilimnion, respectively. z_e (m) is the UML depth and u_* (m s^{-1}) is water friction velocity due to wind stress.

To analyze the stability of shear flows in high-frequency internal wave motions, the gradient Richardson number (Ri_{grad}) was calculated at a temporal resolution of 5 min:

$$Ri_{grad} = \frac{N^2}{(\partial u/\partial z)^2 + (\partial v/\partial z)^2} \quad (3)$$

where u is the longitudinal and v is the transversal horizontal velocity in (m s^{-1}), corresponding to the North and East velocity components.

Classification of thermal stratification – To account for seasonal changes of hydrodynamic processes, we compared statistical properties of measured and estimated parameters according to the thermal regime, which we classified as mixed or stratified. As there is no standard method for this classification, we tested threshold methods for several parameters. For our data, the most suitable was the daily averaged Schmidt Stability, calculated with the data from the thermistor chain. We chose a threshold of 10% of the maximum value of the daily averaged Schmidt stability to distinguish between mixed and stratified conditions, i.e. days with S_T lower than 16.2 J m^{-2} were considered as mixed, or otherwise stratified. A threshold in Schmidt stability was chosen instead of the temperature difference between surface and bottom as its performance for classifying mixed and stratified periods provided the best agreement with observed differences in oxygen concentration between surface and bottom water. Stratified periods coincided with large (> 1.6 mg L^{-1}) differences in oxygen concentrations. Right after or before a mixing event, oxygen differences were more variable with standard deviations around 1.8 mg L^{-1} for bin classes of S_T of 10 J m^{-2}, while at higher thermal stability, the standard deviation was lower than 1 mg L^{-1} (Figure SI 1). According to this classification, weak thermal stratification can persist also during the mixed periods.

Dissipation rates - Dissipation rates of turbulent kinetic energy (ε) were estimated from high-resolution profiles of vertical velocity fluctuations using the structure function method (Wiles et al. 2006; Guerra and Thomson 2017). The maximum along-beam distance over which the structure function was applied was chosen as the integral length scale of turbulent eddies. The integral length scale was obtained as the product of the integral time scale and the mean horizontal velocity calculated for each 10 min interval. The integral time scale of turbulence was determined by numerical integration of the velocity autocorrelation function from zero lag up to the lag distance at which the autocorrelation becomes zero or negative (Kundu and Cohen 2010). The temporal resolution of the dissipation rate estimates was 10 min. Fitting results with negative coefficients and with decreasing velocity variance for increasing separation distance were discarded. The first deployment configuration of the ADCP (from 23 Feb 2018 until 15 Mar 2018) was not favorable for resolving turbulent velocity fluctuations and many dissipation rate estimates had to be rejected. Therefore, we excluded the dissipation rates from this deployment.

High frequency internal waves – Amplitudes of high-frequency internal waves were characterized using band-pass filtered vertical velocity time series (high-resolution vertical velocities). Filter cut-off frequencies were chosen corresponding to periods of 1.5 and 18 min, respectively. Wave amplitudes were calculated as root-mean-square fluctuations of the filtered vertical velocities for 1 h periods and for each vertical measurement location. For further investigation, wave events were chosen through visual inspection of the vertical velocity time series, and selected when they included at least five consecutive wave cycles with peak values exceeding ± 0.5 cm s^{-1}. We analyzed 20 wave events during the mixed period and 45 events during stratification (Table SI 2 and Table SI 3). The kinetic energy of the waves was estimated as the integral of the log averaged velocity spectra of each wave event between 5×10^{-4} to 5×10^{-3} Hz during mixed and 1×10^{-3} to 1×10^{-2} Hz during stratified conditions; these ranges comprehend the observed wave peaks.

Results

Meteorological and hydrological forcing

Monthly mean air temperature varied between 14.2 ± 4.5 °C (mean ± standard deviation) in August 2018 and 23.7 ± 3.7 °C in January 2019. Typical amplitudes of diel air temperature variations were 10 °C throughout the entire year, except for periods of strong decline of air temperature (e.g., middle of April, beginning of August and October, and February 2019 - Figure 2). Monthly averaged wind speed showed no pronounced seasonal pattern and varied from 1.3

± 0.7 m s^{-1} in January 2019 to 2.0 ± 0.9 m s^{-1} in November 2018. Major wind speeds exceeding 8 m s^{-1} occurred in June and in August (Figure 2). The water level in the reservoir varied by less than 1.5 m throughout the year with a maximum level at the beginning of March, when the water depth at the monitoring station was 12.4 m. From April to January, the water level decreased to 10.9 m in January 2019. There was no spillway overflow after May 2018, but the intake kept a mean abstraction rate of 1.7 ± 0.3 $m^3 s^{-1}$. The discharge of the main inflow (Passaúna River) was 1.8 ± 1.4 $m^3 s^{-1}$ on average. The averaged hydraulic residence time during the monitoring period was 325 days.

Thermal Stratification

Water temperature near the intake station followed closely the seasonal cycle of air temperature with maximum monthly mean temperatures of 27.5 ± 1.3 °C at the surface and 21.9 ± 0.2 °C at the bottom in February 2019. Minimum values of water temperature were observed in August 2018, 17.2 ± 0.6 and 16.5 ± 0.2 °C, at surface and bottom, respectively (Figure 2c).

The average Schmidt stability was 47 J m^{-2}, but it varied tenfold throughout the year, with a minimum monthly averaged value in June 2018 (9.5 ± 9.3 J m^{-2}) and a maximum of 122.8 ± 18.5 J m^{-2} in January 2019 (Figure 2d). Based on our threshold, 95 out of 343 days were classified as mixed (S_T < 16.2 J m^{-2}). The reservoir was continuously stratified before April and after October 2018, while alternating periods of mixed and stratified conditions occurred during autumn and winter (Figure 2).

The break-up of thermal stratification was mainly promoted by negative surface heat fluxes (heat loss from the water), in combination with wind speeds above the average (Figure 2b). The first mixing event in the middle of April marked the beginning of the mixed season, when frequent mixing events took place, though there were intermittent periods of weak stratification throughout this period. During the mixed season, thermal stratification was re-established due to positive surface heat flux, but in some cases also due to decreasing water temperature at the bottom of the reservoir. Cooling of the bottom water is an indication of the presence of lateral, density-driven currents. For example on 21 Apr 2018, approximately three days after the first autumn overturn (Figure SI 2), the water temperature measured at the reservoir entrance (Ferraria Bridge) was up to 3 °C lower than the water temperature measured by the thermistor chain at the bottom of the reservoir. Within five subsequent days of bottom-water cooling, the Schmidt stability increased from 8.4 J m^{-2} (mixed) to 30 J m^{-2} (stratified). Without cooling at the

reservoir bottom, the Schmidt stability would have increased to 23 J m^{-2} during the same period, due to warming of the upper part of the water column.

Thermal stratification is closely linked to vertical gradients in concentrations of dissolved substances. Measured dissolved oxygen concentration in the bottom water and its temporal dynamics differed between periods classified as mixed and as stratified. During stratified conditions, the average oxygen concentration at the bottom of the reservoir was 1.7 ± 1.9 mg L^{-1}, which is in the range of hypoxia. During mixed periods, the bottom concentration was on average 5.3 ± 1.7 mg L^{-1}. During stratification, the oxygen concentration consistently decreased at an average rate of 0.3 mg L^{-1} day^{-1}. Each transition from stratified to mixed conditions was accompanied by a sudden increase in oxygen concentration at the bottom (Figure 2d).

The Lake Number describes the dynamic response of stratified water bodies to wind forcing. Approaching periods classified as mixed, L_N fell to values close to unity, indicating that wind forcing could easily promote a complete vertical mixing. Throughout the mixed period L_N was always < 5 and commonly < 1. Although L_N is undefined in the absence of stratification, it is presented for the whole period since weak stratification was observed during the mixed periods (with temperature differences between surface and bottom lower than 1.1°C and maximum S_T of 14.1 J m^{-2}). During summer, the stratification was strong, thus L_N was consistently higher than 10 and most stable conditions were observed in January 2019. On average, L_N was 11.9 ± 15.3 during stratified conditions. During strong wind events in October and November, L_N occasionally dropped to values near unity (Figure 2). Although these periods were classified as stratified, dissolved oxygen concentration at the bottom increased during these events. Nevertheless, persistent differences between oxygen concentration at the bottom and the surface during these events suggest that the water column was only partially mixed.

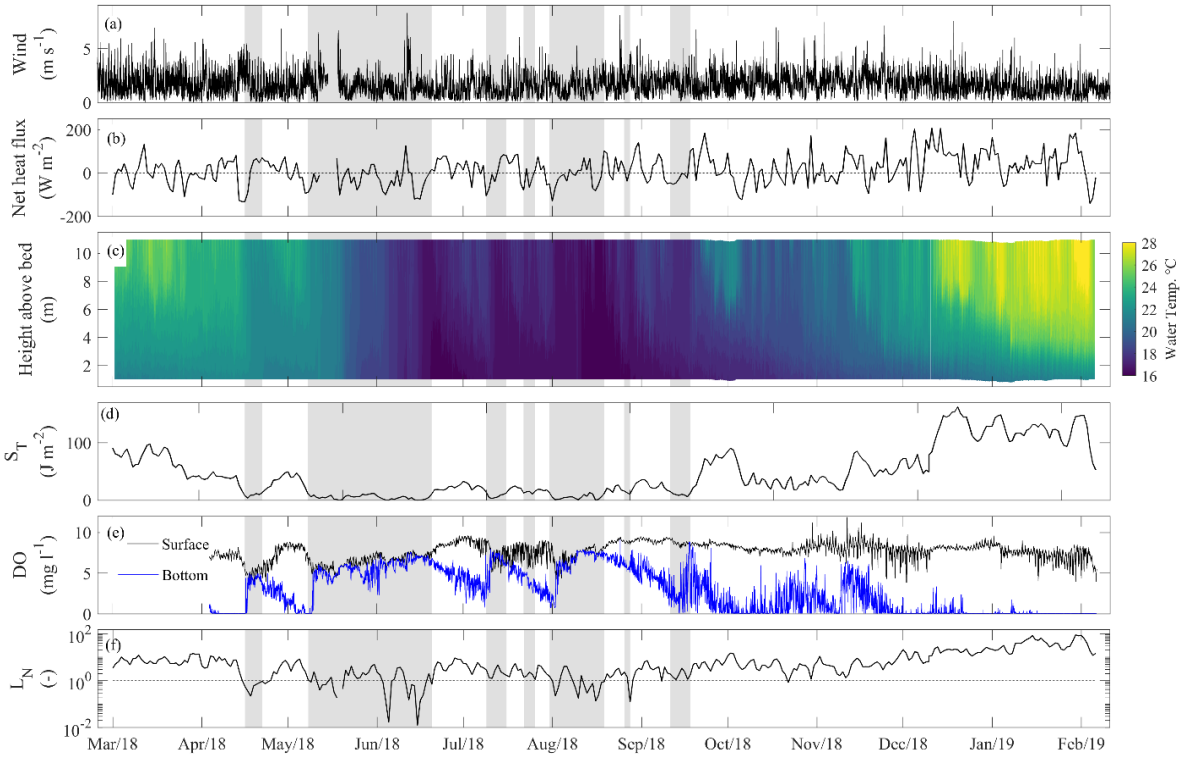

Figure 2: Time series of measurements and derived quantities: ***(a)*** *10 min averaged wind speed.* ***(b)*** *Daily averaged net heat flux at the water surface.* ***(c)*** *Water temperature (1 min resolution).* ***(d)*** *Daily averaged Schmidt stability (S_T).* ***(e)*** *Dissolved oxygen concentration (DO) measured near the surface (black line) and at the bottom (blue line).* ***(f)*** *Daily averaged Lake Number (L_N, solid line). The dotted horizontal line indicates L_N =1. Grey background marks periods classified as mixed, while periods classified as stratified have white background.*

Monthly averaged temperature profiles did not feature well-defined layers of epilimnion, metalimnion and hypolimnion. Water temperature varied rather continuously and smoothly over depth (Figure 3). The absence of a persistent maximum of the buoyancy frequency marking the base of a seasonal mixed layer, i.e. a seasonal thermocline, is remarkable. Instead, the depth of the maximum buoyancy frequency (N_{max}) fluctuated along the total depth during the mixed season and within the upper mixed layer during stratified conditions. The upper mixed layer was strongly affected by diurnal heating and its thickness showed large diel variations. The upper mixed layer temperature varied on average by 0.98 ± 0.63°C within 24 h, while the Schmidt stability changed on average by 32% over the day.

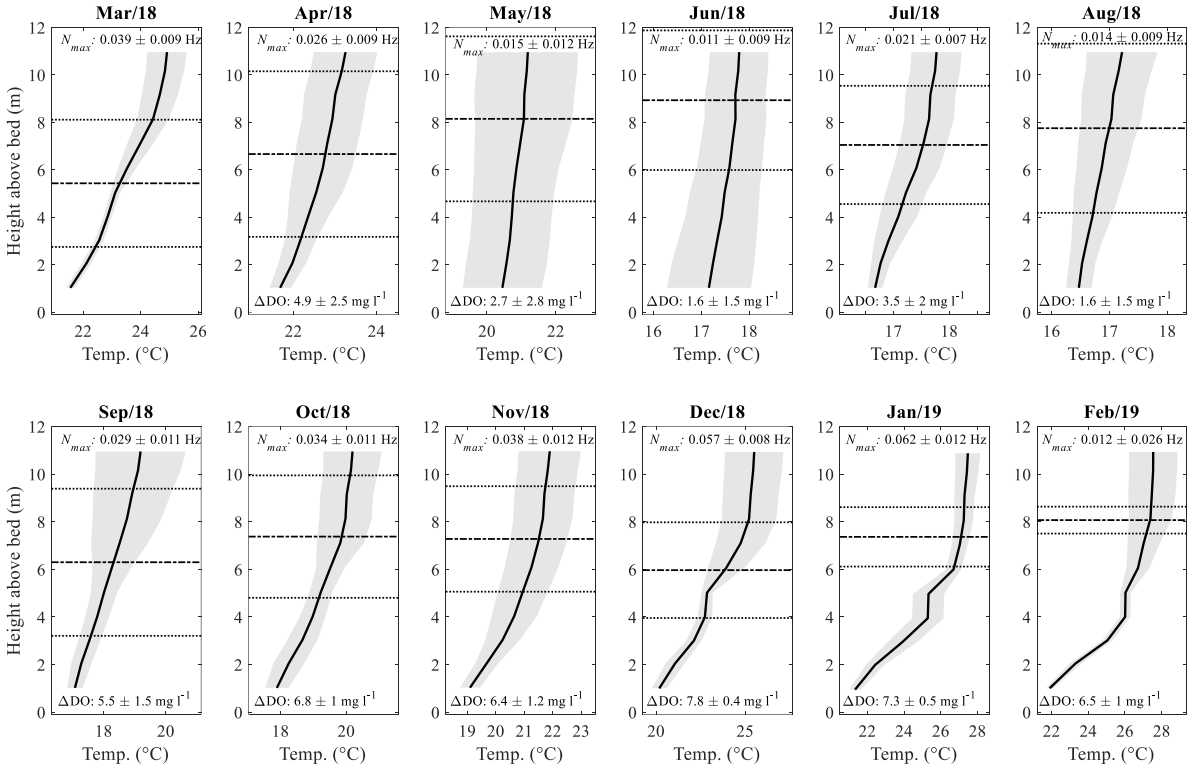

Figure 3: Monthly averaged temperature profiles measured near the water intake. Solid black lines are mean values of temperature and the standard deviation is marked by the gray shaded area. Dashed-dotted lines mark the mean depth of the upper mixed layer (UML), and the dotted lines its standard deviation. Labels in the upper part of each panel provide the monthly averaged value of the maximum buoyancy frequency (N_{max}) ± standard deviation. Text labels in the lower part provide the mean difference of dissolved oxygen concentration between surface and bottom (ΔDO ± standard deviation).

Flow paths of the river inflow

The observations of thermal stratification and temperature profiles described above were undertaken at a deep reservoir location (7 km downstream the main inflow, and 4 km upstream the dam, Figure 1). In the following, we analyze longitudinal variations in water temperature. The temperature of the inflowing water from the Passaúna River was strongly affected by the shallow forebay region (Buffer). Water temperature measured at the transition from the Buffer to the main reservoir (Ferraria Bridge) was consistently higher than the temperature measured in the Passaúna River (Figure SI 3). Due to data logger loss, temperature measurements at Ferraria Bridge are only available for the period March to August 2018. During this period, the daily mean temperature difference between both sampling locations varied between 0.30 ± 0.42 °C on June 8th and 6.33 ± 0.90 °C on March 12th (daily mean ± standard deviation). In comparison to the water temperature observed at the intake station, water temperature at Ferraria Bridge was more variable at seasonal as well as at diel time scales.

We analyzed the path of inflowing water into the main reservoir by comparing the inflow temperature at Ferraria Bridge with the surface and bottom temperature at the monitoring site in the main reservoir. We consider the water temperature observed at Ferraria Bridge as the inflow temperature into the main reservoir. Under consideration of the accuracy of the temperature loggers, we classified the inflow condition as an overflow, if the inflow temperature was exceeding the water surface temperature in the reservoir by 0.2 °C (Figure SI 4b). Similar, we expect an underflow, if the inflow temperature was at least 0.2 °C cooler than the bottom water temperature in the reservoir (Figure SI 4a). All remaining situations are considered as interflow. Underflow and interflow were the most frequent flow paths and accounted for 42% and 45% of all observations, respectively. Flow paths often varied within one day (Figure 4a), owing to the large amplitude of diel variation of water temperature in the forebay (~ 2 °C). At night, water temperature in the forebay frequently decreased to values lower than the bottom temperature in the reservoir and increased to values exceeding surface water temperature in the afternoon. Persistent underflow conditions mainly occurred during mixed periods, while for the flow paths during stratified periods flows paths depended on the season. Before the long mixed period over and inter flow were predominant. After the mixing season, combinations of interflow and underflow were more common. From March to August, 35 out of 164 days featured all three flow paths, 21 of them during stratified periods.

To explore the importance of the forebay region for the path of the inflowing water into the main reservoir, we repeated the above analysis for the hypothetical case that the Passaúna River would flow directly into the main reservoir, without passing through the forebay. Consequently, we used observed river water temperature (upstream of the Buffer) instead of inflow temperature at Ferraria Bridge. Water temperature in Passaúna River was consistently colder, causing the complete absence of overflows (Figure 4b). In addition, the relative occurrence of interflow was reduced, while underflow increased from 42 to 95 % for the period March to August 2018. From September to March, interflow was the most frequent flow path. During a complete annual cycle, underflows would persist for 76 % of the time and interflow could be expected for the remaining 24 % of the year.

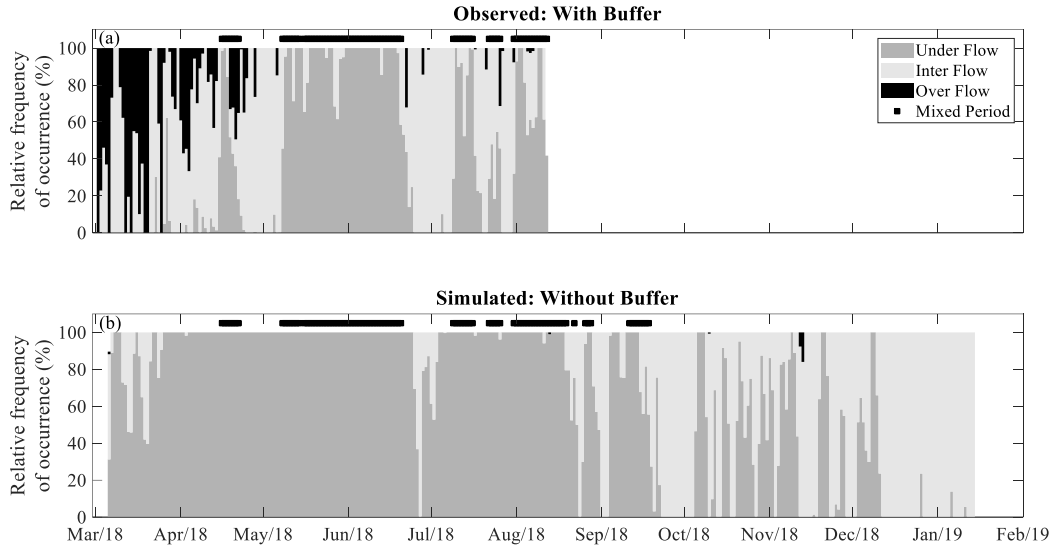

Figure 4: Stacked bar graphs showing the relative frequency of occurrence of different inflow characteristics (flow paths) of the Passaúna River into the main reservoir on a daily basis. ***(a)*** *Based on observed temperature at Ferraria Bridge (due to the loss of the temperature logger used in this analysis the data ends on 12 Aug 2018).* ***(b)*** *Simulations based on river water temperature measured upstream of the forebay. Data are presented as daily averages of the relative contribution of different flow paths. Square symbols above both panels mark time periods classified as mixed.*

Flow conditions

The mean flow speed (velocity magnitude averaged over depth and time) was around 2 cm s^{-1} during low-flow conditions, with frequent events exceeding 4 cm s^{-1} and sporadic periods of velocities up to 10 cm s^{-1} (Figure 5). We used a threshold of 3.5 cm s^{-1} (corresponding to the 90th percentile of all measurements) to identify the occurrence of currents (enhanced flow velocity). Currents were more frequent during stratified than during mixed periods, representing 12% and 6% of the respective periods.

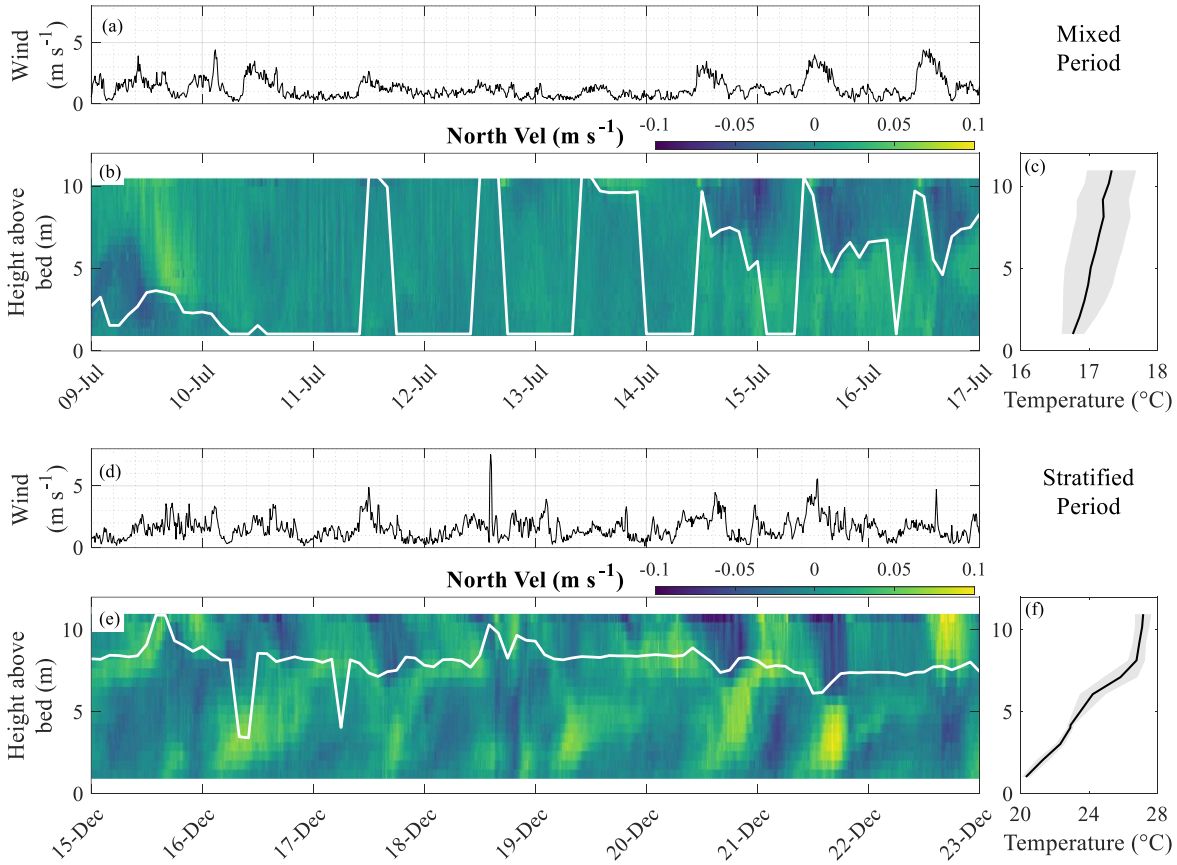

*Figure 5: **(a)** Time series of wind speed for a mixed period. **(b)** Temporally averaged horizontal velocities in south to north direction in m s^{-1} with temporal resolution of 5 min. The white line marks the thermocline depth. **(c)** Time averaged temperature profile for the same time period as in panel (a) and (b), the gray background color marks the standard deviation. **(d)** Time series of wind speed during a stratified period. **(e)** Temporally averaged horizontal north velocities, with the same spatial and temporal resolution as for the mixed period, white line is the thermocline depth. **(f)** Averaged temperature profile for the time period in panel (d) and (e), the gray background color indicates the standard deviation.*

The mean magnitude of the currents during stratified conditions was 4.7 ± 1.2 cm s^{-1} in the bottom layer (lower half of the water column) and 4.9 ± 1.4 cm s^{-1} in the upper water layer (upper half of the water column). During mixed periods, the mean magnitude of the currents was 4.3 ± 0.7 cm s^{-1} for bottom and 4.5 ± 0.9 cm s^{-1} at the surface (Figure SI 5a and 5e). Despite the small differences, a Wilcoxon rank sum test suggested a significant difference of both surface and bottom currents between mixed and stratified conditions (p-value < 0.001). Since one of the main forces generating currents is wind, the data were subdivided according to the thermal regime (mixed or stratified) and different wind speed categories. The wind speed was averaged over 6 h and classified as weak (≤ 1.25 m s^{-1}), moderate (> 1.25 m s^{-1} and ≤ 2.5 m s^{-1}) or strong (> 2.5

m s^{-1}). Wilcoxon rank sum test was applied to each pair of thermal regime for the same depth range and same wind classification. All six classifications showed significantly (p-value < 0.001) smaller currents during mixed conditions.

The short-term dynamics of currents in response to wind revealed that currents were directly driven by wind stress at the water surface, or by a reversed return flow after the wind ceased. For both, mixed and stratified periods, flows were characterized by opposing flow direction between two density layers (Figure 5b and 5e). The return flow was most likely driven by horizontal pressure gradients resulting from longitudinal tilting of the vertical density structure. The motion did not evolve into persistent internal seiches and flow velocities decreased rapidly after the wind has ceased.

We used the mixed-layer Richardson number to compare the observed response of the stratified reservoir to wind shear at the water surface following the classification proposed by Spigel and Imberger (1980). For 77% of the monitoring period pronounced seiches are expected to be excited by wind and to form billows at the thermocline, which have minor effects on the density structure, while most of the energy input is dissipated in the surface mixed layer (Regime 3). This condition occurred mainly during stratified periods. During the mixed period, the classification indicates rapid mixing by wind shear, which causes rapid erosion of vertical density gradients (Regime 1, 16.5% of the monitoring period). In the remaining time (6.5%), Regime 2 was observed during both mixed and stratified conditions, which is characterized by the presence of Kelvin Helmholtz billows due to the shear stress that can provoke significant interface displacements. In this case, the deepening of the thermocline is induced by the shear and upwelling of the thermocline to the water surface at the upwind end of the reservoir may occur (Figure SI 6).

High frequency internal waves

The high-resolution measurements of vertical flow velocities revealed the ubiquitous presence of periodic flow variations with periods between 2 and 17 min (Figure 6). Analysis of band-pass filtered velocity time series for selected periods (Table SI 2 and Table SI 3) showed that the frequencies of the oscillations were correlated with the buoyancy frequency (Figure 6c), suggesting that they are caused by internal waves. On average, wave frequencies were a factor of two smaller than the maximum buoyancy frequency, which describes the upper frequency limit for internal wave motion. Spectral analysis revealed the relevance of high-frequency internal waves for the temporal variability of flow velocity during both stratified and mixed condition. Under

both thermal regimes, the largest share of spectral variance of vertical velocity was associated with internal wave motion. Spectral variance, as a measure of wave energy, increased with increasing distance from the bed. Compared to stratified conditions, internal waves during mixed conditions had longer periods (11.1 ± 3.5 min versus 5.1 ± 2.7 min), but comparable root mean square vertical velocity variations ((1.1 ± 0.6) × 10^{-3} m s^{-1} versus (1.0 ± 0.5) × 10^{-3} m s^{-1}), and kinetic energy (spectral variance of vertical velocity: (2.9 ± 2.7) × 10^{-6} J kg^{-1} versus (2.1 ± 1.3) × 10^{-6} J kg^{-1}). The vertical displacement caused by internal waves was estimated by dividing the root mean square amplitude of the vertical velocities by the respective wave frequency. The mean vertical displacement amplitude during mixed conditions (0.73 ± 0.52 m) was more than twice as high as the mean amplitude during stratified conditions (0.30 ± 0.21 m). During the wave events, the 5th percentile of the gradient Richardson number was 0.16 ± 0.10 during mixed and 0.50 ± 0.35 during stratified conditions.

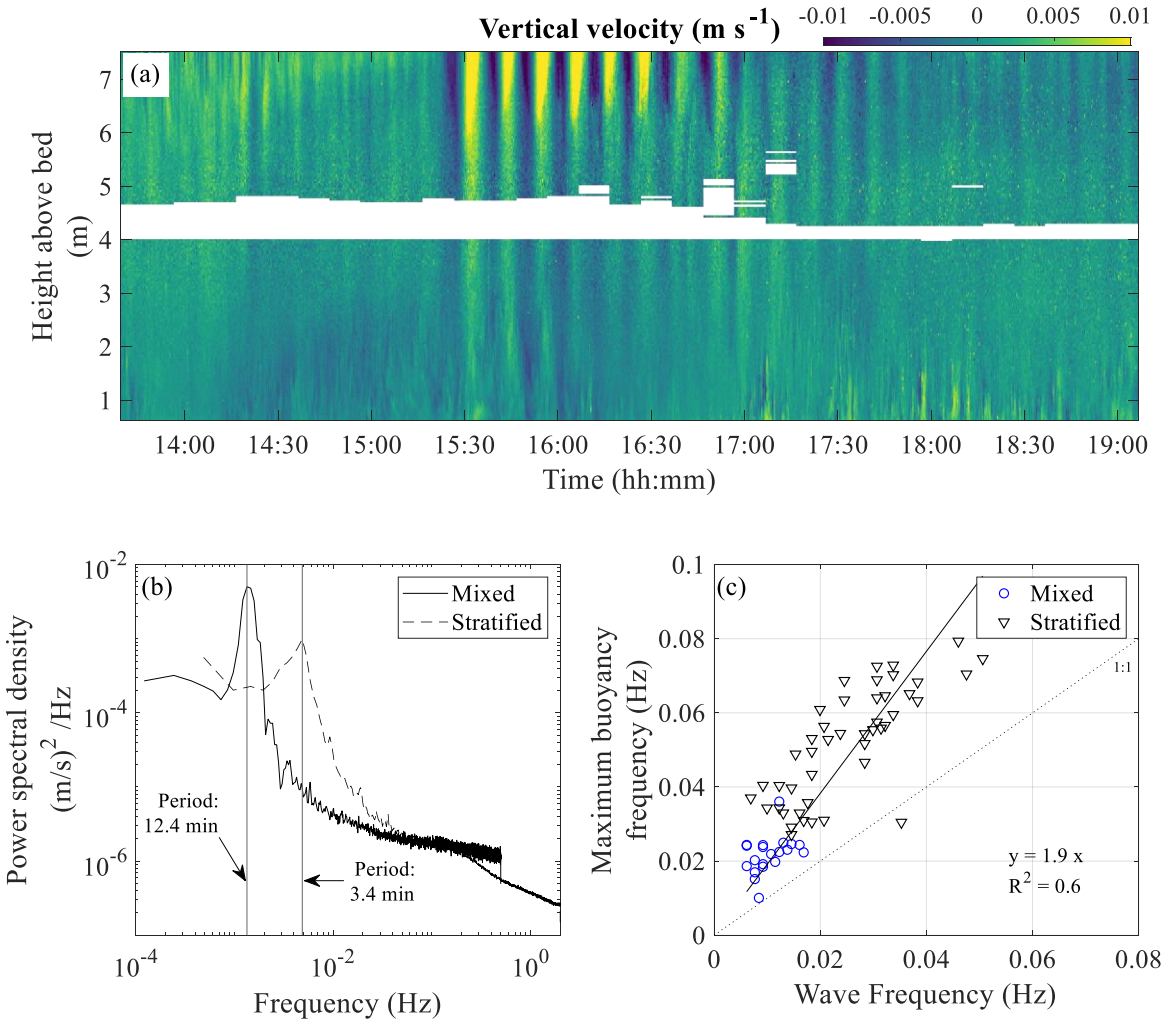

Figure 6: Characteristics of high-frequency internal waves. (a) High-resolution vertical flow velocities with temporal resolution of 1 s exemplifying an internal wave event (14 Jul 2018, wave #2 in Table SI 2). (b) Power spectral density of vertical velocity fluctuations observed during mixed (4 Aug 2018 1800 h to 2330 h, wave #9 in Table SI 2) and during stratified conditions (16 Jan 2019 1000 h to 2330 h, wave #41 in Table SI 3). (c) Maximum buoyancy frequency versus peak frequencies of internal waves for mixed (blue circles) and stratified (black triangles) conditions. The dashed line shows a 1:1 relationship and the solid lines is a linear regression according to the equation provided in the graph.

Turbulence

Dissipation rates of turbulent kinetic energy (ε) for the entire period varied between 10^{-10} – 10^{-9} W kg^{-1}. During the strongest wind events, ε increased to 10^{-6} W kg^{-1} at the upper end of the high-resolution profile (~ 8 m above the bed), but those were sporadic events. Mean (log-averaged) ε during mixed conditions (7.2×10^{-10} W kg^{-1}) did not differ significantly from those observed during stratified conditions (5.2×10^{-10} W kg^{-1}). During both periods, ε were nearly constant over the observed depth range (0.5 to 8 m above the bed), but decreased slightly towards the bed (Figure 7a).

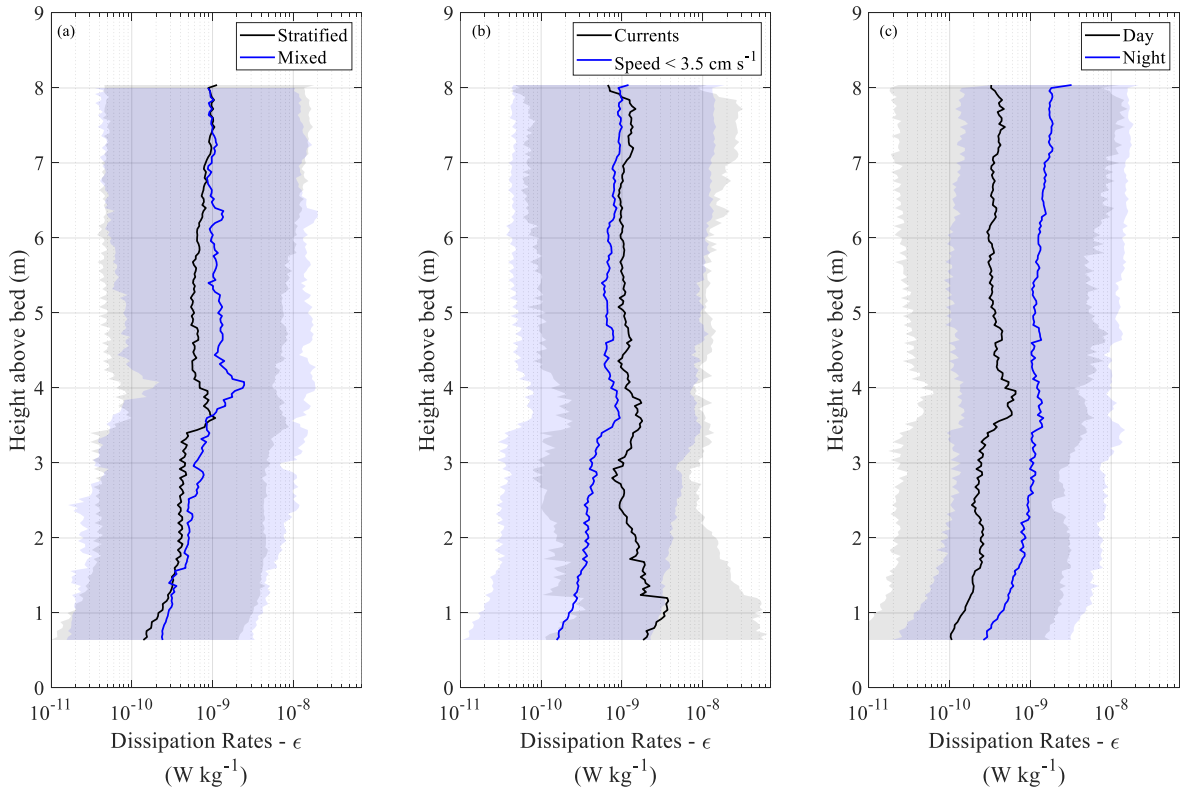

*Figure 7: Vertical profiles of mean dissipation rates of turbulent kinetic energy (solid lines) and range of variability (filled area shows the 5th to 95th percentile): **(a)** Averaged over all measurements during mixed (blue) and during stratified (black) conditions. The peak at a range of 4 m above the bed can be an artifact of the bad data band in this region (see Fig. 7a). **(b)** Averaged over periods of low flow velocity (flow speed < 3.5 cm s^{-1}) and over periods of enhanced flow (currents, flow speed > 3.5 cm s^{-1}). **(c)** Mean dissipation rates during day (black: 0800 h to 1600 h) and during night (blue: 2000 h to 0400 h).*

When mean horizontal velocities were large ε was higher in the lower part of the water column and increased towards to bed (Figure 7b). Near to the bottom ε was about one order of magnitude higher (2×10^{-9} W kg^{-1}) than during calm periods (3.3×10^{-10} W kg^{-1}).

Most pronounced differences in ε were found between day and night (Figure 7c). Log-averaged ε at night (from 2000 h to 0400 h: 1.0×10^{-9} W kg^{-1}) were consistently one order of magnitude larger than during daytime (0800 h to 1600 h: 2.7×10^{-10} W kg^{-1}). The diel variation of turbulent ε followed periodic changes in acoustic backscatter strength (Figure SI 7), although no significant correlation between dissipation rates and echo intensity was observed (Figure SI 9). The regular appearance of high backscatter intensity during nighttime and lower values at daytime was observed at varying intensity during all seasons and suggests the presence of zooplankton performing diel vertical migration. To check if the velocity measurements or the applicability of the structure function approach for estimating dissipation rates were compromised by the presence of zooplankton, we visually compared observed and fitted structure functions (Figure SI 8). Under both conditions, observed velocity variations along the beam followed the expected structure function dependence on distance.

Discussion

Peculiarities of a subtropical reservoir

Stratification

Passaúna reservoir was continuously stratified during spring and summer, while frequent periods of mixing and episodic stratification were observed throughout autumn and winter. The mixing regime can be classified as discontinuous warm polymictic (Lewis Jr 1983), which is characterized by more than one mixing period throughout the year. According to Lewis Jr (1996), this regime can be considered as typical for tropical lakes with 3 – 10 m mean depth. Passaúna is located slightly south of the Tropic of Capricorn, therefore the temperature difference between surface and bottom was larger than in reservoirs of comparable size located at lower latitudes (Antenucci et al. 2012; Xing et al. 2014). Similar to an embayment of Lake Victoria (MacIntyre et al. 2002), these reservoirs were characterized by complete mixing and stratification on a daily basis (i.e. continuous warm polymictic), although the former observations did not cover a complete annual cycle.

Despite the persistent seasonal stratification, a seasonal thermocline did not exist in Passaúna reservoir and the temporarily averaged temperature profiles had a nearly continuous

vertical gradient. Although the temperature difference between the reservoir surface and bottom was small in comparison to those typically observed in temperate lakes with a seasonal thermocline, the corresponding density difference and strength of stratification was of comparable magnitude, owing to the higher coefficient of thermal expansion of water at higher temperature. Therefore the maximum buoyancy frequency had values comparable to those found in the seasonal thermocline of temperate lakes (Boegman et al. 2003; Pernica and Wells 2012), although the depth at which the maximum occurred varied strongly in time.

The lack of a seasonal thermocline and the large amplitude of diel variations of near-surface temperature rendered common metrics for estimating mixed layer depth and mixing status based on maximum buoyancy frequency, or based on temperature differences as problematic. Instead, we used a threshold value for the Schmidt stability corresponding to 10% of its seasonal maximum value for distinguishing between mixed and stratified conditions. Even though under mixed conditions there can be weak stratification, the criterion performed well in identifying periods of bottom water dissolved oxygen depletion and renewal.

Flow Conditions and High Frequency Internal Waves

Flow velocities were generally low and currents, i.e. flow speeds exceeding 3.5 cm s^{-1}, were less frequent and had smaller magnitudes during mixed periods. These flows were mainly driven by wind, or were opposing return flows after the wind has ceased. Basin-scale internal wave oscillations after excitation by wind were not observed. This is in contrast to many lakes and reservoirs with a seasonal thermocline, and to predictions from the classification scheme proposed by Spigel and Imberger (1980). The absence of internal seiches can probably be attributed to the combination of weak wind and continuous stratification over depth. In addition, the rather complex shape and curvature of the reservoir could be a reason for the absence of internal seiches in Passaúna. However, Imam et al. (2020) showed that under homogeneous wind, the fundamental mode of internal seiches can also be excited in multibasin reservoirs, while seiches in sub-basins are mainly generated by spatial heterogeneous winds. Thus, considering that all sub-basins of Passaúna Reservoir have similar orientation and assuming that wind direction was similar in all sections, we expected that the Lake Number could be suitable indicator for internal wave dynamics in our study.

In contrast, high-frequency (propagating) internal waves were present during all seasons. In most of our observations, they were generated along shear layers, for instance at the interface between the opposing currents shown in Figure 5b and 5e, suggesting that they are generated

by Kelvin-Helmholtz instabilities (Thorpe et al. 1977; De Silva et al. 1996). Spectral analysis of our high-resolution velocity measurements revealed that most of the velocity variance in the reservoir interior was associated with high-frequency internal waves during both mixed and stratified conditions.

Most longer-term observations of high-frequency internal waves have been conducted in temperate lakes with a seasonal thermocline and did not include measurements during mixed periods (Thorpe et al. 1996; Saggio and Imberger 1998; Antenucci and Imberger 2001). Measurements in the littoral zone of temperate Lake Constance showed that high-frequency internal wave activity was restricted to the stratified season (Lorke et al. 2006), with no detectable wave motion in winter, although the observations did not include the entire water column of the deep lake. The year-round internal wave activity in Passaúna reservoir can be explained by the comparably strong density stratification caused by small vertical variations of temperature in tropical and subtropical regions.

Turbulence

Average dissipation rates of turbulent kinetic energy did not differ between mixed and stratified conditions and were within the range of typical values reported for the interior of seasonally stratified, temperate lakes (Wüest and Lorke 2003). ε did not increase towards the bed when horizontal velocities were smaller than 3.5 cm s^{-1}, which represents 90% of the total measurement period. We consider the low ε near the bed as an indication of flow laminarization in the bottom boundary layer at low flow velocity. When currents were present, turbulent bottom boundary layers developed, causing an intensification of ε towards the bottom by bed shear. Since our measurements started ~ 50 cm above the bed, the turbulent boundary layer may have been compressed to a thin layer near-bed region at low flow conditions.

When compared to the few reported measurements of ε made in the tropics, the observed values are indeed small. In shallow lakes of the amazon flood plain (MacIntyre et al. 2019), where winds hardly exceed 2 m s^{-1} and turbulence was found to be mainly controlled by the heat flux at the water surface, ε was low (2×10^{-9} W kg^{-1}), but still one order of magnitude larger than the mean ε observed in Passaúna. However, our measurement range ended 3-4 m below the water surface and did not resolve the surface layer.

Low ε throughout the water column under both stratified and mixed conditions indicate weak vertical mixing, which complies with the rapid and persistent build-up of thermal stratification and associated decline in bottom-water dissolved oxygen concentration. An upper

bound of the vertical eddy diffusivity (K_z) can be estimated from simultaneous measurements of ε and stratification by assuming a constant (maximum) mixing efficiency Γ, where $K_z = \Gamma\varepsilon/N^2$, and Γ = 0.2 as suggested by Osborn (1980). Although the continuing debate about the appropriate mixing efficiency, the value of 0.2 was supported in recent reviews (Gregg et al. 2018; Monismith et al. 2018). Hence, based on day and night averaged values of ε, vertical eddy diffusivity in Passaúna reservoir can range from 3.1×10^{-8} to 1.3×10^{-7} W kg^{-1}, which is lower than or comparable to the molecular diffusivity of heat and only one to two order of magnitude higher than molecular diffusivities of dissolved quantities, such as oxygen.

Our observations suggest that shear instabilities and high-frequency internal waves may contribute to vertical mixing throughout the water column. Laboratory experiments suggest that stratified shear flows becomes unstable if the gradient Richardson number falls below a critical value of 0.25 (Miles 1961), which occurred in our observations more frequently during internal wave events. Laboratory experiments and observations from temperate lakes and reservoirs showed that these propagating internal waves dissipate most of their energy by shoaling at the sloping boundaries along the basin (Imberger and Ivey 1993; Boegman et al. 2005; Lorke 2007), thereby strongly contributing to basin-scale vertical mixing (MacIntyre et al. 1999; Gloor et al. 2000; Wüest and Lorke 2003). Although our measurements did not resolve these boundary mixing processes, the ubiquitous nature of high-frequency internal waves during all seasons suggest, that they play an important role in controlling the weak vertical mixing in Passaúna reservoir.

Our measurements did not allow for a conclusive explanation for the enhanced turbulence during nighttime. Because ε were enhanced throughout the entire water column, also under conditions of strong thermal stratification, nighttime convective mixing can be ruled out as a potential forcing for the enhanced turbulence. Interestingly, in Valle de Bravo a tropical reservoir in Mexico, where turbulence is mainly driven by the wind at daytime, average values of ε are larger during the daytime, in the order of 10^{-6} W kg^{-1} and 10^{-7} W kg^{-1} than at nighttime (Anis and Singhal 2006). Therefore, the coincidence with variations in acoustic backscatter strength, which was supposedly caused by migrating zooplankton, may suggest a strong contribution of swimming zooplankton to small-scale turbulence. However, no direct correlation between ε and acoustic backscatter could be observed. We believe that the causes are low frequency variation of the backscatter strength in the long-term records and the likely presence of more than one species of zooplankton with different contributions to backscatter strength (Lorke et al. 2004). As

recently reviewed by Kunze (2019), the potential contribution of swimming zooplankton to vertical mixing in the ocean has been controversy discussed in the literature. Laboratory measurements with migrating freshwater zooplankton point toward negligible contribution to energy dissipation and vertical mixing in stratified lakes (Noss and Lorke 2014). Field measurements on the potential of vertical migrators to generate biomixing in lakes supported this conclusion (Simoncelli et al. 2018), although observations are rare (Simoncelli et al. 2017).

Role of the forebay on flowpaths

The forebay region promoted heat exchange with the atmosphere more rapidly than the main reservoir, which affected the density-driven flow paths of the river into the reservoir. Forebays, or purposely constructed pre-dams, are features of many reservoirs. The effect of upstream located dams on the flow paths and stratification in downstream reservoirs has been studied for reservoir cascades at larger scales (Hocking and Straškraba 1994; Wiejaczka et al. 2018; Long et al. 2019). Smaller pre-dams and impoundments, like the forebay region studied here, received less attention, although they may have a similar or more significant impact on stratification and mixing than differential cooling from side arms observed in tropical lakes and reservoirs (Verburg et al. 2011; Yang et al. 2019).

At Passaúna Reservoir the particularly higher temperatures at Ferraria Bridge during spring and winter caused a frequent occurrence of overflows and interflows. The inflowing water affected the temperature stratification in the main reservoir mainly by adding cooler water to the bottom layer as underflows (as observed in middle April), which is an important process affecting vertical stratification in low latitude lakes (Lewis Jr 2000; Xing et al. 2014). It can be expected, that the inflow of warmer water as an overflow also contributed to vertical density stratification. However, the configuration of our measurements did not allow to quantify the corresponding increase in stability. With a mean horizontal flow speed of 2 cm s^{-1}, the water travel time from Ferraria Bridge to the thermistor chain at the monitoring site was around four days. During that time, the surface temperature was affected by several heating and cooling cycles due to heat exchange with the atmosphere.

Due to ongoing siltation of the forebay, a scenario has been analyzed in which the forebay was completely filled with sediment and the inflow enters the reservoir with river water temperature. Thus, the inflow would change to predominantly underflows. Lower bottom water temperature would promote stronger stratification and reduce the frequency and duration of mixing events in the reservoir. However, bottom water renewal may also reduce the duration of

anoxic periods. The flow paths of the river into the reservoir not only affect stratification, mixing and bottom-water oxygen concentration, it additionally can be relevant for algal growth, if the inflowing waters are a main source of nutrients for the reservoir. Overflows deliver nutrients to the photic zone and can be expected to promote algae blooms (Rueda et al. 2007), and also interflows followed by mixing with the upper mixed layer can increase primary production (MacIntyre et al. 2006).

In our analysis of flow paths, we considered water temperature as the main factor influencing water density, therefore the effect of total solids was neglected. The maximum concentration of total solids during an extreme event was 0.16 g L^{-1} and the dissolved part was 0.14 g L^{-1} during our sampling period (Oliveira et al. 2019). Density differences lower than 0.14 g L^{-1}, which could lead to a wrong flow path classification, represented 14% of the observed situation with the forebay, and 11% of the simulated period. The consideration of total solids would increase the density of the inflow and the likelihood of underflows. As underflows were already the predominant flow paths in our simulations, we expect that the simulation results are not affected by neglecting the contribution of total solids to water density.

Conclusions

High-resolution measurements of an annual cycle of stratification, flow, and turbulence revealed detailed insights into the hydrodynamics of a subtropical reservoir classified as discontinuous warm polymictic. The thermal regime was characterized by persistent stratification from spring to summer, and alternating periods of mixing and stratification during winter. Density stratification was particularly stable, related to the strong temperature dependence of density at high water temperature.

In addition to meteorological forcing, stratification was affected by lateral flows related to river inflow. The density-driven flow paths of the main river inflow were affected by the shallow forebay in the inflow region, a structure similar to widespread pre-dam areas. The forebay has a faster heat exchange than the rest of the reservoir, therefore, it strongly influenced the variation of the flow paths of the inflowing water and supposedly also on the thermal regime in the reservoir. Future research on the importance of such forebays and on the their potential in controlling mixing and water quality in the reservoir as engineering measures, should include more detailed experimental and numerical characterization of the density current propagation and dispersion.

Currents in the reservoir were mainly driven by wind and basin-scale internal waves were absent, most likely because of continuous, rather than layered vertical stratification. Propagating,

high-frequency internal waves, in contrast, were present throughout all seasons. Turbulence and turbulent transport in the reservoir interior was weak. As a consequence, dissolved oxygen concentration near the bottom decreased rapidly even during shorter periods of stratification during the mixing season. Turbulence in the pelagic zone was possibly affected by migrating zooplankton.

The observed hydrodynamic characteristics is potentially representative for a large number of small to medium sized lakes and for a growing number of reservoirs located in the tropical and subtropical zones. Future research should therefore aim at assessing the broader relevance as well as at gaining more detailed understanding of (i) the conditions that lead to the suppression of basin-scale internal waves, (ii) the generation mechanism of high frequency waves and their importance for boundary mixing processes, and (iii) the role of biogenic mixing in this type of aquatic system. As the two latter processes are not resolved in commonly applied numerical models, they potentially limit our capabilities to predict hydrodynamic conditions and water quality in tropical reservoirs.

Acknowledgments

We thank the German Federal Ministry of Education and Research (BMBF) for funding the MuDak-WRM project (grant number 02WGR1431 B), SANEPAR for providing data on reservoir operation, Stephan Hilgert and Regina Kishi for the dissolved oxygen data and also the field organization, Michael Mannich for the valuable comments on the manuscript, and besides those already mentioned all the team from the Postgraduate Program in Water Resources and Environmental Engineering of the Federal University of Paraná and Christoph Bors for field support. And all the MuDak-WRM team for helping to bring together different information that supported this work. Tobias Bleninger acknowledges also the support from the productivity stipend from CNPq (Brazilian Council for Reserch), grant number. 8786885193878624, call: CNPq N º 12/2017.

References

Anis A, Singhal G. 2006. Mixing in the surface boundary layer of a tropical freshwater reservoir. Journal of Marine Systems. 63(3-4):225-243.

Antenucci JP, Imberger J. 2001. On internal waves near the high-frequency limit in an enclosed basin. Journal of Geophysical Research: Oceans. 106(C10):22465-22474.

Antenucci JP, Tan KM, Eikaas HS, Imberger J. 2012. The importance of transport processes and spatial gradients on in situ estimates of lake metabolism. Hydrobiologia. 700(1):9-21.

Bastviken D, Cole J, Pace M, Tranvik L. 2004. Methane emissions from lakes: Dependence of lake characteristics, two regional assessments, and a global estimate. Global Biogeochemical Cycles. 18(4):n/a-n/a.

Baulch HM, Dillon PJ, Maranger R, Schiff SL. 2011. Diffusive and ebullitive transport of methane and nitrous oxide from streams: Are bubble-mediated fluxes important? Journal of Geophysical Research: Biogeosciences. 116(G4).

Best J. 2019. Anthropogenic stresses on the world's big rivers. Nature Geoscience. 12(1):7-21.

Boegman L, Imberger J, Ivey GN, Antenucci JP. 2003. High-frequency internal waves in large stratified lakes. Limnology and Oceanography. 48(2):895-919.

Boegman L, Ivey G, Imberger J. 2005. The degeneration of internal waves in lakes with sloping topography. Limnology and oceanography. 50(5):1620-1637.

Carneiro C, Kelderman P, Irvine K. 2016. Assessment of phosphorus sediment–water exchange through water and mass budget in Passaúna Reservoir (Paraná State, Brazil). Environmental Earth Sciences. 75(7). English.

Cortés A, Fleenor W, Wells M, de Vicente I, Rueda F. 2014. Pathways of river water to the surface layers of stratified reservoirs. Limnology and Oceanography. 59(1):233-250.

De Silva I, Fernando H, Eaton F, Hebert D. 1996. Evolution of Kelvin-Helmholtz billows in nature and laboratory. Earth and Planetary Science Letters. 143(1-4):217-231.

Deemer BR, Harrison JA, Li S, Beaulieu JJ, DelSontro T, Barros N, Bezerra-Neto JF, Powers SM, Dos Santos MA, Vonk JA. 2016. Greenhouse gas emissions from reservoir water surfaces: a new global synthesis. BioScience. 66(11):949-964.

Fer I, Lemmin U, Thorpe S. 2002. Winter cascading of cold water in Lake Geneva. Journal of Geophysical Research: Oceans. 107(C6).

Fonseca Xavier C, Neiva Dias L, Brunkow RF. 2017. Qualidade das águas dos reservatórios do estado do Paraná. IAP - Instituto Ambiental do Paraná.

Friedl G, Wüest A. 2002. Disrupting biogeochemical cycles-Consequences of damming. Aquatic Sciences. 64(1):55-65.

Gloor M, Wüest A, Imboden DM. 2000. Dynamics of mixed bottom boundary layers and its implications for diapycnal transport in a stratified, natural water basin. Journal of Geophysical Research: Oceans. 105(C4):8629-8646.

Goring DG, Nikora VI. 2002. Despiking acoustic Doppler velocimeter data. Journal of hydraulic engineering. 128(1):117-126.

Gregg MC, D'Asaro EA, Riley JJ, Kunze E. 2018. Mixing Efficiency in the Ocean. Annual Review of Marine Science. 10(1):443-473.

Guerra M, Thomson J. 2017. Turbulence measurements from 5-beam acoustic Doppler current profilers. Journal of Atmospheric and Oceanic Technology.(2017).

Hocking G, Straškraba M. 1994. An analysis of the effect of an upstream reservoir by means of a mathematical model of reservoir hydrodynamics. Water Science and Technology. 30(2):91.

Imam YE, Laval B, Pieters R, Lawrence G. 2020. The baroclinic response to wind in a multiarm multibasin reservoir. Limnology and Oceanography. 65(3):582-600.

Imberger J. 1998. Flux paths in a stratified lake: A review. Physical processes in lakes and oceans. 54:1-17.
Imberger J, Hamblin PF. 1982. Dynamics of lakes, reservoirs, and cooling ponds. Annual Review of Fluid Mechanics. 14(1):153-187.
Imberger J, Ivey G. 1993. Boundary mixing in stratified reservoirs. Journal of Fluid Mechanics. 248:477-491.
Imboden DM, Wüest A. 1995. Mixing mechanisms in lakes. Physics and chemistry of lakes. Springer; p. 83-138.
Kundu PK, Cohen IM. 2010. Fluid Mechanics. 4 ed. Elsevier Science.
Kunze E. 2019. Biologically generated mixing in the ocean. Annual review of marine science. 11:215-226.
Lehner B, Liermann CR, Revenga C, Vörösmarty C, Fekete B, Crouzet P, Döll P, Endejan M, Frenken K, Magome J. 2011. High-resolution mapping of the world's reservoirs and dams for sustainable river-flow management. Frontiers in Ecology and the Environment. 9(9):494-502.
Lemmin U. 2020. Insights into the dynamics of the deep hypolimnion of Lake Geneva as revealed by long-term temperature, oxygen, and current measurements. Limnology and Oceanography. 65(9):2092-2107.
Lewis Jr WM. 1983. A Revised Classification of Lakes Based on Mixing. Canadian Journal of Fisheries and Aquatic Sciences. 40(10):1779-1787.
Lewis Jr WM. 1987. Tropical limnology. Annual review of ecology and systematics. 18(1):159-184.
Lewis Jr WM. 1996. Tropical lakes: how latitude makes a difference. Perspectives in tropical limnology. 4364.
Lewis Jr WM. 2000. Basis for the protection and management of tropical lakes. Lakes & Reservoirs: Research & Management. 5(1):35-48.
Long L, Ji D, Liu D, Yang Z, Lorke A. 2019. Effect of Cascading Reservoirs on the Flow Variation and Thermal Regime in the Lower Reaches of the Jinsha River. Water. 11(5):1008.
Lorke A. 2007. Boundary mixing in the thermocline of a large lake. Journal of Geophysical Research. 112(C9).
Lorke A, McGinnis DF, Spaak P, Wüest A. 2004. Acoustic observations of zooplankton in lakes using a Doppler current profiler. Freshwater Biol. 49:1280-1292.
Lorke A, Peeters F, Bäuerle E. 2006. High-frequency internal waves in the littoral zone of a large lake. Limnology and oceanography. 51(4):1935-1939.
MacIntyre S, Fernandes Amaral JH, Barbosa PM, Cortés A, Forsberg BR, Melack JM. 2019. Turbulence and Gas Transfer Velocities in Sheltered Flooded Forests of the Amazon Basin. Geophysical Research Letters. 46(16):9628-9636.
MacIntyre S, Flynn KM, Jellison R, Romero JR. 1999. Boundary mixing and nutrient fluxes in Mono Lake, California. Limnology and Oceanography. 44(3):512-529.
MacIntyre S, Romero JR, Kling GW. 2002. Spatial-temporal variability in surface layer deepening and lateral advection in an embayment of lake Victoria, East Africa. Limnol Oceanogr. 47(3):656-671.
MacIntyre S, Sickman JO, Goldthwait SA, Kling GW. 2006. Physical pathways of nutrient supply in a small, ultraoligotrophic arctic lake during summer stratification. Limnology and Oceanography. 51(2):1107-1124.
Mendonça R, Müller RA, Clow D, Verpoorter C, Raymond P, Tranvik LJ, Sobek S. 2017. Organic carbon burial in global lakes and reservoirs. Nature communications. 8(1):1694.

Miles JW. 1961. On the stability of heterogeneous shear flows. Journal of Fluid Mechanics. 10(4):496-508.
Monismith SG, Koseff JR, White BL. 2018. Mixing Efficiency in the Presence of Stratification: When Is It Constant? Geophysical Research Letters. 45(11):5627-5634.
Noss C, Lorke A. 2014. Direct observation of biomixing by vertically migrating zooplankton. Limnology and Oceanography. 59(3):724-732.
Oliveira JdSd, Wosiacki LFK, Gurski LKK, Prado LLd, Knapik HG, Rauen WB, Hilgert S, Fernandes CVS, Bleninger T. 2019. Concentração de sólidos em um reservatório de abastecimento: Do campo para o laboratório e o gestor. conference annals presented at: XXIII Simpósio brasileiro de recursos hídricos; 24-28 November 2019; Foz do Iguaçu - PR - Brazil.
Osborn TR. 1980. Estimates of the local rate of vertical diffusion from dissipation measurements. J Phys Oceanogr. 10:83-89.
Pernica P, Wells M. 2012. Frequency of episodic stratification in the near surface of Lake Opeongo and other small lakes. Water Quality Research Journal of Canada. 47(3-4):227.
Read JS, Hamilton DP, Jones ID, Muraoka K, Winslow LA, Kroiss R, Wu CH, Gaiser E. 2011. Derivation of lake mixing and stratification indices from high-resolution lake buoy data. Environmental Modelling & Software. 26(11):1325-1336.
Rueda FJ, Fleenor WE, de Vicente I. 2007. Pathways of river nutrients towards the euphotic zone in a deep-reservoir of small size: uncertainty analysis. Ecological modelling. 202(3-4):345-361.
Saggio A, Imberger J. 1998. Internal wave weather in a stratified lake. Limnology and oceanography. 43(8):1780-1795.
SANEPAR CdSdP. 2013. Plano Diretor SAIC: Sistema de Abastecimento de Água Integrado de Curitiba e Região Metropolitana. Curitiba: Sanepar.
Simoncelli S, Thackeray SJ, Wain DJ. 2017. Can small zooplankton mix lakes? Limnology and Oceanography Letters. 2(5):167-176.
Simoncelli S, Thackeray SJ, Wain DJ. 2018. On biogenic turbulence production and mixing from vertically migrating zooplankton in lakes. Aquatic Sciences. 80(4).
Sotiri K, Hilgert S, Fuchs S. 2019. Sediment classification in a Brazilian reservoir: Pros and cons of parametric low frequencies. Advances in Oceanography and Limnology. 10(1).
Spigel RH, Imberger J. 1980. The classification of mixed-layer dynamics of lakes of small to medium size. Journal of physical oceanography. 10(7):1104-1121.
Stevens CL. 1999. Internal waves in a small reservoir. Journal of Geophysical Research: Oceans. 104(C7):15777-15788.
Thorpe S, Hall A, Taylor C, Allen J. 1977. Billows in Loch Ness. Deep Sea Research. 24(4):371-IN373.
Thorpe S, Keen J, Jiang R, Lemmin U. 1996. High-frequency internal waves in Lake Geneva. Philosophical Transactions of the Royal Society of London Series A: Mathematical, Physical and Engineering Sciences. 354(1705):237-257.
Verburg P, Antenucci JP, Hecky RE. 2011. Differential cooling drives large-scale convective circulation in Lake Tanganyika. Limnology and Oceanography. 56(3):910-926.
Vörösmarty CJ, Meybeck M, Fekete B, Sharma K, Green P, Syvitski JPM. 2003. Anthropogenic sediment retention: major global impact from registered river impoundments. Global and Planetary Change. 39(1-2):169-190.
Wahl TL. 2003. Discussion of “Despiking acoustic doppler velocimeter data” by Derek G. Goring and Vladimir I. Nikora. Journal of Hydraulic Engineering. 129(6):484-487.

Wiejaczka Ł, Kijowska-Strugała M, Pierwoła P, Nowak M. 2018. Water Temperature Dynamics in a Complex of Reservoirs and Its Effect on the Temperature Patterns of a Mountain River. Water Resources. 45(6):861-872.
Wiles PJ, Rippeth TP, Simpson JH, Hendricks PJ. 2006. A novel technique for measuring the rate of turbulent dissipation in the marine environment. Geophysical Research Letters. 33(21).
Winton RS, Calamita E, Wehrli B. 2019. Reviews and syntheses: Dams, water quality and tropical reservoir stratification. Biogeosciences. 16(8):1657-1671.
Wisser D, Frolking S, Hagen S, Bierkens MF. 2013. Beyond peak reservoir storage? A global estimate of declining water storage capacity in large reservoirs. Water Resources Research. 49(9):5732-5739.
Woolway RI, Simpson JH. 2017. Energy input and dissipation in a temperate lake during the spring transition. Ocean Dynamics. 67(8):959-971.
Wüest A, Lorke A. 2003. Small-scale hydrodynamics in lakes. Annual Review of fluid mechanics. 35(1):373-412.
Xing Z, Fong DA, Yat-Man Lo E, Monismith SG. 2014. Thermal structure and variability of a shallow tropical reservoir. Limnology and Oceanography. 59(1):115-128.
Yang P, Fong DA, Lo EYM, Monismith SG. 2019. Circulation patterns in a shallow tropical reservoir: Observations and modeling. Journal of Hydro-environment Research. 27:75-86.
Yoshimizu C, Yoshiyama K, Tayasu I, Koitabashi T, Nagata T. 2010. Vulnerability of a large monomictic lake (Lake Biwa) to warm winter event. Limnology. 11(3):233-239.
Zarfl C, Lumsdon AE, Berlekamp J, Tydecks L, Tockner K. 2014. A global boom in hydropower dam construction. Aquatic Sciences. 77(1):161-170.

Appendix II

The effect of stream shading on the inflow characteristics in a downstream reservoir

Mayra Ishikawa[1], Ingo Haag[2], Julia Krumm[2], Katharina Teltscher[2], and Andreas Lorke[1]

[1]*Institute for Environmental Sciences, University of Koblenz-Landau, Landau, Germany*

[2]*HYDRON GmbH, Environmental and Hydrological Consulting, Karlsruhe, Germany*

Please click in the following link to read the publication

https://doi.org/10.1002/rra.3821

Received: 11 January 2021 | Revised: 5 May 2021 | Accepted: 6 May 2021
DOI: 10.1002/rra.3821

RESEARCH ARTICLE

WILEY

The effect of stream shading on the inflow characteristics in a downstream reservoir

Mayra Ishikawa[1] | Ingo Haag[2] | Julia Krumm[2] | Katharina Teltscher[2] | Andreas Lorke[1]

[1]Institute for Environmental Sciences, University of Koblenz-Landau, Landau, Germany

[2]HYDRON GmbH, Environmental and Hydrological Consulting, Karlsruhe, Germany

Correspondence
Mayra Ishikawa, Institute for Environmental Sciences, University of Koblenz-Landau, Landau, Rhineland-Palatinate, Germany.
Email: ishikawa@uni-landau.de

Funding information
Bundesministerium für Bildung und Forschung, Grant/Award Numbers: 02WGR1431 B, 02WGR1431 F

Abstract

In thermally stratified reservoirs, inflows form density currents according to the interplay between inflow temperature and reservoir stratification. The temperature of inflowing water is affected by catchment properties, including shading by riparian vegetation. We hypothesize that the degree of shading in the catchment can affect the inflow dynamics in downstream reservoirs by changing inflow temperature and consequently the nature of the density current. We test it for a subtropical drinking water reservoir by combining catchment-scale hydrological and stream temperature modeling with observations of reservoir stratification. We analyze the formation of density currents, defined as under, inter and overflow, for scenarios with contrasting shading conditions in the catchment. Inflow temperatures were simulated with the distributed water-balance model LARSIM-WT, which integrates heat-balance and water temperature. River temperature measurements and simulations are in good agreement with a RMSE of 0.58°C. In simulations using the present state of shading, underflows are the most frequent flow path, 63% of the annual period. During the remaining time, river intrusion form interflows. In a scenario without stream shading, average inflow temperature increased by 2.2°C. Thus, interflows were the most frequent flow path (51%), followed by underflows (34%) and overflows (15%). With this change, we would expect a degradation of reservoir water quality, as overflows promote longer periods of anoxia and nutrient loads would be delivered to the photic zone, a potential trigger for algae blooms. This study revealed a potentially important, yet unexplored aspect of catchment management for controlling reservoir water quality.

KEYWORDS
density currents, reservoirs, riparian vegetation, stream shading, water quality

1 | INTRODUCTION

During the last two decades, dam construction has been increasing and by considering the ongoing construction and planning of new dams this trend is expected to continue (Zarfl, Lumsdon, Berlekamp, Tydecks, & Tockner, 2014). The current boom of dam construction documented by Zarfl et al. (2014) was based on estimates of hydropower dams only, additional dams are constructed for flood control

and water storage for drinking water and irrigation (Grill et al., 2019; Lehner et al., 2011). Dams disrupt natural hydrological, geological and biogeochemical cycles (Friedl & Wüest, 2002; Poff, Olden, Merritt, & Pepin, 2007; Vörösmarty et al., 2003). The consequences of river damming for water quality and biodiversity have been intensively assessed for downstream river reaches and river basins (Bunn & Arthington, 2002; Vörösmarty et al., 2010), but also water quality in the impounded water bodies is of great concern, as it potentially jeopardizes their economic and societal values.

The efficient trapping of nutrients, including phosphorous and nitrogen (Akbarzadeh, Maavara, Slowinski, & Van Cappellen, 2019; Maavara et al., 2015), in combination with prolonged water residence time and the potential development of thermal stratification, promote eutrophication and harmful algae blooms in the impoundments (Winton, Calamita, & Wehrli, 2019). Nutrient enrichment is the primary cause for eutrophication and the occurrence of harmful algae blooms, which nowadays are the main problems related to water quality (Paerl & Otten, 2013; Schindler, 2012; Smith & Schindler, 2009). The possible consequences are the killing of fish due to the depletion of oxygen or the release of toxins from algae and sediments, as well as increased concentration of suspended and dissolved substances that affect odor and color. Such degradation of water quality increases treatment costs (Dodds et al., 2009; Pretty et al., 2003; Walker Jr, 1983).

In addition to climatic and geographic boundary conditions, reservoir water quality is controlled by the inflowing nutrient load and reservoir hydrodynamics. In stratified reservoirs, inflows form density currents that are classified according to their depth of intrusion: underflows follow the reservoir bottom, overflows stay at the reservoir surface, and interflows enter at intermediate depths (Wetzel, 2001). The type of density current depends on inflow temperature and reservoir stratification and eventually controls the distribution of the nutrient load in the reservoir and its availability for algae growth (Ayala, Cortés, Fleenor, & Rueda, 2014; Rueda, Fleenor, & de Vicente, 2007).

Water temperature of the inflowing streams depends on meteorological and hydrological conditions (Caissie, 2006; B. W. Webb, Hannah, Moore, Brown, & Nobilis, 2008). However, stream temperature is also affected by catchment properties, including shading by riparian vegetation. In particular, stream water temperature has been observed to increase following deforestation, or to decrease in response to tree growth in many studies (see reviews in Beschta, Bilby, Brown, Holtby, & Hofstra, 1987; D. R. Moore, Spittlehouse, & Story, 2005). More recently, the impact of riparian vegetation on stream water temperature has been studied using different empirical and modeling approaches. These studies showed, that the magnitude of temperature reduction due to riparian vegetation depends on many different aspects, including vegetation density, vegetation height, stream width, stream orientation, contribution of net shortwave radiation to the overall energy budget, geographical latitude, solar angle and many others (e.g., Dugdale, Malcolm, Kantola, & Hannah, 2018; Garner, Malcolm, Sadler, & Hannah, 2014, 2017; Garner, Malcolm, Sadler, Millar, & Hannah, 2015; Kalny et al., 2017; D. R. Moore et al., 2005; R. Moore, Leach, & Knudson, 2014; Regenauer, Haag, & Aigner, 2019; Trimmel et al., 2018). In general, the effect of dense riparian vegetation is most pronounced during times of high water temperature, when the energy budget is dominated by short wave radiation (e.g., Garner et al., 2014; Hannah, Malcolm, Soulsby, & Youngson, 2008). It is thus well established that riparian vegetation helps to reduce maximum stream water temperatures and thermal variability. Consequently, shading is often considered in catchment management and stream restoration efforts and is among the three most important environmental state variables in assessments of stream restoration success (Feld et al., 2011).

The effect of stream shading on inflow dynamics in downstream reservoirs has not been studied. We hypothesize that the degree of shading in the catchment can affect the inflow dynamics in downstream reservoirs by changing inflow temperature and consequently the nature of the density current. As riparian stream shading is closely related to land use in the catchment, this mechanism would constitute an unexplored influence of catchment management on reservoir water quality. Here we test this hypothesis for a tropical drinking water reservoir. We combine catchment-scale hydrological and stream temperature modeling with observations of reservoir stratification and analyze the formation of density currents for scenarios with contrasting shading conditions in the catchment. We further discuss the potential implications of stream shading for reservoir water quality and the broader relevance of the studied process.

2 | METHODS

2.1 | Study site

Passaúna reservoir is a drinking water reservoir in a tropical to subtropical region in south Brazil (latitude: − 25°30′ and longitude: − 49°22′). It produces around 1.8 $m^3\ s^{-1}$ of drinking water for parts of the city of Curitiba and three neighboring cities (SANEPAR, 2013). The reservoir has a maximum depth of 15 m, a surface area of 9 km^2 and an approximate volume of $60 \times 10^6\ m^3$ (Carneiro, Kelderman, & Irvine, 2016). The catchment of the reservoir covers an area of 143 km^2 (Figure 1). Mean air temperature within the catchment was approximately 18.7°C and mean yearly precipitation approximately 1,650 mm (years 2009 through 2018). A relatively high proportion of the catchment (44% for catchment of gauge Campo Largo) was covered by broad-leaved mainly evergreen forest (Figure 1). Passaúna River is the dominant inflow to the reservoir. It drains an area of approx. 100 km^2 and delivers around 75% of total annual inflow to the reservoir (Carneiro et al., 2016). Simulated mean annual discharge at gauge Campo Largo (84 km^2) reached approx. 2 $m^3\ s^{-1}$ (2010 through 2018).

2.2 | Observational data

The investigation period of the present study covers 1 year from March 2018 through February 2019. During that period, water

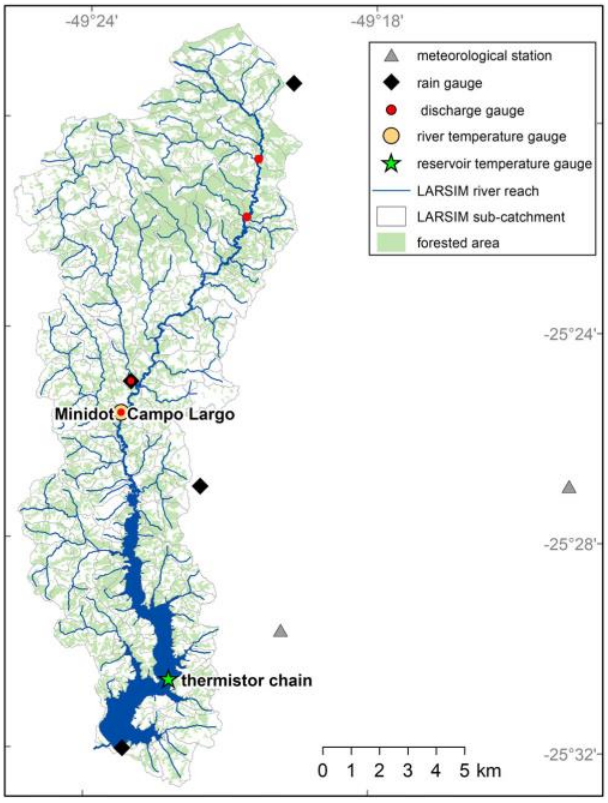

FIGURE 1 Map of the catchment of Passaúna reservoir, including all stream segments and sub-catchments resolved by the model (LARSIM). The locations of water temperature gauges, discharge gauges, rain gauges and meteorological stations used in this study are marked by symbols (see legend) [Color figure can be viewed at wileyonlinelibrary.com]

temperature was monitored in the Passaúna River and reservoir. At Passaúna River, water temperature was measured approximately 3 km upstream of the reservoir inflow near the gauging station Campo Largo using a temperature sensor (miniDOT, Precision Measurement Engineering Inc.) with a temporal resolution of 15 min, an accuracy of ±0.1°C and a resolution of 0.01°C (Figure 1). In the reservoir, a vertical thermistor chain with 11 temperature sensors (Minilog-II-T, Vemco) was deployed close to the intake station of the waterworks (Figure 1), at a mean water depth of 12 m. The chain was fixed at the bottom with the first logger being 1 m above the bed and all remaining sensors were arranged with a fixed vertical spacing of 1 m. The sampling interval was 1 min, precision and accuracy of the sensors was ±0.1°C and of 0.01°C, respectively.

Additional data for modeling discharge and river water temperature was provided by the Federal University of Paraná (UFPR). Measurements of mean daily discharge were available for four gauges within the catchment (Figure 1). These discharge data were used to calibrate and validate the water balance model over a period of several years (see below; Krumm, Haag, & Wolf, 2019). To simulate discharge and river water temperature during the period of investigation (March 2018 through February 2019) we used daily precipitation from four rain gauges within the catchment along with additional measurements of air temperature, global radiation, humidity and wind speed from two meteorological stations west of the catchment (Figure 1).

2.3 | Integrated water balance and stream water temperature modeling

2.3.1 | Model overview

River discharge and stream water temperature were modeled using LARSIM-WT (Large Area Runoff SIMulation Model – Water Temperature – Haag & Luce, 2008). LARSIM is a process-oriented and spatially distributed water balance model, which simulates all major aspects of the terrestrial water cycle (LEG, 2019). LARSIM also includes an optional water temperature module (WT), which simulates water temperature throughout the complete river network on a physical basis (Haag & Luce, 2008).

Heat transport within the river network was modeled using the one-dimensional advection-dispersion equation. The local heat balance, that is, the source-sink term in the advection-dispersion equation, accounts for heat exchange with the atmosphere and at the river bed:

$$\frac{dWT}{dt} = \frac{R_S + R_L + H_S + H_L + H_{bed}}{cp_S \rho_w h} \quad (1)$$

with WT denoting water temperature (°C), t time (s), cp_W the specific heat capacity of water (J kg^{-1}°C^{-1}), ρ_W water density (kg m^{-3}), h average water depth of the river reach (m), R_S net shortwave radiation (W m^{-2}), R_L net longwave radiation (W m^{-2}), H_S turbulent flux of sensible heat (W m^{-2}), H_L turbulent flux of latent heat (W m^{-2}) and H_{bed} the conductive heat flux at the riverbed (W m^{-2}).

In general, the parametrization of the heat fluxes follows the approach of Sinokrot and Stefan (1993) by using relationships, which were originally derived for open water bodies. Applying these open water body formulae to small rivers with riparian vegetation is a simplification. Nonetheless, this simplified approach is well established and validated in the scientific literature on river water temperature modeling and it is commonly used to evaluate the effect of riparian vegetation on river water temperature (e.g., Dugdale, Hannah, & Malcolm, 2017; Garner et al., 2017; Haag & Luce, 2008; Sinokrot & Stefan, 1993; Trimmel et al., 2018). All terms of the heat balance and their parametrization in LARSIM-WT are described in detail in Haag and Luce (2008). For that reason, we only briefly describe the fluxes, which are influenced by riparian vegetation in the following. Net shortwave radiation R_S at the water surface was calculated from measured incoming shortwave radiation R_{glob} (W m^{-2}) and the albedo of the water surface. For the present study, albedo was assumed to be constant at a value of 0.06. To account for shading by riparian vegetation, a shading factor f_{shade} is used, where $f_{shade} = 0$ corresponds to no shading (i.e., a sky view factor of 1) and $f_{shade} = 1$ for complete shading (i.e., a sky view factor of 0):

$$R_S = (1 - f_{shade})(1 - albedo)R_{glob} \quad (2)$$

The turbulent fluxes of latent heat H_L and sensible heat H_s were simulated with an aerodynamic approach:

$$H_L = -\rho_W L K_L (e_{sat,WT} - e_{air}) \quad (3)$$

$$H_s = -\rho_W L K_L \gamma \frac{P}{1013}(WT - T_{air}) \quad (4)$$

with L denoting the latent heat of vaporization (J kg^{-1}), $e_{sat,Wt}$ the saturation vapor pressure (hPa) at the water surface with temperature WT, e_{air} the actual measured vapor pressure in the air (hPa), γ the psychometric constant at normal pressure (0.655 hPa °C^{-1}), P the measured atmospheric pressure (hPa) and T_{air} the measured air temperature (°C). The aerodynamic coefficient for turbulent exchange of water vapor K_L (m s^{-1} hPa^{-1}) was derived as a function of measured wind speed v_{wind} (m s^{-1}) by the approach of Rimsha and Donschemko (1958), which produces realistic results over a wide range of environmental conditions. Within this formula, we accounted for the effect of wind sheltering by riparian vegetation with a wind shield factor f_{wind}, where $f_{wind} = 0$ corresponds to no wind sheltering and $f_{wind} = 1$ corresponds complete wind sheltering:

$$K_L = \frac{0.211 + 0.103 v_{wind}(1 - f_{wind})}{86.4 \times 10^6} \quad (5)$$

Following commonly applied models in stream water temperature modeling (e.g., Bogan, Mohseni, & Stefan, 2003; Bustillo, Moatar, Ducharne, Thiéry, & Poirel, 2014; Sinokrot & Stefan, 1993), we neglected the possible minor effect of stream shading on longwave radiation in the present study. Numerical analysis by Regenauer et al. (2019) demonstrated that this effect is much less important than the shading of shortwave radiation and the wind sheltering especially for situations with high shortwave radiation and high air temperatures.

2.4 | Application to the Passaúna catchment

In LARSIM-WT, the catchment of Passaúna reservoir was represented by sub-catchments and their corresponding river reaches (Figure 1). The sub-catchments and corresponding river reaches were delineated based on a Digital Elevation Model and a digital river dataset. The model was forced by measured data from nearby rain gauges and meteorological stations at daily resolution, which were spatially interpolated within the model. The discharge model was calibrated using measured time series of four discharge gauges (Figure 1). Simulated discharge was in good agreement with observations yielding Nash Sutcliffe efficiencies of 0.77 at gauge Campo Largo (Krumm et al., 2019) (Figure 2).

Forests and riparian vegetation within Passaúna catchment is mainly made up by broad-leaved mostly evergreen trees, resulting in an almost constant mean leaf area index throughout the year. Therefore, with respect to river shading, we did not have to take into account seasonal changes of the leaf area index of riparian vegetation. Moreover, almost all river reaches in the Passaúna catchment were less than approximately 5 m wide. With respect to river shading, we thus assumed that overhanging canopies of typical riparian trees on both banks may cover the river width completely. Consequently, for dense riparian vegetation we assumed a constant sky view factor that is uniformly distributed throughout the complete hemisphere above the river surface. Thus, we did not take into account additional influencing factors for estimating the shading factor f_{shade}, such as height of trees, width of river reaches, solar angle, stream orientation or the proportion of direct and diffuse global radiation (DeWalle, 2008; Garner et al., 2017; R. Moore et al., 2014; Regenauer et al., 2019). Even for river reaches completely covered by dense riparian trees, still a minor part of the shortwave radiation reaches the water surface. Based on literature data we assumed that approximately 15% of R_{glob} reach the water surface when a river reach was completely covered by dense riparian trees (e.g., Garner et al., 2017; Regenauer et al., 2019; Trimmel et al., 2018). Thus, complete shading of a river reach by riparian vegetation was simulated with $f_{shade} = 0.85$. Literature data also indicate that dense riparian vegetation reduces wind speed to approximately 60% of standard measurements, and that shading and wind sheltering are closely correlated. These assumptions are also corroborated by a different study, in which we simulated long-term river water temperature for the complete river network of the federal state of Baden-Württemberg in Germany (approximately 36.000 km^2). Optimizing and validating simulation results at 200 measurement locations indicated that water temperatures of narrow rivers under dense forest vegetation are simulated best by assuming $f_{shade} = 0.85$ and $f_{wind} = 0.4$ (Haag, 2018). Thus, also in the present study completely shaded river reaches were modeled with $f_{shade} = 0.85$ and $f_{wind} = 0.4$, whereas no shading was parameterized by $f_{shade} = 0.0$ and $f_{wind} = 0.0$. For situations between maximum shading and wind sheltering on the one hand and no shading and wind sheltering on the other hand, f_{shade} and f_{wind} values were interpolated linearly (e.g., Caissie, 2006; Regenauer et al., 2019; Sinokrot & Stefan, 1993).

Exact values of the present state of stream shading along the river reaches were not available, since land use data were not accurate enough to account for small strips of riparian vegetation along the rivers and precise ground mapping of riparian vegetation was not existent. Therefore, we used the proportion of forest within each sub-catchment as a proxy for the spatial distribution of the proportion of riparian vegetation. We then introduced a factor to multiply the relative proportion of forest within each sub-catchment to get the relative proportion of riparian vegetation of the river reaches. We optimized this factor to fit the measured stream water temperature with the model, but did not allow f_{shade} to exceed a maximum value of 0.85 in any river reach. Within our approach, we thus assumed that the actual proportion of riparian vegetation was proportional to the proportion of forest within the sub-catchments. We obtained a mean factor of 1.6. Based on observations in the field, this factor seemed reasonable,

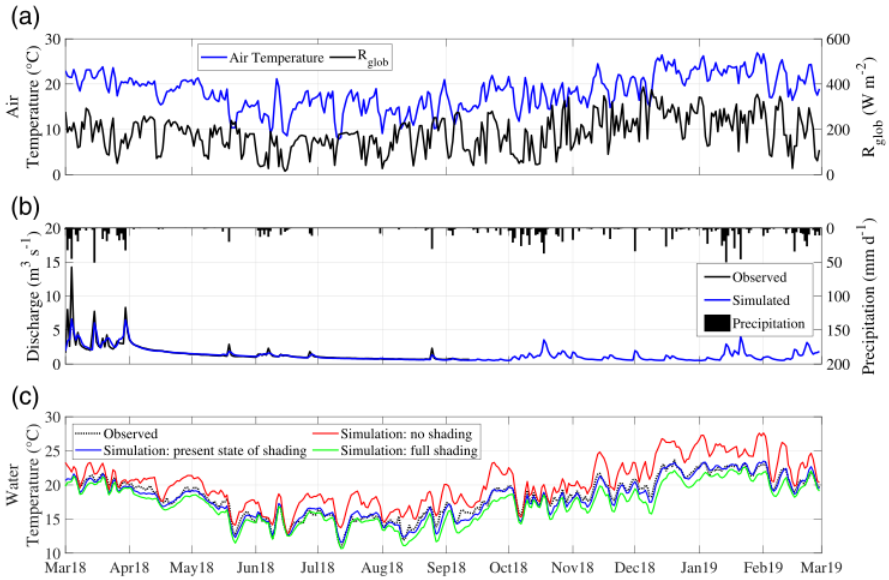

FIGURE 2 (a) Spatial averages of observed air temperature and incoming shortwave radiation R_{glob} within the catchment of gauge Campo Largo in a daily resolution. (b) Observed precipitation along with measured and simulated hydrographs of the Passaúna River at gauge Campo Largo. (c) Time series of observed (dotted black line) and simulated (solid lines) water temperature in the Passaúna River at the temperature gauge (site Minidot). The black dashed line is the observed temperature, blue solid line shows water temperature simulated by the LARSIM-WT model for the present state of shading. The red and green lines show the simulation results for scenarios with no shading and full shading, respectively. All data are shown as daily mean values [Color figure can be viewed at wileyonlinelibrary.com]

since there were many riparian vegetation strips outside forested areas, which increased the first estimate of riparian shading. The optimized factor yielded degrees of shading ranging from 55% to 85% (i.e., f_{shade} varied between 0.55 and 0.85), for the present state of stream shading. The wind shield factor was assumed to vary linearly with the shading factor, as described above. Thus, f_{wind} varied between 0.26 and 0.40.

To analyze the potential effect of stream shading on river water temperatures and inflow dynamics into the reservoir, we defined two scenarios: "full shading" and "no shading." In the full shading scenario for all river reaches we used $f_{shade} = 0.85$ and $f_{wind} = 0.40$. In the no shading scenario, both parameters were fixed at zero for all river reaches.

2.4.1 | Classification of reservoir inflow dynamics

The inflow regime of the river into the reservoir depends on the difference in water density between river water and the seasonally stratified water in the reservoir. Water samples from the analyzed period had maximum total solid concentration of 0.16 g l^{-1} (Oliveira et al., 2019) and the density of the river and reservoir water was mainly controlled by the water temperature.

The intrusion depth of density currents formed at the reservoir entrance was assessed by the difference between the temperature of the inflowing river water and the temperatures observed at the reservoir surface and bottom. The inflow was considered as an overflow, where the river water floats on top of the reservoir, when the temperature of the Passaúna River was higher than the measured surface temperature in the reservoir. When the inflow temperature was lower than the temperature measured close to the reservoir bed, the inflow was classified as underflow, where the river flows along the reservoir bottom. For all other periods, the inflow was considered as interflow, similar to the analysis made by Ishikawa, Bleninger, and Lorke (2021) – accepted at Inland Waters. This analysis was done based on daily mean temperatures.

3 | RESULTS

3.1 | Meteorological conditions and river discharge

During the study period (March 2018–February 2019) average air temperature was 18.3 ± 3.9°C (mean ± *SD*), which was about 0.5°C warmer than the long-term annual average. Air temperature varied seasonally with mean values of 15.1 ± 3.1°C during winter (June to September 2018) and 21.9 ± 2.5°C in summer (March 2018 and December 2018 to February 2019). The average of mean daily shortwave radiation R_{glob} was 184 ± 80 W m^{-2} during the entire year, which was about 17 W m^{-2} more than the long-term average. It also varied seasonally with a winter average of 146 ± 67 W m^{-2} and a summer average of 225 ± 81 W m^{-2} (Figure 2a).

Total precipitation was approximately 1,400 mm for the entire year, which is about 15% below the long-term average of

1,650 mm year^{-1}. The period of investigation started with the relatively wet month of March 2018, followed by a long and extremely dry period from April through September 2018 and it finished with a typical period from October 2018 through February 2019 (Figure 2b).

Discharge of the Passaúna River was successfully calibrated for the 4 year period 2010 through 2013, yielding Nash Sutcliffe efficiencies of 0.77 (Krumm et al., 2019). Based on the simulation results the mean discharge at gauge Campo Largo was 1.4 m^3 s^{-1} during the period of investigation, which is considerably lower than the long-term average of 2 m^3 s^{-1}. The seasonal variation of discharge followed the variation of precipitation: discharge was highest in March 2018. During the following dry season, it gradually dropped to about 0.5 m^3 s^{-1} in September 2018. During the summer 2018/2019 there were some minor peaks, but discharge also frequently dropped to low flow conditions especially, between mid-November and mid-January (Figure 2b). Simulated discharge agreed mostly well with observations at the gauge Campo Largo (measurements were only available until mid-September 2018). Although the major discharge peak in March 2018 was not reproduced well by the model, the minor peaks and in particular, the low flow were simulated very well (Figure 2b).

3.2 | Inflow temperature

Observed river water temperature near the reservoir inflow (location Minidot in Figure 1) varied between 15.3 ± 1.7°C in winter and 21.3 ± 1.2°C in summer. The mean temperature was 18.3 ± 2.9°C, with the lowest temperature (10.9°C) in July and the highest temperature (23.7°C) in December (Figure 2c). In addition to seasonal variations, stream temperature showed strong synoptic variability with rapid temperature changes of up to 5°C at time scales of 5 to 7 days. Water temperature changed mostly synchronously with air temperature and short wave radiation and discharge peaks were often accompanied by rapid drops in water temperature (Figure 2).

Simulated water temperature for the present state of shading was in very good agreement with the measurements, with a RMSE of 0.58°C and a mean absolute error of 0.47°C. Linear regression of measured versus simulated water temperatures resulted in a slope of 1.0, an intercept of −0.27°C and a R^2 of 0.98, indicating that the simulation was unbiased. Moreover, also the temporal dynamics of Passaúna river water temperatures was well reproduced by the model considering the present state of shading (Figure 2c).

The scenario with full shading (f_{shade} = 0.85 for all river reaches) resulted in a moderate reduction of the river water temperature at the reservoir inflow in comparison to the present state (Figures 2 and 3). The simulated temperature differences ranged between −0.1°C and − 2.0°C with an average of −0.8°C. Owing to the already relatively high degree of shading for the present state (f_{shade} = 0.55 through 0.85), maximum shading only showed moderate effects on river water temperature at the reservoir inflow.

The absence of shading (f_{shade} = 0 for all river reaches) resulted in significantly higher inflow temperature (Figures 2 and 3). Compared to

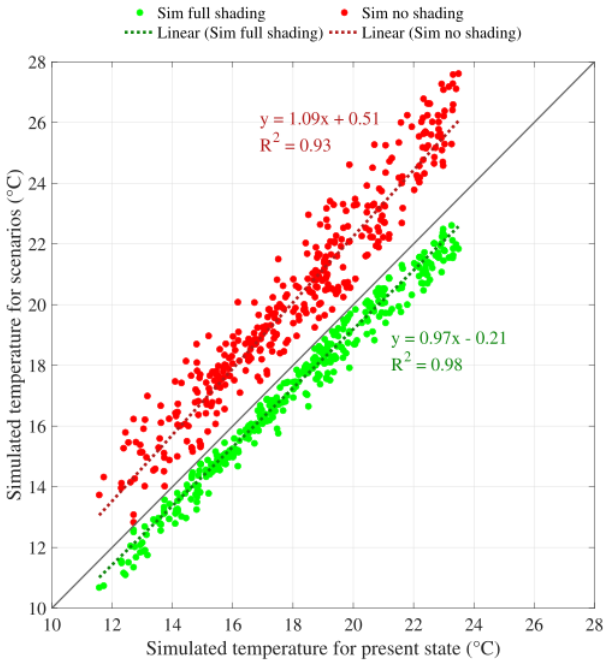

FIGURE 3 Comparison of daily mean stream water temperature at Minidot simulated for the present state of shading with scenarios of full shading (green symbols) and no shading (red symbols) in the upstream stream network. Dotted lines show linear regressions for the two scenarios in the respective color. Regression equations and coefficient of determination (R^2) are provided as text labels. The solid grey line shows a 1:1 relationship [Color figure can be viewed at wileyonlinelibrary.com]

the present state of shading, the increase of daily mean inflow temperature varied between +0.1 and +4.7°C with an average of +2.2°C. This increase is slightly non-linear with higher values in summer, when water temperature was high (Figure 3). This non-linearity is due to the higher contribution of shortwave radiation to the overall energy balance during summer. The largest differences occurred in December 2018, when high shortwave radiation and low flow situations coincided (Figure 2). The difference in water temperature for the two contrasting scenarios without shading and with full shading ranged between +0.3 and +6.7°C with an average difference of +3.0°C (Figure 2c).

3.3 | Reservoir temperature stratification

Water temperature in the reservoir was 21.6 ± 3.5°C at the water surface, and 19.1 ± 2.0°C at the bottom. With persistent temperature differences between the surface and the bottom (1.4 to 7.2°C), the reservoir was stably stratified until the middle of April and from September 2018 (Figure 4). During the stratified period, water surface temperature showed synoptic variability, but with smaller amplitude than stream temperature (Figure 4). The vertical temperature stratification was rather continuous and did not show well-defined layers of

epilimnion, metalimnion and hypolimnion. Below an upper mixed layer of seasonally varying depth, temperature decreased with increasing depth at a nearly constant rate. Bottom water temperature showed little variations and increased nearly linearly over time throughout the stratified period. The stable stratification broke down in April, followed by a period of intermittent mixing and stratification between May and August. The seasonal mixing dynamics of the reservoir can therefore be classified as discontinuous warm polymictic (Lewis Jr, 1983).

3.4 | Reservoir inflow regime

Based on observed daily-mean values of inflow and reservoir water temperature, underflow was the dominant inflow regime of the river in the reservoir, with a relative frequency of occurrence of 63% throughout the monitored period. Interflows were present for the remaining time (37%) and overflows were not existent. Interflows were predominant in spring and summer (Figure 5a), and for the rest of the year underflows were prevalent. The presence of underflows promoted the frequent development of weak stratification also during the mixed period between April and August by transporting cooler river water to the bottom of the reservoir.

In good agreement with the analysis based on measured water temperature, simulated inflow temperature for the present state of shading resulted in a dominance of underflows (67%), whereas overflows were not observed. Also, the seasonal and short-term variability of inflow regimes was well reproduced in the simulations (Figure 5b).

In the simulation for full shading of the stream network, the general distribution of inflow regimes did not change much in comparison to the present state. The relative frequency of occurrence of underflows increased to 81% (Figure 5c), due to the decrease of inflow temperatures (Figure 4).

For the simulated scenario with no shading of the streams, however, inflow regimes changed considerably (Figure 5d). Interflows became the predominant (51%) flow path, and the occurrence of underflows was reduced to 34%. Overflows occurred during 15% of the time. Overflows only occurred during the winter and spring seasons, when the temperature in the Passaúna River exceeded the surface temperatures of the reservoir. During summer, when the temperature was highest, the river temperature was often close to the reservoir surface temperature (Figure 4), but overflows did not occur.

4 | DISCUSSION

4.1 | Effect of riparian shading on stream water temperature

The results presented in this study are based on simulated daily mean water temperature for a relatively well shaded river system at a latitude of −25°30′. According to our results, changing the present state of riparian vegetation to no shading would increase stream water temperature near the reservoir inflow by +2.2°C on average, with a maximum increase of daily mean temperature of +4.7°C. The difference between the no shading scenario and the full shading scenario was +3.1°C on average, with a maximum of +6.7°C.

A quantitative comparison of the observed effect of shading on stream temperature with other investigations is difficult, mainly because of differences in meteorological conditions, in residence times of the water and in methodological approaches. In particular, most other studies were conducted in North America or Europe at higher latitudes with different meteorological conditions. Moreover, results are normally reported for summer conditions and maximum differences only, and not for a yearly average. Nonetheless, our findings may be compared with other results in the literature, qualitatively. For example, several empirical studies, mainly from the Pacific Northwest region in North America (latitude ∼ + 45° to +55°), showed that forest clear-cutting leads to an increase of maximum summer water temperatures of headwater streams commonly in the range of +4°C to +9°C (see reviews in Beschta et al., 1987; D. R. Moore et al., 2005). Empirical studies in the United Kingdom showed that the effect of forest cover as compared to open land on water temperature may vary considerably. Looking at the yearly average, effective shading by forest vegetation in most cases led to moderate

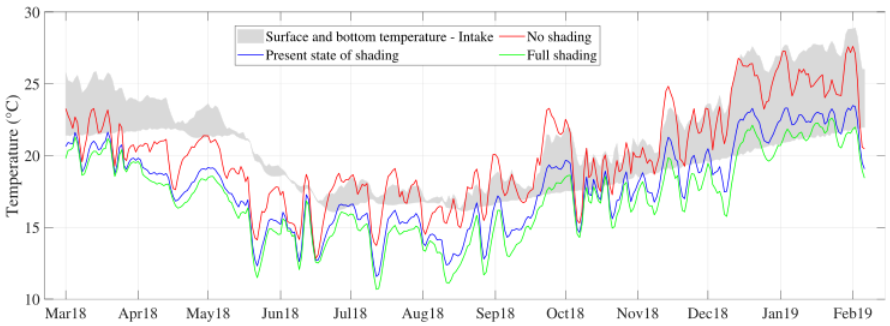

FIGURE 4 Time series of daily-mean water temperature in Passaúna reservoir and its main inflow: The filled gray area marks the range of temperature measured at the surface and the bottom of the reservoir. Colored lines show simulated temperature of the Passaúna River at the reservoir inflow, blue represents the present state of shading, green represents the full shading scenario and red the no-shading scenario of the river network upstream of the reservoir [Color figure can be viewed at wileyonlinelibrary.com]

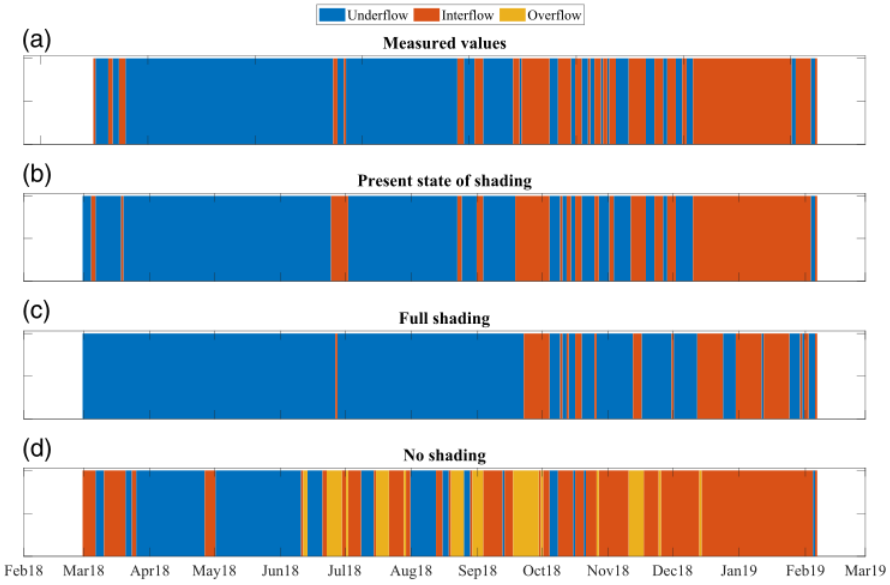

FIGURE 5 Time series of inflow regimes of the Passaúna River into the reservoir. Different flow paths are presented as vertical bars with color denoting underflow (blue), interflow (orange) and overflow (yellow) situations with a temporal resolution of one day. (a) Results based on measured inflow temperature. (b) Result based on simulated river temperatures for the present state of shading of the upstream stream network. (c) Result based on simulated river temperatures for the full shading scenario. (d) Result based on simulated river temperatures for the no shading scenario [Color figure can be viewed at wileyonlinelibrary.com]

temperature reductions of less than 1°C (e.g., Broadmeadow, Jones, Langford, Shaw, & Nisbet, 2011; Brown, Cooper, Holden, & Ramchunder, 2010; Crisp, 1997; Dugdale et al., 2018; Stott & Marks, 2000; B. Webb & Crisp, 2006). However, mean summer temperatures may be reduced more effectively by approximately 1–3°C, and maximum reduction of water temperature may be as high as 5°C (Broadmeadow et al., 2011; Brown et al., 2010; Dugdale et al., 2018; B. Webb & Crisp, 2006).

Recently Garner et al. (2017) investigated the effects of riparian vegetation density, stream orientation and flow velocity in a 1,050 m long reach of the Girnock Burn in Scotland (latitude: +57°) with a sophisticated modeling approach by applying the meteorological conditions of a single summer day with almost clear sky and high rates of solar radiation. For high flow conditions with short residence times of approximately 1.75 hr, stream shading showed a moderate effect on mean daily water temperature in the range of 1.5°C. However, for low flow conditions with a sufficiently long residence time of 12.5 hr, daily mean water temperature for little shading (10–20% canopy density) was about 4.5°C higher than for simulations with a high rate of shading (70–90% canopy density). Similarly, simulation results of Trimmel et al. (2018) for a 50 km reach of the 4–10 m wide river Pinka in Austria (latitude: +47°) demonstrated the potential difference between a no vegetation and a maximum vegetation scenario. According to their results mean water temperatures during the heat wave of August 4 through August 8, 2013 were approximately 4°C lower for the maximum vegetation scenario than for the no vegetation scenario.

The maximum difference between the no shading and the full shading scenario of +6.7°C for Passaúna River is well in the range of the empirical studies for the Pacific North West (D. R. Moore et al., 2005). Also, the difference between the yearly average and the maximum effect in summer is in good accordance with the findings from the United Kingdom (Brown et al., 2010; Dugdale et al., 2018; B. W. Webb et al., 2008). However, our simulated effect of riparian shading on stream water temperature of Passaúna is somewhat higher than the empirical and modeling results from Europe and North America. This may partly be due to differences in residence time. We considered the effect of shading of the complete river network of a relatively large catchment, whereas the other studies mainly looked at small headwater streams with shorter residence times. In the case of river Pinka in Austria only the main river was assumed to be shaded, whereas inflowing tributaries were assumed to have the same temperature in all scenarios. Thus, shorter residence times in other studies may have contributed to the less pronounced effects of shading. Moreover, we neglected the effect of riparian vegetation on longwave radiation in our study, which increases the energy input at the water surface slightly. This might lead to a small systematic overestimation of the effect of stream shading on water temperatures in our study. Finally, and probably most importantly, the effect of riparian shading via blocking of incoming shortwave radiation is likely to be considerably higher at a low latitude of −25° (Passaúna) than at the much higher latitudes of the other study sites (~45° to 57°).

Therefore, in summary, our scenario results for the effect of shading on river water temperature are broadly in line with the literature and can be considered as realistic, even though we could not compare them to other findings from the tropics. Considering the fact that the focus of the present study is not on precise predictions, but results are rather used to demonstrate the potential impact of stream shading in a catchment on a downstream reservoir, the accuracy of our shading scenarios appears to be sufficient.

4.2 | Stream shading in the catchment affects reservoir mixing and stratification

Vertical mixing in reservoirs can be strongly suppressed by temperature stratification, which develops as a consequence of enhanced

water depth and reduced flow velocity in comparison to free-flowing rivers. Vertical temperature gradients develop in response to solar heating of the surface layer, or by lateral density currents formed by inflowing rivers. The latter mechanism depends on stream temperature of the inflow and has been well documented in many reservoirs and studied in laboratory experiments (Alavian, Jirka, Denton, Johnson, & Stefan, 1992; Imberger & Hamblin, 1982; Wells & Nadarajah, 2009). However, the effect of catchment properties on the flow paths of inflowing water has not explicitly been studied. Here, we analyzed the potential effect of riparian stream shading in the catchment on density currents in the reservoir by combining catchment-scale hydrological modeling with temperature observations in a tropical drinking water reservoir. We found that the difference of inflow temperature resulting from the presence and absence of stream shading in the catchment significantly changed the inflow regime, which can affect vertical stratification and mixing in the reservoir. For a high degree of shading, as for the present state of the Passaúna catchment, the stream entered the reservoir predominantly as underflows, along the bottom of the reservoir. In the absence of shading, the higher inflow temperature led to a reduction of the occurrence of underflows and promoted overflow situations. Both types of density currents contribute to vertical temperature stratification in the reservoir. The predicted inflow of warmer water to the reservoir in the absence of shading occurred mainly during winter and spring and can result in increasing the frequency and duration of stratified periods during the mixed season. During the stratified season (summer and autumn), the predicted reduction of underflow situations can be expected to reduce the stability of vertical temperature stratification. Interflows were the most frequent inflow regime in the no-shading scenario and the intrusion depth was shallower compared to the present state. Tracer studies on a plunging river in a Mediterranean reservoir revealed that a fraction (and possibly all) of river inflow entrains into the surface mixed layer, when the density current forms intrusions at the top of the stratified part of the water column (Cortés, Fleenor, Wells, de Vicente, & Rueda, 2014).

4.3 | Implications for reservoir water quality

The observed change in inflow regime for the no shading scenario potentially affects water quality in the reservoir. The occurrence of overflows, which are not present for the present state of shading, facilitates nutrient transport to the photic zone and therewith promotes algae growth (Ayala et al., 2014; Rueda et al., 2007). The combination of excessive nutrient supply at the water surface and reduced vertical mixing during these conditions provide ideal conditions for harmful cyanobacterial blooms (Paerl & Otten, 2013), which are currently not present in Passaúna reservoir. In consequence of the reduced underflows, the transport of oxygen with the inflowing water to greater depths would be reduced, leading to a prolongation of periods of anoxia. Anoxic bottom water further increases internal loading with nutrients from the sediments (Søndergaard, Jensen, & Jeppesen, 2003), as well as the release of anoxic products such as methane, hydrogen sulfide and metals (Beutel & Horne, 1999). In consequence, the water quality in the reservoir can be expected to deteriorate for the scenario without stream shading in the catchment in comparison to the present and full shading conditions.

Given the high degree of forested area in the catchment of Passaúna reservoir (44%), no shading may represent a scenario of extreme land use change at first glance. However, increasing urbanization and agricultural land use in the growing metropolitan area of Curitiba exert a strong anthropogenic pressure on the Passaúna catchment, which may lead to significant deforestation. Furthermore, stream shading does not have an instantaneous effect on water temperature, but rather needs some residence time (i.e., flow distance) to exert its effect (Bartholow, 2000; Kalny et al., 2017; Regenauer et al., 2019). Thus, even if deforestation is restricted to the upstream part of the catchment, it may still lead to increased water temperatures at the downstream inflow of the reservoir.

The strong control of catchment properties on reservoir water quality has been extensively studied in terms of hydrological characteristics and in respect to the input of suspended and dissolved substances, including nutrients and pollutants (Beaver et al., 2014; Jones, Knowlton, & Obrecht, 2008; Knoll et al., 2015). The effect of riparian shading, which is closely linked to land use in the catchment, has not been considered. Our results demonstrate, that changes in stream shading should be included in management scenarios of the catchment area which aim at safeguarding reservoir water quality.

4.4 | Limitations of the present study

The good agreement between stream temperature simulations for the present state of shading with observations suggests that the applied integrated water balance and stream water temperature model LARSIM-WT is a robust tool for estimating the effect of shading on stream water temperature. However, by only considering the temperature difference between the inflowing water and reservoir stratification, we applied a rather crude approach for characterizing the inflow conditions. The plunging depth of density currents in reservoirs is known to depend on geometry of the inflow region and volumetric discharge, wind mixing and many other factors, while the plume formed by the density current is subject to dispersion (Cortés et al., 2014; Imberger & Hamblin, 1982). Moreover, the changing inflow will further change reservoir stratification, which was neglected in this study where we used observed reservoir temperature in all scenarios. In contrast, the most relevant change was the increase of overflows, where the inflowing water stays in the upper mixed layer. Because surface water temperature is mainly driven by air temperature, only minor changes of reservoir stratification are expected in this case. More realistic descriptions of density currents and projected changes in water quality in response to changing inflow temperature requires more detailed hydrodynamic modeling (e.g., Long, Ji, Liu, Yang, & Lorke, 2019; Rueda et al., 2007) and further assumptions on boundary conditions, which would make the results more accurate, but also more case specific.

Our results were obtained for a small reservoir in the tropics, which was chosen for reasons of data and model availability. Although Passaúna reservoir can be considered as being representative for a large number of impoundments in terms of reservoir size, both the effect of riparian shading on stream temperature and the inflow dynamics are affected by many factors, including catchment and reservoir size, water depth and geographic location. For example, in larger rivers (more than approximately 15–30 m wide), shading certainly has limited effect on water temperature, as only a fraction of the water surface is subject to shading by riparian vegetation (e.g., DeWalle, 2008; R. Moore et al., 2014; Regenauer et al., 2019). Given the complex and site-specific conditions of the underlying processes, a more detailed assessment of the relevance of stream shading in the catchment on the inflow regime in reservoirs requires further analysis for a broader range of reservoirs and catchments in future studies.

5 | CONCLUSIONS

Stream shading is a relevant factor for river temperature, and its alteration can significantly affect reservoirs hydrodynamics and potentially water quality. Deforestation in the catchment and the removal of tall vegetation along riparian zones of streams may lead to increased river water temperatures, as can be predicted robustly by a combined water balance and water temperature model, such as LARSIM-WT. These changes of the water temperature of inflowing rivers can be expected to lead to a degradation of water quality in the downstream reservoir due to changes in reservoir hydrodynamics. Despite rather crude assumptions with respect to the hydrodynamics at the reservoir inflow and site-specific simulations, our findings revealed a so-far overlooked mechanism by which reservoir water quality can be affected and potentially also manipulated by catchment properties and land use management. Given the potential relevance of this process for reservoir water quality, the site-specific effects of riparian shading in the catchment should be considered with more realistic approaches to the hydrodynamics at the inflow and for a broader range of reservoirs.

ACKNOWLEDGEMENTS

The German Federal Ministry of Education and Research (BMBF) provided funding for the MuDak-WRM project (grant numbers 02WGR1431 B and 02WGR1431 F). We thank the project team, in particular SANEPAR, Tobias Bleninger and the team of the Postgraduate Program in Water Resources and Environmental Engineering of the Federal University of Paraná for support during field work and for providing data.

Open access funding enabled and organized by Projekt DEAL.

CONFLICT OF INTEREST

The authors declare that there is no conflict of interest.

DATA AVAILABILITY STATEMENT

The data that support the findings of this study are openly available at https://doi.org/10.5281/zenodo.4746288.

ORCID

Mayra Ishikawa https://orcid.org/0000-0001-6680-1570
Ingo Haag https://orcid.org/0000-0001-6409-0373
Andreas Lorke https://orcid.org/0000-0001-5533-1817

REFERENCES

Akbarzadeh, Z., Maavara, T., Slowinski, S., & Van Cappellen, P. (2019). Effects of damming on river nitrogen fluxes: A global analysis. *Global Biogeochemical Cycles*, *33*(11), 1339–1357. https://doi.org/10.1029/2019GB006222

Alavian, V., Jirka, G. H., Denton, R. A., Johnson, M. C., & Stefan, H. G. (1992). Density currents entering lakes and reservoirs. *Journal of Hydraulic Engineering*, *118*(11), 1464–1489. https://doi.org/10.1061/(ASCE)0733-9429(1992)118:11(1464)

Ayala, A. I., Cortés, A., Fleenor, W. E., & Rueda, F. J. (2014). Seasonal scale modeling of river inflows in stratified reservoirs: Structural vs. parametric uncertainty in inflow mixing. *Environmental Modelling & Software*, *60*, 84–98. https://doi.org/10.1016/j.envsoft.2014.06.011

Bartholow, J. M. (2000). Estimating cumulative effects of clearcutting on stream temperatures. *Rivers*, *7*(4), 284–297.

Beaver, J. R., Manis, E. E., Loftin, K. A., Graham, J. L., Pollard, A. I., & Mitchell, R. M. (2014). Land use patterns, ecoregion, and microcystin relationships in U.S. lakes and reservoirs: A preliminary evaluation. *Harmful Algae*, *36*, 57–62. https://doi.org/10.1016/j.hal.2014.03.005

Beschta, R. L., Bilby, R. E., Brown, G. W., Holtby, L. B., & Hofstra, T. D. (1987). Stream temperature and aquatic habitat: fisheries and forestry interactions. In E. O. Salo and T. W. Cundy (eds), *Streamside Management: Forestry and Fishery Interactions*. University of Washington: Institute of Forest Resources Contribution No. 57, pp. 191–232.

Beutel, M. W., & Horne, A. J. (1999). A review of the effects of hypolimnetic oxygenation on lake and reservoir water quality. *Lake and Reservoir Management*, *15*(4), 285–297. https://doi.org/10.1080/07438149909354124

Bogan, T., Mohseni, O., & Stefan, H. G. (2003). Stream temperature-equilibrium temperature relationship. *Water Resources Research*, *39*(9), SWC 7 - 1–SWC 7 -12. https://doi.org/10.1029/2003WR002034

Broadmeadow, S., Jones, J., Langford, T., Shaw, P., & Nisbet, T. (2011). The influence of riparian shade on lowland stream water temperatures in southern England and their viability for brown trout. *River Research and Applications*, *27*(2), 226–237. https://doi.org/10.1002/rra.1354

Brown, L., Cooper, L., Holden, J., & Ramchunder, S. (2010). A comparison of stream water temperature regimes from open and afforested moorland, Yorkshire dales, northern England. *Hydrological Processes*, *24*(22), 3206–3218. https://doi.org/10.1002/hyp.7746

Bunn, S. E., & Arthington, A. H. (2002). Basic principles and ecological consequences of altered flow regimes for aquatic biodiversity. *Environmental Management*, *30*(4), 492–507. https://doi.org/10.1007/s00267-002-2737-0

Bustillo, V., Moatar, F., Ducharne, A., Thiéry, D., & Poirel, A. (2014). A multimodel comparison for assessing water temperatures under changing climate conditions via the equilibrium temperature concept: Case study of the Middle Loire River, France. *Hydrological Processes*, *28*(3), 1507–1524. https://doi.org/10.1002/hyp.9683

Caissie, D. (2006). The thermal regime of rivers: A review. *Freshwater Biology*, *51*(8), 1389–1406. https://doi.org/10.1111/j.1365-2427.2006.01597.x

Carneiro, C., Kelderman, P., & Irvine, K. (2016). Assessment of phosphorus sediment–water exchange through water and mass budget in Passaúna Reservoir (Paraná State, Brazil). *Environmental Earth Sciences*, *75*(7), 564: 1–564: 12. https://doi.org/10.1007/s12665-016-5349-3

Cortés, A., Fleenor, W., Wells, M., de Vicente, I., & Rueda, F. (2014). Pathways of river water to the surface layers of stratified reservoirs. *Limnology and Oceanography*, *59*(1), 233–250. https://doi.org/10.4319/lo.2014.59.1.0233

Crisp, D. (1997). Water temperature of Plynlimon streams. *Hydrology and Earth System Sciences Discussions*, *1*(3), 535–540.

DeWalle, D. R. (2008). Guidelines for riparian vegetative shade restoration based upon a theoretical shaded-stream model. *JAWRA Journal of the American Water Resources Association*, *44*(6), 1373–1387. https://doi.org/10.1111/j.1752-1688.2008.00230.x

Dodds, W. K., Bouska, W. W., Eitzmann, J. L., Pilger, T. J., Pitts, K. L., Riley, A. J., … Thornbrugh, D. J. (2009). Eutrophication of U.S. freshwaters: analysis of potential economic damages. *Environmental Science & Technology*, *43*(1), 12–19. https://doi.org/10.1021/es801217q.

Dugdale, S. J., Hannah, D. M., & Malcolm, I. A. (2017). River temperature modelling: A review of process-based approaches and future directions. *Earth-Science Reviews*, *175*, 97–113. https://doi.org/10.1016/j.earscirev.2017.10.009

Dugdale, S. J., Malcolm, I. A., Kantola, K., & Hannah, D. M. (2018). Stream temperature under contrasting riparian forest cover: Understanding thermal dynamics and heat exchange processes. *Science of the Total Environment*, *610*, 1375–1389. https://doi.org/10.1016/j.scitotenv.2017.08.198

Feld, C. K., Birk, S., Bradley, D. C., Hering, D., Kail, J., Marzin, A., … Friberg, N. (2011). From natural to degraded rivers and back again: A test of restoration ecology theory and practice. In W. Guy (Ed.), *Advances in ecological research* (Vol. 44, pp. 119–209). London: Academic Press. https://reader.elsevier.com/reader/sd/pii/B9780123747945000080?token=8E96FE0BB0AD040A5CF290111F952E831DFD7C7CB7817F8260900EBBC4E9CD964615ABE8AF0E32A48299FCBF7D9B21BB&originRegion=eu-west-1&originCreation=20210531130652

Friedl, G., & Wüest, A. (2002). Disrupting biogeochemical cycles-Consequences of damming. *Aquatic Sciences*, *64*(1), 55–65. https://doi.org/10.1007/s00027-002-8054-0

Garner, G., Malcolm, I. A., Sadler, J. P., & Hannah, D. M. (2014). What causes cooling water temperature gradients in a forested stream reach? *Hydrology and Earth System Sciences*, *18*(12), 5361. https://doi.org/10.5194/hess-18-5361-2014

Garner, G., Malcolm, I. A., Sadler, J. P., & Hannah, D. M. (2017). The role of riparian vegetation density, channel orientation and water velocity in determining river temperature dynamics. *Journal of Hydrology*, *553*, 471–485. https://doi.org/10.1016/j.jhydrol.2017.03.024

Garner, G., Malcolm, I. A., Sadler, J. P., Millar, C. P., & Hannah, D. M. (2015). Inter-annual variability in the effects of riparian woodland on micro-climate, energy exchanges and water temperature of an upland Scottish stream. *Hydrological Processes*, *29*(6), 1080–1095. https://doi.org/10.1002/hyp.10223

Grill, G., Lehner, B., Thieme, M., Geenen, B., Tickner, D., Antonelli, F., … Zarfl, C. (2019). Mapping the world's free-flowing rivers. *Nature*, *569*(7755), 215–221. https://doi.org/10.1038/s41586-019-1111-9

Haag, I. (2018). *Regionalisierung und Simulation der Wassertemperatur – Ergebnisse und Bewertungen*. Paper presented at the 6. KLIWA-Symposium 22. und 23. Mai 2017, Baden-Baden, Baden-Baden.

Haag, I., & Luce, A. (2008). The integrated water balance and water temperature model LARSIM-WT. *Hydrological Processes*, *22*(7), 1046–1056. https://doi.org/10.1002/hyp.6983

Hannah, D. M., Malcolm, I. A., Soulsby, C., & Youngson, A. F. (2008). A comparison of forest and moorland stream microclimate, heat exchanges and thermal dynamics. *Hydrological Processes: An International Journal*, *22*(7), 919–940. https://doi.org/10.1002/hyp.7003

Imberger, J., & Hamblin, P. F. (1982). Dynamics of lakes, reservoirs, and cooling ponds. *Annual Review of Fluid Mechanics*, *14*(1), 153–187. https://doi.org/10.1146/annurev.fl.14.010182.001101

Ishikawa, M., Bleninger, T., & Lorke, A. (2021). Hydrodynamics and mixing mechanisms in a subtropical reservoir. *Inland Waters* (accepted). https://doi.org/10.1080/20442041.2021.1932391.

Jones, J. R., Knowlton, M. F., & Obrecht, D. V. (2008). Role of land cover and hydrology in determining nutrients in mid-continent reservoirs: Implications for nutrient criteria and management. *Lake and Reservoir Management*, *24*(1), 1–9. https://doi.org/10.1080/07438140809354045

Kalny, G., Laaha, G., Melcher, A., Trimmel, H., Weihs, P., & Rauch, H. P. (2017). The influence of riparian vegetation shading on water temperature during low flow conditions in a medium sized river. *Knowledge and Management of Aquatic Ecosystems*, *418*, 5. https://doi.org/10.1051/kmae/2016037

Knoll, L., Hagenbuch, E., Stevens, M., Vanni, M., Renwick, W., Denlinger, J., … Gonzalez, M. (2015). Predicting eutrophication status in reservoirs at large spatial scales using landscape and morphometric variables. *Inland Waters*, *5*(3), 203–214. https://doi.org/10.5268/IW-5.3.812

Krumm, J., Haag, I., & Wolf, N. (2019, March 28-29). *Adaption des Wasserhaushaltsmodells LARSIM zur Anwendung bei veränderter Datenlage und unter subtropischen Bedingungen am Beispiel des Passaúna (Brasilien)*. Paper presented at the Forum für Hydrologie und Wasserbewirtschaftung, Karlsruhe, Germany.

Leg, L.-E. (2019). Das Wasserhaushaltsmodell LARSIM. Modellgrundlagen und Anwendungsbeispiele.

Lehner, B., Liermann, C. R., Revenga, C., Vörösmarty, C., Fekete, B., Crouzet, P., … Magome, J. (2011). High-resolution mapping of the world's reservoirs and dams for sustainable river-flow management. *Frontiers in Ecology and the Environment*, *9*(9), 494–502. https://doi.org/10.1890/100125

Lewis, W. M., Jr. (1983). A revised classification of lakes based on mixing. *Canadian Journal of Fisheries and Aquatic Sciences*, *40*(10), 1779–1787. https://doi.org/10.1139/f83-207

Long, L., Ji, D., Liu, D., Yang, Z., & Lorke, A. (2019). Effect of cascading reservoirs on the flow variation and thermal regime in the lower reaches of the Jinsha River. *Water*, *11*(5), 1008. https://doi.org/10.3390/w11051008

Maavara, T., Parsons, C. T., Ridenour, C., Stojanovic, S., Dürr, H. H., Powley, H. R., & Van Cappellen, P. (2015). Global phosphorus retention by river damming. *Proceedings of the National Academy of Sciences of the United States of America*, *112*(51), 15603–15608. https://doi.org/10.1073/pnas.1511797112

Moore, D. R., Spittlehouse, D. L., & Story, A. (2005). Riparian microclimate and stream temperature response to forest harvesting: A review. *JAWRA Journal of the American Water Resources Association*, *41*(4), 813–834. https://doi.org/10.1111/j.1752-1688.2005.tb03772.x

Moore, R., Leach, J., & Knudson, J. (2014). Geometric calculation of view factors for stream surface radiation modelling in the presence of riparian forest. *Hydrological Processes*, *28*(6), 2975–2986. https://doi.org/10.1002/hyp.9848

Oliveira, J. d. S. d., Wosiacki, L. F. K., Gurski, L. K. K., Prado, L. L. D., Knapik, H. G., Rauen, W. B., … Bleninger, T. (2019). *Concentração de sólidos em um reservatório de abastecimento: Do campo para o laboratório e o gestor*. Paper presented at the XXIII Simpósio brasileiro de recursos hídricos, Foz do Iguaçu - PR - Brazil. conference annals. Retrieved from http://anais.abrh.org.br/works/5863

Paerl, H. W., & Otten, T. G. (2013). Harmful cyanobacterial blooms: Causes, consequences, and controls. *Microbial Ecology*, *65*(4), 995–1010. https://doi.org/10.1007/s00248-012-0159-y

Poff, N. L., Olden, J. D., Merritt, D. M., & Pepin, D. M. (2007). Homogenization of regional river dynamics by dams and global biodiversity implications. *Proceedings of the National Academy of Sciences of the United States of America*, *104*(14), 5732–5737. https://doi.org/10.1073/pnas.0609812104

Pretty, J. N., Mason, C. F., Nedwell, D. B., Hine, R. E., Leaf, S., & Dils, R. (2003). Environmental costs of freshwater eutrophication in England and Wales. *Environmental Science & Technology*, *37*(2), 201–208. https://doi.org/10.1021/es020793k.

Regenauer, J., Haag, I., & Aigner, D. (2019). *2-Grad-Ziel für unsere Bäche – Wassertemperatur und Beschattung*. Intermediate Report on behalf of

the Environmental Agencies of the federal States of Bavaria, Baden-Württemberg, Hesse and Rhineland-Palatine

Rimsha, V. A., & Donschemko, K. (1958). Untersuchungen des Wärmeverlustes offener Wasserflächen im Winter. *Trudy GGJ*, *65*.

Rueda, F. J., Fleenor, W. E., & de Vicente, I. (2007). Pathways of river nutrients towards the euphotic zone in a deep-reservoir of small size: Uncertainty analysis. *Ecological Modelling*, *202*(3-4), 345–361. https://doi.org/10.1016/j.ecolmodel.2006.11.006

Sanepar, C. D. S. D. P. (2013). *Plano Diretor SAIC: Sistema de Abastecimento de Água Integrado de Curitiba e Região Metropolitana*. Curitiba, Curitiba: Sanepar.

Schindler, D. W. (2012). The dilemma of controlling cultural eutrophication of lakes. *Proceedings of the Biological Sciences*, *279*(1746), 4322–4333. https://doi.org/10.1098/rspb.2012.1032

Sinokrot, B. A., & Stefan, H. G. (1993). Stream temperature dynamics: Measurements and modeling. *Water Resources Research*, *29*(7), 2299–2312. https://doi.org/10.1111/j.1752-1688.2005.tb03772.x

Smith, V. H., & Schindler, D. W. (2009). Eutrophication science: Where do we go from here? *Trends in Ecology & Evolution*, *24*(4), 201–207. https://doi.org/10.1016/j.tree.2008.11.009

Søndergaard, M., Jensen, J., & Jeppesen, E. (2003). Role of sediment and internal loading of phosphorus in shallow lakes. *Hydrobiologia*, *506-509*(1-3), 135–145. https://doi.org/10.1023/B:HYDR.0000008611.12704.dd

Stott, T., & Marks, S. (2000). Effects of plantation forest clearfelling on stream temperatures in the Plynlimon experimental catchments, mid-Wales. *Hydrology and Earth System Sciences Discussions*, *4*(1), 95–104.

Trimmel, H., Weihs, P., Leidinger, D., Formayer, H., Kalny, G., & Melcher, A. (2018). Can riparian vegetation shade mitigate the expected rise in stream temperatures due to climate change during heat waves in a human-impacted pre-alpine river? *Hydrology and Earth System Sciences*, *22*(1), 437. https://doi.org/10.5194/hess-22-437-2018

Vörösmarty, C. J., McIntyre, P. B., Gessner, M. O., Dudgeon, D., Prusevich, A., Green, P., … Davies, P. M. (2010). Global threats to human water security and river biodiversity. *Nature*, *467*(7315), 555–561. https://doi.org/10.1038/nature09440

Vörösmarty, C. J., Meybeck, M., Fekete, B., Sharma, K., Green, P., & Syvitski, J. P. M. (2003). Anthropogenic sediment retention: Major global impact from registered river impoundments. *Global and Planetary Change*, *39*(1–2), 169–190. https://doi.org/10.1016/s0921-8181(03)00023-7

Walker, W. W., Jr. (1983). Significance of eutrophication in water supply reservoirs. *Journal-American Water Works Association*, *75*(1), 38–42. https://doi.org/10.1002/j.1551-8833.1983.tb05056.x

Webb, B., & Crisp, D. (2006). Afforestation and stream temperature in a temperate maritime environment. *Hydrological Processes: An International Journal*, *20*(1), 51–66. https://doi.org/10.1002/hyp.5898

Webb, B. W., Hannah, D. M., Moore, R. D., Brown, L. E., & Nobilis, F. (2008). Recent advances in stream and river temperature research. *Hydrological Processes*, *22*(7), 902–918. https://doi.org/10.1002/hyp.6994

Wells, M., & Nadarajah, P. (2009). The intrusion depth of density currents flowing into stratified water bodies. *Journal of Physical Oceanography*, *39*(8), 1935–1947. https://doi.org/10.1175/2009JPO4022.1

Wetzel, R. G. (2001). Water movements. *Limnology: Lake and river ecosystems*. San Diego: Gulf Professional Publishing.

Winton, R. S., Calamita, E., & Wehrli, B. (2019). Reviews and syntheses: Dams, water quality and tropical reservoir stratification. *Biogeosciences*, *16*(8), 1657–1671. https://doi.org/10.5194/bg-16-1657-2019

Zarfl, C., Lumsdon, A. E., Berlekamp, J., Tydecks, L., & Tockner, K. (2014). A global boom in hydropower dam construction. *Aquatic Sciences*, *77*(1), 161–170. https://doi.org/10.1007/s00027-014-0377-0

How to cite this article: Ishikawa, M., Haag, I., Krumm, J., Teltscher, K., & Lorke, A. (2021). The effect of stream shading on the inflow characteristics in a downstream reservoir. *River Research and Applications*, 1–12. https://doi.org/10.1002/rra.3821

Appendix III

Effects of dimensionality on the performance of hydrodynamic models for stratified lakes and reservoirs

Mayra Ishikawa[1], Wendy Gonzalez[2], Orides Golyjeswski[3], Gabriela Sales[3], J. Andreza Rigotti[4], Tobias Bleninger[5], Michael Mannich[5], and Andreas Lorke[1]

[1]*Institute for Environmental Sciences, University of Koblenz-Landau, Landau, Germany*

[2]*Institute for Water and River Basin Management, Karlsruhe Institute of Technology, Karlsruhe, Germany*

[3]*Graduate Program in Environmental Engineering, Federal University of Paraná, Curitiba, Brazil*

[4]*Graduate Program in Water Resources and Environmental Engineering, Federal University of Paraná, Curitiba, Brazil*

[5]*Department of Environmental Engineering, Federal University of Paraná, Curitiba, Brazil*

Please click in the following link to read the publication

https://doi.org/10.5194/gmd-15-2197-2022

Geosci. Model Dev., 15, 2197–2220, 2022
https://doi.org/10.5194/gmd-15-2197-2022

Geoscientific Model Development
Open Access
EGU

Effects of dimensionality on the performance of hydrodynamic models for stratified lakes and reservoirs

Mayra Ishikawa[1], Wendy Gonzalez[2], Orides Golyjeswski[3], Gabriela Sales[3], J. Andreza Rigotti[4], Tobias Bleninger[5], Michael Mannich[5], and Andreas Lorke[1]

[1]Institute for Environmental Sciences, University of Koblenz – Landau, Landau, 76829, Germany
[2]Institute for Water and River Basin Management, Karlsruhe Institute of Technology, Karlsruhe, 76131, Germany
[3]Graduate Program in Environmental Engineering, Federal University of Paraná, Curitiba, 82590-300, Brazil
[4]Graduate Program in Water Resources and Environmental Engineering,
Federal University of Paraná, Curitiba, 81531-990, Brazil
[5]Department of Environmental Engineering, Federal University of Paraná, Curitiba, 82590-300, Brazil

Correspondence: Mayra Ishikawa (ishikawa@uni-landau.de)

Received: 21 July 2021 – Discussion started: 20 September 2021
Revised: 28 January 2022 – Accepted: 8 February 2022 – Published: 16 March 2022

Abstract. Numerical models are an important tool for simulating temperature, hydrodynamics, and water quality in lakes and reservoirs. Existing models differ in dimensionality by considering spatial variations of simulated parameters (e.g., flow velocity and water temperature) in one (1D), two (2D) or three (3D) spatial dimensions. The different approaches are based on different levels of simplification in the description of hydrodynamic processes and result in different demands on computational power. The aim of this study is to compare three models with different dimensionalities and to analyze differences between model results in relation to model simplifications. We analyze simulations of thermal stratification, flow velocity and substance transport by density currents in a medium-sized drinking-water reservoir in the subtropical zone, using three widely used open-source models: GLM (1D), CE-QUAL-W2 (2D) and Delft3D (3D). The models were operated with identical initial and boundary conditions over a 1-year period. Their performance was assessed by comparing model results with measurements of temperature, flow velocity and turbulence. Our results show that all models were capable of simulating the seasonal changes in water temperature and stratification. Flow velocities, only available for the 2D and 3D approaches, were more challenging to reproduce, but 3D simulations showed closer agreement with observations. With increasing dimensionality, the quality of the simulations also increased in terms of error, correlation and variance. None of the models provided good agreement with observations in terms of mixed layer depth, which also affects the spreading of inflowing water as density currents and the results of water quality models that build on outputs of the hydrodynamic models.

1 Introduction

A wide variety of different numerical models have been used for simulating temperature and hydrodynamics in lakes and reservoirs, as well as the biogeochemical and ecological processes that depend on them (e.g., Dissanayake et al., 2019; Guseva et al., 2020; Wang et al., 2020; Xu et al., 2021). While the mechanistic description of underlying physical processes is similar in all models, they differ in their dimensionality, i.e., the number of spatial dimensions that are considered in the model.

One-dimensional (1D) models usually resolve the vertical direction only (water depth), while considering homogeneity of all relevant quantities along horizontal directions. They are attractive due to their easy connection to ecological and biogeochemical modules. In addition, the comparably low number of required input parameters and fast computational time allow for evaluations of scenarios and sensitivity analyses, which facilitate their application for assessing long-term dynamics and resilience of lakes and reservoirs in response to climatic, hydrological and land use changes (Bruce et al.,

2018; Sabrekov et al., 2017; Hipsey et al., 2019). Therefore, 1D models such as DYRESM (Imberger and Patterson, 1981; Hetherington et al., 2015), SimStrat (Goudsmit et al., 2002; Stepanenko et al., 2014) and GLM (Hipsey et al., 2019; Fenocchi et al., 2017; Bruce et al., 2018; Soares et al., 2019) have been extensively used in scientific and applied studies. On the other hand, detailed studies of hydrodynamic effects and spatially varying flow and transport mechanisms, such as density currents at river inflow locations, require models with a higher dimensionality. Two-dimensional (2D) models can provide additional insights into the hydrodynamics of lakes and reservoirs while keeping computational costs low when compared to 3D models. The 2D models that neglect variations in the vertical dimension, 2DH, are suitable for shallow lakes, where gradients along depth are minor, but they are mainly used for flood maps, river flows, hydraulics structures and sediment transport. Alternatively, the models that resolve the vertical dimension and one horizontal (longitudinal) dimension, 2DV, are suitable for elongated deep-water bodies where vertical thermal stratification plays a major role, e.g., CE-QUAL-W2 (Gelda et al., 2015; Kobler et al., 2018; Mi et al., 2020). Finally, three-dimensional (3D) models provide highly detailed spatial data but require larger computational effort in terms of time and storage. Regardless of their complexity, 3D models are widely applied, e.g., POM (Beletsky and Schwab, 2001; Song et al., 2004), ELCOM (Carpentier et al., 2017; Marti et al., 2011; Zhang et al., 2020) and Delft3D-FLOW (Soulignac et al., 2017; Bermúdez et al., 2018; Baracchini et al., 2020; Guénand et al., 2020).

The choice of model dimensionally often represents a trade-off between required accuracy, availability of boundary conditions and computational costs, and it depends on the objectives of the simulation, the water body characteristics and the availability of computer resources. Different models can complement each other, and model intercomparisons can significantly contribute to process understanding of the studied system, as well as to the assessment of model limitations. Within the framework of the Lake Model Intercomparison Project (LakeMIP; Stepanenko et al., 2010), the performance of different 1D models was compared for a number of reference sites, targeting also at the improvement of model parameterizations (Stepanenko et al., 2013, 2014; Thiery et al., 2014; Guseva et al., 2020). Perroud et al. (2009) compared four different 1D models, which were previously applied to small water bodies, to the large Lake Geneva, and Mesman et al. (2020) investigated the performance of three 1D models under extreme weather events like storms and heat waves. Most of the comparison among 3D models focused on systems where circulation patterns and internal waves had a major influence. For example, Huang et al. (2010) compared three 3D models for Lake Ontario, where variations in surface temperature are caused by circulation patterns and upwelling or downwelling of the thermocline. Dissanayake et al. (2019) applied ELCOM and Delft3D to simulate internal wave motions and surface currents in Upper Lake Constance. Zamani and Koch (2020) compared AEM3D and MIKE3 models in a reservoir with complex morphology.

Comparison of models with different dimensionalities is more difficult, since the interpretation of each result also depends on model considerations and simplifications. Polli and Bleninger (2019) compared water temperature simulations of a thermally stratified reservoir using MTCR-1 (1D model) and Delft3D (3D model), and they found that 1D simulations may provide similar information as 3D models in terms of thermal structure. Therefore, the study recommended one-dimensional models as a first approach for assessing reservoir stratification patterns and the application of a 3D model if the horizontal substance transport is of interest. Following the same idea, Man et al. (2021) recommended the application of a 1D model for parameter estimation that is subsequently used in 3D simulations, because of the shorter computational time of the 1D model. In their simulations the 1D model showed better agreement with measurements only for specific periods (when stratification or mixing were stable). The Geologic Survey of Israel and Tahal (Gavrieli et al., 2011) developed numerical models with three different dimensionalities for the simulation of the hydrodynamics and temperature stratification of the Dead Sea: a 1D model using the software 1D-DS-POM, a 2D laterally averaged model using CE-QUAL-W2 and a 3D model using the software POM2 K. The models were used in a complementary manner, taking advantage of their respective strengths: the 1D model was used to simulate decades in order to study future scenarios, the 2DV model was used to investigate the changes in the thermal structure of the reservoir due to changes in the multiple inflows, and the 3D model allowed for the study of currents and the 3D thermohaline structure. Nevertheless, the performance of the three different model approaches was not compared within this study and neither were comparisons with respect to velocities where shown. It is important to note that the selection of a higher dimensionality does not imply better simulation results (Wells, 2020). DeGasperi (2013) compared the performance of CE-QUAL-W2 and CH3D-Z (3D model) in simulating the water temperature of Lake Sammamish in the USA. Both models presented similar results with slightly better performance statistics for the 2DV model. Al-Zubaidi and Wells (2018) evaluated the capacity of CE-QUAL-W2 and a three-dimensional adaptation of the same software known as W3 in modeling the temperature stratification at Laurance Lake, Oregon, USA. For this study, the simulations from both models were in comparable agreement with measurements, but running the 3D model was 60 times more expensive in terms of computational time.

The aim of this study is to compare three models with different dimensionalities and to analyze the results based on the simplification of the physical processes caused by model dimensionality. We analyze simulations of thermal stratification, horizontal flow velocity and substance transport by density currents in a medium-sized drinking-water reservoir in the subtropical zone using three widely used

open-source models: GLM (1D), CE-QUAL-W2 (2D) and Delft3D-FLOW (3D). The models were run with identical initial and boundary conditions over a 1-year period. Their performance was assessed by comparing model results with measurements of temperature, flow velocity and turbulence over a 1-year period. We aim at providing a reference study for supporting the selection of models and the assessment of model accuracy, as well as at improving the mechanistic understanding of model performance at reduced dimensionality.

2 Description of the models

2.1 General Lake Model (GLM)

General Lake Model (version 3.1.8) (Hipsey et al., 2019) is a one-dimensional vertical model, freely available, and is designed to simulate the water balance and the vertical stratification of lacustrine systems. The model computes the vertical profiles of temperature, salinity and density by considering hydrological and meteorological forcing. GLM adopts a flexible Lagrangian layer structure (Imberger et al., 1978; Imberger and Patterson, 1981), which allows the layer thicknesses to change dynamically by contraction and expansion, according to density changes driven by surface heating, mixing, inflows and outflows. The number of layers is adapted throughout the simulation to maintain homogeneous properties within them, while the water volume in each layer is determined based on the site-specific hypsographic curve.

The thickness of the surface mixed layer is described in terms of a balance of turbulent kinetic energy, comparing the available energy with that required for vertical mixing. The available kinetic energy calculation considers surface wind stress, convective mixing, shear production between layers and Kelvin–Helmholtz billowing. Mixing in the deeper hypolimnion is modeled using a constant turbulent diffusivity or a derivation by Weinstock (1981), in which the diffusivity is calculated as a function of the strength of stratification (described by the Brunt–Väisälä frequency) and the dissipation rate of turbulent kinetic energy.

The general heat budget equation for the uppermost layer considers the balance of shortwave and longwave radiation fluxes and sensible and latent heat fluxes. The effect of heating or cooling by the sediment can additionally be included. The rate of temperature change in each layer is a function of the temperature gradient and of the relative area of the layer that is in contact with the bottom.

Inflows can be characterized by temperature, salinity and other scalar concentration data. Initial mixing is estimated by the inflow entrainment coefficient, which is calculated using a bottom drag coefficient and water column stability characterized by the Richardson number. The inflow Richardson number, in turn, is computed according to the channel geometry and assuming a typically small velocity and Froude number for the drag coefficient (Imberger and Patterson, 1981). Thereafter, the inflow is placed in a layer of neutral buoyancy along the water column. Thus, a new layer is created, with a thickness dependent on the inflow volume.

2.2 CE-QUAL-W2

CE-QUAL-W2 (version 3.7) (Cole and Wells, 2006) is a laterally averaged (2DV) model, resulting from the integration in one horizontal direction of the differential equations of conservation of mass, momentum and energy. It is an open-source Eulerian model using a structured orthogonal grid that uses a bathymetric map as geometry input and shortwave radiation, cloud cover, air temperature, dew point temperature, wind speed, wind direction and precipitation as meteorological forcing. Hydrodynamic output data include water temperature and longitudinal flow velocity. Laterally averaged models are based on the shallow water equations (Reynolds-averaged Navier–Stokes equations using the hydrostatic pressure assumption in the vertical, thus neglecting vertical accelerations) and are used for modeling hydrodynamics, water quality, and density stratification in lakes and reservoirs for which the transversal gradients of those properties are small compared to gradients in the longitudinal and vertical directions. The assumption of lateral homogeneity can be well suited for describing long and narrow water bodies. The equations are applied in a finite difference grid.

The default turbulence closure model (W2) uses the layer thickness as the mixing length and a formulation for the turbulent viscosity derived by Cole and Buchak (1995). It is also possible to use Nikuradse, parabolic, RNG (renormalization group) and TKE (turbulent kinetic energy, k–ε model) closure schemes. The k–ε closure is frequently used and was chosen for the study.

2.3 Delft3D-FLOW

Delft3D-FLOW (version 4.04.01) (Deltares, 2013), from now on referred to as Delft3D, is a 3D open-source software for simulating the flow and transport of constituents in water bodies. For the simulation of the hydrodynamics, the numerical algorithms behind Delft3D solve the shallow water equations (3D Reynolds-averaged Navier–Stokes equations with the hydrostatic approximation for the vertical direction). The simulation of the transport of matter and heat is achieved through the solution of the advection–diffusion equation. The mentioned equations are solved on a structured finite-difference grid using case-appropriate initial and boundary conditions. Delft3D considers user-defined (constant) background viscosities and diffusivities. They represent all forms of mixing that are not parameterized through the turbulence closure scheme. In order to calculate the heat exchange between the water surface and the air, five different heat flux models are implemented in Delft3D. Those models

consider the short- and longwave radiation balances, evaporation and sensible heat fluxes.

The spatial discretization in the horizontal plane can be performed using curvilinear or rectangular grids, with the former having variable cell size. In the vertical direction a Z- or σ-layer configuration can be employed. In the Z model, the number of layers is not constant over the basin and varies with local bathymetry.

3 Field data

Passaúna Reservoir is a drinking-water reservoir located in southern Brazil (25.50° S, 49.38° W), which has been in operation since 1990. The reservoir is around 11 km long, has 9 km^2 of surface area and has a maximum depth of 16.5 m close to its dam (Sotiri et al., 2019). The main tributary is the Passaúna River with a mean discharge of 2.4 $m^3 s^{-1}$, delivering approximately 75 % of the total inflow to the reservoir (Carneiro et al., 2016). Passaúna River enters the reservoir through a small forebay formed at the upstream region of the reservoir due to a bridge (Ferraria Bridge). This forebay has an average depth of 1 m and approximately 0.28 km^2 of area (Fig. 1). The outflows from the reservoir are the abstraction for the water treatment station, the bottom outlet at the dam (ensuring a minimum discharge of $\sim 0.4\,m^3\,s^{-1}$ in the downstream river) and the free overflow spillway. Reservoir bathymetry and its hypsographic curve were obtained from a high-resolution echo-sounder survey (Sotiri et al., 2019). The field measurements described below have been analyzed in detail in Ishikawa et al. (2021a).

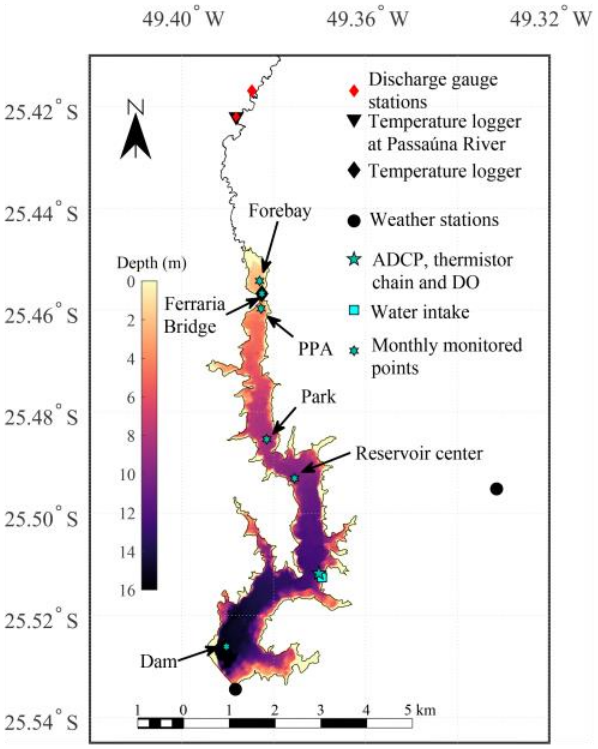

Figure 1. Bathymetric map of Passaúna Reservoir with color representing depth in meters in relation to the crest of the spillway (data provided by Sotiri et al., 2019). The inflow of the Passaúna River is in the north, upstream of a bridge forming a forebay. Monitoring stations and main facilities are marked by symbols with their respective names and/or explained in the legend.

3.1 Meteorological data

Relative humidity, downwelling shortwave radiation, wind (speed and direction at 10 m height) and dew point temperature were measured at a meteorological station located 4 km east of the reservoir. This station is operated by the Technology Institute of Paraná (TECPAR) and measured every 1 min, here averaged to 1 h. The company operating the reservoir (Sanitation Company of Paraná, SANEPAR) measured precipitation nearby the dam, and starting from May 2018, they also measured air temperature at the same location (temporal resolution of 10 min, later averaged to 1 h). Starting from this date, the air temperature data were taken from this station. Cloud cover data were downloaded from the ERA5 database from Copernicus (Hersbach et al., 2018) with hourly resolution.

Air temperature varied seasonally with a lowest monthly-mean value of 14.0 ± 4.3 °C (mean $\pm$ standard deviation of hourly time series) in August 2018 and the highest temperature in January 2019 (23.7 ± 3.6 °C). Large diel temperature variations followed the daily cycle in shortwave radiation. Wind speed was generally low with a total mean value of $2.0 \pm 1.0\,m\,s^{-1}$. A slight seasonal variation was observed where the lowest monthly averaged wind speed occurred during winter (in June 2018, $1.6 \pm 1.0\,m\,s^{-1}$) and the largest during spring (November 2018, $2.5 \pm 1.0\,m\,s^{-1}$). No seasonal pattern was observed for the remaining parameters (Fig. 2).

3.2 Inflow, outflow and water level

Daily-averaged discharge and temperature of the inflows were modeled using the Large Area Runoff Simulation Model (LARSIM-WT; Haag and Luce, 2008). The model was calibrated with data from four gauging stations (the two most downstream stations are shown on the map in Fig. 1) for the period 2010 to 2013 with a Nash–Sutcliffe efficiency of 0.77 (for further information see Ishikawa et al., 2021d). In 2018, the model underestimated the peaks of discharges but had good agreement during baseflow conditions. Simulated water temperature for the year of 2018 had a Nash–Sutcliffe efficiency of 0.96.

Starting from March 2018, a temperature logger was installed in the Passaúna River and measured inflow temperature was used instead of the simulated values (sampling resolution of 10 min, here averaged to 1 h). The measurement

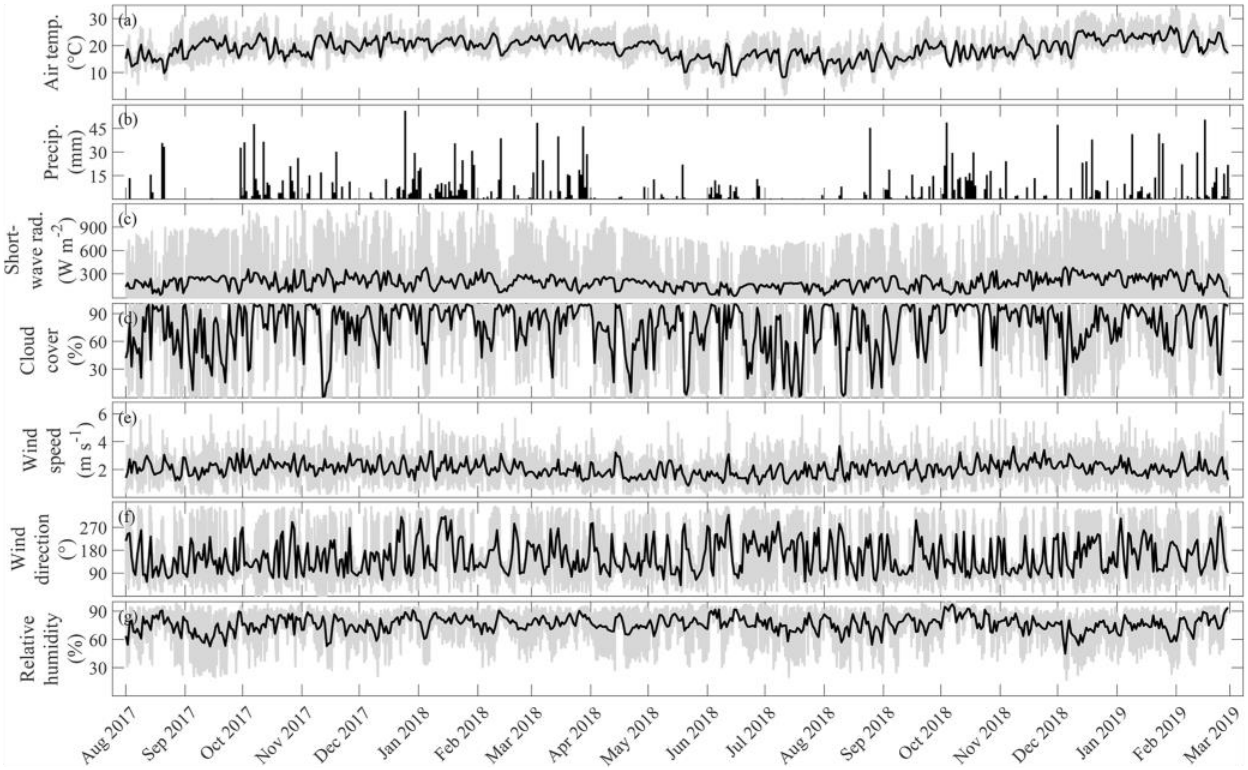

Figure 2. Time series of meteorological parameters. The gray lines show data with 1 h resolution, and black lines are daily averages. Wind direction is measured in degrees clockwise from north.

was made with an accuracy of ±0.1 °C and resolution of 0.01 °C using a temperature–oxygen sensor (miniDOT, Precision Measurement Engineering, Inc.).

Water abstraction rate at the intake facility was provided by SANEPAR, measured with an inductive flow meter, and provided at hourly resolution. The operator also provided reservoir water level measured by an ultrasonic probe in a 30 min temporal resolution. Outflow discharge at the ground outlet and the spillway were calculated based on standard hydraulic structure design equations, according to the structure's geometry. The discharge coefficients were adjusted using a few downstream discharge measurements (MuDak-WRM project; Fuchs et al., 2019) but also considering the overall water balance, where simulated inflows minus calculated outflows should correspond to the measured water level changes.

3.3 Temperature

Close to the intake facility, where the water depth is about 12 m, a thermistor chain was deployed from 1 March 2018 to 6 February 2019. The chain was fixed at the bottom and had 11 temperature loggers with 1 m vertical spacing, starting from 1 m above the bed. The loggers (Minilog-II-T, Vemco) measured at a sampling interval of 1 min with a precision of ±0.1 °C and 0.01 °C resolution. An additional logger of the same type was placed under the Ferraria Bridge, with the same configuration from 2 March 2018 to 12 August 2018. In addition, temperature profiles were collected with a CTD (conductivity–temperature–depth profiler, SonTek CastAway) at five locations along the reservoir (Fig. 1) in February, April, May, June, August, November and December 2018, as well as February 2019.

3.4 Flow velocities

An upward-looking acoustic Doppler current profiler (ADCP Signature 1000, Nortek AS) was deployed close to the thermistor chain (< 50 m distance) at the bottom of the reservoir to measure vertical profiles of flow velocity. The device was deployed and recovered for data download and battery replacement several times from 23 February 2018 to 5 February 2019. Its configuration was modified between individual deployments (Table S1 in the Supplement) to improve the data quality and also to adjust power consumption (measurement duration) to the monitoring program. Mean values of the three-dimensional flow velocities were recorded along a vertical profile starting at 0.7 m above the bed up to 1.5 m below the water surface with vertical and temporal resolution of 0.5 m and 5 or 10 min, respectively. High-resolution pro-

files of vertical velocities were used for turbulence analysis. These profiles covered a depth range of 7.4 m, starting 0.6 m above the bed with a spatial (vertical) resolution of 4 cm and a sampling frequency of 1 or 4 Hz. High-resolution data are not available for the first ADCP deployment.

4 Model setup

The simulation period started on 1 August 2017 and ended on 28 February 2019. The first 6 months were considered a spinup period for the models; it was decided to start the simulations in August when the reservoir was vertically mixed. Therefore, all models started with uniform temperature of 17 °C and water level at 887.01 m a.s.l. In addition, conservative tracers were implemented to observe the transport of substances from Passaúna River; hence, the river had a constant concentration of 1 kg m^{-3} starting from 1 August 2017.

4.1 Model calibration

Parameters that could be used for calibration are related to the exchange of heat and momentum at the water surface and include coefficients for wind drag, light extinction, and sensible and latent heat transfer. Scaling factors were not considered in the calibration process. The light extinction coefficient was intended to have a fixed value for all models based on Secchi disk depth measurements (which the average along the longitudinal and over time was 2 m, resulting in a light extinction coefficient of 0.85 m^{-1}). However, it was noticed that the results of the 2D model could be improved based on this coefficient; therefore, it was considered an additional calibration parameter.

Each model underwent a manual calibration procedure, in which the listed coefficients (see Table 1) were modified in order to reduce the mean absolute error (MAE) of the water temperature. Automatic calibration procedures are available for GLM but were not applied, and its calibration processes were similar to those of the 2D and 3D models. The specific choice of model parameters is presented in Table 1.

Each model used different time steps; nevertheless, the difference between 2D and 3D models was minor. For Delft3D, the time step was defined based on the estimation of Courant number in order to reach numerical stability. In GLM, the default time step of 1 h was used, which was applied in several other studies using the same model (e.g., Farrell et al., 2020; Gal et al., 2020; Ladwig et al., 2021). Due to the relatively large difference between the 1D and the other models, we ran the GLM model with time steps ranging from 1 to 86400 s and compared the simulations with measurements (Fig. S1 in the Supplement). The simulation results differed due to the variable number of vertical layers. The default time step had one of the smallest centered root-mean-square errors and was used for the model comparison. The usage of different time steps should not affect the comparison, once all models were stable and calibrated.

4.2 Boundary conditions

The same boundary conditions were used for all three models, with temporal resolutions according to the availability of data and model requirements. The boundary conditions are the following: air temperature, relative humidity, downwelling shortwave radiation, wind speed, wind direction, precipitation, cloud cover, outflow discharge (for water intake and continuous discharge of ground outlet), and inflow discharge and temperature. The water level at the spillway was used as a boundary condition as it represents an open boundary in the 3D model.

4.2.1 Bathymetry and grids

Bathymetric information was interpolated on the grids of Delft3D and CE-QUAL-W2, whereas GLM only used the hypsographic curve. The CE-QUAL-W2 grid was built using a QGIS 3.2 plugin developed by Bornstein (2019). It contains a maximum of 20 layers (vertical direction), two branches (longitudinal direction) and 82 segments divided among the two branches (Fig. 3b).

The Delft3D grid was built using the grid generator of Delft3D (RGFGRID). The resolution is higher in the forebay–bridge area in order to better represent the formation of density currents in this region (Fig. 3e and f). The refinement of the grid in the forebay region was made using the RGFGRID module, and where needed the bathymetry and grid was edited using the Quickin module for a better representation of the reservoir.

4.2.2 Inflow

GLM and CE-QUAL-W2 used inflow discharge and temperature with daily resolution, which was required for GLM, while the 3D model used temperatures with 10 min temporal resolution for the Passaúna River after the installation of a temperature logger.

In GLM the inflows were divided into three: the two main tributaries (Passaúna River and Ferraria River) and the 60 other minor tributaries as a single discharge, their discharges were summed up and the temperatures averaged. In CE-QUAL-W2 and Delft3D, each tributary was implemented as a single discharge at the closest respective segment or cell. The intrusion depth for CE-QUAL-W2 was defined as the layer having the same density, and for Delft3D it was uniformly distributed over depth.

4.2.3 Intake

The intake facility had withdrawal flow rates implemented in daily resolution for the 1D and 2D models and in hourly resolution for the 3D model. The abstraction of water occurred

Table 1. Specification of model parameters and settings. Coefficients indicated with ⋆ were calibrated, and default values are in parenthesis.

	GLM	CE-QUAL-W2	Delft3D
Horizontal grid	Not applicable	two branches Main branch: 72 segments Sec. branch: 5 segments Branch width: ∼ 150 m	Curvilinear Cell grids of ∼ 40 m × 40 m
Vertical grid resolution	Mixed layers scheme Maximum number of layers: 500 Min layer volume: 0.025 * Min–max: 0.1–0.5 m	Z – 20 layers 0.85 m	Z – 20 layers 0.83 m
Time step	3600 s	1 s	12 s
Computational time Specifications: Intel® Core™ i5-8400 CPU at 2.80 GHz 2.81 GHz. All source codes were written in FORTRAN	5 s	3.69 min	85.2 h
Surface heat flux approach	Longwave radiation: calculated by the model internally from the cloud cover and air temperature. Solar radiation flux: albedo calculation option 4 – sub-daily approximation	*Term-by-term model* Longwave radiation: calculated by the model internally from the cloud cover and air temperature. Solar radiation flux: albedo is calculated according to solar altitude	*Ocean heat flux model* Longwave radiation: calculated by the model as total net longwave radiation, as a function of cloud cover, relative humidity, and air and water surface temperature Solar radiation flux: constant albedo (0.06)
Evaporative heat flux approach	Estimated by the vapor pressure differences and wind-driven convection as a function of air density and pressure	Estimated by the vapor pressure differences and wind-driven convection with constant empirical coefficients	Estimated from relative humidity, summing the forced (wind dependent) and free convection of latent heat
Coefficient for latent heat transfer (–)	⋆ 0.002–(0.0013)	–	⋆ 0.0013–(0.0013)
Coefficient for sensible heat transfer (–)	⋆ 0.0015–(0.0013)	0.47 mm Hg °C^{-1} (Bowen's coeff.)	⋆ 0.0013–(0.0013)
Drag coefficient	⋆ Bulk aerodynamic transfer coefficient for momentum (–): 0.0013–(0.0013)	⋆ Wind roughness height (m): 0.001–(0.001)	⋆ Wind drag coeff. (–): Wind intensity coeff. 0–1.25 m s^{-1} 0.003 1.25–3.00 m s^{-1} 0.0025 > 3.00 m s^{-1} 0.0018
Light extinction coefficient (m^{-1})	⋆ 0.85–(0.50)	⋆ 0.50–(0.45)	⋆ 0.85–(0.85)
Heat exchange with the sediment	Neglected	Neglected	Not applicable
Turbulence closure model	Option 2: derivation by Weinstock (1981) whereby diffusivity increases with dissipation and decreases with increasing stratification	k–ε model	k–ε model

* Layer thickness is not fixed and changes within a range with daily temporal resolution.

Table 1. Continued.

	GLM	CE-QUAL-W2	Delft3D
Horizontal eddy viscosity ($m^2 s^{-1}$)	Not applicable	⋆ 1.0–(1.0)	⋆ Background 0.0–(10)
Horizontal eddy diffusivity ($m^2 s^{-1}$)	Not applicable	⋆ 1.0–(1.0)	⋆ Background 0.0–(10)
Vertical eddy viscosity ($m^2 s^{-1}$)	Molecular kinematic viscosity of water: 1.14×10^{-6}	⋆ Maximum 1.0–(1.0)	⋆ Background 0.0–(10^{-6})
Vertical eddy diffusivity ($m^2 s^{-1}$)	–	–	⋆ Background 0.0–(10^{-6})
Bottom friction	–	Manning 0.035	Manning 0.035

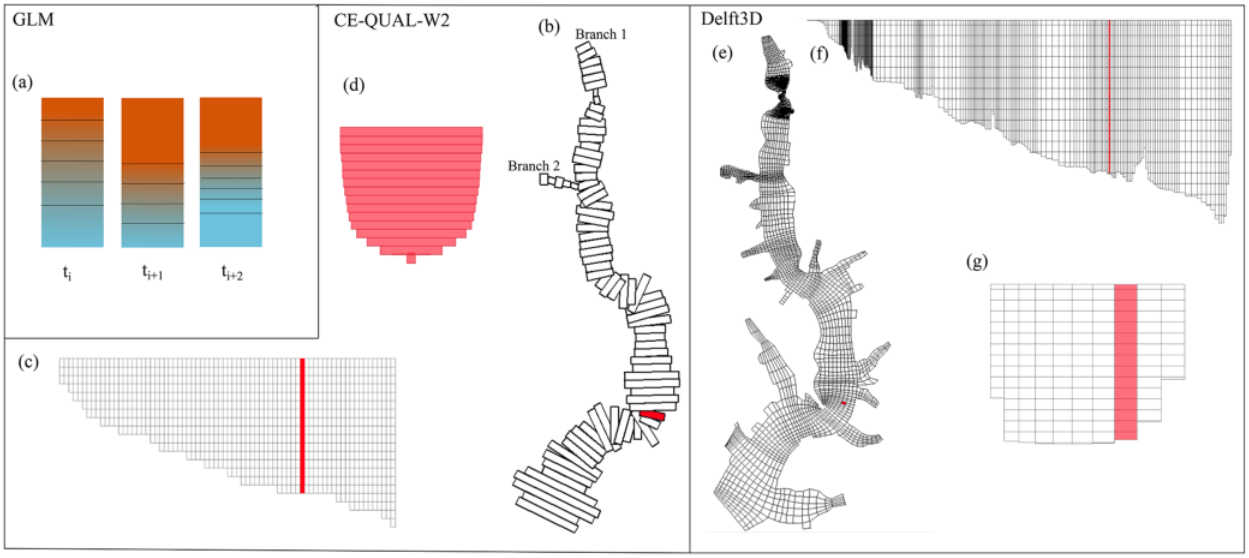

Figure 3. Overview of grids. **(a)** Representation of GLM cells (vertical layers) that expand or contract according to mixing, thus changing their total number during simulations. CE-QUAL-W2 grid in **(b)** top view, **(c)** longitudinal view and **(d)** transversal view of the marked segment in panel **(b)**. Delft3D grid in **(e)** top view, **(f)** longitudinal view and **(g)** transversal view. Red background represents the cells that were used for comparison with monitoring data near the intake station.

close to the surface; therefore, for GLM and CE-QUAL-W2, the abstraction level was set up as 885 m a.s.l., and the surface cell was defined for Delft3D. The abstraction location was defined for the 2D and 3D models, and for the 1D model only the level was required.

4.2.4 Ground outlet

The ground outlet flow rate was almost constant ($0.44 \pm 0.07\ m^3 s^{-1}$) over the simulation period, as there were only a few gate operations, and small water level variations. This flow rate was abstracted from all models in a daily temporal resolution. Similar to the intake withdrawal, GLM required as additional information the level of the outlet (872 m a.s.l.). For CE-QUAL-W2 and Delft3D, the second deepest cell was selected.

4.2.5 Spillway

The spillway was set up as an open boundary in the three models. For GLM and CE-QUAL-W2, its discharge was computed through the following equations:

$$Q_{\text{spillway}} = \alpha \Delta h^{1.5}, \quad (1)$$

where Q_{spillway} ($m^3 s^{-1}$) is the volumetric flow over the spillway, and Δh (m) is the difference between water level and

spillway crest. For GLM, α was calculated as

$$\alpha = 2/3 C_{\mathrm{Dspill}} \sqrt{2g} W_{\mathrm{spill}}, \quad (2)$$

which depends on spillway width, $W_{\mathrm{spill}} = 60$ m, and associated drag coefficient $C_{\mathrm{Dspill}} = 0.62$, and g is the acceleration due to gravity ($\mathrm{m\,s^{-2}}$), while in CE-QUAL-W2 it was defined as an empirical coefficient = 110.3.

For Delft3D, this open boundary was defined as water level dependent, where the measured water levels were applied in temporal resolution of 30 min. The outflow discharge thus depends on the water level and the bathymetry at the open boundary grid cells.

4.2.6 Shorelines, bed and water surface

Shorelines and bed are considered to be closed boundaries with no-flux condition. For Delft3D and CE-QUAL-W2, a uniform roughness coefficient was specified at the bed (Table 1). Surface heat fluxes are described in Table 1, and wind direction was not used in the 1D model. Precipitation was uniformly distributed over the water surface.

4.2.7 Meteorological data

GLM and CE-QUAL-W2 used meteorological data with a temporal resolution of 1 h. For GLM, this resolution is equivalent to the minimum time step. For Delft3D, meteorological data with 10 min temporal resolution were used.

5 Indices for comparison

To compare model simulations to observations, the following parameters were calculated for the cells being closest to the sampling location. For CE-QUAL-W2, segment 55 was selected (indicated in Fig. 3a–c); for Delft3D, cell [193, 28] was selected (Fig. 3d–f), and for GLM the first 12 m of depth was selected. Simulated values were linearly interpolated to match with the sampling depths, and indices were calculated only for the period of interest: 1 March 2018 to 28 February 2019.

The assessed variables were water level, spillway discharge, evaporation rate, water temperature, flow velocities, energy dissipation rates and substance transport. Variables that required additional processing for the analysis are described below; otherwise, the variables were assessed through time series provided by the models.

5.1 Statistics

The model simulations were compared with observations in terms of mean absolute error (MAE), centered root-mean-square error (cRMSE), standard deviation (σ), correlation coefficient (R) and coefficient of determination (r). These parameters were calculated as follows:

$$\mathrm{MAE} = \frac{1}{n}\sum_{i=1}^{n}(s_i - m_i), \quad (3)$$

$$\mathrm{cRMSE} = \sqrt{\frac{1}{n}\sum_{i=1}^{n}[(s_i - \overline{s}) - (m_i - \overline{m})]^2}, \quad (4)$$

$$\sigma = \sqrt{\frac{1}{n-1}\sum_{i=1}^{n}(a_i - \overline{a})^2}, \quad (5)$$

where n is the number of observations, a_i is one observation and $\overline{a}$ is the mean of all samples (measured or simulated).

$$R = \frac{\frac{1}{n}\sum_{i=1}^{n}(s_i - \overline{s})(m_i - \overline{m})}{\sigma_{\mathrm{s}}\sigma_{\mathrm{m}}}, \quad (6)$$

where s denotes the simulated value and m the measured value.

$$r^2 = 1 - \frac{SS_{\mathrm{res}}}{SS_{\mathrm{tot}}}, \quad (7)$$

where SS_{res} is the sum of the squared residuals, and SS_{tot} is the sum of squared data.

Taylor diagrams (Taylor, 2001) are used to assess the simulation results of the vertical temperature distribution. The diagram provides a concise overview of results through comparison with observations in terms of standard deviation (σ), correlation coefficient (R) and centered root-mean-square error (cRMSE) in one plot.

In addition, descriptive statistics (mean, standard deviation, percentiles and percentage differences) were calculated to compare simulated and observed values.

5.2 Mixing and stratification

Following Ishikawa et al. (2021a), the water column was classified as mixed or stratified based on a threshold of the Schmidt stability (S_{T}). Days with daily-averaged Schmidt stability equal or lower than 10 % of the annual maximum Schmidt stability (calculated with the measured data as $16.3\,\mathrm{J\,m^{-2}}$) were considered mixed, while days with higher S_{T} were classified as stratified.

Schmidt stability was calculated using the software Lake Analyzer (Read et al., 2011) as

$$S_{\mathrm{T}} = \frac{g}{A_{\mathrm{S}}}\int_0^{z_{\mathrm{D}}}(z - z_{\mathrm{v}})\rho_z A_z \mathrm{d}z, \quad (8)$$

where g ($\mathrm{m\,s^{-2}}$) is the gravitational acceleration, A_{S} is the reservoir surface area, A_z is the area at depth z, ρ_z is the water density at depth z, z_{D} is the maximum depth and z_{v} is depth of the reservoir center of volume calculated as $z_{\mathrm{v}} = \int_0^{z_{\mathrm{D}}} z A_z \mathrm{d}z / \int_0^{z_{\mathrm{D}}} A_z \mathrm{d}z$.

The thickness of the upper mixed layer (UML) was also computed by Lake Analyzer using a threshold for the vertical density gradient, which depends on the density gradient of the entire water column (see Read et al., 2011, for details).

5.3 Temperature

Due to the dynamic mixed layers of GLM, its results were linearly interpolated for each 0.5 m over depth. To calculate errors, the measured temperatures correspondent to the timestamp of simulation results were selected, and simulation results were linearly interpolated to match with the observations over depth. This procedure was followed for the three models.

5.4 Flow velocities

CE-QUAL-W2 provided one horizontal velocity component (longitudinal velocity), being positive in the downstream direction and negative in the upstream direction. To compare flow velocities, the longitudinal component of Delft3D and the measurements were computed by aligning the flow in the same direction as the 2D model; thus, the transversal velocity component was not considered in our analysis.

5.5 Density currents and substance transport

Water from inflowing rivers can take different flow paths after entering the reservoir, which are affected by density stratification in the reservoir and inflow conditions. Density-driven inflows can be classified as underflows, interflows, or overflows, where the first is spreading along the reservoir bottom, the second at an intermediate water depth and the last at the reservoir surface.

Substance transport in models was analyzed by simulating the transport of a conservative tracer that was added continuously to the inflowing water. Tracer concentrations at the intake region were assessed to observe substance transport from the Passaúna River to the monitoring site through vertical profiles of the daily maximum value of tracer concentration. The GLM model was set up with a maximum water depth of 17 m, while the water depth at the point of analysis was ~ 12 m. For this reason, we present model outputs up to a maximum depth of 12.5 m. If the maximum tracer concentration was below this depth, the inflow regime was categorized as underflow. For CE-QUAL-W2 and Delft3D, the closest cell to the station was selected, which represents the actual water depth at the monitoring site.

6 Results

6.1 Water level and water storage

At the end of the simulation period, all three models presented a lower water level than the measured. The last measurement was 886.81 m a.s.l., and the closest value simulated was in Delft3D with 886.49 m a.s.l., which was also the one with the lowest error (MAE = 7.4 cm). GLM simulated a final water level of 886.44 m a.s.l., and CE-QUAL-W2 estimated 886.36 m a.s.l., with respective MAE values of 10.5 and 10.8 cm (Fig. S2a in the Supplement). Additional statistical metrics are presented in the Supplement (Table S2).

The largest discrepancies in water level occurred when it raised over the spillway crest. GLM and Delft3D had water above the crest for a longer period than observed, and their levels kept being larger than the measurements until a sharp increase in October 2018, which none of the models reproduced. Total spillway discharge had its largest volume in CE-QUAL-W2: 2.93×10^7 m^3, GLM had a spillway volume as the 2D model of 2.87×10^7 m^3, and Delft3D simulated 3.7 % less spillway discharge than CE-QUAL-W2 (2.83×10^7 m^3) (Fig. S2b).

Evaporation values in all models were in the same order of magnitude but significantly different (one-way ANOVA test with p value $= 5 \times 10^{-17}$, with the null hypothesis that both pieces of data have the same mean). The 1D, 2D and 3D model estimated daily-mean evaporation rates were 2.9 ± 1.3, 2.7 ± 1.0 and 3.4 ± 1.4 mm d^{-1}, respectively. Comparing the volumes due to evaporation with the reservoir volume (7.0×10^7 m^3), over the year GLM lost the equivalent of 12.0 % of the reservoir volume, CE-QUAL-W2 with the lowest evaporation rate lost 11.0 % and Delft3D lost 14.3 %.

6.2 Temperature

6.2.1 Vertical profile at the intake region

From the measurements made with the thermistor chain, it was observed that the reservoir was thermally stratified at the beginning of the monitoring period (end of summer). The first autumn overturn took place in mid-April, but after a few days the reservoir became stratified again. These dynamics of mixing and stratification repeated several times throughout autumn and winter, characterizing a warm polymictic mixing regime (Lewis, 1983; Ishikawa et al., 2021a). Thermal stratification developed in spring and persisted throughout the summer.

The observed seasonal pattern of stratification and mixing was reproduced by all three models (Fig. 4). At the water surface, simulated temperatures were highly correlated with observations with comparable correlation coefficient (> 0.99) for all three models (Fig. 5b). The net surface heat fluxes simulated by the models were not statistically different (p value $= 0.14$, one-way ANOVA test with null hypothesis that the two groups have the same mean). Observed water surface temperature was 21.6 ± 3.5 °C (mean value and standard deviation) for the whole period. In the simulations, surface temperature was 22.2 ± 4.0 °C in GLM, 21.1 ± 3.7 °C in CE-QUAL-W2, and 22.4 ± 3.7 °C in Delft3D. With increasing depth, the error increased, and the correlation between

measured and simulated temperatures decreased (Fig. 5). In the deepest layer, temperature was on average 19.1 ± 2.0 °C, while GLM, CE-QUAL-W2 and Delft3D simulated 18.6 ± 2.2, 18.2 ± 2.3 and 19.3 ± 2.3 °C, respectively.

In the 2D model, errors increased rather continuously with increasing depth, showing maximum cRMSE of 0.6 °C at around 10.5 m depth. Meanwhile, GLM and Delft3D showed the largest errors around the middle of the lower half of the water column, GLM at a depth of 6.7 m with cRMSE of 0.94 °C, and Delft3D at around 8.6 m depth with an error of 0.6 °C.

The average water temperature in the GLM simulations was about 0.5 °C warmer at the surface and colder at the bottom, which lead to stronger thermal stratification than in the observations. CE-QUAL-W2 simulated lower temperatures at the surface and bottom (-0.5 and -0.9 °C, respectively), and Delft3D estimated warmer temperatures at surface and bottom ($+0.8$ and $+0.2$ °C, respectively).

According to the classification based on Schmidt stability, Passaúna Reservoir was mixed on 95 d out of 343 d of the monitoring period, with the longest continuous period of mixing from 8 May to 20 June 2018 (Fig. 6a). In GLM, stratification was generally more stable and the reservoir was classified as mixed only on 68 d. Periods with homogeneous temperature were shorter and discontinuous, and the last mixing event in early September was not resolved by the model. The simulated Schmidt stability was strongly correlated with those estimated from observations (Pearson's correlation coefficient with null hypothesis of no relationship, $R = 0.98$, p value $= 0$); however, it was overestimated by a factor of 1.64 on average (Fig. 6b). CE-QUAL-W2 provided the closest match of the number of mixed days with observations (95 d). Due to the lower simulated bottom temperature, the Schmidt stability was overestimated by a factor of 1.19 on average (Fig. 6c), but simulations and observations were highly correlated ($R = 0.95$, p value $= 0$). During the mixed season, the intermittent stratification was attenuated in the 2D model, and the mixed periods were slightly longer. Delft3D had the best correlation and a lower overestimation of Schmidt stability than GLM ($R = 0.98$, p value $= 0$, factor of 1.12), however the number of mixed days in the simulations was underestimated by about 25 % (72 mixed days) (Fig. 6c).

The upper mixed layer (UML) depths estimated from measurements were compared to UMLs estimated for each model, and all of them presented poor coefficient of determination ($r^2 < 0.6$) for linear regressions (Pearson's correlation coefficients with null hypothesis of no relationship are the following: for 1D $R = 0.42$, for 2D $R = 0.33$, and for 3D $R = 0.68$, and all had p value $= 0$ – see Fig. S3 in the Supplement). GLM and Delft3D presented rather thinner UMLs, whilst CE-QUAL-W2 had a larger variance, ranging between deeper and shallower UMLs.

The Taylor diagram presented in Fig. 7 was calculated for temperature simulations throughout the entire period, and all depths demonstrate that the three models had good correlations (> 0.95) and similar standard deviations of residuals (all models had a standard deviation lower than 0.5 °C for residuals of the difference between measured and simulated temperature). The cRMSE had the most significant differences between models, with Delft3D as the closest to observations (0.50 °C), followed by CE-QUAL-W2 (0.56 °C) and GLM (0.84 °C).

6.2.2 Longitudinal temperature variations

To compare temperature simulations along longitudinal cross-sections of the reservoir, CTD profile measurements were interpolated and compared with simulations of the 2D and the 3D model (Fig. 8). The models were capable of reproducing the different temperature distributions during the sampling dates. In February 2018 and 2019, the reservoir was stratified in the upstream region with a growing UML along its longitudinal axis. During the remaining surveys in August, November and December 2018, the reservoir showed different patterns of vertical stratification with only minor longitudinal variations. Similar to the mean temperature analyzed above, CE-QUAL-W2 had colder temperatures, while Delft3D had higher temperatures, and both had a comparable strength in stratification and were in agreement with the measurements.

As the 1D model considers horizontally averaged temperature, the temperature profiles measured along the longitudinal cross-section of the reservoir were averaged for the comparison with GLM simulations (Fig. 9). The simulations were generally in good agreement with the averaged temperature profile. The best agreement occurred in August 2018, when the reservoir was mixed. In November 2018 and February 2019, the low water temperature in the upstream part of the reservoir affected the surface temperature of the averaged profiles, leading to a greater difference compared to the simulations.

In addition, simulated temperatures from the 2D and 3D models were horizontally averaged and compared to the continuous temperature profile observed at the intake. The cRMSE values of both were very similar to the original comparison with the closest segment or cell to the monitoring station (Fig. S4 in the Supplement). The similarity with the original comparison can be explained by the fact that a large part of the reservoir was indeed homogeneous over the horizontal (approximately until 5000 m of distance from the dam) and had a comparable water depth as at the monitoring station.

6.3 Hydrodynamics

6.3.1 Flow velocities

The total averaged horizontal flow velocity (the magnitude of the horizontal velocity components averaged in time and

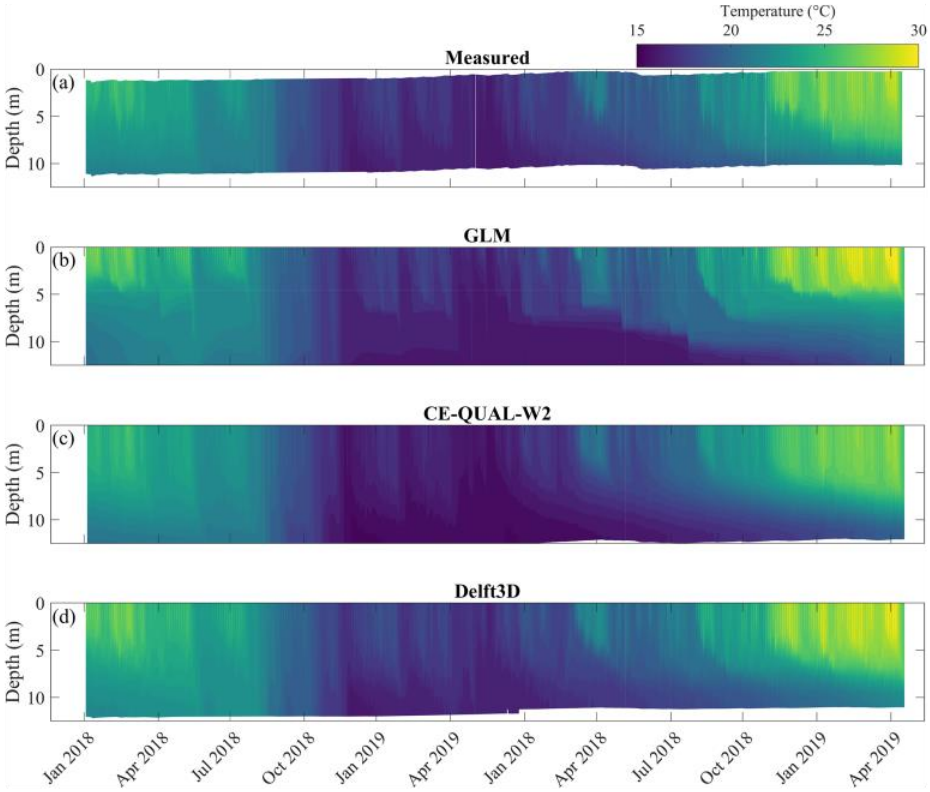

Figure 4. Contour plots of vertical temperature profiles at the location of the thermistor chain near the intake region of the reservoir (Fig. 1). **(a)** Measured temperature with $\Delta t = 1$ h and $\Delta z = 1$ m; **(b)** simulation result of GLM ($\Delta t = 1$ h and $\Delta z = 0.5$ m); **(c)** simulation result of CE-QUAL-W2 ($\Delta t = 1$ h and $\Delta z = 0.85$ m); **(d)** simulation result of Delft3D ($\Delta t = 1$ h and $\Delta z = 0.83$ m).

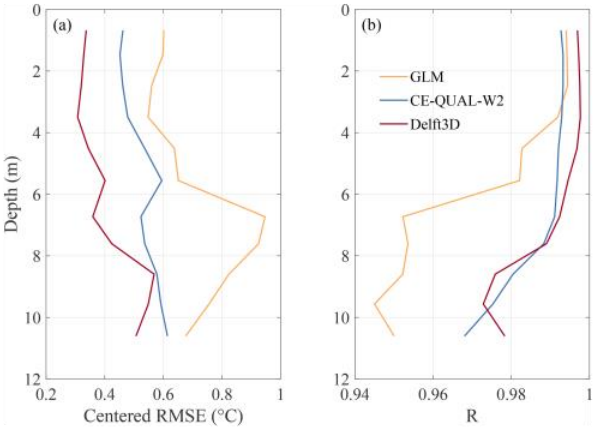

Figure 5. Performance of temperature simulations from GLM, CE-QUAL-W2 and Delft3D for the intake region. Panel **(a)** shows the centered root-mean-square error (cRMSE), and panel **(b)** shows the correlation coefficient (R) along depth for each model.

over depth) was around $2\,\mathrm{cm\,s^{-1}}$. Following the analysis of hydrodynamics in Passaúna Reservoir in Ishikawa et al. (2021a), flow velocities larger than $3.5\,\mathrm{cm\,s^{-1}}$ ($\sim$ 90th percentile) were defined as currents. They were forced by wind and had the upper part of the water column flowing towards an opposite direction as the lower part (see Fig. 10a–d). The currents, and consequently the total averaged flow velocity, were significantly (p value $= 1 \times 10^{-181}$, with null hypotheses of both having a similar distribution) more frequent and more intense during stratified periods when compared to mixed periods. The same analysis, only considering the magnitude of the longitudinal component, was made for the 2D and 3D simulation results (Table 2).

For the total period and all depths, CE-QUAL-W2 had a cRMSE $= 2.1\,\mathrm{cm\,s^{-1}}$ and a negative correlation coefficient with observations (-0.04, p value $= 4 \times 10^{-40}$, with null hypothesis of no relationship), while Delft3D had cRMSE $= 1.7\,\mathrm{cm\,s^{-1}}$ and correlation coefficient of 0.50 (p value $= 0$). The two models had errors in the same order of magnitude, but the simulations of the 2D model had a lower standard deviation ($0.8\,\mathrm{cm\,s^{-1}}$), while the 3D simulations had a standard deviation closer to the observed value ($1.4\,\mathrm{cm\,s^{-1}}$, being the observed $1.9\,\mathrm{cm\,s^{-1}}$). Both models showed the largest er-

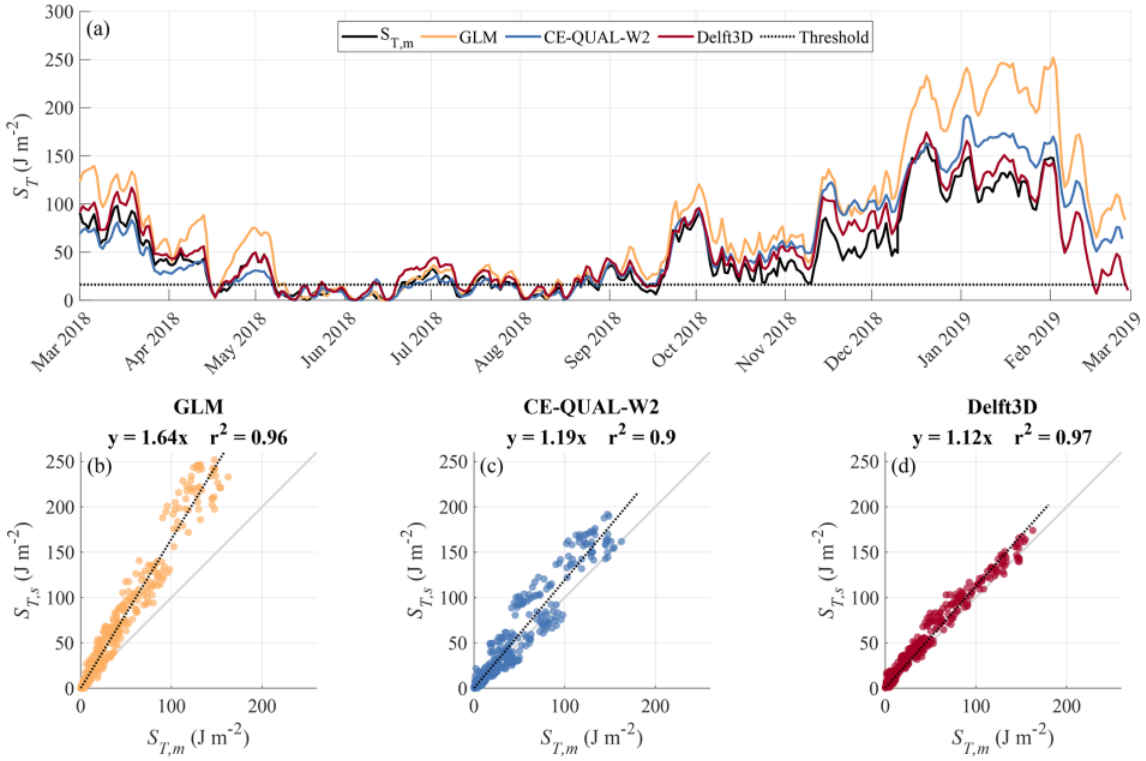

Figure 6. **(a)** Time series of daily-averaged Schmidt stability (S_T) estimated from observed ($S_{T,m}$) and simulated ($S_{T,s}$) temperature stratification. The dotted line marks the threshold ($S_T = 16.3\,J\,m^{-2}$) used to classify mixed and stratified conditions. Comparison between S_T estimated from measurements and simulation results; linear regression with zero intercept (black dashed lines) equations and coefficient of determination (r^2) are provided as panel title for **(b)** GLM, **(c)** CE-QUAL-W2 and **(d)** Delft3D.

Table 2. Comparison of magnitude of longitudinal flow velocities (mean ± standard deviation) between measurements and simulations. Measurements and processing are described in Ishikawa et al. (2021a).

	Period	Currents ($cm\,s^{-1}$), i.e., mag. of long. vel. > 90th percentile	Total longitudinal vel. ($cm\,s^{-1}$), i.e., all mag. of long. vel.	Relative occurrence of currents
Measured	Mixed	4.0 ± 0.7	1.3 ± 1.0	6.4 %
90th percentile: 3.1	Stratified	4.4 ± 1.2	1.5 ± 1.3	10.8 %
	Total	4.3 ± 1.2	1.5 ± 1.3	
CE-QUAL-W2	Mixed	2.4 ± 0.6	0.9 ± 0.8	14.9 %
90th percentile: 1.8	Stratified	2.4 ± 0.7	0.7 ± 0.7	9.0 %
MAE: 1.7, cRMSE: 2.1	Total	2.5 ± 0.8	0.8 ± 0.8	
Delft3D	Mixed	3.3 ± 1.0	0.9 ± 0.9	7.3 %
90th percentile: 2.4	Stratified	3.5 ± 1.1	1.1 ± 1.1	10.7 %
MAE: 1.3, cRMSE: 1.7	Total	3.5 ± 1.1	1.1 ± 1.0	

rors at the surface, where the 3D model is closer to the observations than the 2D model (Fig. 11). In contrast to the temperature simulations, the simulated flow velocities had the smallest errors near the bottom. Despite the comparable magnitude of cRMSE of both models, the correlation between simulated and observed velocities differed remarkably (Fig. 11b). While it was generally low (< 0.1) and fluctuated around zero along the water column for CE-QUAL-W2, it varied between 0.4 and 0.6 for Delft3D.

The longitudinal velocities of CE-QUAL-W2 had a 90th percentile of $1.8\,cm\,s^{-1}$ and a MAE of $1.7\,cm\,s^{-1}$, its total mean value was $0.8\,cm\,s^{-1}$, and it is possible for the wind in-

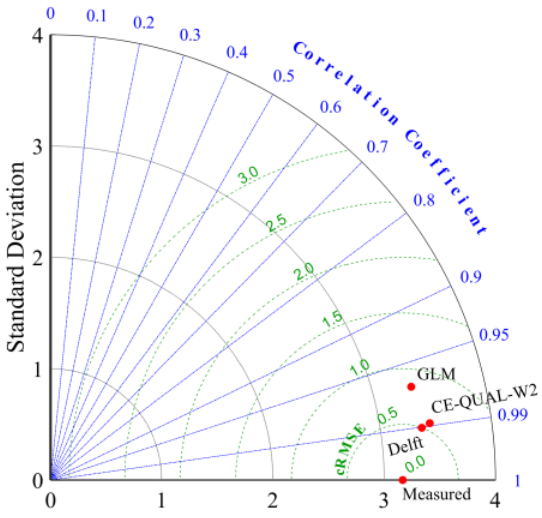

Figure 7. Taylor diagram of the total simulated period of temperature profiles at the intake region. Green lines indicate centered root-mean-square error (cRMSE) isolines. Angular coordinate, in blue, represents the correlation coefficient (R). Standard deviation (black dashed line) is represented in radial coordinate with the reference measured data in center. Measured is the baseline where correlation is 1 and cRMSE is zero. The red dots represent model performance.

fluence on formation of currents to be observed (Fig. 10a, b, e and f). The occurrence of currents differed between mixed and stratified conditions and were statistically different (p value $= 0$, Kruskal–Wallis test with null hypothesis that the two groups are from the same distribution). Their relative occurrence was larger during mixed conditions, which is the opposite from that observed. In general the simulated flow velocities were lower than observed velocities. For Delft3D, MAE was 1.3 cm s^{-1}, and its longitudinal velocities were in general lower than observed with a total average of 1.1 cm s^{-1} and 90th percentile of 2.4 cm s^{-1}. As in the observations, the occurrence of currents was significantly different (p value $= 2.98 \times 10^{-285}$) between mixed and stratified conditions. The simulated currents presented clear opposing directions of flow between upper and lower depths (Fig. 10g and h). In addition, their relative occurrence was within 1 % difference from the observed data.

6.3.2 Turbulence

Only Delft3D provided simulated energy dissipation rates (ε). The estimation of ε based on measurements is described in Ishikawa et al. (2021a), and due to the limited measurement range of the high-resolution mode of the ADCP, estimations were only made up to 8 m height above the bed.

Observed energy dissipation rates were basically the same during mixed and stratified conditions (respective log averages along depth and time: 7.5 and 5.5×10^{-10} W kg^{-1}). In Delft3D, ε was approximately 1 order of magnitude larger at mid-depth under mixed conditions. Log-averaged dissipation rates for the depth range with observations were 8.0×10^{-10} W kg^{-1} under mixed and 1.0×10^{-10} W kg^{-1} under stratified conditions (Fig. 12a and b).

While simulations from Delft3D had log-averaged profiles with higher ε towards the bed, the estimations only had the same trend during the presence of currents (magnitude of longitudinal velocities $>$ 90th percentile). The increase for the estimations started around 3 m above the bed; for simulations, the flow velocities under the current threshold also had ε increasing towards the bottom, and in the presence of currents ε started to be larger at around 6 m above the bed (Fig. 12c and d).

6.3.3 Density currents and substance transport

The models had similar overall distributions until August 2018 (Fig. 13). The tracer transport changed from interflows to underflows (or to deeper interflows) after the first autumn overturn, with differences at the depth of daily-averaged maximum concentrations.

Underflows and interflows at greater depths were predominant in autumn and winter and overflows and interflows closer to the surface were more frequent in spring and summer. GLM predicted interflows with the maximum concentrations at shallower depths than the other models from March to mid-April. After this time, GLM and Delft3D simulations showed underflows more frequently, while CE-QUAL-W2 results had the interflows moved to deeper regions and presented less underflows when compared to the 1D and 3D models. Starting from August 2018, the maximum concentration of the tracer showed different patterns in each model. In the 1D simulations, underflows persisted until the middle of October, and after that interflows formed at $\sim$ 5 m depth. In the 2D simulations, the inflow formed interflows at a slightly deeper depth ($\sim$ 7 m), while maximum tracer concentrations were widely scattered over the upper water column in the 3D simulations, with their lower bound following the 2D simulations (Fig. 13).

We calculated the relative frequency of occurrence of each flow path by assigning overflows when the maximum concentration was at the water surface (uppermost depth cell), underflows when it was at the bottom (lowest depth cell or deeper than 12 m for GLM) and interflows otherwise. For GLM, there were no overflows, while for most of the time underflows were observed (57.6 %) and interflows for the remaining time. For CE-QUAL-W2 and Delft3D, interflows were the most frequent, with 75.1 % for the 2D model and 67.1 % for the 3D model; overflows and underflows were almost equally distributed for Delft3D, with, respectively, 14.9 % and 18.0 %, and CE-QUAL-W2 simulated more frequent underflows (21.4 %) than overflows 3.5 %.

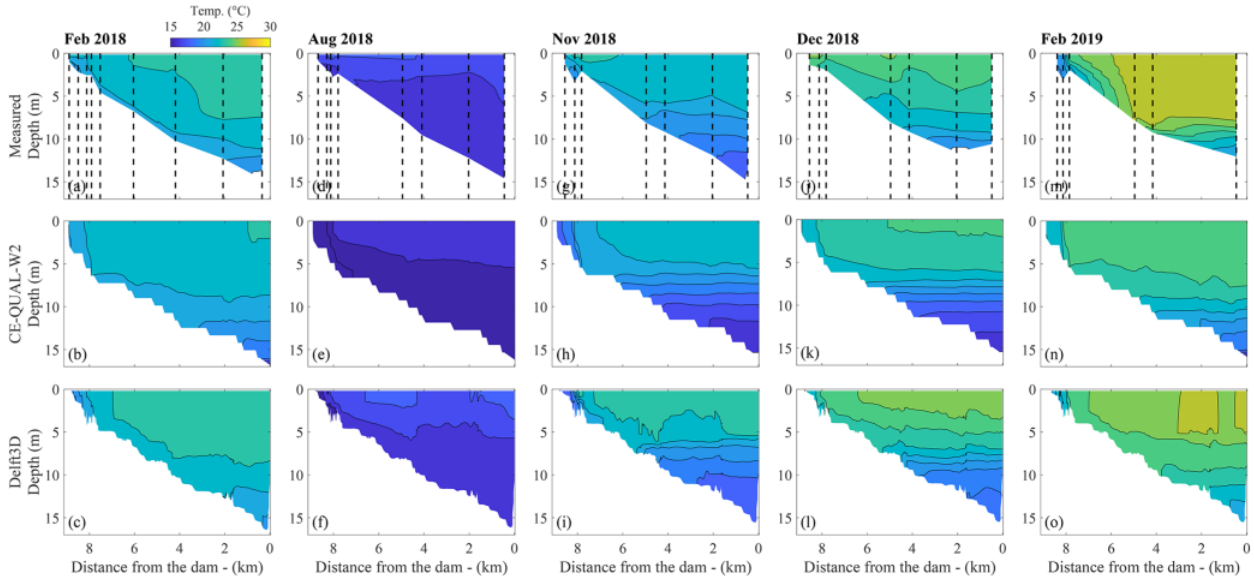

Figure 8. Contour plots of temperature along a longitudinal cross-section of the reservoir from the forebay to the dam. Each column represents one sampling campaign; the first row shows the measurements (interpolated from vertical CTD profiles at locations marked by the dashed vertical lines). The second row shows the simulation results of CE-QUAL-W2 for which we show every segment of the grid and all the respective depth cells. The third row of panels shows simulation results from Delft3D; a way along the thalweg of the reservoir was drawn by selecting several grid cells, and the entire depth of each cell was used.

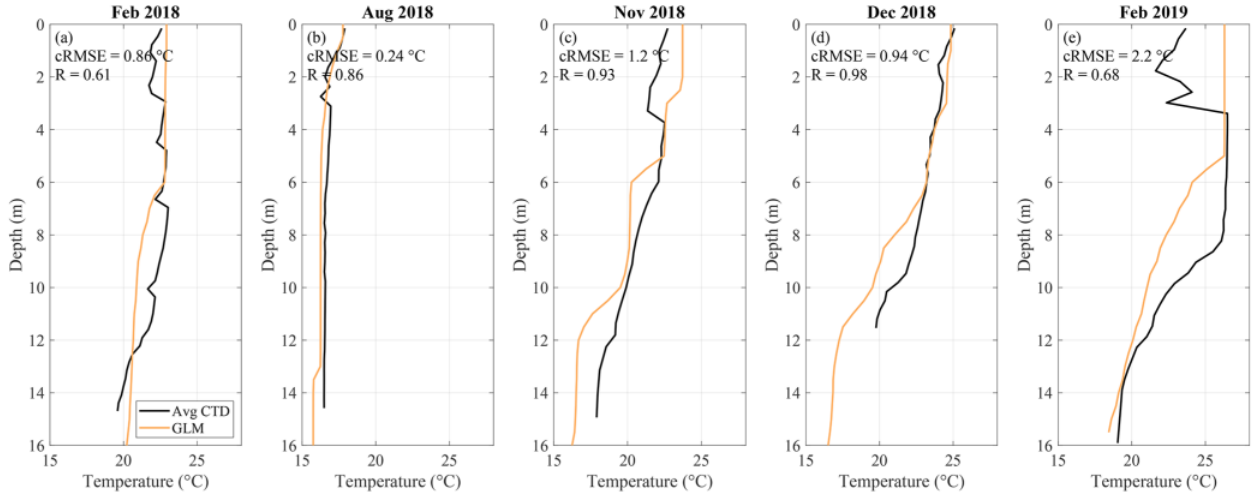

Figure 9. Comparison of spatially averaged temperature measurements with 1D (GLM) model simulations for different sampling days **(a–e**, sampling month is provided at the top of each panel**)**. The black lines show horizontally averaged profiles measured with a CTD, and the orange line shows GLM simulations. The respective errors and correlation coefficients are provided in each panel.

7 Discussion

7.1 Water storage

Regarding the water balance, all models had errors of comparable magnitude: 1D, 2D and 3D models had errors in stored water volume of −4.4 %, −4.9 % and −3.7 %. The error in terms of water level was similar for all models (∼ 10 cm) and is in the range of errors reported in the literature (e.g., Dai et al., 2013; Jeznach et al., 2014; Chen et al., 2016; Bueche et al., 2020). GLM had a constant water level from January to May 2018, corresponding to the maximum level defined by the hypsographic curve due to the spillway crest elevation. CE-QUAL-W2 had lower water levels and a larger discharge

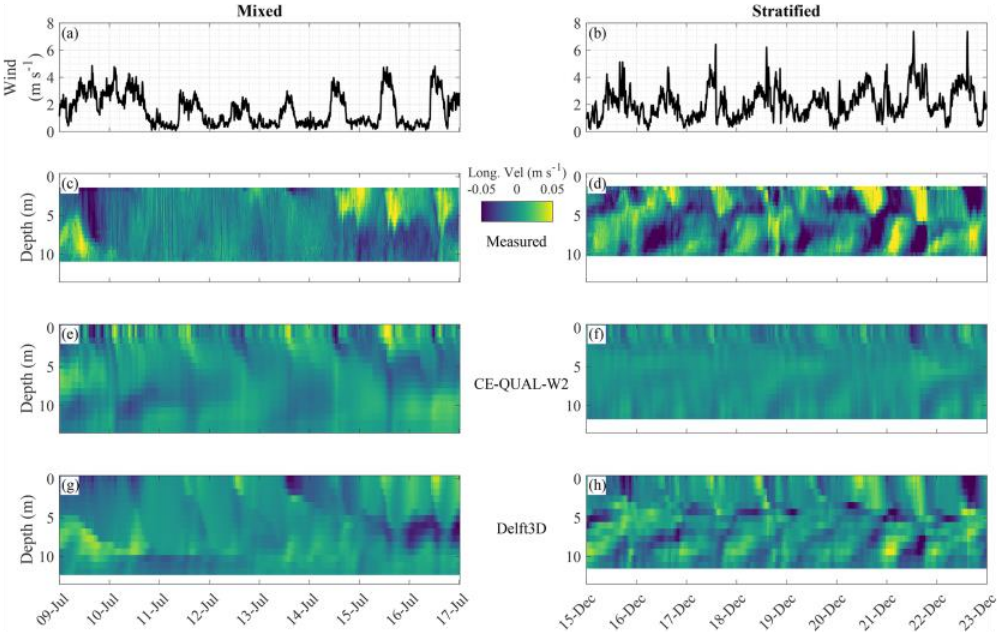

Figure 10. Panels **(a)** and **(b)** show time series of wind speed for two selected periods during mixed (9 July 2018 to 17 July 2018) and stratified (15 December 2018 to 23 December 2018) conditions. The other panels show contour plots of the longitudinal flow velocities at the monitoring site (positive values correspond to downstream flow); panels **(c)** and **(d)** show observations made by the ADCP, panels **(e)** and **(f)** show simulation results from CE-QUAL-W2, and panels **(g)** and **(h)** show simulation results from Delft3D.

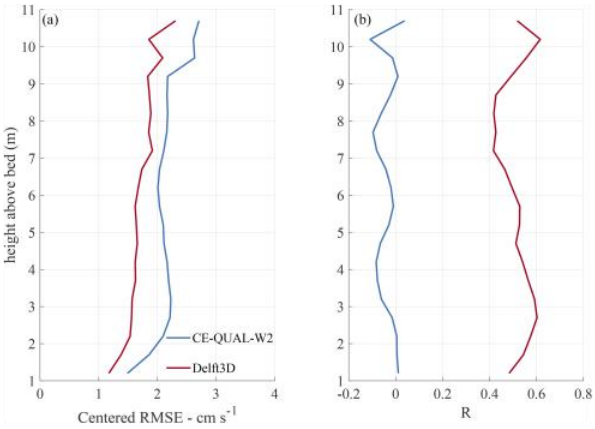

Figure 11. Performance of longitudinal flow velocity simulations from CE-QUAL-W2 and Delft3D for the intake region. Panel **(a)** shows the centered root-mean-square error (cRMSE), and panel **(b)** shows correlation coefficient (R) along depth for each model.

over the spillway. Both models calculated the discharge by empirical equations. Delft3D was forced by the measured water level as an open boundary at the spillway location. For water level elevations higher than the bathymetry at the outflow cells, water will leave the domain. For water level elevations lower than the bathymetry at the outfall cells, no water should flow at all. However, as the bathymetry at the outflowing cells could not reproduce the spillway geometry, periods of water flowing into the domain were observed, which is obviously an artifact. Despite similar results in terms of storage volume, discharges through the spillway and evaporation differed among models, with Delft3D having the largest evaporation loss and CE-QUAL-W2 the lowest. The differences can be attributed to the differences in how the models describe and implement the boundary conditions. We cannot affirm which model is most precise, because the modeled processes (e.g., evaporation or flow over spillway) were not directly measured. In addition, measured data are also associated with uncertainties. There is an underestimation of peaks of inflow discharge from LARSIM-WT and poor data accuracy on outflows of the bottom outlet at the dam and the spillway discharge, which were important parameters that contributed for the discrepancies of the water balance of the reservoir. Thus, care has to be taken when defining boundary conditions in all models, and the first step should always be to check water balance and flows at the boundaries.

7.2 Temperature

All three models simulated the dynamics of temperature stratification in reasonable agreement with observations. Resulting errors are in the same order of magnitude as values reported in other model applications (e.g., Bruce et al.,

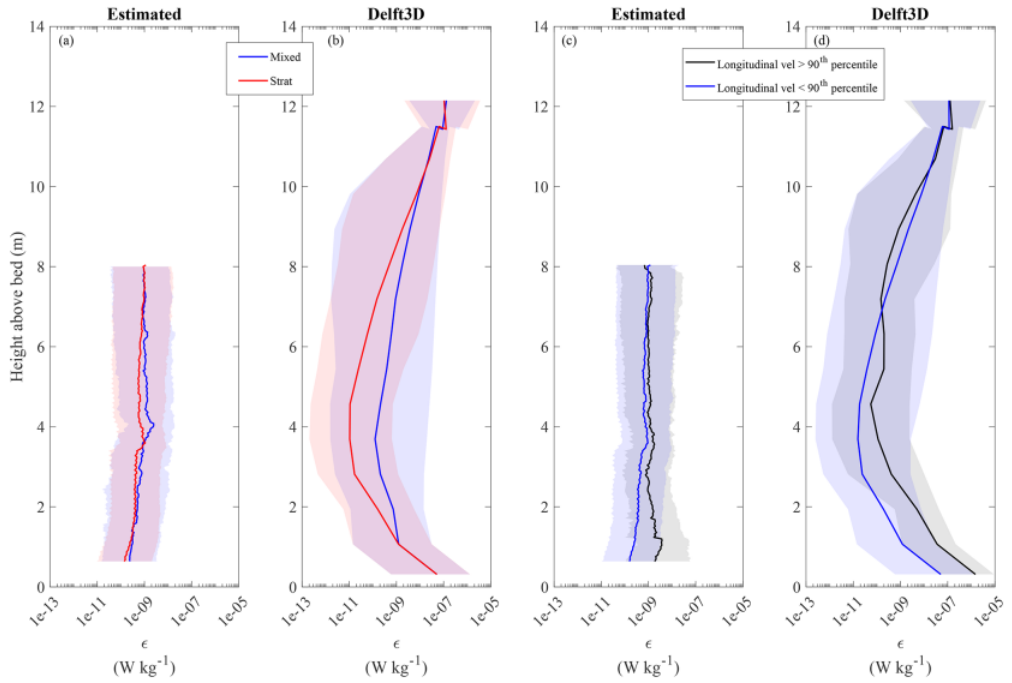

Figure 12. Solid lines show depth profiles of log-averaged energy dissipation rates (ε). Background shades mark the range between the 5th and 95th percentiles of the temporal variations. Panels **(a)** and **(b)** show estimated and simulated (Delft3D) dissipation rates separated between mixed and stratified conditions. Panels **(c)** and **(d)** show estimated and simulated dissipation rates divided in periods of longitudinal flow velocity magnitudes exceeding ($>$) or being smaller ($<$) than their 90th percentile.

2018; Weber et al., 2017; Kobler et al., 2018; Mi et al., 2020; Chanudet et al., 2012; Dissanayake et al., 2019).

Stratification is mostly driven by heat exchange associated with absorption of solar radiation, net longwave radiation, evaporation, precipitation and sensible heat transfer at the water–air interface. Despite the different parameterizations of the surface heat flux, which also included downwelling longwave radiation that was not measured, and the use of different coefficients (see Table 1); daily averages of net surface heat flux of the three models had no significant difference among each other. Other processes that influence the temperature stratification are inflows, surface runoff, groundwater inflow and heat exchange with the sediment (Wetzel, 2001). Out of those, only river inflow temperatures were known and implemented in all models. The others were considered to be negligible. Regarding the heat exchange with sediment, Stepanenko et al. (2013) showed that it did not have significant influence on simulations of bottom water temperature of a shallow lake for a comparable temperature range as observed in Passaúna Reservoir. Even though the errors were of comparable magnitude, the model simulations of thermal stability differed among the models, with underestimated temperature in the 2D simulations and overestimated temperature in the 3D simulations. We assume that the differences were related to model dimensionality and the parameterization of vertical mixing and inflows.

The 1D model imposes the largest simplification by neglecting horizontal variations in flow and water temperature, even though an initial mixing of inflows due to entrainment is parameterized in the model. It is important to point out that the continuous temperature measurements at a single sampling location are not ideal for comparison with 1D simulations, and spatially averaged temperature profiles are more representative for the horizontally homogenous conditions assumed by the 1D model. The lower temperatures in the deeper layers can be explained by the cold inflow temperatures combined with the inability of reproducing the enhanced heat exchange of the inflowing water with the atmosphere in the shallow forebay. In addition, the surface temperature was overestimated by GLM, which explains the larger number of stratified days and increased thermal stability. Another factor that can potentially contribute to errors is the selection of the first 12 m in depth for comparison with measurements, thus excluding the bottom boundary layer of the 1D vertical grid. On the other hand, the 2D and 3D models had a better representation of the strength of vertical density stratification, despite having overall divergent results – respectively colder and warmer temperatures than measured. These differences can be at least partially explained by the calibration process, which becomes more difficult for increased dimensionality. Due to the short computational time required for 1D models, it is possible to per-

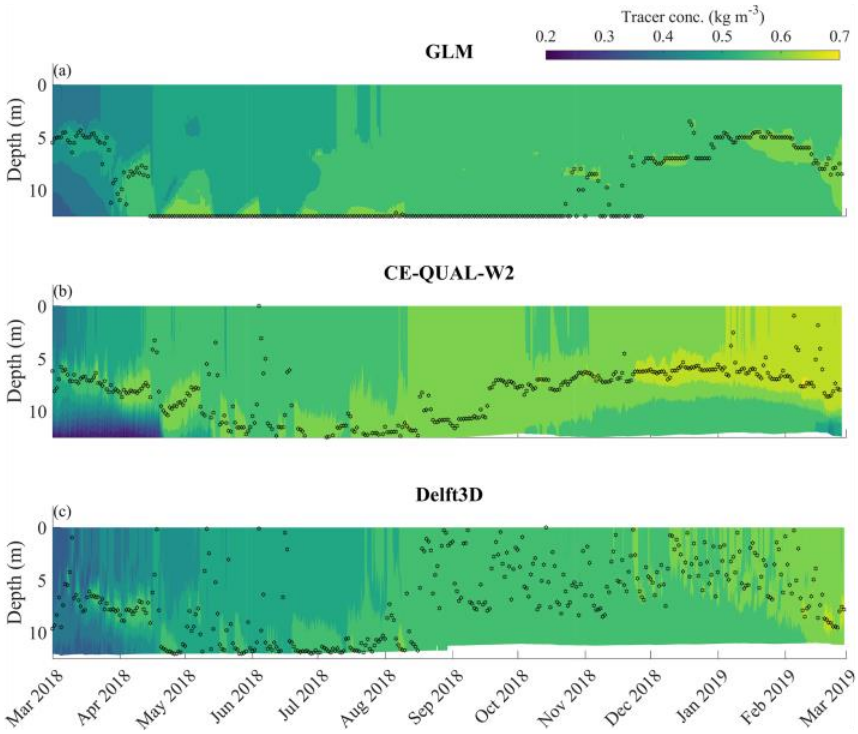

Figure 13. Contour plots showing simulated time series of tracer concentration along water depth at the intake region obtained from **(a)** GLM, **(b)** CE-QUAL-W2 and **(c)** Delft3D simulations. Black markers indicate the depth of the maximum daily-mean concentration. The tracer was introduced continuously in the Passaúna River inflow with a constant concentration of 1 kg m^{-3}.

form repeated runs with varying calibration parameters (e.g., light extinction coefficient) and to improve agreement with data during model calibration. Moreover, tools for automated model calibration are available (Bueche et al., 2020).

CE-QUAL-W2 estimated 92 d with mixed conditions, which is in closest agreement with the observations (95 d), but their temporal dynamics differed from observations especially during winter. The intermittency between mixing and stratification was more frequent; mixed periods were longer from June to August and the last mixing event shorter. In the Delft3D simulations, the shorter mixed periods are missing, which reduced the total duration of mixed conditions to 78 % of the observed.

7.3 Longitudinal processes

Both 2D and 3D simulations of temperature distributions along the longitudinal cross-section of the reservoir were in good agreement with observed temperature distributions. The 1D simulations reproduced the horizontally averaged temperature distributions, with better results when the reservoir was relatively homogeneous. The close agreement between the 2D and 3D simulations with measurements indicates that transversal gradients are of minor importance for the stratification in Passaúna Reservoir. This is further supported by the good agreement between both models for the simulated tracer transport from the river inflow to the water intake station. Nevertheless, the tracer analysis showed how the differences in temperature simulated by each model also affected the inflow pathways.

These results highlight the advantages of CE-QUAL-W2 and Delft3D, as they are capable of representing the observed longitudinal gradient, especially considering the inflow region, where colder river water flows downwards as an underflow. This underflow is responsible for transporting not only cold water but also dissolved nutrients and suspended sediment over long distances into the deeper parts of the reservoir. Those dynamics are represented in GLM only in a very simplified manner, explaining the weaker performance of GLM with respect to water temperatures at higher depths (Fig. 5).

Tracer dynamics observed with GLM complies with the hypothesis that the lower temperature at the bottom was caused by inflow pathways of mostly underflows because of the absence of the forebay. Fenocchi et al. (2017) demonstrated that, in order to reproduce the thermal response to inflows in a subalpine lake with GLM, it was necessary to use an impractical coefficient of light extinction. The general colder temperatures simulated by CE-QUAL-W2 placed the inflow at deeper depths and confined them in layers. This

behavior was observed because the longitudinal flows were located below the UML, thus showing the higher concentrations of tracer especially after September (Fig. 13). For Delft3D, the opposite was observed: the density currents were within the UML, which diluted the tracer concentration, and the depth of its maximum was strongly variable over the last 6 months. The travel times of the tracer was evaluated by identifying the first time that the tracer concentration was larger than $10^{-3}\,\mathrm{kg\,m^{-3}}$ at the intake after the release of the tracer at Passaúna River. The transport in CE-QUAL-W2 was faster with travel times of 2.2 and 3.5 d in Delft3D, which can be associated with the higher tracer concentrations of the 2D model. This information is important for management of reservoirs during spilling accidents (e.g., Jeznach et al., 2014); for GLM it is not possible to estimate time travel, since inflows are directly placed at defined layers. Studies assessing the inflow pathways through modeling demonstrated a good agreement between simulations and observations, e.g., Marti et al. (2011) and Zamani et al. (2020) with 3D models and Jeznach et al. (2014) with CE-QUAL-W2.

Despite similar seasonality of stratification and mixing predicted by the three models, the tracer analysis demonstrated how the spatial simplification affects the transport of substances. This was clear especially for the 1D model that differed considerably from the 2D and 3D models. CE-QUAL-W2 and Delft3D presented similar seasonal patterns for density currents, which influenced the stratification in the reservoir mainly by underflows that added a layer of colder water at the bottom and were strongly present in the simulations during winter. Ishikawa et al. (2021a) analyzed the distribution of density currents, categorized as underflows, interflows and overflows, based on the comparison of the measured temperature between the forebay region and the main reservoir (only available for the first half of the total period) with the temperature profile at the intake. Overflows were assigned when the forebay temperature was larger than the surface of the measured profile, and underflows were assigned when lower than the bottom; otherwise, they were interflows. A similar classification of density currents was made using the location of the maximum tracer concentration of the models (Fig. S4). Processes such as entrainment, mixing, diffusion and dilution of inflow are neglected in this approach; therefore, overflows were frequent in March and April 2018, while of minor importance in the simulations. However, the underflow season that was expected in the prior analysis was at some extension reproduced by CE-QUAL-W2 and Delft3D. It was mainly present during the winter, with shifts of 1 month among analyses made based on observations and simulations, matching with the period where the process is relevant for stratification.

For the second half of the simulated annual cycle, the flow paths of 2D and 3D models differed the most with respect to the occurrence of overflows, which is explained by the location of the density currents in relation to the UML depth (Figs. 13 and S4). All models had poor results for UML depth estimated from measurements. For this reason, the 2D model presented a smoothed error along the depth (Fig. 5), while the 1D and 3D models simulated consistently shallower UML depths, causing the peak in the error and correlation profiles. The predictions of thickness of the mixed layer and the slope of the thermoclines are generally challenging for models, as reported for other model applications (Perroud et al., 2009; Huang et al., 2010).

7.4 Flow velocities and vertical mixing

Simulation of flow velocities showed less agreement with measurements than temperature, although errors were in the same range of other work with Delft3D (Chanudet et al., 2012; Dissanayake et al., 2019). The magnitudes of simulated longitudinal flow velocities were generally lower than observations, but Delft3D was capable of reproducing the overall characteristic of larger magnitudes of longitudinal flow velocities during stratification and larger relative occurrence of currents (> 90th percentile), while flow velocities simulated by CE-QUAL-W2 showed no agreement in magnitude or dynamics with observations. For a fair comparison with the 2D model, laterally averaged flow velocity observations would be required, which are not accessible from longer-term observations. However, the transversal flow velocity component of observations and simulations of Delft3D were disregarded in the comparison (0.96 ± 0.98 and $0.54 \pm 0.64\,\mathrm{cm\,s^{-1}}$, respectively). The ratios of mean transversal and longitudinal velocity components are 0.7 for measurements and 0.5 for Delft3D, which indicates that potential transversal flow processes are not resolved by CE-QUAL-W2.

The poor results regarding magnitude and direction of flow velocities in both models can be associated with the fact that flow velocities in Passaúna Reservoir were generally small, internal seiches were not observed and circulation patterns are absent. In studies where those properties are relevant, better agreement between observations and 3D simulations were reported (Huang et al., 2010; Chanudet et al., 2012; Dissanayake et al., 2019), and a simulation in Lake Erie with CE-QUAL-W2 reproduced the oscillation frequency of basin-scale seiches but not their amplitudes (Boegman et al., 2001). Further, the direction of flow velocities is highly affected by the inaccuracy of wind direction measurements, and weak wind intensities are expected to have lower correlation with flow velocities, since they potentially change direction more frequently (Dissanayake et al., 2019), which is the case in Passaúna. Moreover, the correlation between observed and simulated flow velocities increased towards the bottom, probably because the bottom is a better represented boundary for the process, whereas it is the opposite is the case for temperature.

The turbulent closure models are relevant for the vertical mixing, thus the different approaches implemented in

the models can be considered to contribute to the variation among simulated UML thicknesses. GLM is the one with the thinner UML and poorest correlation; its simplification in dimensionality and the structure of the model in mixed layers can be the cause for lower mixing. CE-QUAL-W2 neglects transversal flows, which may contribute to the shear profile and cause errors in turbulence production. Lastly, Delft3D resolved all three dimensions, but dissipation rates simulated by the model differ from those estimated from measurements of flow velocities. The log-averaged profiles of dissipation rates computed by the 3D model follow an expected profile with a turbulent surface boundary layer, a low energetic interior and increasing dissipation rates towards the bottom (Wüest and Lorke, 2003). Only few studies in the literature reported comparisons of measured and simulated dissipation rates. In general they presented good agreement, but all of them were performed in high energetic environments such as ocean regions with the presence of breaking waves, near to the surface, and large lakes (Stips et al., 2005; Jones and Monismith, 2008; Paskyabi and Fer, 2014; Moghimi et al., 2016). In spite of all uncertainties regarding the estimated dissipation rates, in our study the results from the 3D simulations revealed that the model has limitations in reproducing all processes contributing to energy dissipation in a medium-sized reservoir.

8 Conclusions

Three commonly used hydrodynamic models with different dimensionalities were applied to a subtropical reservoir using identical boundary conditions. The simulation results were compared to measurements covering a complete annual cycle. All models were capable of providing valuable information about the water balance and reproduced the overall pattern of seasonal thermal stratification and mixing. Flow velocities, only available from the 2D and 3D models, were more challenging to reproduce, particularly because of low flow velocities and the lack of large-scale circulation pattern in the reservoir. In terms of the mean absolute error for water level, temperature and flow velocity, the three models had a maximum variation among each other of 30 %, but the time required to run the simulations increased by nearly 5 orders of magnitude, from 5 s with GLM, 3.7 min with CE-QUAL-W2 and 3.5 d with Delft3D (Table 1). Passaúna is a medium-sized reservoir, so for larger systems computational time can turn into a more constraining factor.

Nevertheless, each model has its advantages and limitations, and their application should be chosen in accordance with the parameters to investigate.

1D.

- Water balance and water level are fundamental for the management of reservoirs.
- Seasonal operations that depend on stratification are important, e.g., selecting intake and outflow depths that will have better results depending on the mixing condition (Weber et al., 2017).
- The good trade-off between computational costs and provided accuracy in simulating seasonal thermal stratification and vertical mixing is attractive, and 1D models have been increasingly employed in larger-scale studies including a large number of water bodies (e.g., Read et al., 2014; Woolway and Merchant, 2019).

2D.

- Assisting in actions and time response regarding substance transport are important, e.g., in case of contamination of the principal inflow (Jeznach et al., 2014). However, specific determination of layers containing the density currents is uncertain, and it will depend on initial mixing of inflow and depths of UML and thermocline, which none of the models could reproduce with precision, although the 3D model had better correlation.
- Seasonal pattern of the density currents is important.

3D.

- Field of flow velocities is important. Although Passaúna Reservoir had low kinetic energy, the 3D model presented positive correlation with measurements. In addition, wind speeds were low and were measured a few kilometers apart from the monitored site, where it could have different directions and could reduce the agreement between observation and simulation. Flow velocities can be important for processes that depend on circulation patterns, e.g., the transport of nutrients that are related to algae blooms (León et al., 2005; Chung et al., 2014).

Challenges faced by all models were the water balance and the UML thickness. The first was rather because of the poor monitoring; thus, it is of paramount importance to have good measurements of the volumetric discharge of inflows and outflows, including engineering structures such as spillways. Otherwise it is difficult to identify sources of errors related to the models themselves. The thickness of the mixed layer can have large effects on subsequent simulations of water quality. The categorization of density currents as overflows, interflows or underflows depends on that and will have a direct impact on the fate of nutrients and organic matter inside the reservoir (Rueda et al., 2007). Similarly, the dynamics and vertical distribution of dissipation rates of turbulent kinetic energy could not be reproduced. This quantity can be relevant not only for hydrodynamic applications but also for the prediction of air–water gas exchange (Katul and Liu, 2017), sediment–water fluxes (Lorke and Peeters, 2006; Grant and Marusic, 2011) or the development of algal blooms (Aparicio

Medrano et al., 2013). By taking these general and model-specific limitations into consideration, models are valuable tools not only for managing water resources but also for scientific applications (e.g., Sabrekov et al., 2017; Mi et al., 2020; de Carvalho Bueno et al., 2021).

Data availability. The current versions of the models used in this study are available at their respective websites.

GLM – https://github.com/AquaticEcoDynamics/ (last access: 26 October 2021); Delft3D-FLOW – https://oss.deltares.nl/web/delft3d/get-started (last access: 26 October 2021), both under the GNU General Public License v3.0 (https://www.gnu.org/licenses/gpl-3.0.html, last access: 6 November 2021); and CE-QUAL-W2: http://www.ce.pdx.edu/w2/ (last access: 26 October 2021). The source codes for the exact versions of each model used to produce the results are archived at https://doi.org/10.5281/zenodo.5613653 (Ishikawa et al., 2021b).

Data and scripts supporting the findings of this study are openly available at https://doi.org/10.5281/zenodo.5600497 (Ishikawa et al., 2021c).

Supplement. The supplement related to this article is available online at: https://doi.org/10.5194/gmd-15-2197-2022-supplement.

Author contributions. MI contributed to the conceptualization of the article, application of Delft3D, formal analysis, and investigation. WG was responsible for finishing the setup of Delft3D, adjustment of grids, bathymetry, and analysis of water balance. OG made the first setup of Delft3D and the application of CE-QUAL-W2. GS and JAR were responsible for the application of GLM. TB was the supervisor of GS and OG master theses and also advised in all models and concepts. MM was the co-supervisor of GS and advisor for the article concept. AL was the supervisor of MI PhD thesis and advisor for the article concept. Writing of the original draft was performed by MI, WG, JAR, GS, and OG. AL, TB, and MM also contributed to writing, reviewing, and editing the article.

Competing interests. The contact author has declared that neither they nor their co-authors have any competing interests.

Disclaimer. Publisher's note: Copernicus Publications remains neutral with regard to jurisdictional claims in published maps and institutional affiliations.

Acknowledgements. All measurements and analysis presented in this paper were part of the MuDak-WRM project: https://www.mudak-wrm.kit.edu/ (last access: 28 January 2022) (Fuchs et al., 2019). Project partners provided data to support this specific study, such as the bathymetry and the inflows discharges and temperatures. We also thank SANEPAR and the Postgraduate Program in Water Resources and Environmental Engineering from the Federal University of Paraná for collaborating during the field work and providing data. Tobias Bleninger acknowledges the productivity stipend from the National Council for Scientific and Technological Development – CNPq, call no. 09/2020. Gabriela Sales and Orides Golyjeswski acknowledge the financial support from Coordenação de Aperfeiçoamento de Pessoal de Nível Superior (CAPES, code no. 001) scholarships.

Financial support. This research has been supported by the Bundesministerium für Bildung und Forschung (grant nos. 02WGR1431 B and 02WGR1431A) and the Conselho Nacional de Desenvolvimento Científico e Tecnológico (grant no. 312211/2020-1, call no. 09/2020).

Review statement. This paper was edited by Jeffrey Neal and reviewed by Victor Stepanenko and Laura M. V. Soares.

References

Al-Zubaidi, H. A. M. and Wells, S. A.: Comparison of a 2D and 3D Hydrodynamic and Water Quality Model for Lake Systems, World Environmental and Water Resources Congress 2018, 3–7 June 2018, Minneapolis, Minnesota, 74–84, https://doi.org/10.1061/9780784481400.007, 2018.

Aparicio Medrano, E., Uittenbogaard, R. E., Dionisio Pires, L. M., van de Wiel, B. J. H., and Clercx, H. J. H.: Coupling hydrodynamics and buoyancy regulation in Microcystis aeruginosa for its vertical distribution in lakes, Ecol. Model., 248, 41–56, https://doi.org/10.1016/j.ecolmodel.2012.08.029, 2013.

Baracchini, T., Wüest, A., and Bouffard, D.: Meteolakes: An operational online three-dimensional forecasting platform for lake hydrodynamics, Water Res., 172, 115529, https://doi.org/10.1016/j.watres.2020.115529, 2020.

Beletsky, D. and Schwab, D. J.: Modeling circulation and thermal structure in Lake Michigan: Annual cycle and interannual variability, J. Geophys. Res.-Oceans, 106, 19745–19771, https://doi.org/10.1029/2000JC000691, 2001.

Bermúdez, M., Cea, L., Puertas, J., Rodríguez, N., and Baztán, J.: Numerical Modeling of the Impact of a Pumped-Storage Hydroelectric Power Plant on the Reservoirs' Thermal Stratification Structure: a Case Study in NW Spain, Environ. Model. Assess., 23, 71–85, https://doi.org/10.1007/s10666-017-9557-3, 2018.

Boegman, L., Loewen, M. R., Hamblin, P. F., and Culver, D. A.: Application of a two-dimensional hydrodynamic reservoir model to Lake Erie, Can. J. Fish. Aquat. Sci., 58, 858–869, https://doi.org/10.1139/f01-035, 2001.

Bornstein, Y.: Creating a bathimetry file for CE-QUAL-W2 in QGIS using the CE-QUAL-W2_Bathimetry plugin, GitHub [code], https://github.com/WQDSS/qgis-cequalw2-bath (last access: 6 March 2020), 2019.

Bruce, L. C., Frassl, M. A., Arhonditsis, G. B., Gal, G., Hamilton, D. P., Hanson, P. C., Hetherington, A. L., Melack, J. M., Read, J. S., Rinke, K., Rigosi, A., Trolle, D., Winslow, L., Adrian, R., Ayala, A. I., Bocaniov, S. A., Boehrer, B., Boon, C., Brookes, J. D., Bueche, T., Busch, B. D., Copetti, D., Cortés, A., de Eyto, E., Elliott, J. A., Gallina, N., Gilboa, Y., Guyennon, N., Huang, L., Kerimoglu, O., Lenters, J. D., MacIn-

tyre, S., Makler-Pick, V., McBride, C. G., Moreira, S., Özkundakci, D., Pilotti, M., Rueda, F. J., Rusak, J. A., Samal, N. R., Schmid, M., Shatwell, T., Snorthheim, C., Soulignac, F., Valerio, G., van der Linden, L., Vetter, M., Vinçon-Leite, B., Wang, J., Weber, M., Wickramaratne, C., Woolway, R. I., Yao, H., and Hipsey, M. R.: A multi-lake comparative analysis of the General Lake Model (GLM): Stress-testing across a global observatory network, Environ. Modell. Softw., 102, 274–291, https://doi.org/10.1016/j.envsoft.2017.11.016, 2018.

Bueche, T., Wenk, M., Poschlod, B., Giadrossich, F., Pirastru, M., and Vetter, M.: glmGUI v1.0: an R-based graphical user interface and toolbox for GLM (General Lake Model) simulations, Geosci. Model Dev., 13, 565–580, https://doi.org/10.5194/gmd-13-565-2020, 2020.

Carneiro, C., Kelderman, P., and Irvine, K.: Assessment of phosphorus sediment–water exchange through water and mass budget in Passaúna Reservoir (Paraná State, Brazil), Environ. Earth Sci., 75, 564, https://doi.org/10.1007/s12665-016-5349-3, 2016.

Carpentier, D., Haas, J., Olivares, M., and De la Fuente, A.: Modeling the Multi-Seasonal Link between the Hydrodynamics of a Reservoir and Its Hydropower Plant Operation, Water, 9, 367, https://doi.org/10.3390/w9060367, 2017.

Chanudet, V., Fabre, V., and van der Kaaij, T.: Application of a three-dimensional hydrodynamic model to the Nam Theun 2 Reservoir (Lao PDR), J. Great Lakes Res., 38, 260–269, https://doi.org/10.1016/j.jglr.2012.01.008, 2012.

Chen, G., Fang, X., and Devkota, J.: Understanding flow dynamics and density currents in a river-reservoir system under upstream reservoir releases, Hydrolog. Sci. J., 61, 2411–2426, https://doi.org/10.1080/02626667.2015.1112902, 2016.

Chung, S., Imberger, J., Hipsey, M., and Lee, H.: The influence of physical and physiological processes on the spatial heterogeneity of a Microcystis bloom in a stratified reservoir, Ecol. Model., 289, 133–149, https://doi.org/10.1016/j.ecolmodel.2014.07.010, 2014.

Cole, T. M. and Buchak, E. M.: CE-QUAL-W2: A Two-Dimensional, Laterally Averaged, Hydrodynamic and Water Quality Model, Version 2.0. User Manual, Army Engineer Waterways Experiment Station Vicksburg MS Environmental Lab, 1995.

Cole, T. M. and Wells, S. A.: CE-QUAL-W2: A two-dimensional, laterally averaged, hydrodynamic and water quality model, version 3.5, Instruction Report EL-06-1, US Army Engineering and Research Development Center, Vicksburg, MS, http://archives.pdx.edu/ds/psu/12049, 2006.

Dai, H., Mao, J., Jiang, D., and Wang, L.: Longitudinal hydrodynamic characteristics in reservoir tributary embayments and effects on algal blooms, PloS one, 8, e68186, https://doi.org/10.1371/journal.pone.0068186, 2013.

de Carvalho Bueno, R., Bleninger, T., and Lorke, A.: Internal wave analyzer for thermally stratified lakes, Environ. Modell. Softw., 136, 104950, https://doi.org/10.1016/j.envsoft.2020.104950, 2021.

DeGasperi, C.: Predicting Climate Change Effects on Kokanee Habitat Suitability in Lake Sammamish, Washington, Report prepared for U.S. Fish and Wildlife Service, Lacey, Washington, King County Water and Land Resources Division, Department of Natural Resources and Parks, Seattle, Washington, 46 pp., 2013.

Deltares, D. D.-F.: Simulation of multi-dimensional hydrodynamic flows and transport phenomena, including sediments, Deltares, Rotterdamseweg, the Netherlands, 1–706, 2013.

Dissanayake, P., Hofmann, H., and Peeters, F.: Comparison of results from two 3D hydrodynamic models with field data: internal seiches and horizontal currents, Inland Waters, 9, 239–260, https://doi.org/10.1080/20442041.2019.1580079, 2019.

Farrell, K. J., Ward, N. K., Krinos, A. I., Hanson, P. C., Daneshmand, V., Figueiredo, R. J., and Carey, C. C.: Ecosystem-scale nutrient cycling responses to increasing air temperatures vary with lake trophic state, Ecol. Model., 430, 109134, https://doi.org/10.1016/j.ecolmodel.2020.109134, 2020.

Fenocchi, A., Rogora, M., Sibilla, S., and Dresti, C.: Relevance of inflows on the thermodynamic structure and on the modeling of a deep subalpine lake (Lake Maggiore, Northern Italy/Southern Switzerland), Limnologica, 63, 42–56, https://doi.org/10.1016/j.limno.2017.01.006, 2017.

Fuchs, S., Hilgert, S., Sotiri, K., Wagner, A., Ishikawa, M., Kern, J., Jirka, S., Klassen, I., Krumm, J., Malewski, C., Rohr, H., and Pakzad, K.: Sustainable management of reservoirs – defining minimum data needs and model complexity, GRoW- Water as a Global Resource – Status Seminar 2019, Frankfurt am Main, Germany, 20–21 February 2019, 2019.

Gal, G., Yael, G., Noam, S., Moshe, E., and Schlabing, D.: Ensemble Modeling of the Impact of Climate Warming and Increased Frequency of Extreme Climatic Events on the Thermal Characteristics of a Sub-Tropical Lake, Water, 12, 1982, 2020.

Gavrieli, I., Lensky, N., Abelson, M., Ganor, J., Aharon, O., Brenner, S., Lensky, I., Shalev, E., Yechieli, Y., Dvorkin, Y., Gertman, I., Scott, W., Ehud, S., Rosentraub, Z., and Reznik, I.: Red Sea – 75 Dead Sea Water Conveyance Study Program – Dead Sea Study, Project final report, Tahal Group in association with Geological Survey of Israel and associates, 348 pp., 2011.

Gelda, K. R., King, T. A., Effler, W. S., Schweitzer, A. S., and Cowen, A. E.: Testing and application of a two-dimensional hydrothermal/transport model for a long, deep, and narrow lake with moderate Burger number, Inland Waters, 5, 387–402, https://doi.org/10.5268/IW-5.4.804, 2015.

Goudsmit, G. H., Burchard, H., Peeters, F., and Wüest, A.: Application of k-ϵ turbulence models to enclosed basins: The role of internal seiches, J. Geophys. Res.-Oceans, 107, 23-21–23-13, https://doi.org/10.1029/2001jc000954, 2002.

Grant, S. B. and Marusic, I.: Crossing Turbulent Boundaries: Interfacial Flux in Environmental Flows, Environ. Sci. Technol., 45, 7107–7113, https://doi.org/10.1021/es201778s, 2011.

Guénand, Y., Perga, M.-E., Chanudet, V., and Bouffard, D.: Hydropower operations modulate sensitivity to meteorological forcing in a high altitude reservoir, Aquat. Sci., 82, 60, https://doi.org/10.1007/s00027-020-00734-y, 2020.

Guseva, S., Bleninger, T., Jöhnk, K., Polli, B. A., Tan, Z., Thiery, W., Zhuang, Q., Rusak, J. A., Yao, H., Lorke, A., and Stepanenko, V.: Multimodel simulation of vertical gas transfer in a temperate lake, Hydrol. Earth Syst. Sci., 24, 697–715, https://doi.org/10.5194/hess-24-697-2020, 2020.

Haag, I. and Luce, A.: The integrated water balance and water temperature model LARSIM-WT, Hydrol. Process., 22, 1046–1056, https://doi.org/10.1002/hyp.6983, 2008.

Hersbach, H., Bell, B., Berrisford, P., Biavati, G., Horányi, A., Muñoz Sabater, J., Nicolas, J., Peubey, C., Radu, R., Rozum,

I., Schepers, D., Simmons, A., Soci, C., Dee, D., and Thépaut, J.-N.: ERA5 hourly data on single levels from 1979 to present. Copernicus Climate Change Service (C3S) Climate Data Store (CDS) [data set], https://doi.org/10.24381/cds.adbb2d47, 2018.

Hetherington, A. L., Schneider, R. L., Rudstam, L. G., Gal, G., DeGaetano, A. T., and Walter, M. T.: Modeling climate change impacts on the thermal dynamics of polymictic Oneida Lake, New York, United States, Ecol. Model., 300, 1–11, https://doi.org/10.1016/j.ecolmodel.2014.12.018, 2015.

Hipsey, M. R., Bruce, L. C., Boon, C., Busch, B., Carey, C. C., Hamilton, D. P., Hanson, P. C., Read, J. S., de Sousa, E., Weber, M., and Winslow, L. A.: A General Lake Model (GLM 3.0) for linking with high-frequency sensor data from the Global Lake Ecological Observatory Network (GLEON), Geosci. Model Dev., 12, 473–523, https://doi.org/10.5194/gmd-12-473-2019, 2019.

Huang, A., Rao, Y. R., Lu, Y., and Zhao, J.: Hydrodynamic modeling of Lake Ontario: An intercomparison of three models, J. Geophys. Res., 115, C12076, https://doi.org/10.1029/2010jc006269, 2010.

Imberger, J. and Patterson, J. C.: A Dynamic Reservoir Simulation Model – DYRESM: 5, in: Transport Models/Inland and Coastal Waters, edited by: Fischer, H. B., Academic Press, San Diego, 310–361, 1981.

Imberger, J., Loh, I., Hebbert, B., and Patterson, J.: Dynamics of reservoir of medium size, J. Hydr. Eng. Div.-ASCE, 104, 725–743, 1978.

Ishikawa, M., Bleninger, T., and Lorke, A.: Hydrodynamics and mixing mechanisms in a subtropical reservoir, Inland Waters, 11, 286–301, https://doi.org/10.1080/20442041.2021.1932391, 2021a.

Ishikawa, M., Gonzalez, W., Golyjeswski, O., Sales, G., Rigotti, J. A., Bleninger, T., Mannich, M., and Lorke, A.: Models source code: GLM (version 3.1.8), CE-QUAL-W2 (version 3.7), Delft3D-FLOW (version 4.04.01) – Preprint: Effects of dimensionality on the performance of hydrodynamic models, Zenodo [code], https://doi.org/10.5281/zenodo.5613653, 2021b.

Ishikawa, M., Gonzalez, W., Golyjeswski, O., Sales, G., Rigotti, J. A., Bleninger, T., Mannich, M., and Lorke, A.: Dataset of preprint: Effects of dimensionality on the performance of hydrodynamic models, Zenodo [data set], https://doi.org/10.5281/zenodo.5600497, 2021c.

Ishikawa, M., Haag, I., Krumm, J., Teltscher, K., and Lorke, A.: The effect of stream shading on the inflow characteristics in a downstream reservoir, River Res. Appl., 37, 943–954, https://doi.org/10.1002/rra.3821, 2021d.

Jeznach, L. C., Tobiason, J. E., and Ahlfeld, D. P.: Modeling conservative contaminant effects on reservoir water quality, J. Am. Water Works Ass., 106, E295–E306, https://doi.org/10.5942/jawwa.2014.106.0062, 2014.

Jones, N. L. and Monismith, S. G.: Modeling the influence of wave-enhanced turbulence in a shallow tide- and wind-driven water column, J. Geophys. Res.-Oceans, 113, C03009, https://doi.org/10.1029/2007JC004246, 2008.

Katul, G. and Liu, H.: Multiple mechanisms generate a universal scaling with dissipation for the air-water gas transfer velocity, Geophys. Res. Lett., 44, 1892–1898, https://doi.org/10.1002/2016GL072256, 2017.

Kobler, U. G., Wüest, A., and Schmid, M.: Effects of Lake–Reservoir Pumped-Storage Operations on Temperature and Water Quality, Sustainability, 10, 1968, https://doi.org/10.3390/su10061968, 2018.

Ladwig, R., Hanson, P. C., Dugan, H. A., Carey, C. C., Zhang, Y., Shu, L., Duffy, C. J., and Cobourn, K. M.: Lake thermal structure drives interannual variability in summer anoxia dynamics in a eutrophic lake over 37 years, Hydrol. Earth Syst. Sci., 25, 1009–1032, https://doi.org/10.5194/hess-25-1009-2021, 2021.

León, L. F., Imberger, J., Smith, R. E., Hecky, R. E., Lam, D. C., and Schertzer, W. M.: Modeling as a tool for nutrient management in Lake Erie: a hydrodynamics study, J. Great Lakes Res., 31, 309–318, 2005.

Lewis Jr., W. M.: A revised classification of lakes based on mixing, Can. J. Fish. Aquat. Sci., 40, 1779–1787, https://doi.org/10.1139/f83-207, 1983.

Lorke, A. and Peeters, F.: Toward a unified scaling relation for interfacial fluxes, J. Phys. Oceanogr., 36, 955–961, https://doi.org/10.1175/JPO2903.1, 2006.

Man, X., Lei, C., Carey, C. C., and Little, J. C.: Relative Performance of 1-D Versus 3-D Hydrodynamic, Water-Quality Models for Predicting Water Temperature and Oxygen in a Shallow, Eutrophic, Managed Reservoir, Water, 13, 88, https://doi.org/10.3390/w13010088, 2021.

Marti, C. L., Mills, R., and Imberger, J.: Pathways of multiple inflows into a stratified reservoir: Thomson Reservoir, Australia, Adv. Water Resour., 34, 551–561, https://doi.org/10.1016/j.advwatres.2011.01.003, 2011.

Mesman, J. P., Ayala, A. I., Adrian, R., De Eyto, E., Frassl, M. A., Goyette, S., Kasparian, J., Perroud, M., Stelzer, J. A. A., Pierson, D. C., and Ibelings, B. W.: Performance of one-dimensional hydrodynamic lake models during short-term extreme weather events, Environ. Modell. Softw., 133, 104852, https://doi.org/10.1016/j.envsoft.2020.104852, 2020.

Mi, C., Shatwell, T., Ma, J., Xu, Y., Su, F., and Rinke, K.: Ensemble warming projections in Germany's largest drinking water reservoir and potential adaptation strategies, Sci. Total Environ., 748, 141366, https://doi.org/10.1016/j.scitotenv.2020.141366, 2020.

Moghimi, S., Thomson, J., Özkan-Haller, T., Umlauf, L., and Zippel, S.: On the modeling of wave-enhanced turbulence nearshore, Ocean Model., 103, 118–132, https://doi.org/10.1016/j.ocemod.2015.11.004, 2016.

Paskyabi, M. B. and Fer, I.: Turbulence structure in the upper ocean: a comparative study of observations and modeling, Ocean Dynam., 64, 611–631, https://doi.org/10.1007/s10236-014-0697-6, 2014.

Perroud, M., Goyette, S., Martynov, A., Beniston, M., and Annevillec, O.: Simulation of multiannual thermal profiles in deep Lake Geneva: A comparison of one-dimensional lake models, Limnol. Oceanogr., 54, 1574–1594, https://doi.org/10.4319/lo.2009.54.5.1574, 2009.

Polli, B. A. and Bleninger, T.: Comparison of 1D and 3D reservoir heat transport models and temperature effects on mass transport, RBRH, 24, e30, https://doi.org/10.1590/2318-0331.241920190023, 2019.

Read, J. S., Hamilton, D. P., Jones, I. D., Muraoka, K., Winslow, L. A., Kroiss, R., Wu, C. H., and Gaiser, E.: Derivation of lake mixing and stratification indices from high-resolution

lake buoy data, Environ. Modell. Softw., 26, 1325–1336, https://doi.org/10.1016/j.envsoft.2011.05.006, 2011.

Read, J. S., Winslow, L. A., Hansen, G. J. A., Van Den Hoek, J., Hanson, P. C., Bruce, L. C., and Markfort, C. D.: Simulating 2368 temperate lakes reveals weak coherence in stratification phenology, Ecol. Model., 291, 142–150, https://doi.org/10.1016/j.ecolmodel.2014.07.029, 2014.

Rueda, F. J., Fleenor, W. E., and de Vicente, I.: Pathways of river nutrients towards the euphotic zone in a deep-reservoir of small size: uncertainty analysis, Ecol. Model., 202, 345–361, https://doi.org/10.1016/j.ecolmodel.2006.11.006, 2007.

Sabrekov, A. F., Runkle, B. R. K., Glagolev, M. V., Terentieva, I. E., Stepanenko, V. M., Kotsyurbenko, O. R., Maksyutov, S. S., and Pokrovsky, O. S.: Variability in methane emissions from West Siberia's shallow boreal lakes on a regional scale and its environmental controls, Biogeosciences, 14, 3715–3742, https://doi.org/10.5194/bg-14-3715-2017, 2017.

Soares, L. M. V., Silva, T. F. D. G., Vinçon-Leite, B., Eleutério, J. C., Lima, L. C. D., and Nascimento, N. D. O.: Modelling drought impacts on the hydrodynamics of a tropical water supply reservoir, Inland Waters, 9, 422–437, https://doi.org/10.1080/20442041.2019.1596015, 2019.

Song, Y., Semazzi, F. H. M., Xie, L., and Ogallo, L. J.: A coupled regional climate model for the Lake Victoria basin of East Africa, Int. J. Climatol., 24, 57–75, https://doi.org/10.1002/joc.983, 2004.

Sotiri, K., Hilgert, S., and Fuchs, S.: Sediment classification in a Brazilian reservoir: Pros and cons of parametric low frequencies, Advances in Oceanography and Limnology, 10, https://doi.org/10.4081/aiol.2019.7953, 2019.

Soulignac, F., Vinçon-Leite, B., Lemaire, B. J., Scarati Martins, J. R., Bonhomme, C., Dubois, P., Mezemate, Y., Tchiguirinskaia, I., Schertzer, D., and Tassin, B.: Performance Assessment of a 3D Hydrodynamic Model Using High Temporal Resolution Measurements in a Shallow Urban Lake, Environ. Model. Assess., 22, 309–322, https://doi.org/10.1007/s10666-017-9548-4, 2017.

Stepanenko, V., Jöhnk, K. D., Machulskaya, E., Perroud, M., Subin, Z., Nordbo, A., Mammarella, I., and Mironov, D.: Simulation of surface energy fluxes and stratification of a small boreal lake by a set of one-dimensional models, Tellus A, 66, 21389, https://doi.org/10.3402/tellusa.v66.21389, 2014.

Stepanenko, V. M., Goyette, S., Martynov, A., Perroud, M., Fang, X., and Mironov, D.: First steps of a Lake Model Intercomparison Project: LakeMIP, Boreal Environ. Res., 15, 191–202, 2010.

Stepanenko, V. M., Martynov, A., Jöhnk, K. D., Subin, Z. M., Perroud, M., Fang, X., Beyrich, F., Mironov, D., and Goyette, S.: A one-dimensional model intercomparison study of thermal regime of a shallow, turbid midlatitude lake, Geosci. Model Dev., 6, 1337–1352, https://doi.org/10.5194/gmd-6-1337-2013, 2013.

Stips, A., Burchard, H., Bolding, K., Prandke, H., Simon, A., and Wüest, A.: Measurement and simulation of viscous dissipation in the wave affected surface layer, Deep-Sea Res. Pt. II, 52, 1133–1155, https://doi.org/10.1016/j.dsr2.2005.01.012, 2005.

Taylor, K. E.: Summarizing multiple aspects of model performance in a single diagram, J. Geophys. Res.-Atmos., 106, 7183–7192, https://doi.org/10.1029/2000JD900719, 2001.

Thiery, W. I. M., Stepanenko, V. M., Fang, X., Jöhnk, K. D., Li, Z., Martynov, A., Perroud, M., Subin, Z. M., Darchambeau, F., Mironov, D., and Van Lipzig, N. P. M.: LakeMIP Kivu: evaluating the representation of a large, deep tropical lake by a set of one-dimensional lake models, Tellus A, 66, 21390, https://doi.org/10.3402/tellusa.v66.21390, 2014.

Wang, X., Zhang, H., Bertone, E., Stewart, R. A., and O'Halloran, K.: Numerical Study of the Hydrodynamic and Sediment Transport Process in a Subtropical Water Reservoir: the Impacts of Storms and Winds, Environ. Model. Assess., 25, 843–860, https://doi.org/10.1007/s10666-020-09719-5, 2020.

Weber, M., Rinke, K., Hipsey, M. R., and Boehrer, B.: Optimizing withdrawal from drinking water reservoirs to reduce downstream temperature pollution and reservoir hypoxia, J. Environ. Manage., 197, 96–105, https://doi.org/10.1016/j.jenvman.2017.03.020, 2017.

Weinstock, J.: Vertical turbulence diffusivity for weak or strong stable stratification, J. Geophys. Res.-Oceans, 86, 9925–9928, https://doi.org/10.1029/JC086iC10p09925, 1981.

Wells, S. A.: Modeling Thermal Stratification Effects in Lakes and Reservoirs, in: Inland Waters-Dynamics and Ecology, IntechOpen, https://doi.org/10.5772/intechopen.91754, 2020.

Wetzel, R. G.: Limnology: lake and river ecosystems, gulf professional publishing, Academic Press, ISBN 978-0-12-744760-5, 2001.

Woolway, R. I. and Merchant, C. J.: Worldwide alteration of lake mixing regimes in response to climate change, Nat. Geosci., 12, 271–276, https://doi.org/10.1038/s41561-019-0322-x, 2019.

Wüest, A. and Lorke, A.: Small-scale hydrodynamics in lakes, Annu. Rev. Fluid Mech., 35, 373–412, https://doi.org/10.1146/annurev.fluid.35.101101.161220, 2003.

Xu, H., Yan, M., Long, L., Ma, J., Ji, D., Liu, D., and Yang, Z.: Modeling the Effects of Hydrodynamics on Thermal Stratification and Algal Blooms in the Xiangxi Bay of Three Gorges Reservoir, Frontiers in Ecology and Evolution, 8, 610622, https://doi.org/10.3389/fevo.2020.610622, 2021.

Zamani, B. and Koch, M.: Comparison Between Two Hydrodynamic Models in Simulating Physical Processes of a Reservoir with Complex Morphology: Maroon Reservoir, Water, 12, 814, https://doi.org/10.3390/w12030814, 2020.

Zamani, B., Koch, M., and Hodges, B. R.: Effects of morphology in controlling propagation of density currents in a reservoir using uncalibrated three-dimensional hydrodynamic modeling: Effects of morphology in propagation of density currents, J. Limnol., 79, https://doi.org/10.4081/jlimnol.2020.1942, 2020.

Zhang, F., Zhang, H., Bertone, E., Stewart, R., Lemckert, C., and Cinque, K.: Numerical study of the thermal structure of a stratified temperate monomictic drinking water reservoir, Journal of Hydrology: Regional Studies, 30, 100699, https://doi.org/10.1016/j.ejrh.2020.100699, 2020.

Appendix IV

Hydrodynamic drivers of nutrient and phytoplankton dynamics in a subtropical reservoir

Mayra Ishikawa[1], Luziadne Gurski[2], Tobias Bleninger[2], Harald Rohr[3], Nils Wolf[4], and Andreas Lorke[1]

[1]*Institute for Environmental Sciences, University of Koblenz-Landau, Landau, Germany*

[2]*Graduate Program in Water Resources and Environmental Engineering, Federal University of Paraná, Curitiba, Brazil*

[3]*TriOS Mess- und Datentechnik GmbH, Rastede, Germany*

[4]*EFTAS GmbH, Münster, Germany*

Please click in the following link to read the publication

https://doi.org/10.3390/w14101544

water

MDPI

Article

Hydrodynamic Drivers of Nutrient and Phytoplankton Dynamics in a Subtropical Reservoir

Mayra Ishikawa [1,*], Luziadne Gurski [2], Tobias Bleninger [2], Harald Rohr [3], Nils Wolf [4] and Andreas Lorke [1]

[1] Institute for Environmental Sciences, University of Koblenz-Landau, 76829 Landau, Germany; lorke@uni-landau.de
[2] Graduate Program in Water Resources and Environmental Engineering, Federal University of Paraná, Curitiba 82590-300, Brazil; luziadne@ufpr.br (L.G.); bleninger@ufpr.br (T.B.)
[3] TriOS Mess- und Datentechnik GmbH, 26180 Rastede, Germany; rohr@trios.de
[4] EFTAS GmbH, 48145 Münster, Germany; nils.wolf@eftas.com
* Correspondence: ishikawa@uni-landau.de

Abstract: Chlorophyll-a (chla) is an important parameter to assess water quality in lakes and reservoirs, since it is a proxy for phytoplankton biomass and primary production. The increasing availability of data with high spatial and temporal resolution allows assessing short-term dynamics and small-scale variations of chla within larger water bodies. In freshwater reservoirs, the nutrient concentrations and the physical conditions that control phytoplankton growth vary along their longitudinal extend. Here, we analyze how the flow paths of the inflowing river water into density-stratified reservoirs affect the vertical and longitudinal distribution of nutrients and chla. We combine spatially resolved and high-frequency measurements of chla from satellite remote sensing and in-situ sensors, with numerical simulations using a three-dimensional hydrodynamic model to assess the influence of density currents on chla dynamics along a subtropical drinking water reservoir in the south of Brazil. Chla did not have pronounced seasonal dynamics (4.9 ± 1.2 µg L^{-1}, at the continuous measurement station); instead, spatial variability along the reservoir was more pronounced (4.4 ± 2.1 µg L^{-1}, all monitored points within the euphotic zone). Most of the nutrients from the inflowing river were consumed in the upstream region, and phytoplankton in the lacustrine zone depended on internal loading. Temporal variability was observed only in the upstream region, and phytoplankton produced in that area was transported downstream by density currents, resulting in large concentrations of chla below the euphotic zone. The results of a hydrodynamic model that simulates the present state are in good agreement with the observations. Two simulated scenarios, where the density current patterns were altered, resulted only in slight variations in density currents, indicating that the influence of the main inflow was of minor relevance in chla concentrations in downstream regions of the reservoir. Our results highlight the importance of two-dimensional hydrodynamic processes in regulating phytoplankton dynamics in reservoirs.

Keywords: water quality; reservoirs; chlorophyll-a; nutrients; density currents

Citation: Ishikawa, M.; Gurski, L.; Bleninger, T.; Rohr, H.; Wolf, N.; Lorke, A. Hydrodynamic Drivers of Nutrient and Phytoplankton Dynamics in a Subtropical Reservoir. *Water* **2022**, *14*, 1544. https://doi.org/10.3390/w14101544

Academic Editors: Roohollah Noori, Rabin Bhattarai and Soroush Abolfathi

Received: 20 April 2022
Accepted: 7 May 2022
Published: 11 May 2022

1. Introduction

The water quality in lakes and reservoirs is often assessed by the concentration of chlorophyll-a (chla), which is a proxy of the biomass and primary production of phytoplankton, and an important parameter for determining the index of trophic state [1,2]. For this reason, the prediction of chla is essential for the management of inland waters. Linear relationships between the concentration of total phosphorus in water and chla have been observed for many lakes [3,4]. Therefore, it became common practice to predict chla in lakes and reservoirs based on linear models using total phosphorus as a predictor [4–7]. Such relationships have been continuously revisited, due to the increasing amount of data and better approaches that can provide more robust estimates. For example, Stow and Cha [7] suggested that linear relationships would only hold for lakes with similar features. Most

recently, Quinlan, et al. [8] estimated that total phosphorus explained 44% of chla variation among 3874 lakes across 47 countries, though most of them were located in North America and Europe. A sigmoidal relationship was found between the two parameters, and the regions where the linear relationship was not valid were in either most cold or hot climates. Similarly, existing studies show that the linear relationships are rather poor predictors for chla in lakes located at low latitudes [9], and that the relationships between both parameters are not strictly linear [10]. Shuvo, et al. [11] demonstrated that additional factors can be relevant for chla, such as regional climate and the morphology of the water body. Most of the relationships between chla and total phosphorus were estimated using data from lakes, which are most abundant at higher latitudes [12], whereas there is a general lack of limnological studies in tropical and subtropical regions [13].

Freshwater reservoirs have been constructed globally for different purposes, with recent estimates suggesting a number of 38,000 existing dams [14]. Hotspots for the ongoing construction and planning of new dams are located in tropical zones [15]. Water quality in reservoirs has become a global concern, particularly in drinking water reservoirs, where their degradation caused by eutrophication and rising temperature may abate the services that they provide [16–18]. In distinction to lakes, reservoirs can be divided into three distinct zones along their longitudinal extent from the inflow region to the dam, namely the riverine, transitional, and the lacustrine zone. These zones differ in temperature, underwater light availability, turbidity, and nutrient concentration [19]. For this reason, the spatial variations and dynamics of primary production in reservoirs differs from natural lakes, although the drivers are identical [20]. According to Kimmel, Lind, and Paulson [19], nutrient availability, suspended particle concentration, and light limitation in reservoirs decrease toward the dam. Therefore, phytoplankton production has its maximum in the transition zone, where nutrients are still largely available and light limitation is reduced due to sedimentation of suspended particles. In the lacustrine zone, light and flow conditions are more favorable for phytoplankton growth, but the nutrients are limited, and growth depends on internal loading, i.e., from the release of remineralized nutrients from the sediment. In addition, besides nutrient loads, factors such as the hydraulic residence time have an impact on the trophic state of reservoirs [21].

The relationships between total phosphorus and chla have mostly been analyzed using longer-term data and for annual mean values of measurements obtained at a single location or for the average of several sampling points (e.g., [7,8]). The increasing availability of data with high spatial and temporal resolution, however, also lead to usage of trophic state indices to explain short-term dynamics and small-scale variations within larger water bodies (e.g., [22]). Remote sensing techniques have become useful tools to monitor and evaluate the quality of inland waters, measuring qualitative parameters of water with spatial and temporal variations [23].

For assessing spatial variations and temporal dynamics, the hydrodynamic conditions and, in the case of reservoirs, longitudinal gradients need to be taken into account. The flow path of inflowing waters into density-stratified reservoirs can be classified according to its depth distribution. The vertical position of the inflow depends on reservoir stratification and the density of the inflowing water, which enters at a depth of neutral buoyancy. Accordingly, the density currents are defined as under-, inter-, and overflows, where in the first the river, water flows along the reservoir bottom, in the second at an intermediate water depth, and in the latter along the water surface. The potential importance of density currents for reservoir water quality has been analyzed in recent years [24–26]. These studies addressed the hypothesis that overflows and interflows promote the growth of phytoplankton, as they can deliver nutrients directly to the euphotic zone.

The aim of the present study is to analyze the role of reservoir hydrodynamics for the longitudinal variations and the temporal dynamics of the relationships between nutrient concentration and chla in a subtropical reservoir. We combine spatially resolved and high-frequency measurements of chla from satellite remote sensing and in-situ sensors, with numerical simulations using a three-dimensional hydrodynamic model. We analyze

to what extent nutrient concentration and prevailing density currents can explain the dynamics of chla in different regions along the reservoir. In addition, we assessed two scenarios for projected changes of density currents due to changing inflow temperature and changing reservoir morphology. Our results provide information about the applicability of fixed relationships between nutrient concentration and water quality in reservoirs located at low latitude, and advance the understanding of the role of physical processes in these relationships.

2. Methods

2.1. Study Site

The study site is a drinking water reservoir located in a subtropical region in South Brazil at latitude 25.50° S. Passaúna Reservoir is of small to medium size and used for the abstraction of on average 1.8 m^3 s^{-1} of potable water for about one half million people (Sanitation Company of Paraná—SANEPAR [27]). The maximum water depth close to the dam is 17.5 m, the surface area is 8.5 km^2, and it has a storage volume of 48 × 10^6 m^3. In the upstream region of the reservoir, a forebay was formed due to the presence of a bridge (Figure 1). The main inflow is the Passaúna River that represents, on average, 77% of all incoming discharge. The outflows are the bottom outlet at the dam that had a continuous discharge of ~0.5 m^3 s^{-1}, the spillway at the dam, and the intake for the water treatment plant. Data on air temperature and wind speed are available from two stations. Until May 2018, data were provided by the Technology Institute of Paraná (TECPAR), located 4 km from the reservoir in the east direction. After that, measurements were provided by a station near to the dam and operated by SANEPAR. Both stations provided observations with a temporal resolution of 10 min. Precipitation was measured at the dam station for the entire period.

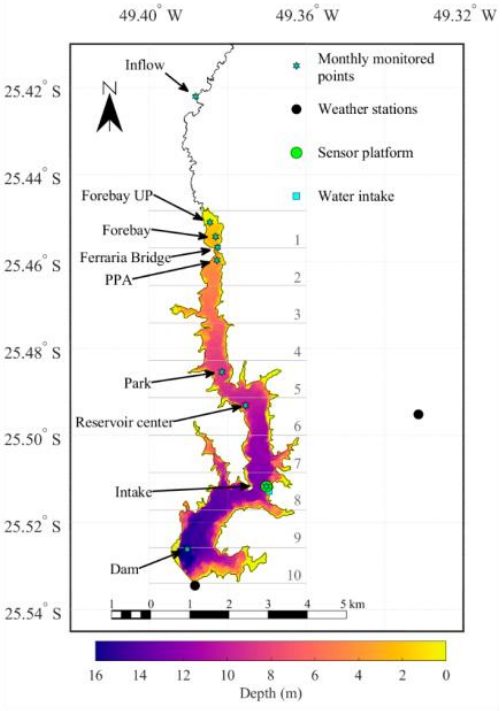

Figure 1. Map of Passaúna Reservoir. The color map shows the reservoir bathymetry (adopted from Sotiri, et al. [28]); the location of the dam, the intake station, and the main river inflow are indicated by text labels. Symbols mark the location of sampling sites for continuous sensor observations and monthly water quality sampling (see legend). The latitudinal sections (numbered as 1 to 10) are used in the spatial analysis of model simulations and remote sensing data.

2.2. Monitoring Program

Passaúna Reservoir was monitored for one year, starting from February 2018. The monitoring program was composed of three extensive and seven smaller sampling campaigns; the latter had fewer sampling locations along the reservoir. Water sampling and in-situ measurements with sensors were performed from 3 to 10 sampling sites during seven campaigns, and additional continuous sensor measurements along longitudinal, a transect crossing the complete reservoir, were measured during the three extensive campaigns. In addition to the sampling campaigns, continuous sensor measurements of surface water properties were obtained at a fixed platform near the water intake (Figure 1). The sampling schedule and the location and water depths of the measurements conducted during the campaigns are provided in Table S1. Detailed descriptions of sensor measurements and water sample analyses are provided in the following sections. In addition, Secchi disk depth (z_{SD}) was measured at each location, which were used to estimate euphotic zone depths (z_e) following Luhtala and Tolvanen [29]:

$$z_e = 3.7489 \times z_{SD}^{0.7506} \quad (1)$$

2.2.1. Sensors

Several sensors were used to measure vertical profiles at the selected sampling locations, for measuring longitudinal transects at the reservoir surface, and for continuous time series at the platform location (Table 1).

Table 1. Sensor's specification regarding variables measured, type of measurement, range, accuracy, and temporal resolution.

Equipment	Fluorometer	Spectrometer	Fluorometer	Conductivity, Temperature, and Depth Profiler
Equipment model	nanoFlu	OPUS	FluoroProbe III	CastAway-CTD
Manufacturer	TriOS	TriOS	bbe moldaenke	Sontek
Origin	Rastede, Germany	Rastede, Germany	Schwentinental, Germany	San Diego, United States
Variables measured	chla	Nitrate(N-NO_3)	chla with the determination of algae classes	conductivity, temperature, and depth
Range	0 to 200 µg L^{-1}	0.03 to 10 mg L^{-1}	0 to 500 µg L^{-1}	
AccuracyResolution	±5%	±5%	0.01 µg L^{-1}	0.1 PSU and 0.05 °C
Measurements	continuous time series	continuous time series	continuous time series, longitudinal transects, and vertical profiles	Vertical profiles
Temporal resolution	15 min	15 min	for continuous measurement 1 h, and 1 s for transects and profiles	Sampling in a rate of 5 Hz.

OPUS is an UV spectral sensor that, through the analysis of the full spectrum, determines concentrations of nitrate (N-NO_3). Both nanoFlu and the FluoroProbe (bbe moldaenke) are fluorometers; however, the last one makes the assessment of chla with the determination of five different algae classes.

Fluorometer-based measurements potentially underestimate chla concentration in the presence of daylight due to photochemical quenching [30], which was observed in our measurements with both chla probes. For this reason, data acquired between 8 am and 8 pm were excluded from the continuous measurements at the platform, and the remaining data were averaged to provide daily estimates of chla. The sensor data were

calibrated using a linear regression of daily averaged sensor data and the data obtained from laboratory analysis of water samples collected during the campaigns (Figure S1). The factory calibrations resulted in averaged overestimations of a factor of 1.46 for the nanoFlu, and 2.13 for the FluoroProbe. The same correction was applied for measurements done during campaigns, even though they were performed during daytime. Measurements of $N\text{-}NO_3$ made with the sensor were in good agreement with laboratory analyses (Figure S2).

2.2.2. Laboratory Analyses

Water samples were collected during the campaigns at each sampling site (Figure 1) using a Van Dorn sampler. The sampled depths included the water surface (0.2 m depth), the near-bottom layer (~0.5 m above the bottom), and up to three additional depths according to the measured temperature stratification (Table S1). The sampling depths were defined after the assessment of the temperature profile to resolve the vertical gradients sufficiently. Polyethylene bottles were used for sample collection of chla analyses, and glass bottles for nutrient analysis. Chla samples were stored in darkness until analysis in the laboratory.

Chemical analyses of water samples included total nitrogen (TN), organic nitrogen (Organic N), ammonium ($N\text{-}NH_4$), nitrate ($N\text{-}NO_3$), nitrite ($N\text{-}NO_2$), total phosphorus (TP), total dissolved phosphorus (TDP), particulate phosphorus (particulate P), orthophosphate ($P\text{-}PO_4$), and chla. Sampling, preservation, and analytical protocols were following standard methods for surface waters [31].

Samples for TN and TP determination were kept unfiltered, and the remaining samples were filtered using a 0.45-micron membrane filter. Measurements of $N\text{-}NO_3$, $P\text{-}PO_4$, and $N\text{-}NH_3$ were conducted within 24 h from sample collection. The remaining samples were stored at 4 °C with minimum exposure to light and air until analyzed within 10 days after sampling. Prior to analysis, water samples were equilibrated to ambient temperature.

TN concentration was determined with the persulfate method, by oxidation of all nitrogenous compounds to nitrate. $N\text{-}NH_3$ concentrations were measured by the phenate method, and $N\text{-}NO_3$ and $N\text{-}NO_2$ concentrations were analyzed by the cadmium reduction method [31]. Organic N concentration was obtained as the difference between TN and inorganic nitrogen forms ($N\text{-}NH_3$, $N\text{-}NO_3$, and $N\text{-}NO_2$).

TP and TDP concentrations were determined with acid digestion, followed by the ascorbic acid method. $P\text{-}PO_4$ concentrations were quantified using the ascorbic acid method. Particulate phosphorus was determined as the difference between TP and TDP.

Chla concentration was determined according to CETESB [32]. The water samples were vacuum filtered onto a glass fiber filter and preserved frozen until quantification. The filter was macerated and steeped in 90% acetone to extract chlorophyll from the algal cells, followed by sample clarification through centrifugation. The absorbance of the clarified extract was then measured in a UV-visible spectrophotometer (Kazuaki IL-0082-BI) before and after HCl acidification.

All analysis results were quality-checked by careful standardization, procedural blank measurements, and triplicated analyses, in which samples were measured three times and averaged.

2.3. Remote Sensing Images

Chla in the surface water of Passaúna Reservoir was estimated from Sentinel-2 single scenes which are available every 5 days if the investigation area is cloud-free. The spatial resolution is 20 m. We used the "Case 2 Regional Coast Colour" Processor (C2RCC), which is implemented in the SNAP Toolbox [33]. The C2RCC processor provides several trained neural networks (we selected C2X) that map Sentinel-2 Level 1C data (top-of-atmosphere radiance) to (atmospherically corrected) surface reflectance and chla concentration.

In total, 15 images from cloud-free observations are available for the study period: 1 March 2018, 20 April 2018, 10 May 2018, 30 May 2018, 14 July 2018, 23 August 2018, 7 September 2018, 11 November 2018, 11 December 2018, 10 January 2019, 30 January 2019,

9 February 2019, and 19 February 2019. A linear regression was performed between the measured chla (from the time series of the continuous sensor measurement near the intake station, and from sampling stations during the campaign of 11 December 2018) and the estimated chla from satellite images. For the comparison with in-situ measurements, an area of 60 m × 60 m around the sampling location was averaged. To assess the longitudinal gradient of concentrations, the reservoir was divided in 10 sections of equal width of the forebay (Figure 1).

2.4. Reservoir Hydrodynamics

Reservoir hydrodynamics were assessed in previous studies in terms on the spatial variations and temporal dynamics of thermal stratification and density currents based on measurements [34] and modeling [35]. In both studies, mixed periods were defined based on Schmidt Stability (S_T) calculated from the vertical temperature profile measured at the Intake point. Therefore, the reservoir was classified as mixed when $S_T \leq 16.3$ J m^{-2} (10% of the annual maximum).

The applied three-dimensional hydrodynamic model was capable of reproducing stratification and large-scale flow features in Passaúna Reservoir [35]. In the present study, three sets of simulations are used: (i) The simulations of the monitoring period (February 2018 to February 2019) using present reservoir morphology, observed inflow temperature, and measured atmospheric forcing (including wind and heat fluxes); (ii) A scenario with the forebay removed, where we assessed its influence on density currents, since it is a region that can potentially disappear either due to siltation or reduced water levels during a drought period. The underlying hypothesis was that underflows were expected to become more frequent due to lower inflow temperatures, once the forebay increases surface heat exchange due to the relatively large superficial area and low water depths [34]. One of the parameters to estimate river water temperature is the percentage of stream shading in the catchment. In scenario (iii), the inflow temperature was changed according to simulations with warmer river temperature that considered the lack of stream shading (0%) in the catchment [26]. In this case, the inflow temperatures became higher and an increased occurrence of overflows was expected [26].

As an extension of the previous simulations, we assessed the distribution and dynamics of density currents along the reservoir using the simulated transport of a numerical tracer, which was added to the inflow of the Passaúna River with a constant concentration of 1 kg L^{-1}. To avoid accumulation of the tracer in the reservoir, its concentration is decreasing over time with a first-order decay rate of 0.01 d^{-1}. A dynamic classification of density currents along a longitudinal cross section of the reservoir, according to the 10 sections, was performed for the remote sensing analysis. The classification was based on the vertical tracer distribution, expressed as the tracer ratio *Tr*:

$$Tr = 1 - \frac{d_{MaxTr}}{d} \quad (2)$$

where d_{MaxTr} is the depth of the maximum value of the laterally averaged simulated tracer concentration, and d is the mean water depth of the respective section. Thus, values of $Tr \leq 0.33$ are defined as underflows, $Tr \geq 0.67$ as overflows, and the intermediate range as interflows.

2.5. Statistical Metrics

For the comparison of different data, statistical tests were applied: the one-way ANOVA test, which compares the variance of two groups of normally distributed data; and the Kruskal–Wallis test, which is the equivalent of ANOVA for non-parametric distributions.

Chla estimated through remote sensing images were compared to the in-situ estimations by means of root mean squared error (*RMSE*), calculated as following:

$$RMSE = \sqrt{\frac{1}{n}\sum_{i=1}^{n}(\hat{y}_i - y_i)^2} \quad (3)$$

where $\hat{y}$ is the predicted value (estimation by remote sensing), y is the observed value (by in-situ sensing), and n is the number of predictions/observations. In addition, the Pearson correlation coefficient (R) was calculated.

3. Results

3.1. Continuous Observations

Air temperature had diel and seasonal variations (Figure 2a), and varied between 1.7 °C on 11 July 2018 and 33.9 °C on 29 January 2019. Wind speed was generally low, with a maximum value of 6.8 m s^{-1} and an average ± standard deviation of 2.0 ± 1.0 m s^{-1} (Figure 2b). March 2018 was a wet month regarding precipitation, which was followed by a dry period that extended until September (Figure 2b). From October on, precipitation occurred more regularly; in total, there was around 1400 mm of precipitation during the monitoring period. Regarding stratification, the reservoir is discontinuous warm polymictic, with stable thermal stratification during spring and summer, and intermittently mixing during autumn and winter (Figure 2, [34]).

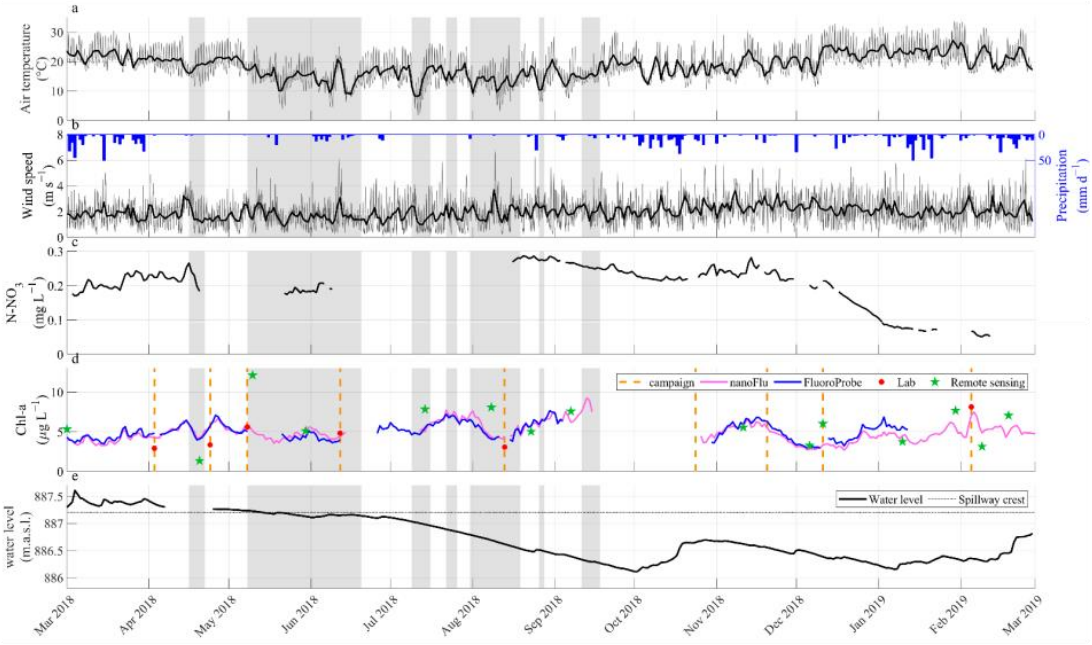

Figure 2. (**a**) Time series of daily mean air temperature. (**b**) Time series of wind speed (left *y*-axis, the gray fine line shows hourly averaged values and the black thick line shows daily means) and daily mean precipitation in mm d^{-1} (right *y*-axis) adopted from [26,34]. (**c**) Time series of N-NO_3 measured by the OPUS sensor. (**d**) Time series of chla measured by sensors with daily resolution (nanoFlu (pink) and FluoroProbe (blue) solid lines), laboratorial analysis (red symbols), and remote sensing (green symbols). The dashed vertical orange lines mark the days where field campaigns were performed. Gray background color marks periods of vertical mixing in all panels; during the remaining time, the reservoir was thermally stratified (adopted from Ishikawa, Bleninger, and Lorke [34]). (**e**) Time series of water level in meters above sea level (m.a.s.l.) in black thick line, the dotted line shows the crest of the spillway.

Chla measured continuously at the platform location at 1.5 m depth was relatively constant throughout the year (mean ± std: 5.2 ± 1.5 µg L^{-1}), and a marked seasonal behavior was not clear from visual inspection. However, the decrease of concentration over mixing events, followed by peaks of concentration were noted. Dividing the data in two series, concentrations over the mixed period (between the first and the last mixing event, 17 April to 17 September 2018) were significantly larger (7.2 ± 1.5 µg L^{-1}) than during stable stratification (5.7 ± 1.3 µg L^{-1}) according to a one-way ANOVA test (p-value << 0.01). Concentrations of N-NO_3 presented more consistent patterns over prolonged periods of time (Figure 2c). For example, the low concentrations in January and February 2019 did not affect chla concentrations, indicating that nitrogen is not a limiting nutrient in Passaúna Reservoir.

Water level fluctuations in Passaúna Reservoir were minor: over the monitored year, it varied between 886.1 and 887.6 m.a.s.l. From the middle of May, the level was constantly under the spillway crest, thus outflow at the dam occurred only through the bottom outlet.

3.2. Longitudinal Variations

Regarding the temperature stratification of the reservoir, only two campaigns were conducted during mixed periods (12 June 2018 and 13 August 2018), whereas during the remaining campaigns, the reservoir was thermally stratified (Figure 2d). Dissolved oxygen concentrations dropped to hypoxic conditions in a near-bottom layer, downstream of the Reservoir Center station, except for the two campaigns during the mixed period (Figure S3).

Nutrient concentrations (N-NO_3, N-NH_4, P-PO_4, TN, and TP) did not vary strongly between campaigns, but showed consistent longitudinal gradients along the reservoir (Figure 3). The concentrations generally decreased from higher concentrations in the inflow region to the smallest values near the dam. A particularly strong decrease was observed around station PPA (approximately 7 km from the inflow), indicating that most of the nutrients were taken up or settled before and around this location (Figure 3). Downstream of the station park (8 km from the inflow), the concentrations remained at relatively constant low levels. A different pattern was observed for N-NH_3, which remained relatively constant along the reservoir, and was strongly increased in the reservoir outflow.

Contrary to nutrient concentrations, chla was lowest in the river inflow, but increased rapidly within the reservoir, with the highest values and largest variability between the forebay and station PPA (Figure 3f). Beyond these sampling locations, chla gradually decreased towards the dam. Surprisingly, chla was comparable within the euphotic zone and below. Moreover, larger chla concentrations near the bed than at the water surface were frequently observed during the campaigns (Figure 4 and Figure S3).

During the lab analysis, it was observed that the samples collected below the euphotic zone had a brownish color, indicating that at least part of the phytoplankton was dead. The pattern of larger concentrations in deeper layers was also observed for nutrient concentrations (Figure 3).

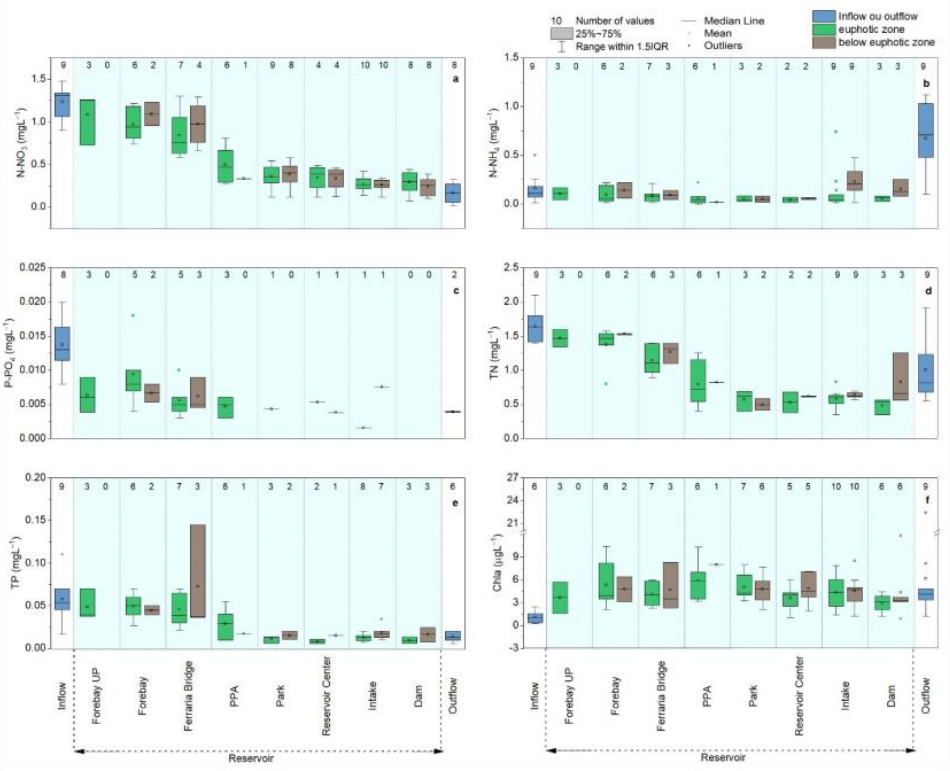

Figure 3. Box plots of water quality data estimated through laboratorial analysis and sensor measurements during all sampling campaigns at different locations along the reservoir (from inflow to outflow, see Figure 1 for the location of sampling sites). Data from different sampling sites are separated by vertical gray lines. Blue boxplots show measurements in the inflow and outflow; green boxplots show data from within the euphotic zone; and grey boxplots show data from below the euphotic zone. Numbers on the top of each boxplot represent total of samples; see the legend for an explanation of the box plot elements. Each panel presents one parameter indicated in each *y*-axis. Each panel presents the concentration of one substance: (**a**) N-NO_3; (**b**) N-NO_4; (**c**) P-PO_4; (**d**) TN; (**e**) TP; and (**f**) chla.

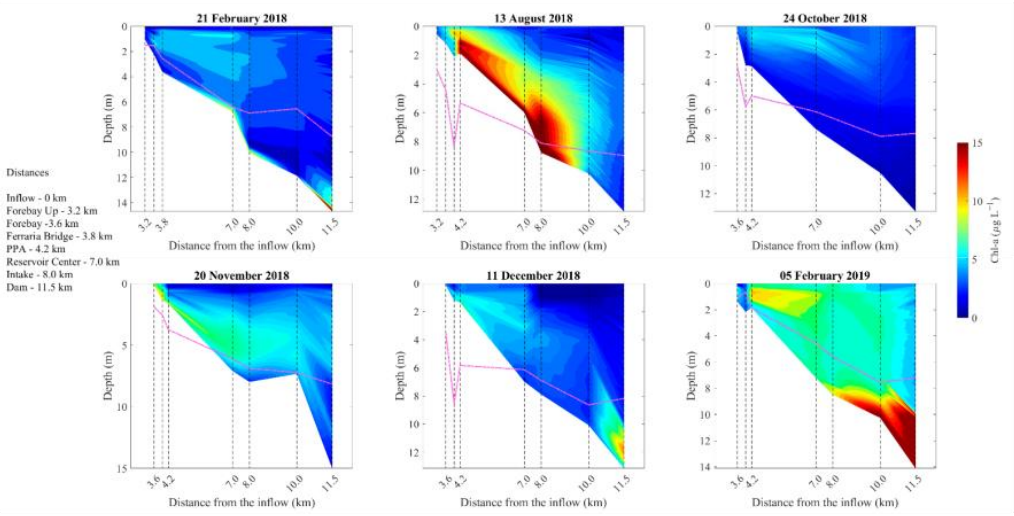

Figure 4. Contour plots of chla concentrations along a cross section of Passaúna Reservoir observed

during different sampling campaigns (the sampling date is indicated in the title of each panel). The *y*-axis is depth, and the *x*-axis is the distance along the longitudinal. The location of the sampling sites at which vertical profiles with the FluoroProbe sensor were measured is indicated by black dashed vertical lines. The profiles were interpolated along the longitudinal direction. The magenta dashed line shows the estimated depth of the euphotic zone.

3.3. Spatial Variations of Chla at the Water Surface

The three longitudinal transects had the highest concentrations between the forebay and the side arm with the Ferraria River, with the highest chla concentrations in February 2019 and the lowest in August 2018 (Figure 5).

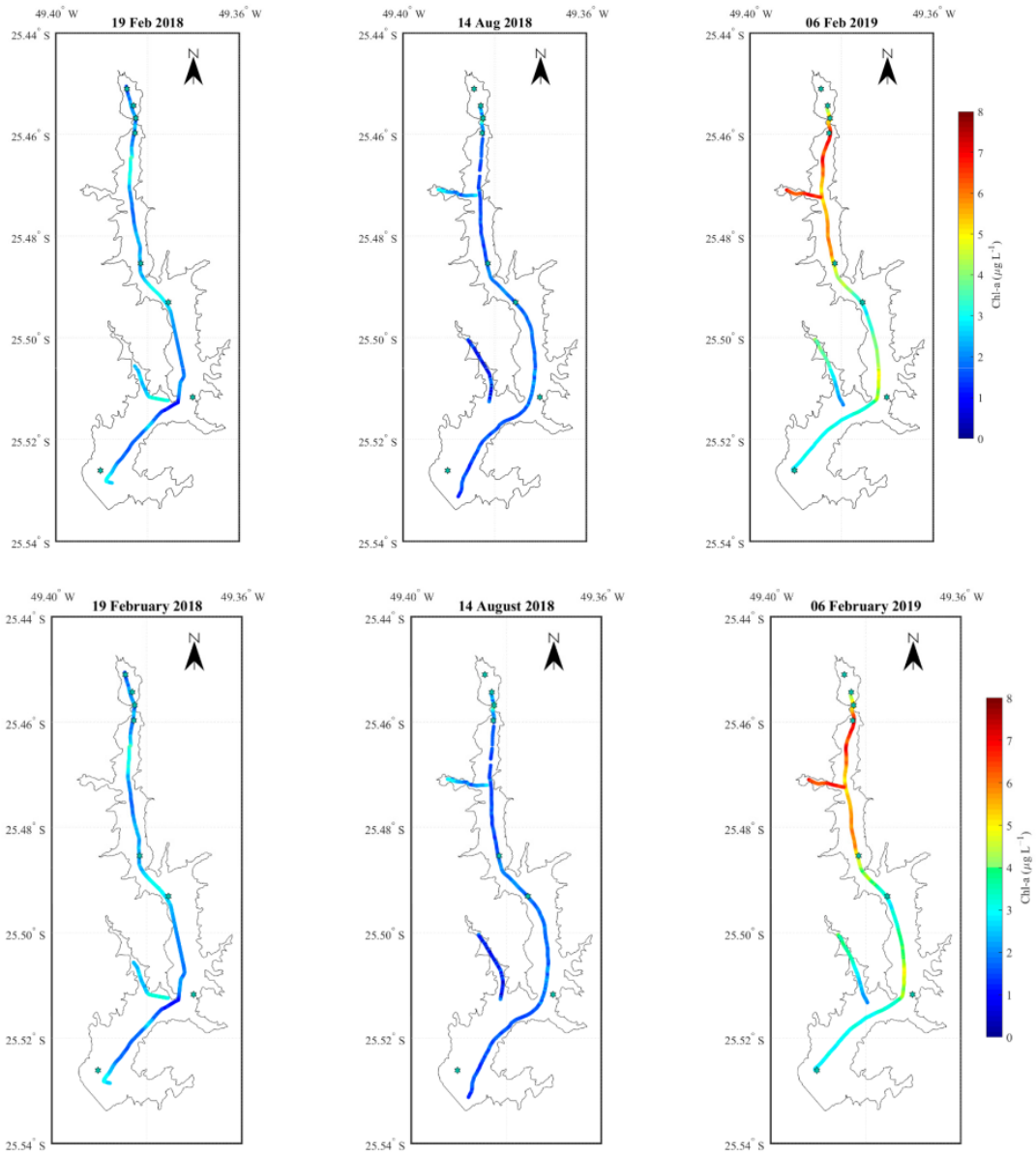

Figure 5. Longitudinal transects of chla at the water surface (~1 m depth), measured with the FluoroProbe sensor during the three extensive sampling campaigns (the sampling date indicated in the title of each panel).

Chla estimated from remote sensing images, in comparison to sensor measurements at the intake platform and the campaign in December 2018, had a root mean squared error (*RMSE*) of 3.7 µg L^{-1}. The Pearson correlation coefficient with lab measurements was poor and not significant: $R = 0.11$ (p-value = 0.56, n = 31). When keeping only the data from the intake sampling location, there was a slight improvement of agreement (*RMSE* = 2.8 µg L^{-1}, $R = 0.32$, p-value = 0.12, n = 24). A systematic error was not observed through a linear regression between laboratory measurements and remote sensing estimates (Figure S4).

Despite the poor correlation, the remote sensing observations provided values in the same magnitude and longitudinal gradients similar to the observations during the in-situ measurements (Figure 6). Therefore, the dataset can support the findings of the study, especially because of the better spatial resolution at the water surface. Considering all remote sensing estimates, the mean chla concentration ± standard deviation was 5.8 ± 4.2 µg L^{-1}.

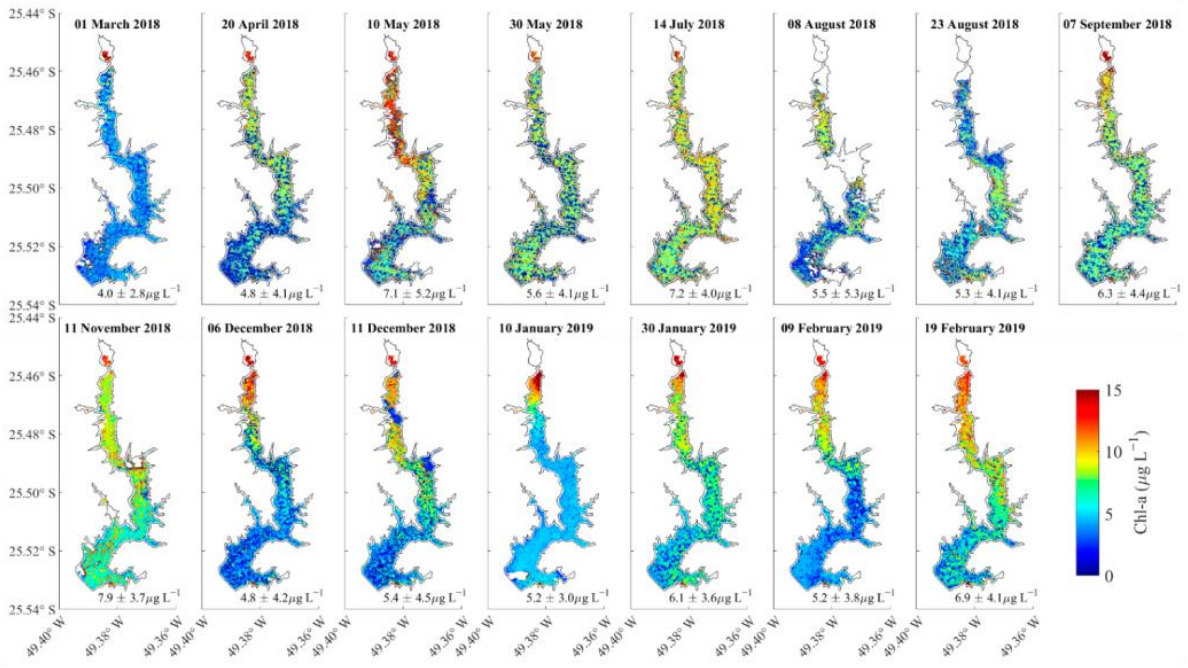

Figure 6. Maps of remote sensing estimates of chla concentrations for the days indicated in the title of each panel. The mean (±standard deviation) concentration is presented as a text label below each map.

3.4. Linking Water Quality to Physical Processes

Former analysis found seasonal variations of the density current patterns at the intake sampling station, which changed from predominantly interflows from March to mid-April 2018, to underflows during the period of frequent mixing, and to inter- and overflows starting from mid-August 2018 [35]. Here, we extended this analysis to other regions of the reservoir. The longitudinal pattern of the density current could be well followed by the simulated transport and decay of a tracer in the main inflow river (see Figure S5 for a sample distribution).

3.4.1. Temporal and Spatial Variations

In-situ sampling of the monitoring points within the euphotic zone were grouped according to the sections, since the points had variable distances among each other. In this way, the largest concentrations of chla were observed in section 2, (Figure 7b). The continuous surface transects (Figure 5) were also divided according to the sections, and

a similar longitudinal distribution to the samples was observed (Figure 7b). According to a Kruskal–Wallis test, none of the sections were significantly different from each other (p-value = 0.26 and 0.93, for measurements made through sampling and with the sensor, respectively).

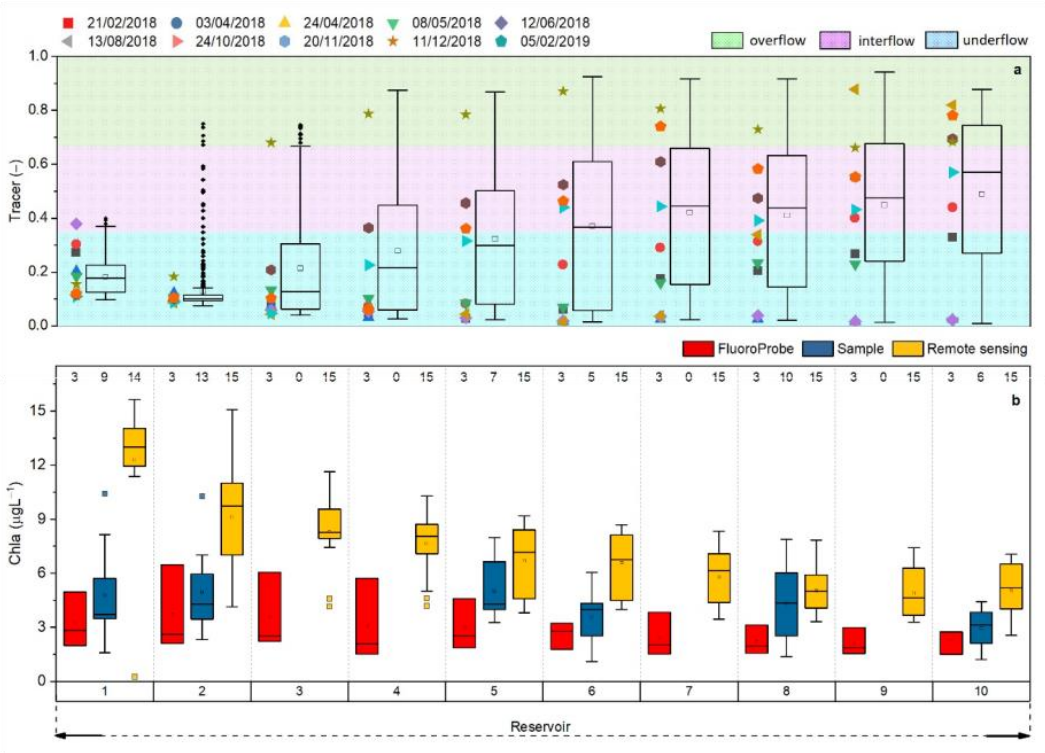

Figure 7. (**a**) Box plots of the temporal variations of the tracer ratio (*Tr*, Equation (1)) averaged for each section. The background color marks the thresholds for the three classifications of density currents (see legend). Each campaign is marked as a scatter plot. (**b**) Box plots showing the variability of different estimates of chla in the 10 longitudinal zones (vertical grey lines indicate each section as divided in panel (**a**). Yellow box plots represent the temporal variation of chla from remote sensing. Blue box plots represent the temporal variation of chla measured by analyses of water samples, for which sampling points were grouped according to sections. Red box plots represent the temporal variation of chla measured during the three continuous longitudinal transects with the FluoroProbe sensor (Figure 5).

The longitudinal pattern of the chla estimates from remote sensing differed from that of the in-situ measurements by showing gradually decreasing concentrations from the inflow region towards the dam (Figure 7b). The Kruskal–Wallis test showed that, in this case, chla concentration distribution in sections 1 to 4 were significantly different from sections 8 to 10, whereas sections 5 to 7 were only significantly different from section 1 (p-value < 0.001).

The longitudinal distribution of the tracer ratio for the entire analysis period showed the smallest values in section 2 (average of 0.13), followed by a gradual increase towards the dam (Figure 7a). Underflows dominated the forebay, representing 98% of the simulated period, as well as sections 2 and 3 (96% and 76%, respectively). In sections 4 and 5, the inflow was mostly present as underflows (65% and 54%), but also inter- and overflows occurred more frequently than in the sections upstream. From section 6, the flow path was present as interflows for 34% of the period, indicating a separation of the flow paths from the bed. The occurrence of overflow situations was observed only downstream of section 4,

where its occurrence gradually increased towards the dam (at section 10, it had a share of 37%). The opposite longitudinal pattern was observed for the occurrence of underflows.

The inflow regimes during the campaigns were classified using the tracer box plots (Figure 7a). At section 1, only the campaign in 12 June 2018 was an interflow, which was at the edge of being classified as underflow. Then, in section 2, all campaigns were within underflows. The campaign in 11 December 2018 is the only one that was classified as overflow over most of the sections. The first three campaigns were consistent underflows along all sections, whereas the others shifted to interflow and eventually to overflow (e.g., 13 August 2018 and 5 February 2019). It was also possible to identify a seasonal variation in the density current pattern: underflows occur mainly during autumn and winter, and overflows during spring and summer (Figure S6).

To assess the influence of thermal stability, chla concentrations were analyzed separately for mixed and for conditions, based on the temperature difference between surface and bottom water. The difference was calculated from in-situ measurements, whenever they were available; otherwise, they were estimated from the model simulations (Figure 8a,b).

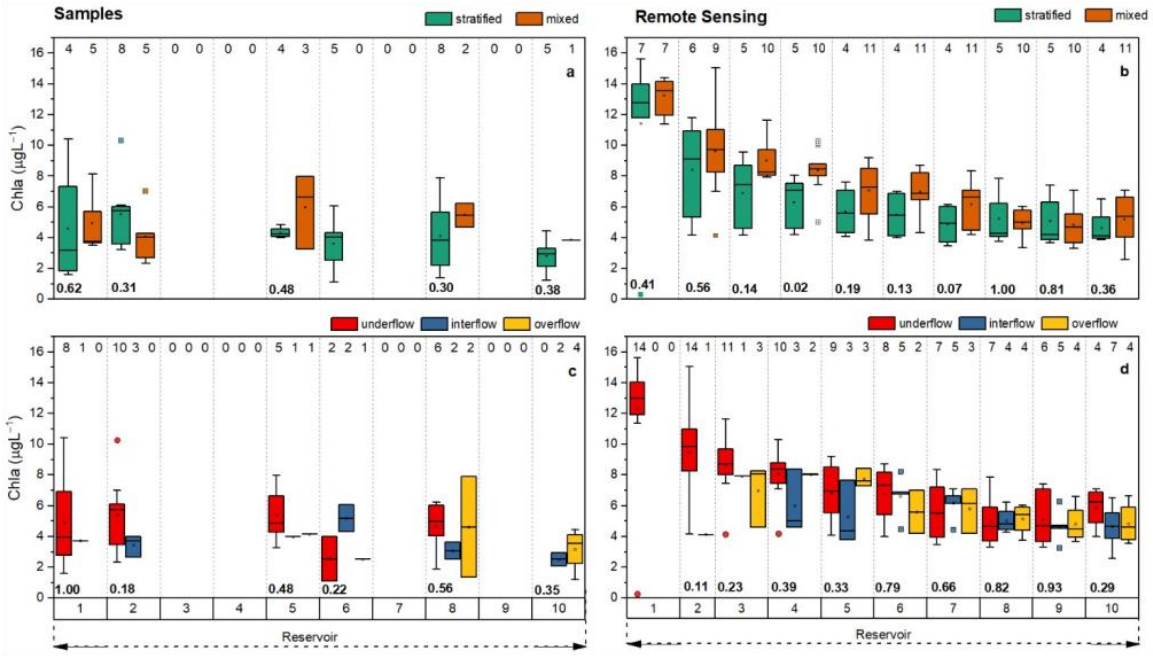

Figure 8. Box plots of chla concentrations observed during mixed (green) and stratified (orange) conditions from (**a**) laboratory analyses of water samples and (**b**) remote sensing estimates. Box plots of chla concentrations observed for different types of density currents: (**c**) laboratory analyses and (**d**) remote sensing. Each color represents one group according to the legends. Numbers at the bottom are the *p*-value of the Kruskal–Wallis test between the two groups within the section with the null hypothesis that both groups come from the same distribution.

The median values of chla estimated from situ data were consistently larger during mixed compared to stratified conditions, except for section 2. However, the chla concentration obtained from laboratory analyses of water samples did not differ significantly between mixed and stratified conditions (p-values > 0.05, Figure 8a), maybe due to the few and unevenly distributed samples. In addition, no consistent longitudinal trend was observed. The number of samples became more limiting when comparing chla measurements obtained during different types of density currents. For example, some sections had only one or no observation for some flow path groups (Figure 8c). No significant

differences between the distributions of chla concentrations from in-situ observations could be observed for the different types of density currents.

Contrary to the in-situ estimates, the chla concentrations estimated by remote sensing in the different longitudinal sections of the reservoir had consistently higher median values during stratified conditions compared to mixed conditions. However, only for section 4, the difference was significant (p-value = 0.02, Figure 8b). Only in sections 1, 8, and 9, the observed chla concentrations under mixed conditions had the maximum averaged observation larger than during stratified conditions. The division according to density currents did not present any systematic pattern, and all groups were similar (p-value > 0.05, Figure 8d).

We compared the original simulation of the tracer ratio to two additional scenarios (without the forebay, and without stream shading in the catchment) to understand how the changes could affect the flow paths of the density currents (Figure 9).

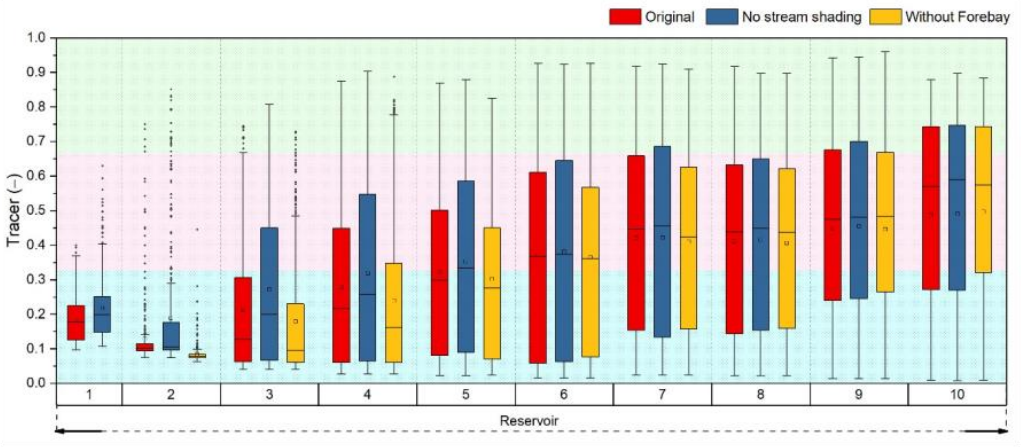

Figure 9. Box plots of tracer ratio for the original simulation and two scenarios (without the forebay and no stream shading in the catchment—indicated by the legend). Each subplot is one section, indicated by the title. The background color marks the thresholds for the three classifications of density current. Blue background represents the threshold for underflows, pink background for interflows, and green background for overflows.

The two scenarios presented the expected variations for density currents, but the changes were generally small. The most pronounced shift happened at section 2, which is right after the forebay, where, in the original simulation, underflows represented 95% of the density currents, it increased to 99% without the forebay, and decreased to 86% without stream shading. Similar differences were observed until section 4, whereas in more downstream sections, the distributions were unaffected, indicating that, from section 6, the influence of the inflow temperature was of minor relevance.

3.4.2. Correlations

For each of the 10 longitudinal sections of the reservoir, we calculated Pearson correlation coefficients between chla estimated from in-situ measurements and from remote sensing with the following parameters: inflow concentration of TP, P-PO_4, TN, N-NO_3, N-NH_4 (interpolated to a daily resolution from the in-situ measurements); Schmidt stability (S_T); average temperature difference between surface and bottom at each section (ΔT, model results); inflow temperature; and tracer ratio (Tr) (Figure 10). The sampled chla within the euphotic zone was correlated only with the temperature difference ΔT in section 2 (positive correlation). Remote sensing estimates of chla were positively correlated with Schmidt stability, ΔT, and inflow temperature in sections 1 and 2. Section 2 also had a positive correlation with P-PO_4, and a negative correlation with N-NO_3. From sections

4 to 6, negative correlations with ΔT were observed. Then, only section 6 had a negative correlation with Schmidt stability.

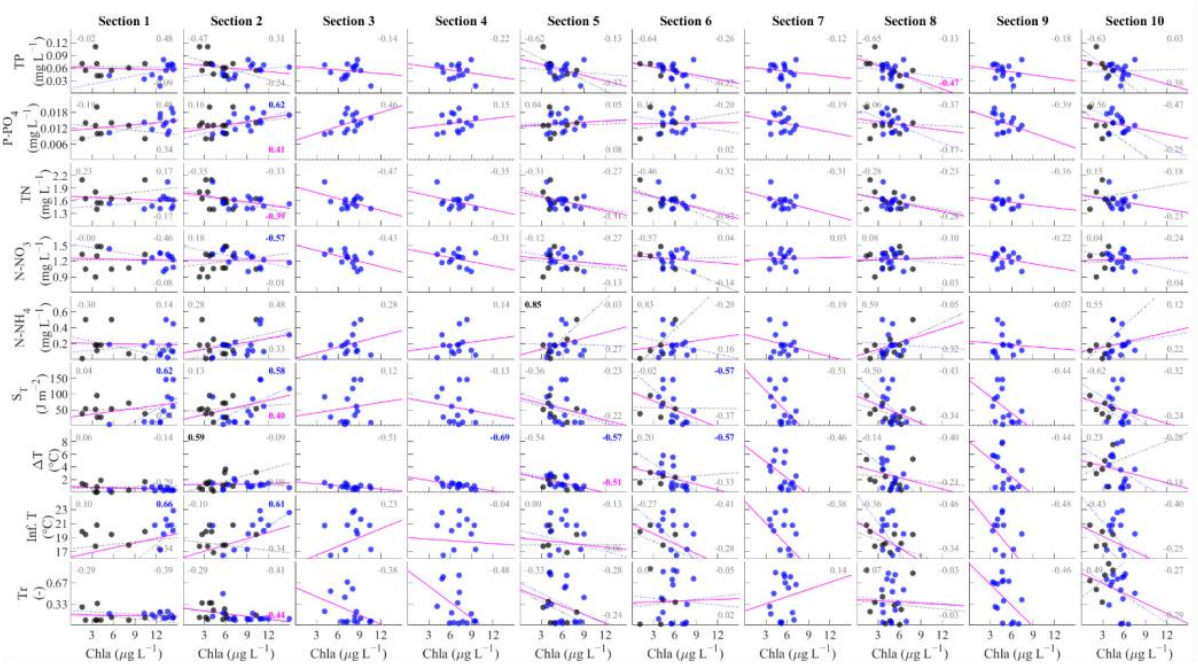

Figure 10. Correlations of chla obtained from samples (black dots) and remote sensing images (blue dots) with: measured inflow concentration of TP, P-PO_4, TN, N-NO_3, N-NH_4, Schmidt stability (S_T), the mean temperature difference between surface and bottom water (ΔT), measured inflow temperature (Inf. T), and tracer ratio (Tr). The columns represent data for 10 longitudinal sections, and rows represent the different parameters. All panels present the Pearson correlation coefficient for sampling (**top left**), remote sensing (**top right**), and both combined (**bottom right**) chla estimates. Numbers in gray indicate that the correlation was not significant ($p > 0.05$).

When combining both data (samples and remote sensing), the correlations did not improve much. Section 2 had significant correlations with P-PO4, TN, S_T, ΔT, and tracer ratio. Correlation with TP was negative in all sections (and significant in section 8). In addition, the correlation coefficients tended to shift their sign along the sections. For example, the inflow temperature was positively correlated with chla until section 3, and thereafter, the correlation became negative.

4. Discussion

4.1. Temporal and Spatial Variations of Nutrients and Chlorophyll

Concentration of dissolved nutrients and chla were more variable along the longitudinal extent of the reservoir than over time. The productivity in aquatic ecosystems in tropical to subtropical regions is known to have lower seasonal variability when compared to lakes and reservoirs in the temperate zone [36]. Nevertheless, there are several factors that can drive seasonal variability in tropical regions, including the prevalence of dry and wet seasons, flow regulation, and reservoir operation [37]. For Passaúna Reservoir, the several mixing episodes observed over the year prevented the development of a consistent seasonal pattern, as it is commonly found in studies in temperate regions (e.g., [38]). Due to the polymictic condition, the lacustrine zone of tropical reservoirs tend to have a more efficient recycling of nutrients in the sediment and in the hypolimnion [12]. Thus, the observed decrease of concentration of chla right after the mixing events is most likely explained by dilution due to vertical mixing, and the followed increase in chla supported

by internal loading with nutrients [39,40]. This is further supported by higher nutrient concentrations in deeper layers than near the water surface (Figure 3). In addition, averaged chla concentrations were larger over the periods where the mixing events occurred: during the autumn and winter seasons.

There are indications of N limitation in tropical lakes [41]; however, the continuous measurements at the monitoring platform at the intake suggested that the large variations of the N-NO_3 did not affect the chla dynamics, indicating that the N limitation was not relevant. In addition, the P limitation at Passaúna Reservoir was observed through the assessment of the annual average of inflow concentrations of TP and TN according to the scheme presented by Sterner [42].

The observed longitudinal decrease of nutrients (TN and TP) in Passaúna Reservoir (Figure 3) supports the conceptual model of [20] and observations in other reservoirs (e.g., [43,44]). The observed chla concentrations were in accordance with the proposed framework, showing the largest concentrations in a region between the riverine and lacustrine zones. This was more evident when grouping the sampled data in sections of equal distance (Figure 7b). When evaluating each point individually, chla concentrations had their largest values at the forebay and PPA. Between these two sampling locations, there was Ferraria Bridge, where concentrations were lower at the water surface than in deeper layers. At this point, the reservoir is laterally constraint to a channel-like region (see Figure 1), which may have influenced the vertical distribution (Figure 3). When grouping the data in sections, the second section presented the largest concentrations of chla, and a similar pattern was observed in the continuous longitudinal sensor transect (Figure 5). However, the concentration distributions of the different sections were not significantly different among each other. TP and TN had lower concentrations in the outflow from the reservoir compared to the inflow, indicating the trapping of nutrients by the dam. This was observed for all chemical nutrient speciation, except for N-NH_4, which had the largest concentrations at the outflow, a feature caused by the anoxic conditions found at the deepest layers close to the dam. Hence, most of the outflow was from the bottom outlet (all during the period when the water level was lower than the spillway crest—Figure 2e), and outflow concentrations were similar to the ones found in the deepest regions around the dam. On the other hand, chla had larger concentrations at the outflow than at the inflow.

The distinct longitudinal distribution of chla in reservoirs has not been observed in all studies, with many examples in which the largest concentration of chla was observed at the riverine zone [43–45], and at the lacustrine zone due to the mobilization of nutrients from the sediment [45]. A quantitative criterion for the definition or the prediction of the reservoir sections belonging to the riverine, transitional, and lacustrine zones is not trivial. Their location depends on morphological characteristics, flow velocities, light availability, and nutrient levels. Moreover, these zones can expand and compress over time [46]. Whereas other studies defined those regions through data clustering of the aforementioned parameters [37,47], we tried to do the same analysis, but the results were inconsistent. We believe that the main causes are the uneven distribution of sampling points along the longitudinal, and the missing measurements upstream between April and June (Table S1). A classification based on model results was also attempted; in this case, the variables used were morphological (depth and width) and flow velocities. For this reason, we evaluated the gradients according to the longitudinal distribution of nutrients and chla, which is more relevant than defined zones. In addition, for reservoirs with a dendritic shape, or with more than one relevant inflow, the zonation can become less meaningful.

In contrast to the in-situ measurements, chla estimated by remote sensing had its largest concentrations in the most upstream regions, and it decreased continuously until the dam. The greatest differences between remote sensing and in-situ chla estimates occurred in section 1, and the difference was gradually decreasing along the reservoir. However, the remote-sensing-based estimates had a root mean square error of ± 3.7 μg L^{-1}, which is smaller than the expected error for chla estimations from the Sentinel-2 observation of $5-10$ μg L^{-1} [48,49]. Thus, for the low range of chla values in Passaúna Reservoir from

the in-situ reference (mostly between 4 and 7 µg L^{-1}, see Figure 2c), a strong correlation between observed and estimated chla variations over time cannot be expected. Yet, spatial patterns observed in individual remote sensing scenes may be meaningful, in that it may be a systematic error per scene. The comparison of remote-sensing-based and in-situ measurements time series suggests that the remote-sensing-based method is sensitive to small temporal changes. There are several sources contributing to the disagreement of in-situ and remote-sensing-based values, such as the mismatch of the field of view of in-situ and remote optical sensors, temporal mismatch, remote sensing model error, and in-situ sensor error (disagreement between sensor and lab analysis). However, we cannot estimate the individual contribution of each error source.

In laboratory analyses, although the samples were kept in the dark for their preservation, they were filtered several hours after sample collection (when they arrived in the laboratory). Further, chlorophyll was extracted from the samples by manual maceration. Each step is susceptible to add uncertainties. On the other hand, sensor measurements have the advantage of taking measurements in-situ, but can be affected by the sunlight, and present a limitation on the measurement range depending on the optical path. As the laboratorial analysis is a well-established method, we usually take its result as the reference for the comparison with sensor and remote-sensing-based estimates.

4.2. Effects of Density Currents

The results from the numerical model showed good agreement with observed temperatures (*RMSE* = 0.77 °C) [35], and for Passaúna Reservoir, the main driver of changes in inflow density is temperature [34]. Thus, the simulated tracer transport is considered a good approach for evaluating the flow paths of density currents. This is supported by previous studies using numerical tracers as a proxy for density currents, which showed good agreement with in-situ observations of dye tracers [50].

The sampling campaigns on 13 August 2018 and on 5 February 2019 were conducted for similar nutrient concentrations in the reservoir inflow (TN = 1.5 and 1.6 mg L^{-1}, TP = 0.04 and 0.05 mg L^{-1}), yet the longitudinal transects showed that chla at the water surface was about a factor of two lower in August than in February (Figure 5). Based on the tracer ratio analysis from the numerical model (Figure 9), the campaign in August was dominated by an underflow (except in the two last sections), and the other campaign varied from underflow in sections 1 to 4, and to inter- and overflow in the rest of the reservoir. In addition, sensor profiling (Figure 4) showed that the highest concentrations of chla in August were in the deeper layers. This indicates that nutrients were consumed in the upstream region, where the euphotic zone encompassed the entire water column, and the algae were transported by the density current to larger depths. When dividing the sampled data set in groups of under-, inter-, and overflow (Figure 8c), chla had the largest concentrations in interflows (section 6) and overflows (sections 8 and 10). However, the groups were statistically similar, which agrees with the generally small temporal variability of chla.

Density currents varied seasonally (Figure S6), and it was expected that they could promote seasonal variations in chla [24,35]; however, this was not observed. One explanation for not seeing a significant difference according to the flow path over time is related to water depth in relation to the euphotic zone. Until section 4 (maximum water depth ~7 m), the estimated depth of the euphotic zone was larger than the water depth on some occasions. Therefore, even when nutrients were delivered directly to the bottom, they were within the euphotic zone available for algal growth. Because of the shallower depths, the region mixed more frequently than downstream regions, making the surface concentrations of chla independent of the density current pattern. Since inflow concentrations were rather constant, temporal variations were minor.

Regarding the simulated scenarios, simulation without the forebay increased the formation of underflows significantly until section 3 (p-values < 0.001). The other scenario, with higher inflow temperatures due to the removal of stream shading in the catchment,

increased the formation of overflows until section 4 (p-values ≤ 0.03). In both simulations, the density currents were not influenced by the inflow conditions downstream of this section. In that regard, our simulations confirm previous analyses of the expected changes of density currents in both scenarios [26,34]. In these studies, density currents were classified based on inflow temperature and on the vertical temperature profile measured at the intake (section 8), which excluded vertical mixing during transport along the longitudinal extent of the reservoir. Indeed, there was the increase of under- or overflows depending on the scenario; however, these changes could not be seen at the intake. According to the model, the shift is only seen until the park station. The inflowing water can be mixed vertically before it is transported longitudinally to regions with water depths exceeding that of the surface mixed layer. In this way, it is possible that the currents classified as interflows or underflows move forward along to the water surface. This was observed in the tracer simulations, and due to the small water depth until section 5, it was common to have a vertical mixing over the entire water column during the entire year.

Sotiri, et al. [51] assessed the sediment thickness of Passaúna Reservoir, and identified two major zones of sedimentation, which correspond to sections 2 and 9 of this study. The first region upstream is linked to sedimentation from inflow, where we found most algal growth. Our observations show that the second sedimentation zone, closer to the dam, is likely formed by the enhanced deposition of algae that are transported there from the inflow region by density currents. This is supported by the assessment of organic matter content in the sediment presented in Marcon, et al. [52], where at section 2, organic matter was <10% of the sediment content, and in the downstream regions, it was >30%. Enhanced deposition of autochthonous organic matter explains the persistent formation of anoxic conditions of the deeper layers in the downstream region of the reservoir, as they were observed in most campaigns (Figure S3) and in previously analyzed continuous oxygen measurements performed near the intake station [34]. Using the sediment surface area and reservoir water volume for water depth exceeding 9 m, the areal hypolimnetic oxygen deficit (AHOD, Hutchinson [53]) calculated from the temporal rate of decrease of dissolved oxygen concentration in the hypolimnion observed in [34] was approximately 1.0 g of O_2 m^{-2} day^{-1}. The AHOD observed in Passaúna is in the same range as eutrophic lakes in the temperate zone [54], though Passaúna is classified as mesotrophic. Moreover, the two regions with high sedimentation rates are characterized by the highest emissions and production rates of methane [52].

4.3. Correlations between Nutrient and Chlorophyll Concentrations

With an annual mean inflow concentration of total phosphorous (TP) of 0.06 mg L^{-1}, the averaged concentration of chla measured in-situ (at all depths and all campaigns) of 4.4 µg L^{-1} in Passaúna Reservoir is in the lower range of values predicted by linear models between both variables that have been established for different lakes and reservoirs, and range between 5.0 and 30.2 µg L^{-1} (Table S2). The relationship that provided the closest result to the observations was the one presented by Stow and Cha [7], though its relationship was found for Lake Huron; nevertheless, other results were within the error margin.

Correlations between spatial and temporal variations of chla and TP in Passaúna Reservoir were generally poor, and the same was observed for correlation with other parameters. Carneiro, et al. [55], and Klippel, Macêdo, and Branco [1] also found poor results for direct relationships between total phosphorus and chla in Brazilian reservoirs. They considered data for periods of one month and three years, respectively. Cunha, Finkler, Lamparelli, Calijuri, Dodds, and Carlson [2] found better linear relationships between TP and chla using annual mean values from six reservoirs in Brazil for a period of nine years. An increase in sample number by merging the in-situ and remote sensing data did not improve the correlations. Nevertheless, remote-sensing-based chla estimates had the largest difference in regard to longitudinal pattern in the two first sections when compared to in-situ measurements, which can put the results from these zones into question. For sections

where there was not much difference between the two datasets (e.g., section 6), Schmidt stability had negative correlations, which agrees with the observation of declining chla concentrations during mixing, and higher values during restratification periods (Figure 2c). In the data from continuous measurements of chla and Schmidt stability, the correlation between both parameters was poor, most likely because the trigger for the increased algal growth is the mixing event, i.e., change of the strength of stratification.

From the poor correlations between observed chla variability and environmental conditions, we comprehend that the processes that are controlling phytoplankton dynamics are more complex than linear relationships, and additional processes should be considered when assessing results at different spatial and temporal scales. For example, during the campaign in October 2018, the total phosphorus concentration in Passaúna River was highest; however, the chla concentrations in the reservoir were the smallest. This counterintuitive observation can potentially be explained by a rain event that occurred in this month, which mobilized nutrients, increased the flow rates, and reduced the residence time, which are not favorable for phytoplankton growth [56]. Another feature was the concentration maximum of chla at deeper, near-bed layers, where the concentration frequently exceeded those measured near the water surface. Our analysis suggests that they were transported by density currents from upstream regions. Depending on the mixing condition, type of density current, and euphotic zone depth, concentrations of chla can be highest at the water surface, even in the presence of underflows.

5. Conclusions

The use of fast in-situ probes on a moving boat, combined with remote sensing techniques and 3D hydrodynamic modeling allowed us to map and link water quality and hydrodynamic features in a drinking water reservoir located in the subtropical zone. Despite the seasonal variation of density currents and thermal stratification, the chlorophyll-a concentration (chla) did not follow a seasonal pattern (standard deviation of 1.2 µg L^{-1}, at the continuous measurement station), whereas spatial variability was more pronounced (standard deviation of 2.1 µg L^{-1}, among all monitored points within the euphotic zone). The small temporal variability was caused by the shallow depth of water in the productive upstream region of the reservoir, where the entire water column was within the euphotic zone and was frequently mixed throughout the year. Thus, even with the delivery of nutrients to deeper layers by inflowing river water as underflows, they were available for the growth of phytoplankton. The algae grown in the upstream region of the reservoir were transported downstream by the density currents, resulting in the highest concentrations of chla below the euphotic zone at larger water depths. Most nutrients were consumed in the upstream region, and primary production in the lacustrine zone depended on internal loading, and was promoted by mixing events.

Linear correlations between temporal variations of the concentration of chla and total phosphorus (TP), thermal stability, and density current patterns at specific points in the reservoir were generally poor. On the other hand, the annual mean values of chla and TP were in the lower range of linear models relating both parameters across different lakes and reservoirs. Such relationships can inform about seasonal and basin-scale mean chla concentrations, but fail in reproducing its spatial and temporal dynamics, for which the distribution and dynamics of both nutrients and algae are strongly influenced by hydrodynamic processes.

We expect that the dynamics of nutrient delivery and phytoplankton transport by density currents observed in Passaúna Reservoir are representative of a large number of reservoirs. For deeper reservoirs, where the euphotic zone is restricted to a smaller longitudinal extent, or flow velocities are larger (pushing the transitional zone towards larger water depth), more pronounced seasonal variations of chla could be induced by variations of density currents. Under such conditions, the simulated scenarios with increasing occurrence of overflow situations in the upstream reservoir region could increase the primary production of the system. For Passaúna Reservoir, a significant increase of nutrient

concentration in the inflow would probably be required to compromise its water quality, if nutrients would not be consumed completely in the upstream region and became available also for the lacustrine regions. However, our analyses suggest that phytoplankton growth in the lacustrine zone of the reservoir is controlled by internal loading. Internal loading can increase over time due to the increasing accumulation of phosphorus in the sediment, and due to higher temperatures that increase organic matter decomposition rates, and cause more persistent water column stratification with anoxic conditions in the hypolimnion. Additionally, drought periods with lower water levels and intensified near-bed mixing can increase internal loading episodically. Therefore, internal loading can become a trigger for degradation of water quality in the lacustrine region.

For spatial variations within the reservoir and temporal variability of chlorophyll dynamics, linear statistical models were not sufficient to provide predictions. These features can potentially be resolved by applying coupled hydrodynamic and water quality models. The persistent longitudinal gradients and the importance of density currents for the transport and distribution of nutrients, algae, and detritus revealed in our analyses suggest that at least two dimensions (depth and longitudinal) should be considered in hydrodynamic and water quality models for reservoirs.

Supplementary Materials: The following supporting information can be downloaded at: https://www.mdpi.com/article/10.3390/w14101544/s1, Figures S1–S6; Tables S1 and S2.

Author Contributions: Conceptualization, M.I., A.L., L.G. and T.B.; field campaigns, M.I., L.G., H.R. and T.B.; laboratorial analysis, L.G.; validation of sensor's data, H.R., L.G. and M.I.; formal analysis, M.I. and L.G.; remote sensing images acquisition, processing, and validation, N.W.; writing—original draft preparation, M.I. and L.G.; writing—review and editing, A.L., T.B., N.W. and H.R.; supervision, A.L. and T.B. All authors have read and agreed to the published version of the manuscript.

Funding: This research was funded by the Federal Ministry of Education and Research by the MuDak-WRM project under the grant numbers: 02WGR1431B, 02WGR1431G, and 02WGR1431E. In addition, Bleninger acknowledges the productivity stipend from the National Council for Scientific and Technological Development—CNPq, grant no. 312211/2020-1, call 09/2020. This study was financed in part by the Coordenação de Aperfeiçoamento de Pessoal de Nível Superior—Brasil (CAPES)—Finance Code 001. Luziadne Gurski acknowledges CAPES for financial support and Ph.D. scholarship.

Data Availability Statement: The data that support the findings of this study are available upon request from the authors.

Acknowledgments: The authors are thankful for all of the team involved in the campaign planning, execution, platform maintenance, and sample analysis, which include people from MuDak-WRM project, the Sanitation Company of Paraná (SANEPAR), and the Graduate Program of Water Resources and Environmental Engineer of Federal University of Paraná, especially Heloise Knapik and Luciane Prado.

Conflicts of Interest: The authors declare no conflict of interest.

References

1. Klippel, G.; Macêdo, R.L.; Branco, C.W.C. Comparison of different trophic state indices applied to tropical reservoirs. *LakesReserv. Sci. Policy Manag. Sustain. Use* **2020**, *25*, 214–229. [CrossRef]
2. Cunha, D.G.F.; Finkler, N.R.; Lamparelli, M.C.; Calijuri, M.d.C.; Dodds, W.K.; Carlson, R.E. Characterizing Trophic State in Tropical/Subtropical Reservoirs: Deviations among Indexes in the Lower Latitudes. *Environ. Manag.* **2021**, *68*, 491–504. [CrossRef]
3. Megard, R.O. Phytoplankton, Photosynthesis, And Phosphorus In Lake Minnetonka, Minnesota1. *Limnol. Oceanogr.* **1972**, *17*, 68–87. [CrossRef]
4. Havens, K.E.; Nürnberg, G.K. The Phosphorus-Chlorophyll Relationship in Lakes: Potential Influences of Color and Mixing Regime. *Lake Reserv. Manag.* **2004**, *20*, 188–196. [CrossRef]
5. Dillon, P.J.; Rigler, F.H. The phosphorus-chlorophyll relationship in lakes1,2. *Limnol. Oceanogr.* **1974**, *19*, 767–773. [CrossRef]
6. Phillips, G.; Pietiläinen, O.P.; Carvalho, L.; Solimini, A.; Lyche Solheim, A.; Cardoso, A.C. Chlorophyll–nutrient relationships of different lake types using a large European dataset. *Aquat. Ecol.* **2008**, *42*, 213–226. [CrossRef]

7. Stow, C.A.; Cha, Y. Are Chlorophyll a–Total Phosphorus Correlations Useful for Inference and Prediction? *Environ. Sci. Technol.* **2013**, *47*, 3768–3773. [CrossRef]
8. Quinlan, R.; Filazzola, A.; Mahdiyan, O.; Shuvo, A.; Blagrave, K.; Ewins, C.; Moslenko, L.; Gray, D.K.; O'Reilly, C.M.; Sharma, S. Relationships of total phosphorus and chlorophyll in lakes worldwide. *Limnol. Oceanogr.* **2021**, *66*, 392–404. [CrossRef]
9. Abell, J.M.; Özkundakci, D.; Hamilton, D.P.; Jones, J.R. Latitudinal variation in nutrient stoichiometry and chlorophyll-nutrient relationships in lakes: A global study. *Fundam. Appl. Limnol.* **2012**, *181*, 1–14. [CrossRef]
10. Filstrup, C.T.; Wagner, T.; Soranno, P.A.; Stanley, E.H.; Stow, C.A.; Webster, K.E.; Downing, J.A. Regional variability among nonlinear chlorophyll—phosphorus relationships in lakes. *Limnol. Oceanogr.* **2014**, *59*, 1691–1703. [CrossRef]
11. Shuvo, A.; O'Reilly, C.M.; Blagrave, K.; Ewins, C.; Filazzola, A.; Gray, D.; Mahdiyan, O.; Moslenko, L.; Quinlan, R.; Sharma, S. Total phosphorus and climate are equally important predictors of water quality in lakes. *Aquat. Sci.* **2021**, *83*, 16. [CrossRef]
12. Lewis, W.M., Jr. Tropical lakes: How latitude makes a difference. In *Perspectives in Tropical Limnology*; SPB Academic Publishing: Amsterdam, The Netherlands, 1996; Volume 4364.
13. Winton, R.S.; Calamita, E.; Wehrli, B. Reviews and syntheses: Dams, water quality and tropical reservoir stratification. *Biogeosciences* **2019**, *16*, 1657–1671. [CrossRef]
14. Mulligan, M.; van Soesbergen, A.; Sáenz, L. GOODD, a global dataset of more than 38,000 georeferenced dams. *Sci. Data* **2020**, *7*, 31. [CrossRef]
15. Zarfl, C.; Lumsdon, A.E.; Berlekamp, J.; Tydecks, L.; Tockner, K. A global boom in hydropower dam construction. *Aquat. Sci.* **2014**, *77*, 161–170. [CrossRef]
16. Yasarer, L.M.W.; Sturm, B.S.M. Potential impacts of climate change on reservoir services and management approaches. *Lake Reserv. Manag.* **2016**, *32*, 13–26. [CrossRef]
17. Fadel, A.; Sharaf, N.; Siblini, M.; Slim, K.; Kobaissi, A. A simple modelling approach to simulate the effect of different climate scenarios on toxic cyanobacterial bloom in a eutrophic reservoir. *Ecohydrol. Hydrobiol.* **2019**, *19*, 359–369. [CrossRef]
18. Weber, C.J.; Weihrauch, C. Autogenous Eutrophication, Anthropogenic Eutrophication, and Climate Change: Insights from the Antrift Reservoir (Hesse, Germany). *Soil Syst.* **2020**, *4*, 29. [CrossRef]
19. Kimmel, B.L.; Lind, O.T.; Paulson, L.J. Reservoir primary productivity. In *Reservoir Limnology: Ecological Perspectives*; John Wiley & Sons, Inc.: Hoboken, NJ, USA, 1990; Volume 1, pp. 133–199.
20. Kimmel, B.L.; Groeger, A.W. Factors Controlling Primary Production In Lakes And Reservoirs: A Perspective. *Lake Reserv. Manag.* **1984**, *1*, 277–281. [CrossRef]
21. Noori, R.; Ansari, E.; Jeong, Y.-W.; Aradpour, S.; Maghrebi, M.; Hosseinzadeh, M.; Bateni, S.M. Hyper-Nutrient Enrichment Status in the Sabalan Lake, Iran. *Water* **2021**, *13*, 2874. [CrossRef]
22. Sun, H.; Lu, X.; Yu, R.; Yang, J.; Liu, X.; Cao, Z.; Zhang, Z.; Li, M.; Geng, Y. Eutrophication decreased CO2 but increased CH4 emissions from lake: A case study of a shallow Lake Ulansuhai. *Water Res.* **2021**, *201*, 117363. [CrossRef]
23. Gholizadeh, M.H.; Melesse, A.M.; Reddi, L. A Comprehensive Review on Water Quality Parameters Estimation Using Remote Sensing Techniques. *Sensors* **2016**, *16*, 1298. [CrossRef] [PubMed]
24. Rueda, F.J.; Fleenor, W.E.; de Vicente, I. Pathways of river nutrients towards the euphotic zone in a deep-reservoir of small size: Uncertainty analysis. *Ecol. Model.* **2007**, *202*, 345–361. [CrossRef]
25. Cortés, A.; Fleenor, W.; Wells, M.; de Vicente, I.; Rueda, F. Pathways of river water to the surface layers of stratified reservoirs. *Limnol. Oceanogr.* **2014**, *59*, 233–250. [CrossRef]
26. Ishikawa, M.; Haag, I.; Krumm, J.; Teltscher, K.; Lorke, A. The effect of stream shading on the inflow characteristics in a downstream reservoir. *River Res. Appl.* **2021**, *37*, 943–954. [CrossRef]
27. Sanepar, C.d.S.d.P. Plano Diretor SAIC: Sistema de Abastecimento de Água Integrado de Curitiba e Região Metropolitana. *Curitiba Sanepar* **2013**. Available online: https://site.sanepar.com.br/arquivos/saicplanodiretor.pdf (accessed on 30 September 2020).
28. Sotiri, K.; Hilgert, S.; Fuchs, S. Sediment classification in a Brazilian reservoir: Pros and cons of parametric low frequencies. *Adv. Oceanogr. Limnol.* **2019**, *10*. [CrossRef]
29. Luhtala, H.; Tolvanen, H. Optimizing the Use of Secchi Depth as a Proxy for Euphotic Depth in Coastal Waters: An Empirical Study from the Baltic Sea. *ISPRS Int. J. Geo-Inf.* **2013**, *2*, 1153–1168. [CrossRef]
30. Rousso, B.Z.; Bertone, E.; Stewart, R.A.; Rinke, K.; Hamilton, D.P. Light-induced fluorescence quenching leads to errors in sensor measurements of phytoplankton chlorophyll and phycocyanin. *Water Res.* **2021**, *198*, 117133. [CrossRef]
31. APHA. *Standard Methods for the Examination of Water and Wastewater*, 21st ed.; American Public Health Association: Washington, DC, USA, 2005.
32. COMPANHIA AMBIENTAL DO ESTADO DE SÃO PAULO (CETESB). *L5.306: Determinação de Clorofila a e Feofitina a: Método Espectrofotométrico*, 3rd ed.; Companhia Ambiental do Estado de São Paulo: São Paulo, Brazil, 2014.
33. Brockmann, C.; Doerffer, R.; Peters, M.; Kerstin, S.; Embacher, S.; Ruescas, A. Evolution of the C2RCC Neural Network for Sentinel 2 and 3 for the Retrieval of Ocean Colour Products in Normal and Extreme Optically Complex Waters. In Proceedings of the conference: Living Planet Symposium 2016, Prague, Czech Republic, 1 August 2016; p. 54.
34. Ishikawa, M.; Bleninger, T.; Lorke, A. Hydrodynamics and mixing mechanisms in a subtropical reservoir. *Inland Waters* **2021**, *11*, 286–301. [CrossRef]
35. Ishikawa, M.; Gonzalez, W.; Golyjeswski, O.; Sales, G.; Rigotti, J.A.; Bleninger, T.; Mannich, M.; Lorke, A. Effects of dimensionality on the performance of hydrodynamic models for stratified lakes and reservoirs. *Geosci. Model Dev.* **2022**, *15*, 2197–2220. [CrossRef]

36. Wetzel, R.G. *Limnology: Lake and River Ecosystems*; Academic Press: San Diego, CA, USA; London, UK, 2001.
37. de Oliveira, T.F.; de Sousa Brandão, I.L.; Mannaerts, C.M.; Hauser-Davis, R.A.; Ferreira de Oliveira, A.A.; Fonseca Saraiva, A.C.; de Oliveira, M.A.; Ishihara, J.H. Using hydrodynamic and water quality variables to assess eutrophication in a tropical hydroelectric reservoir. *J. Environ. Manag.* **2020**, *256*, 109932. [CrossRef]
38. Shatwell, T.; Adrian, R.; Kirillin, G. Planktonic events may cause polymictic-dimictic regime shifts in temperate lakes. *Sci. Rep.* **2016**, *6*, 24361. [CrossRef]
39. Soranno, P.A.; Carpenter, S.R.; Lathrop, R.C. Internal phosphorus loading in Lake Mendota: Response to external loads and weather. *Can. J. Fish. Aquat. Sci.* **1997**, *54*, 1883–1893. [CrossRef]
40. Mesman, J.P.; Ayala, A.I.; Goyette, S.; Kasparian, J.; Marcé, R.; Markensten, H.; Stelzer, J.A.A.; Thayne, M.W.; Thomas, M.K.; Pierson, D.C.; et al. Drivers of phytoplankton responses to summer wind events in a stratified lake: A modeling study. *Limnol. Oceanogr.* **2022**, *67*, 856–873. [CrossRef]
41. Lewis Jr., W. Biogeochemistry of tropical lakes. *Int. Ver. fÜR Theor. Angew.Limnol. Verh.* **2010**, *30*, 1595–1603. [CrossRef]
42. Sterner, R.W. On the Phosphorus Limitation Paradigm for Lakes. *Int. Rev. Hydrobiol.* **2008**, *93*, 433–445. [CrossRef]
43. Caputo, L.; Naselli-Flores, L.; OrdoÑEz, J.; Armengol, J. Phytoplankton distribution along trophic gradients within and among reservoirs in Catalonia (Spain). *Freshw. Biol.* **2008**, *53*, 2543–2556. [CrossRef]
44. Rychtecký, P.; Znachor, P. Spatial heterogeneity and seasonal succession of phytoplankton along the longitudinal gradient in a eutrophic reservoir. *Hydrobiologia* **2011**, *663*, 175–186. [CrossRef]
45. Gomes Nogueira, M. Phytoplankton composition, dominance and abundance as indicators of environmental compartmentalization in Jurumirim Reservoir (Paranapanema River), São Paulo, Brazil. *Hydrobiologia* **2000**, *431*, 115–128. [CrossRef]
46. Freire, R.; Calijuri, M.; Santaella, S. Longitudinal patterns and variations in water quality in a reservoir in the semiarid region of NE Brazil: Responses to hydrological and climatic changes. *Acta Limnol. Bras.* **2009**, *21*, 251–262.
47. de Moura-Júnior, E.G.; Severi, W.; Kamino, L.H.Y.; de Lemos-Filho, J.P. To what degree do spatial and limnological predictors explain the occurrence of a submerged macrophyte species in lotic and semi-lotic/lentic environments of a dammed river? *Limnology* **2021**, *22*, 101–110. [CrossRef]
48. Soomets, T.; Uudeberg, K.; Jakovels, D.; Brauns, A.; Zagars, M.; Kutser, T. Validation and Comparison of Water Quality Products in Baltic Lakes Using Sentinel-2 MSI and Sentinel-3 OLCI Data. *Sensors* **2020**, *20*, 742. [CrossRef]
49. Ogashawara, I.; Kiel, C.; Jechow, A.; Kohnert, K.; Ruhtz, T.; Grossart, H.-P.; Hölker, F.; Nejstgaard, J.C.; Berger, S.A.; Wollrab, S. The Use of Sentinel-2 for Chlorophyll-a Spatial Dynamics Assessment: A Comparative Study on Different Lakes in Northern Germany. *Remote Sens.* **2021**, *13*, 1542. [CrossRef]
50. Owens, E.M.; Effler, S.W.; O'Donnell, D.M.; Matthews, D.A. Modeling the Fate and Transport of Plunging Inflows to Onondaga Lake. *JAWRA J. Am. Water Resour. Assoc.* **2014**, *50*, 205–218. [CrossRef]
51. Sotiri, K.; Hilgert, S.; Mannich, M.; Bleninger, T.; Fuchs, S. Implementation of comparative detection approaches for the accurate assessment of sediment thickness and sediment volume in the Passaúna Reservoir. *J. Environ. Manag.* **2021**, *287*, 112298. [CrossRef]
52. Marcon, L.; Sotiri, K.; Bleninger, T.; Lorke, A.; Männich, M.; Hilgert, S. Acoustic Mapping of Gas Stored in Sediments of Shallow Aquatic Systems Linked to Methane Production and Ebullition Patterns. *Front. Environ. Sci.* **2022**, *10*. [CrossRef]
53. Hutchinson, G.E. On the Relation between the Oxygen Deficit and the productivity and Typology of Lakes. *Int. Rev. Gesamten Hydrobiol. Hydrogr.* **1938**, *36*, 336–355. [CrossRef]
54. Müller, B.; Bryant, L.D.; Matzinger, A.; Wüest, A. Hypolimnetic Oxygen Depletion in Eutrophic Lakes. *Environ. Sci. Technol.* **2012**, *46*, 9964–9971. [CrossRef]
55. Carneiro, F.M.; Nabout, J.C.; Vieira, L.C.G.; Roland, F.; Bini, L.M. Determinants of chlorophyll-a concentration in tropical reservoirs. *Hydrobiologia* **2014**, *740*, 89–99. [CrossRef]
56. Chen, G.; Fang, X.; Devkota, J. Understanding flow dynamics and density currents in a river-reservoir system under upstream reservoir releases. *Hydrol. Sci. J.* **2016**, *61*, 2411–2426. [CrossRef]